1-1-2013

Investigations of the Non-Covalent CH-Π Interactions Using Molecular Torsional Balances

Chen Zhao
University of South Carolina

INVESTIGATIONS OF THE NON-COVALENT CH–π INTERACTIONS USING MOLECULAR TORSIONAL BALANCES

by

Chen Zhao

Bachelor of Science
University of Science and Technology of China, 2008

Submitted in Partial Fulfillment of the Requirements

For the Degree of Doctor of Philosophy in

Chemistry and Biochemistry

College of Arts and Sciences

University of South Carolina

2013

Accepted by:

Ken D. Shimizu, Major Professor

Qian Wang, Committee Member

John L. Ferry, Committee Member

Harry J. Ploehn, Committee Member

Lacy Ford, Vice Provost and Dean of Graduate Studies

ACKNOWLEDGEMENTS

I would like to thank my parents for their selfless and endless support. Confucius once said, "While his parents are alive, the son may not go abroad to a distance." Thank you for forgiving me being further away from home and could not spend much time with you. I promise I will be back to your side when I become a person who is reliable enough to take over all these responsibilities, and sorry that it takes too long. Also many thanks to Bin, my dear husband, for all these trusts he offered. Being in a long-distant relationship for five years sounds almost impossible, but I am glad that we made it eventually.

My greatest thanks also go to my academic advisor, Dr. Ken Shimizu. The expertise I got while working in your group will benefit me for the rest of my life. Your guidance and advice showed me the right way to do research, not just reactions. Your wisdom and passion on the academic set a role model for me to follow about how to be a fine chemist, and your patience and kindness on supervising us showed me the right way to be a great teacher. I will always be thankful for all the things you have taught me, and will respect you with my highest sincerity.

Thank Dr. Qian Wang for being my committee chair and always acting strict when asking questions. Your rigorous attitude reminds me that I should always keep conscious and have high objective. Also thanks to Dr. Perry Pellachia for his assistant in the use of NMR, and Dr. Mark Smith for every beautiful crystal structure he solved. Your contribution to my work is of great significance.

Thanks to my group members, past and present. Thank Bill for helped me get started in this lab and handed me this wonderful project, and thank Brent for all his good suggestions. Thank Ping and Irene for taking over my project. Thanks to Di, Yang, and Yinyan, for making the lab such a fun place to work. Thank my friends, Yuyuan, Chunxue, Weiwei, and many others, for bringing so much joy to me. Especially Eve, for acting crazy sometimes and showing me a way living with enthusiasm.

Thank you all for being an irreplaceable part of my life. My gratitude is way beyond the words.

ABSTRACT

Several bicycle *N*–arylimide based molecular balances were designed to study aliphatic CH–π interactions and aromatic CH–π interactions (edge-to-face arene-arene interactions). In each case, the geometries of the interactions were characterized in the solid-state via X-ray analysis, and the strengths of interactions were characterized in solution by their *folded*/*unfolded* ratios, as measured by integration of their ^{1}H NMR spectra.

The balances are very sensitive to variations in the strengths of weak non-covalent interactions. Several different aspects of the CH–π interactions were studied, such as sterics, conformational entropy, cooperativity, deuterium isotope effect, substitution effects, and solvent effects. It showed that due to the weak nature of CH–π interactions, many forces can contribute on determining their interacting energies with similar magnitudes. Approaches using "double-mutant cycles" to isolate the interactions of interest from secondary effects were presented. The balances can also be used to the study of other non-covalent interaction, and the investigations were included in the last chapter.

TABLE OF CONTENTS

ACKNOWLEDGEMENTS iii

ABSTRACT v

LIST OF FIGURES x

LIST OF TABLES xvii

CHAPTER 1: INTRODUCTION TO NON-COVALENT INTERACTIONS AND MOLECULAR BALANCES 1

1.1 NON-COVALENT INTERACTIONS 1

1.2 NON-COVALENT INTERACTIONS OF ARENES 4

1.2.1 ARENE-ARENE INTERACTIONS 6

1.2.2 CH–π INTERACTIONS 7

1.2.3 CATION–π INTERACTIONS 7

1.3 MOLECULAR BALANCES FOR MEASURING NON-COVALENT INTERACTIONS 8

1.3.1 TRIPTYCENE-BASED TORSIONAL BALANCES 9

1.3.2 WILCOX'S MOLECULAR BALANCES 10

1.3.3 DIBENZOBICYCLO[3.2.2]-NONANE DERIVATIVES 11

1.3.4 EARLY MODEL SYSTEM FROM OUR GROUP 12

1.4 CONCLUSION 13

CHAPTER 2: GENERAL EXPERIMENTAL DESIGN FOR THE MEASUREMENT OF CH–π INTERACTIONS WITH MOLECULAR BALANCES 15

2.1 STRUCTURES OF BALANCES 16

2.2 GENERAL SYNTHETIC ROUTE 18

2.3 QUANTIFICATION OF FOLDED AND UNFOLDED CONFORMERS 19

2.4 Calculation of the Interacting Energies 20

2.5 Thermodynamic Studies 21

2.6 Conclusion 23

Chapter 3: Molecular Balances for Measureing Aliphatic CH–π Interactions with the Existence of Lone Pair–π Interactions 24

3.1 Designs of the Structures of Molecular Balances 25

3.2 Characterization of CH–π Interactions in Solid State 25

3.3 Quantification of CH–π Interactions in Solution 27

3.3.1 Comparison Between Methoxy and Ethoxy Balances 28

3.3.2 Balances with Large Alkoxy Groups 29

3.3.3 Comparison of Entropy and Enthalpy Values 30

3.3.4 Solvent Study 32

3.4 Conclusion 33

3.5 Experimental Section 34

3.5.1 Synthesis 34

3.5.2 Van't Hoff Plots 57

Chapter 4: Molecular Balances for Measuring Multiple Aliphatic CH–π Interactions 62

4.1 Designs of the Structures 62

4.2 Solid-State Structures 64

4.2.1 Geometries of CH_3–π Interactions 64

4.2.2 Geometries of Multiple CH–π Interactions 65

4.2.3 Control Balances 66

4.3 Measuring CH–π Interactions in Solution 66

4.3.1 Control Balances 67

4.3.2 Strength of Multiple CH–π interactions 68

4.4 Entropic and Enthalpic Values 69

4.5 Solvent Effects 71

4.6 Conclusion 72

4.6 Experimetnal Section 72

4.6.1 Synthesis 73

4.6.2 Variable Temperature ^{1}H NMR Experiments: 96

Chapter 5: Investigation of Deuterium Isotope Effect on Aliphatic CH–π Interactions 102

5.1 Design of Balances 103

5.2 Solid-State Structures 104

5.3 Comparison of Folding Energies of CH_3 and CD_3 Balances 107

5.4 Thermodynamic Experimetns 109

5.5 Conclusion 109

5.6 Experimental Section 110

5.6.1 Synthesis and Spectrums 111

5.6.2 Folding Energies in Acetone-D_6 120

5.6.3 Van't Hoff Plots 121

Chapter 6: Measuring Aromatic CH–π Interactions using Molecular Balances 127

6.1 Ba;ance Designs 128

6.2 Solid-State Structures 128

6.3 Edge-to-Face Arene–Arene Interactions in Solution 130

6.3.1 Measurement of Rotational Barrier 130

6.3.2 Comparison of Balances with Naphthalene and Quinoline Rotors 131

6.3.3 Substituent Effect 132

6.3.4 Solvent Effects 133

6.3.5 Balances with Quinoline and *iso*-Quinoline as Rotors 136

6.4 Conclusion 137

6.5 Synthesis 137

Chapter 7: Other Notable Works 143

7.1 Double-Mutant Cycles for Measuring Non-Covalent Interactions 143

7.1.1 Structures of Molecular Balances 144

7.1.2 Folding Energies of Balances **22** and **23** 145

7.1.3 General Design of Double-Mutant Cycles 146

7.1.4 Measuring π–π Stacking Interactions with Double-Mutant Cycle 147

7.1.5 Double-Mutant Cycle for Measuring CH–π Interactions 148

7.1.6 Double-Mutant Cycle for Comparing CH–π interactions to O–π and π–π Stacking Interactions 149

7.1.7 Conclusion 149

7.2 Solvent Effects on Balances with Different Linkers 150

7.3 Molecular Balance for Study NH_2–Π Interaction 152

7.4 Molecular Balance for Study Imidazole–Π Interaction 154

7.5 Molecular Balance with Split Phenyl Rings on Shelf 155

7.6 Synthesis 156

References 164

LIST OF FIGURES

Figure 1.1: Examples of a) an ion–induced dipole interaction between a sodium cation and a water molecule, b) a dipole–induced dipole interaction between a water molecule and an oxygen molecule. 2

Figure 1.2: Comparison of the interacting surface areas and boiling points of ethane, *n*-pentane, and neopentane. 3

Figure 1.3: Illustration of a hydrogen bond between two alcohol molecules. 4

Figure 1.4: Illustration of the aggregation of two solute molecules in solution caused by the solvophobic effect. 4

Figure 1.5: Examples for different types of non-covalent interactions of arenes: a)π–π stacking interactions, b) perpendicular arene–arene interactions, c) XH–π (X = C, N, or O) interactions, and d) ion–π interactions. 5

Figure 1.6: Depiction of the quadrupole of a benzene molecule: top view and side view. 6

Figure 1.7: Relationship between the π–π interaction and the orientation of dimers based on Hunter's electrostatic model. 6

Figure 1.8: Simplified representation based on the theory by Hunter *et al*.[44] showing the folding equilibrium between *unfolded* and *folded* conformers of a molecular torsion balance in solvent. 8

Figure 1.9: Equilibrium between different conformers of 1,9-disubstituted triptycenes used to study intramolecular interactions between the Y and Z groups. 9

Figure 1.10: Wilcox's molecular torsion balance for measuring CH–π and edge-to-face arene–arene interactions. 10

Figure 1.11: Motherwell's balances for quantifying functional group–π interactions in organic solvent. 11

Figure 1.12: The *syn* and *anti* conformers for the naphthalene diimide molecular balances for measuring π–stacking interactions.....12

Figure 1.13: The equilibrium between *unfolded* and *folded* bicyclic molecular balances for measuring π–π stacking interactions. 13

Figure 2.1: The equilibrium between folded and unfolded conformers of the bicyclic *N*-arylimide molecular balance for study the face-to-face π–π interaction. 15

Figure 2.2: Molecular balances A and B designed to measure aliphatic CH–π interactions and balances C to measure aromatic CH–π interactions (or edge-to-face arene–arene interactions). 16

Figure 2.3: One-armed (**1a**–**e**), two-armed (**1f**, **1g**, and **2c**), and control (**2a**–**b**, **3a**) molecular balances designed to measure CH–π interaction. 17

Figure 2.4: General route for the synthesis of balances **1–3** (X = CO, O, or CH_2; Y = H or Ph). 18

Figure 2.5: ^{1}H NMR spectra of balance **1a** in $CDCl_3$ allowed for quantification of *folded*/*unfolded* ratios. 19

Figure 2.6: ^{1}H NMR spectra of a balance with ethylene shelf in $CDCl_3$ allowed for quantification of *folded*/*unfolded* conformations. 20

Figure 2.7: The van't Hoff plots of the molecular balance **1b** in $CDCl_3$ (25°C–55°C). .. 22

Figure 3.1: One-armed (**1a**–**e**), two-armed (**1f**, **1g**, and **2c**), and control (**2a**–**b**, **3a**) molecular balances designed with alkoxy arm groups to measure CH–π interaction. 24

Figure 3.2: X-ray structures of (a) balance **1d**, and (b) balance **3a**, both shown in *unfolded* conformation. 25

Figure 3.3: X-ray structures of the two-armed balances (a) **1f**, (b) **1g**, and (c) **2b**. 26

Figure 3.4: Folding energy (ΔG), enthalpy (ΔH) and entropy ($T\Delta S$) values with error bars in $CDCl_3$ for balance **1a**, **2a**, **1b**, **2b**, **3a** measured from van't Hoff plots (25–55 °C). 30

Figure 3.5: Measured $-\Delta G$ of (a) balance **1a** and **1b** and (b) balances **1a**, **2a** and **3a** in a series of solvents versus the $E_T(30)$ for each solvent. 32

Figure 3.6: Overview of the synthesis of balances **1–3** via condensation between aniline **4** and anhydride **5**. 34

Figure 3.7: 400 MHz ^{1}H NMR spectrum of balance **1a** in $CDCl_3$. 41

Figure 3.8: 100 MHz ^{13}C NMR spectrum of balance **1a** in $CDCl_3$. 41

Figure 3.9: 400 MHz ^{1}H NMR spectrum of balance **1b** in $CDCl_3$. 43

Figure 3.10: 100 MHz ^{13}C NMR spectrum of balance **1b** in $CDCl_3$. 43

Figure 3.11: 300 MHz ^{1}H NMR spectrum of balance **1c** in $CDCl_3$. 44

Figure 3.12: 100 MHz ^{13}C NMR spectrum of balance **1c** in $CDCl_3$. 45

Figure 3.13: 300 MHz 1H NMR spectrum of balance **1d** in CDCl3. 46

Figure 3.14: 100 MHz ^{13}C NMR spectrum of balance **1d** in $CDCl_3$. 46

Figure 3.15: 400 MHz ^{1}H NMR spectrum of balance **1e** in $CDCl_3$. 47

Figure 3.16: 100 MHz ^{13}C NMR spectrum of balance **1e** in $CDCl_3$. 48

Figure 3.17: 400 MHz ^{1}H NMR spectrum of balance **1f** in $CDCl_3$. 49

Figure 3.18: 100 MHz ^{13}C NMR spectrum of balance **1f** in $CDCl_3$. 49

Figure 3.19: 400 MHz ^{1}H NMR spectrum of balance **1g** in $CDCl_3$. 50

Figure 3.20: 100 MHz ^{13}C NMR spectrum of balance **1g** in $CDCl_3$. 51

Figure 3.21: 400 MHz ^{1}H NMR spectrum of balance **2a** in $CDCl_3$. 52

Figure 3.22: 100 MHz ^{13}C NMR spectrum of balance **2a** in $CDCl_3$. 52

Figure 3.23: 400 MHz ^{1}H NMR spectrum of balance **2b** in $CDCl_3$.....53

Figure 3.24: 100 MHz ^{13}C NMR spectrum of balance **2b** in $CDCl_3$. 54

Figure 3.25: 400 MHz ^{1}H NMR spectrum of balance **2c** in $CDCl_3$. 55

Figure 3.26: 100 MHz ^{13}C NMR spectrum of balance **2c** in $CDCl_3$. 55

Figure 3.27: 300 MHz ^{1}H NMR spectrum of balance **3a** in $CDCl_3$. 56

Figure 3.28: Van't Hoff plot of balances **1a**, **1b**, **2a**, **2b**, and **3a** in $CDCl_3$ based on the information in Table 3.3, Table 3.4, and Table 3.5. 58

Figure 3.29: Van't Hoff plot of balances **1a**, **1b**, **2a**, **2b**, and **3a** in acetone-d_6 based on the information in Table 3.7, Table 3.8 and Table 3.9. 60

Figure 4.1: Structures of balances **7**–**10** designed for measuring multiple CH–π interactions. 63

Figure 4.2: Illustration of (a) single CH–π interaction in balance **7a**, (b, c) multiple CH–π interactions in balance **7b** and **7d**, and (d) the long pair–π interaction in previous balance with oxygen linker. 63

Figure 4.3: X-ray structures of balances (a) **7a**, (b) **8a**, (c) **7b**, (d) **7d**, (e) **9a** and (f) **10a** that obtain the *folded* conformation. 64

Figure 4.4: Polts showing the compensation between ΔH and $-T\Delta S$ values of balances **7–10**. 70

Figure 4.5: Solvent trends for balances **7a–7d** in a series of solvents with different $E_T(30)$ values. 71

Figure 4.6: Overview of synthesis of balances **7–10** via condensation between aniline **11** and anhydride **5**. 73

Figure 4.7: ^{1}H NMR spectrum of anhydride **5b** ($CDCl_3$, 400 MHz). 76

Figure 4.8: ^{13}C NMR spectrum of anhydride **6b** ($CDCl_3$, 100 MHz). 76

Figure 4.9: ^{1}H NMR spectrum of balance **7c** ($CDCl_3$, 400 MHz). 79

Figure 4.10: ^{13}C NMR spectrum of balance **7c** ($CDCl_3$, 100 MHz). 79

Figure 4.11: ^{1}H NMR spectrum of balance **7d** ($CDCl_3$, 400 MHz). 80

Figure 4.12: ^{13}C NMR spectrum of balance **7d** ($CDCl_3$, 100 MHz). 81

Figure 4.13: ^{1}H NMR spectrum of balance **8a** ($CDCl_3$, 400 MHz). 82

Figure 4.14: ^{13}C NMR spectrum of balance **8a** ($CDCl_3$, 100 MHz). 82

Figure 4.15: ^{1}H NMR spectrum of balance **8b** ($CDCl_3$, 400 MHz). 83

Figure 4.16: ^{13}C NMR spectrum of balance **8b** ($CDCl_3$, 100 MHz). 84

Figure 4.17: ^{1}H NMR spectrum of balance **8c** ($CDCl_3$, 400 MHz). 85

Figure 4.18: ^{1}H NMR spectrum of balance **8d** ($CDCl_3$, 400 MHz). 86

Figure 4.19: ^{13}C NMR spectrum of balance **8d** ($CDCl_3$, 100 MHz). 86

Figure 4.20: ^{1}H NMR spectrum of balance **14a** ($CDCl_3$, 400 MHz). 88

Figure 4.22: ^{1}H NMR spectrum of balance **9b** ($CDCl_3$, 400 MHz). 89

Figure 4.23: ^{13}C NMR spectrum of balance **9b** ($CDCl_3$, 100 MHz). 90

Figure 4.24: ^{1}H NMR spectrum of balance **9c** ($CDCl_3$, 400 MHz). 91

Figure 4.25: ^{13}C NMR spectrum of balance **9c** ($CDCl_3$, 100 MHz). 91

Figure 4.26: ^{1}H NMR spectrum of balance **9d** ($CDCl_3$, 400 MHz). 92

Figure 4.27: ^{13}C NMR spectrum of balance **9d** ($CDCl_3$, 100 MHz). 93

Figure 4.28: ^{1}H NMR spectrum of balance **10c** ($CDCl_3$, 400 MHz). 95

Figure 4.29: ^{13}C NMR spectrum of balance **10c** ($CDCl_3$, 100 MHz). 95

Figure 4.30: Van't Hoff plot of balances **7a–7d** in $CDCl_3$ based on the information in Table 4.3 and Table 4.4. 97

Figure 4.31: Van't Hoff plot of balances **8a–8d** in $CDCl_3$ based on the information in Table 4.5 and Table 4.6. 98

Figure 4.32: Van't Hoff plot of balances **9a–9d** in $CDCl_3$ based on the information in Table 4.7 and Table 4.8. 99

Figure 4.33: Van't Hoff plot of balances **10a–10d** in $CDCl_3$ based on the information in Table 4.9 and Table 4.10. 100

Figure 5.1: Schematic representation of the *folded*/*unfolded* conformational equilibrium of the molecular balances that can be used to measure changes in the strength of the intramolecular CH–π interactions in the folded conformer. 103

Figure 5.2: *Folded* conformers of protic and deuterated molecular balances **12–15** that were designed to form intramolecular CH–π interactions and control balance **16**. 104

Figure 5.3: X–ray structures of the *folded* conformers of (a) **13a**, (b) **14a**, (c) **15a**, and (d) **16a**. 105

Figure 5.4: Definitions of the distance and angular measurements used to characterize balances **13a**–**16a**. 106

Figure 5.5: Comparison of the *folded*/*unfolded* ratios of balances **12–16** in $CDCl_3$ at 25°C measured by integration of the ^{1}H NMR spectra with a ±5% integration error. ...107

Figure 5.6: Overview of synthesis of balances **13–16** via condensation reactions between deuterated or protic *o*-toluidine and anhydride **5**. 111

Figure 5.7: ^{1}H NMR spectrum of balance **13b** ($CDCl_3$, 400 MHz). 114

Figure 5.8: ^{13}C NMR spectrum of balance **13b** ($CDCl_3$, 100 MHz). 114

Figure 5.9: ^{1}H NMR spectrum of balance **14b** ($CDCl_3$, 400 MHz). 115

Figure 5.10: ^{13}C NMR spectrum of balance **14b** ($CDCl_3$, 100 MHz). 116

Figure 5.11: ^{1}H NMR spectrum of balance **15b** ($CDCl_3$, 400 MHz). 118

Figure 5.12: ^{13}C NMR spectrum of balance **15b** ($CDCl_3$, 100 MHz). 118

Figure 5.13: ^{1}H NMR spectrum of balance **16b** ($CDCl_3$, 400 MHz). 119

Figure 5.14: ^{13}C NMR spectrum of balance **16b** ($CDCl_3$, 100 MHz). 120

Figure 5.15: The van't Hoff plots of balances **13a** and **13b** in $CDCl_3$ and acetone-d_6. . 122

Figure 5.16: The van't Hoff plots of balances **14a** and **14b** in $CDCl_3$ and acetone-d_6... 123

Figure 5.17: The van't Hoff plots of balances **15a** and **15b** in $CDCl_3$ and acetone-d_6. . 124

Figure 5.18: The van't Hoff plots of balances **16a** and **16b** in $CDCl_3$ and acetone-d_6. . 125

Figure 6.1: Equilibrium between the *unfolded* and *folded* conformers of molecular balances used for measuring edge-to-face arene–arene interaction between naphthalene and aromatic rings. 127

Figure 6.2: Structures of balances designed for measuring edge-to-face arene–arene interactions. 128

Figure 6.3: X-ray structures for *folded* conformers of balances **17a**[94] and **17b** suggesting edge-to-face interactions between the edge of rotor rings and phenanthrene-shelf. 129

Figure 6.4: The value of $\ln[(R_{folded/unfolded}-R_{eq})/(R_{folded/unfolded}+1)]$ plotting versus time (at 21°C) indicating the rate for exchange between *folded* and *unfolded* conformers of balance **19a**. 131

Figure 6.5: The folding energies ($-\Delta G$, in kcal/mol) of balances **17b**–**17d** in acetonitrile–d_3 at 25 °C, shown with errors of 0.03 kcal/mol. 133

Figure 6.6: Measured $-\Delta G$ values for balances **17a–17c** in a variety of solvents at 25°C plotted versus $E_T(30)$ values of each solvent. 134

Figure 6.7: Measured $-\Delta G$ values for balances **19a–19c** in a variety of solvents at 25°C plotted versus $E_T(30)$ values of each solvent. 135

Figure 6.8: Measured $-\Delta G$ values for balances **17a–17c** in a series of mixtures of CDCl3 and methanol–d_4 at 25°C plotted versus $E_T(30)$ values. 136

Figure 6.9: Structures of balances **17b**, **20** and **21** with quinoline and *iso*-quinoline arms. 136

Figure 6.10: Folding energies of balances **17b**, **20** and **21** in different solvents at 25°C. 137

Figure 6.11: Overview of synthesis of balances **17a–b**, **18**, and **19** via condensation reactions. 138

Figure 7.1: General schematic representing a supramolecular double-mutant cycle for measuring the intramolecular interaction between X and Y. 144

Figure 7.2: Molecular balances **22** and **23** designed for double-mutant cycles analyzing intramolecular primary interactions and secondary interactions. 144

Figure 7.3: General design of the double-mutant cycle based on our molecular balances for measuring non-covalent interaction between Y and the outer ring on shelf. 146

Figure 7.4: Double-mutant cycle formed by balances **22a**, **22c**, **23a**, **23c** for measuring π–π stacking interaction. 147

Figure 7.5: The double-mutant cycle formed by balances **22b**, **22c**, **23b**, **23c** for measuring π–π stacking interaction. 148

Figure 7.6: Structures of balances **1**, **7**, **24** and **25** with different linkers for the comparison of different solvent effect. 150

Figure 7.7: Comparison of the folding energies (–Δ*G*) of balances **1a**, **1h**, **7b**, **7e** (left) and balances **1h**, **7e**, **24** and **25** (right) in different solvents. 151

Figure 7.8: Structure of balance **26** that designed to form the NH–π interaction and its crystal structure obtained from X–ray analysis. 152

Figure 7.9: Comparison of the folding energies (–Δ*G*) of balances **24** and **26** in different solvents. 153

Figure 7.10: Structure of balance **27** that designed to form the imidazole–π interaction. 154

Figure 7.11: Crystal structure of balance **27** with (a) side view and (b) top view of the stacking interaction. 154

Figure 7.12: Structure of balance **28** with separate phenyl rings on the shelf. 155

Figure 7.13: Crystal structure of balance **28** with (a) side view and (b) front view with both *unfolded* and *folded* conformers. 156

Figure 7.14: Overview of synthesis of balances **22** via Diels-Alder reaction between maleic imides **29** and the diene **30** with phenanthrene shelf. 157

LIST OF TABLES

Table 3.1: Comparison of *folded*/*unfolded* ratios and ΔG_{fold} values for one-armed balances as measured by ^{1}H NMR integrations, in $CDCl_3$ at 23 °C. 28

Table 3.2: Comparison of $\Delta\Delta G$, $\Delta\Delta H$ and $-T\Delta\Delta S$ values for balances for selected pairs of balances (in $CDCl_3$, 25 °C). 31

Table 3.3: Spectral deconvolution integrations for variable temperature ^{1}H NMR of balance **1a** and **1b** in $CDCl_3$. 57

Table 3.4: Spectral deconvolution integrations for variable temperature ^{1}H NMR of balance **2a** and **2b** in $CDCl_3$. 57

Table 3.5: Spectral deconvolution integrations for variable temperature ^{1}H NMR of balance **3a** in $CDCl_3$. 58

Table 3.6: Calculation of ΔG, ΔH, ΔS, and $-T\Delta S$ and their errors of balance **1a**, **1b**, **2a**, **2b**, and **3a** by VT NMR experiments in $CDCl_3$. 59

Table 3.7: Spectral deconvolution integrations for variable temperature ^{1}H NMR of balance **1a** and **1b** in acetone-d_6. 59

Table 3.8: Spectral deconvolution integrations for variable temperature ^{1}H NMR of balance **2a** and **2b** in acetone-d_6. 59

Table 3.9: Spectral deconvolution integrations for variable temperature ^{1}H NMR of balance **3a** in acetone-d_6. 60

Table 3.10: Calculation of ΔG, ΔH, ΔS, and $-T\Delta S$ and their errors for balance **1a**, **1b**, **2a**, **2b**, and **3a** by VT NMR experiments in acetone-d_6. 61

Table 4.1: The folding energies (ΔG) of molecular balances **7–10** in $CDCl_3$ at 25 °C. .. 67

Table 4.2: Comparison of ΔG, ΔH, and $-T\Delta S$ for balances **7–10** in $CDCl_3$ at 25 °C. 69

Table 4.3: Results from variable temperature ^{1}H NMR experiments of balance **7a** and **7b** in $CDCl_3$. 97

Table 4.4: Results from variable temperature ^{1}H NMR experiments of balance **7c** and **7d** in $CDCl_3$ 97

Table 4.5: Results from variable temperature ^{1}H NMR experiments of balance **8a** and **8b** in $CDCl_3$. 98

Table 4.6: Results from variable temperature ^{1}H NMR experiments of balance **8c** and **8d** in $CDCl_3$. 98

Table 4.7: Results from variable temperature ^{1}H NMR experiments of balance **9a** and **9b** in $CDCl_3$. 99

Table 4.8: Results from variable temperature ^{1}H NMR experiments of balance **9c** and **9d** in $CDCl_3$. 99

Table 4.9: Results from variable temperature ^{1}H NMR experiments of balance **10a** and **10b** in CDCl3. 100

Table 4.10: Results from variable temperature ^{1}H NMR experiments of balance **10c** and **10d** in $CDCl_3$. 100

Table 4.11: Calculation of ΔG, ΔH, ΔS, and $-T\Delta S$ and their errors of balance **7–10** by VT NMR experiments in $CDCl_3$. 101

Table 5.1: The d, θ and α measured from the crystal structures of balances **13a**–**16a**. . 106

Table 5.2: The folding energies of protic (ΔG_H) and deuterated (ΔG_D) balances **12**–**16** in $CDCl_3$ at 25 °C. 109

Table 5.3: Comparison of calculated ΔG_{fold} values between protic and deuterated balances **12**–**15** in $CDCl_3$ and acetone–d_6 at 25 °C with errors. 109

Table 5.4: Comparison of folding energies of protic and deuterated balances 12–16 in acetone-d_6 at 25 °C. 120

Table 5.5: *Folded*/*unfolded* ratios obtained from the integrations of corresponding peaks in variable temperature ^{1}H NMR spectrums of balances **13a** and **13b** in $CDCl_3$. 121

Table 5.6: *Folded*/*unfolded* ratios obtained from the integrations of corresponding peaks in variable temperature ^{1}H NMR spectrums of balances **13a** and **13b** in acetone-d_6. ... 121

Table 5.7: *Folded*/*unfolded* ratios obtained from the integrations of corresponding peaks in variable temperature ^{1}H NMR spectrums of balances **14a** and **14b** in $CDCl_3$. 122

Table 5.8: *Folded*/*unfolded* ratios obtained from the integrations of corresponding peaks in variable temperature ^{1}H NMR spectrums of balances **14a** and **14b** in acetone-d_6. ... 122

Table 5.9: *Folded*/*unfolded* ratios obtained from the integrations of corresponding peaks in variable temperature ^{1}H NMR spectrums of balances **15a** and **15b** in $CDCl_3$. 123

Table 5.10: *Folded*/*unfolded* ratios obtained from the integrations of corresponding peaks in variable temperature ^{1}H NMR spectrums of balances **15a** and **15b** in acetone-d_6. 123

Table 5.11: *Folded*/*unfolded* ratios obtained from the integrations of corresponding peaks in variable temperature ^{1}H NMR spectrums of balances **16a** and **16b** in $CDCl_3$. 124

Table 5.12: *Folded*/*unfolded* ratios obtained from the integrations of corresponding peaks in variable temperature ^{1}H NMR spectrums of balances **16a** and **16b** in acetone-d_6. 124

Table 5.13: Calculated ΔG, ΔH, ΔS at 25°C and $T\Delta S$ for balance **13–16** in $CDCl_3$ with errors via VT ^{1}H NMR experiment. 125

Table 5.14: Calculated ΔG, ΔH, ΔS (25°C) and $T\Delta S$ for balance **13–16** in acetone-d_6 with errors via VT ^{1}H NMR experiment. 126

Table 6.1: The *folded*/*unfolded* ratios of balance **17a–17b**, **18a–18b** and **19a–19b** in $CDCl_3$ at 25 °C. 132

Table 7.1: *Folded*/*unfolded* ratios and folding energies of balances **22–23** measured in CDCl3 at 25 °C. 145

CHAPTER 1

INTRODUCTION TO NON-COVALENT INTERACTIONS AND MOLECULAR BALANCES

Non-covalent interactions are ubiquitous in biomolecular systems and play a key role in their functions. They determine the secondary and tertiary structures of proteins,[1] and are the main forces that drive enzyme-ligand binding and base-pairing in nucleic acids.[2] They also play important roles in many chemical processes such as template-directed synthesis,[3] transmission of stereochemical information,[4] and determination of structures and properties of materials.[5] Thus, systematic studies of these interactions are important to gain a better understanding of their natures and to build better predictive models for their applications.

Thus, the topic of this thesis is the application of a series of molecular balances to study weak non-covalent interactions, specifically, CH–π interactions. Before describing the experimental design and results, an introduction to the general types and properties of non-covalent interaction and the development of molecular balances will be provided.

1.1 NON-COVALENT INTERACTIONS

The term of "non-covalent interactions" describes the weak attractive forces between two adjacent atoms. Non-covalent interactions do not involve the sharing of electrons, and thus, are differentiated from covalent interactions.[6] As a result, non-covalent interactions are usually weaker than covalent bonds (0.5–5 kcal/mol versus 50–150 kcal/mol).[7] However, the cooperativity of multiple non-covalent interactions can

provide sufficient attraction to hold interacting functional groups together, such as in large biomolecules such as proteins and nucleic acids.[8] On the other hand, the instability of these interactions can lead to greater flexibility and reversibility, and thus, they can provide dynamic properties such as stimuli-response, allosteric effect, and switching.

There are several general types of non-covalent interactions. These include ionic bonds, hydrogen bonds, dipole interactions, and solvophobic effects. One of the most common types of non-covalent interactions is ionic bonds. The ionic bonds are strong electrostatic attractions between oppositely charged ions. They are the strongest type of non-covalent interaction. The binding energy between a cation and an anion can be over 100 kcal/mol in the gas phase.[6]

The non-covalent interactions of dipoles are also based on electrostatics. These include the attraction between an ion and a polar molecule with a dipole moment (ion–dipole interaction), and the interaction between two polar molecules (dipole–dipole interaction). Finally, dipoles can be induced by a nearby ion (ion–induced dipole interaction) or another dipole (dipole–induced dipole interaction) (Figure 1.1). The strength of a dipole interaction is typically between 0.5–2 kcal/mol.

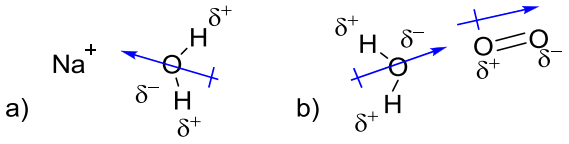

Figure 1.1: Examples of a) an ion–induced dipole interaction between a sodium cation and a water molecule, b) a dipole–induced dipole interaction between a water molecule and an oxygen molecule.

Attractive non-covalent interactions can also arise between two dipoles that are instantaneously generated from the random motions of valence electrons on the surface of molecules. These are known as van der Waals interactions or London dispersion forces.

The CH–π interactions, which are the major interactions of interest in this thesis, can be classified as dispersion interactions. Although dispersion forces are relatively weak (< 1 kcal/mol) compared with the interaction of ions and dipoles, their contribution and influence can be significant, especially when there is a large contact area between the two molecules. For instance, they are the cause of the high boiling point of linear alkanes versus branched alkanes (Figure 1.2). However, because the interactions are a consequence of electron correlation, they cannot be quantitatively modeled with computational studies. Thus, experimental approaches on measuring dispersion forces, which is the major objective of this thesis, are of great significance.

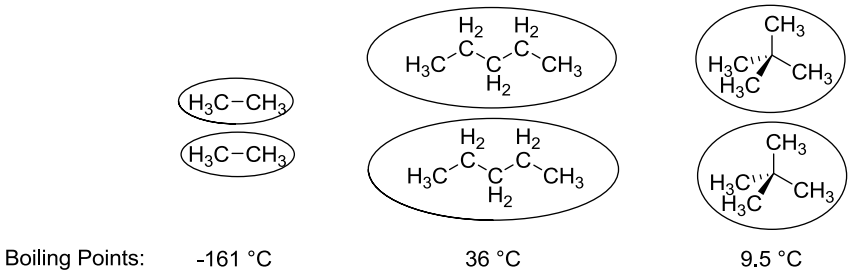

Figure 1.2: Comparison of the interacting surface areas and boiling points of ethane, *n*-pentane, and neopentane.

Another type of non-covalent interactions that have been extensively studied is the hydrogen bond. The strength of hydrogen bonds can range from about 0.1 to 60 kcal/mol.[9-11] Early definitions of hydrogen bonds were limited to the attraction between a hydrogen atom from a polar proton donor (X–H bond, X = O, N, S, halogen) and an electronegative atom having a lone-pair of electrons (e.g., O, N, S, or halogen) (Figure 1.3).[12] These classical hydrogen bonds are highly directional, and are primarily electrostatic interactions. More recently, the definition of hydrogen bonding has been broadened to include a wider range of donor and accepter functional groups.[13] For example, the hydrogen donor can be a weakly polarized C–H bond, and the acceptor can

be a group with a region with high electron-density such as the π-face of an aromatic system. Using this broader definition, many of the non-covalent interactions of arenes can also be considered as weak hydrogen bonds. The driving forces for formation of these weak hydrogen bonds still contain electrostatic component but are dominated by van der Waals interactions.[14]

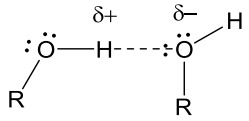

Figure 1.3: Illustration of a hydrogen bond between two alcohol molecules.

In contrast to the interactions introduced above, the solvophobic effect is a non-covalent interaction that does not have electrostatic attraction as its major component. These solutes are not held together because of mutual attraction. Instead, the binding interaction is driven by the release of solvent molecules from the surfaces of each solute and the formation of stronger solvent-solvent interactions. The precise physical origin of solvophobic effect is still being debated. One of the most common solvophobic effect is the hydrophobic effect[15-17] The hydrophobic effect is an important component in controlling biological molecular recognition, and the strongest contributor to protein folding and membrane formation.[18,19]

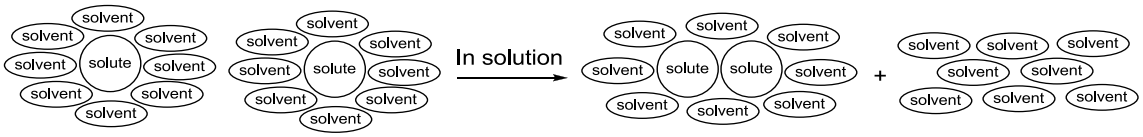

Figure 1.4: Illustration of the aggregation of two solute molecules in solution caused by the solvophobic effect.

1.2 NON-COVALENT INTERACTIONS OF ARENES

Non-covalent interactions involving aromatic rings, including CH–π interactions, are important in molecular biology.[20-22] They can also be the major driving force for the

assembly of molecules[23,24] and the selectivity of asymmetric organic reactions.[25-27] The experimentally measured strength of a non-covalent interactions with arene rings is typically 1–5 kcal/mol.[22] Based on the structures of the complementary functional groups that interact with the arene rings, the non-covalent interactions of aromatic surfaces can be classified into several subtypes, which include π–π interactions, XH–π interactions, and ion–π interactions (Figure 1.5).

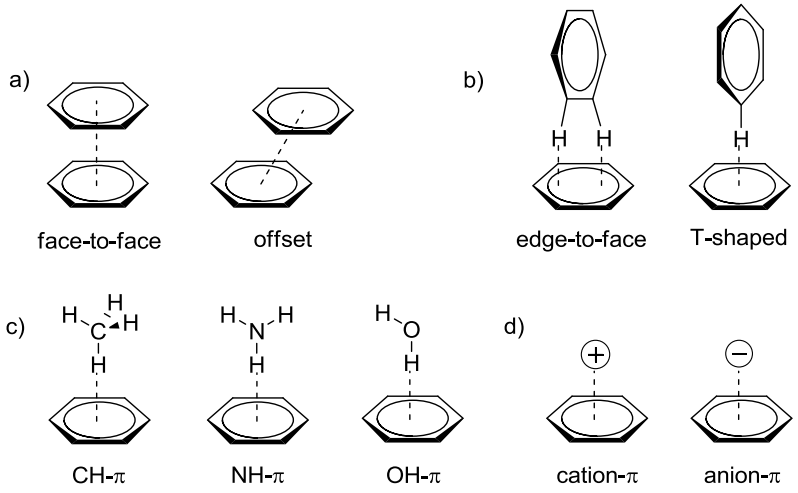

Figure 1.5: Examples for different types of non-covalent interactions of arenes: a)π–π stacking interactions, b) perpendicular arene–arene interactions, c) XH–π (X = C, N, or O) interactions, and d) ion–π interactions.

While each of these interactions has different contributing terms, many of these interactions can be treated as electrostatic hydrogen-bond-type interactions. Although benzene has no dipole moment, the six polarized $C^{\delta-}$–$H^{\delta+}$ bonds leads to a large, permanent quadrupole moment (Figure 1.6). An electrostatic model of a benzene ring can be shown as a sandwich-like structure, with partial negative charges on the two π electron-clouds above and below the faces of the ring, and partial positive charges on the edges of the ring.[28] This model shows how an aromatic ring can act as a hydrogen-bond accepter. Brief descriptions for some of these interactions will be discussed as below.

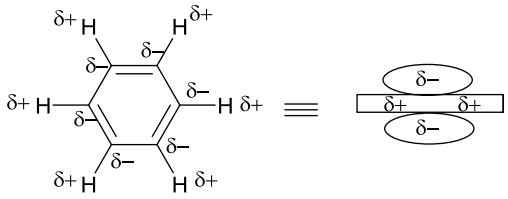

Figure 1.6: Depiction of the quadrupole of a benzene molecule: top view (left) and side view (right).

1.2.1 Arene–Arene Interactions

The attractive interactions between two aromatic rings can be classified into two types: 1) parallel, including the aligned face-to-face and offset (parallel-displaced) stacking interactions (Figure 1.5, a), 2) perpendicular, including edge-to-face and edge-on (T-shape) interactions (Figure 1.5, b).

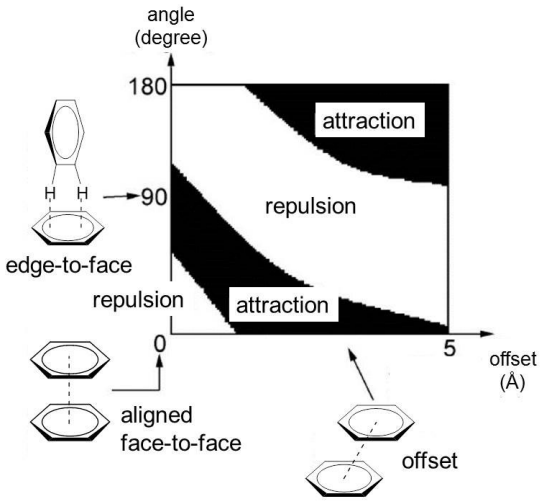

Figure 1.7: Relationship between the π–π interaction and the orientation of dimers based on Hunter's electrostatic model. Adapted with permission from Hunter, C. A.; Sanders, J. K. M. *J. Am. Chem. Soc.* **1990**, *112*, 5525-5534.[28] Copyright © 1990, American Chemical Society.

Hunter *et al.*[28] developed an electrostatic model that describes and predicts the relationship between the interaction strength and the geometry of arene-arene interactions (Figure 1.7). The black areas in the Figure show arene–arene geometries where the interaction is attractive, which includes the offset face-to-face and edge-to-face

geometries. The aligned face-to-face conformation will be a repulsive geometry due to the proximity of the two electronegative π-clouds.

1.2.2 CH–π Interactions

CH–π interactions are generally defined as the interactions between aliphatic CH's and aromatic rings. Sometimes edge-to-face or edge-on arene–arene interactions are also considered as CH–π interactions.[11,29] Both types of the interactions play significant role in conformations of marcomolecules,[30] crystal packing,[31] host-guest chemistry,[32,33] determining reaction selectivities,[34] and biochemical phenomena.[35]

CH–π interactions can be classified as non-classical weak hydrogen bonds (1.5–2.5 kcal/mol). The interactions are primarily stabilized by dispersion forces, with the electrostatic forces as of only minor importance.[36] Studies of the electronic substituent effects,[37] solvent effects[38] and thermodynamic properties[39] of CH–π interactions has provided support for the weak hydrogen-bonding nature of these interactions. Exceptions are that in which the CH's show strong proton-donating properties, such as Cl_3CH–π or C≡CH–π interactions.[13]

1.2.3 Cation–π Interactions

The cation–π interactions are strong attractive interactions between positive charges and the π-clouds of aromatic rings. The strength of these non-covalent interactions are due to their strong electrostatic component.[40] This is confirmed by the ability of simple electrostatic models to accurately describe the stability trends.[41] There are a wide range of structural types, such as those found in proteins and artificial supramolecular receptors.[40,42] Similar interactions have also been observed between cations and π-electrons of isolated alkenes and alkynes.[43]

1.3 MOLECULAR BALANCES FOR MEASURING THE NON-COVALENT INTERACTIONS

Molecular balances are synthetic molecules designed to measure the strength of intramolecular non-covalent interactions. Due to their centrally located rotatable bonds, these structures are able to adopt two or more different conformations, one of which forms an intramolecular non-covalent interaction (Figure 1.8). Thus, the conformational equilibrium ratios are governed by the strength of the intramolecular interaction in the "folded" conformer and the strength of the solvent interactions.

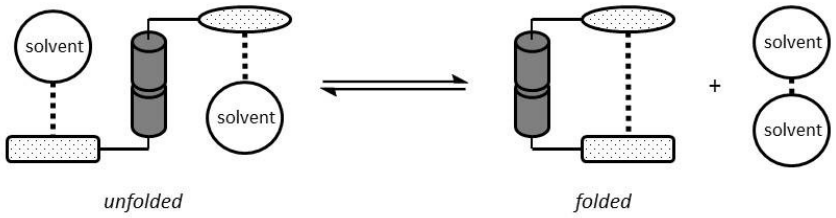

Figure 1.8: Simplified representation based on the theory by Hunter *et al.*[44] showing the folding equilibrium between *unfolded* and *folded* conformers of a molecular torsion balance in solvent.

The difference in the free energy (ΔG_{fold}) between *folded* and *unfolded* conformers of the balance provides a measurement of the strength of the intramolecular non-covalent interaction. To facilitate the measurement of the equilibrium ratios, the rate of the exchange of conformers should be slow enough to show distinct signals for each conformation in the NMR spectra, but rapid enough to allow conformational equilibrium to be reached within a reasonable timescale at room temperature. For room-temperature analysis using ^{1}H NMR, this typically requires a rotational barrier that is larger than 16 kcal/mol.[45] Ideally, the intramolecular interactions in the folded conformation can also be observed and characterized directly in the solid-state using X-ray crystallography.

There are several advantages in using molecular balances for the study of non-

covalent interactions versus biomolecular systems or supramolecular complexes.[46] First, molecular balances are minimal single-molecule systems, which provide better control over the geometries of the interactions. Second, the interaction of interest can be more easily isolated from other intramolecular or intermolecular interactions in these minimal model systems. Thus, the observed behaviors of the molecular balances provide a more accurate measure of the interaction of interest. Finally, modifications of these structures and solvent environment are easier. This makes it easier to systematically study the variables that influence the strength of the interaction, such as substituent and solvent effects. A number of successful molecular balances have been developed, and several examples will be presented in the next section.

1.3.1 Triptycene-Based Torsional Balances

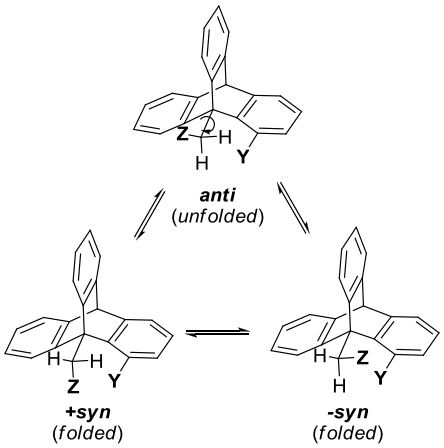

Figure 1.9: Equilibrium between different conformers of 1,9-disubstituted triptycenes used to study intramolecular interactions between the Y and Z groups.[45]

In 1970s, Oki *et al.* measured the rotational barriers of a series of bridge-head-substituted triptycene molecules (Figure 1.9).[47] They found that by increasing the size of substituents at 1– and 9– position, they are able to raise the rotational barrier of the C–C bond,[5] so that distinct signals for different conformers were observed in ^{1}H NMR at low temperatures.[48] Intramolecular interactions were able to be formed between the 1– and

9– substituents in the +/– *syn* conformations, and were broken in the *anti* conformation. By variation of the Y and Z groups, triptycene balances have been applied to the study of a broad range of non-covalent interactions,[49] including CH–O,[50-54] CH–π and oxygen/halogen–π,[55,56] methoxymethyl–π,[57] and π–π stacking interactions.[58-61]

1.3.2 Wilcox's Molecular Balances

Wilcox et al. were the first to coin the term "molecular torsion balance" to define these functional model systems in 1994.[62] Wilcox's molecular balances adopted distinct *folded* and *unfolded* conformers (Figure 1.10) due to the restricted rotation of the aryl–aryl single bond, and the two conformers showed distinct signals in the ^{1}H NMR spectra at room temperature. The folding energies were then used to quantify the stabilities of intramolecular interactions in the *folded* conformers.

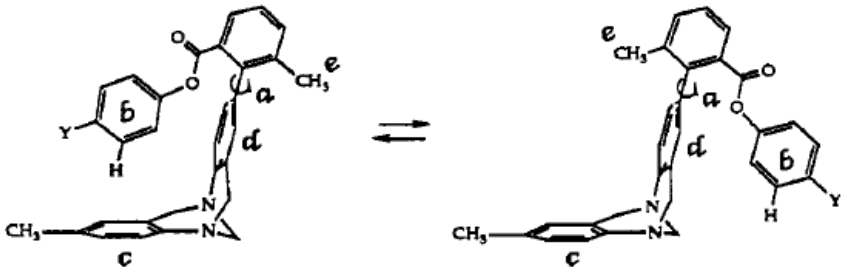

Figure 1.10: Wilcox's molecular torsion balance for measuring CH–π and edge-to-face arene–arene interactions. Reprinted with permission from Paliwal, S.; Geib, S.; Wilcox, C. S. *J. Am. Chem. Soc.* **1994**, *116*, 4497-4498. Copyright © 1994, American Chemical Society.

The balances were original applied to measure edge-to-face arene–arene interactions.[62] By varying the substituents on the two interacting phenyl rings, the electrostatic nature of the interaction was systematically probed. The results showed that the variation of the edge-ring (ring b in Figure 1.10) had a strong influence on the folding behavior of the balances, while variation of the face-ring (ring c in Figure 1.10) only led to a slight change. This second observation was originally used to support the hypothesis

that dispersion forces play a more important role than electrostatic forces in edge-to-face interactions.[63] However, further studies found that the lack of electrostatic trends for the face-ring is due to the solvent molecules screening electrostatic attraction between two phenyl rings.[64-66]

Wilcox's balance system is one of the most extensively studied molecular balances. These molecules were also modified to study aliphatic CH–π interactions,[62,67] halogen–π interactions,[68] and solvent effects.[66,69] This system also inspired a number of computational studies.[44,70]

1.3.3 Dibenzobicyclo[3, 2, 2]-Nonane Derivatives

A series of dibenzobicyclo[3, 2, 2]-nonane-based balances were developed by Motherwell *et al.*[71,72] for the study of the non-covalent interactions of aromatic rings (Figure 1.11). Each of these molecules exist in two conformations, in which either the Y or Z group interacts with the face of an aromatic ring (X = OH or OMe; Y = H, Me, *n*-Bu, CN, or C≡CH). The barrier for the conformational change is relatively low, and the two conformations are in rapid equilibrium on the NMR time-scale. However, accurate ratios of the two conformers could be measured from the ^{1}H NMR *J*-couplings.[71]

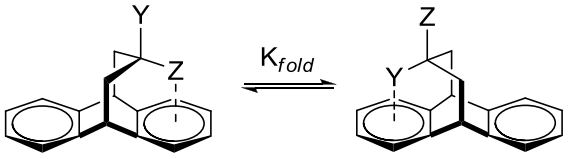

Figure 1.11: Motherwell's balances for quantifying functional group–π interactions in organic solvent.[71,72]

The solvent effects were studied in a balance with Y = CH_3 and Z = OH. In solvents with low polarity (cyclohexane, CCl_4, and benzene), the conformation that forms OH–π interactions dominated. In polar solvents that can act as H-bond acceptors

(pyridine, methanol and DMSO), the equilibrium shifts towards the one that forms the weaker CH–π interactions, allowing the OH group to form hydrogen-bonding interactions with solvent. The balances with Z = NH_2 were also studied, and the NH–π interaction was found to be weaker than the OH–π interaction under the same conditions.[72]

1.3.4 Early Model System from Our Group

A series of naphthalene diimide balances were designed in our group to study parallel face-to-face aromatic stacking interactions (Figure 1.12).[73] The rotational barrier between the *syn* and *anti* conformations was sufficiently high (27 kcal/mol) that the two conformers could be isolated at room temperature. X-ray analysis of the *anti* conformer indicated the formation of two stacking interactions with the central naphthalene diimide surface. Upon heating, the two conformers reached equilibrium in period of (**minutes or hours), and the folding energy could be quantified by the ratios of the two conformers. Different sized arene groups were linked to the "arm" (*label on figure) position, and the folding energies were found to increase with the size of the arene groups. One explanation for this folding trend is that the dispersion forces are stronger for larger aromatic surfaces. Another explanation is solvophobic effects which scales with **. However, no solvent effect was observed for this series of balances.

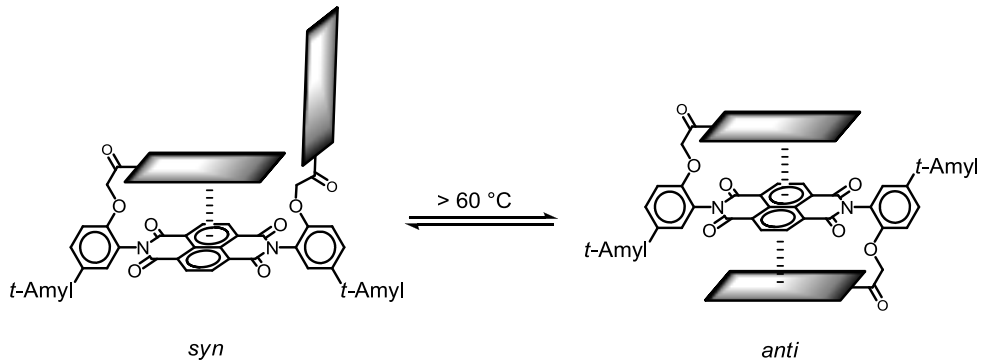

Figure 1.12: The *syn* and *anti* conformers for the naphthalene diimide molecular balances for measuring π–stacking interactions.

More recently, a new series of balances for measuring face-to-face π–stacking interactions were designed based on an *N*–arylsuccinimide phencyclone framework (Figure 1.13).[74] Control balances were made with different sized shelves (***label on Fig). The balances with large shelves (phenanthrene, and pyrene) were found to have higher *folded*/*unfolded* ratios than the ones with smaller benzene shelves which cannot form a π–π interaction with the phenyl ring of the arm, and only forms a repulsive lone pair–π interaction with the oxygen linker. The folding energies for the balances were measured in a series of solvents. The balances were more *folded* in more polar solvents, which is consistent with the theory that solvophobic effects drive the folding of balances.

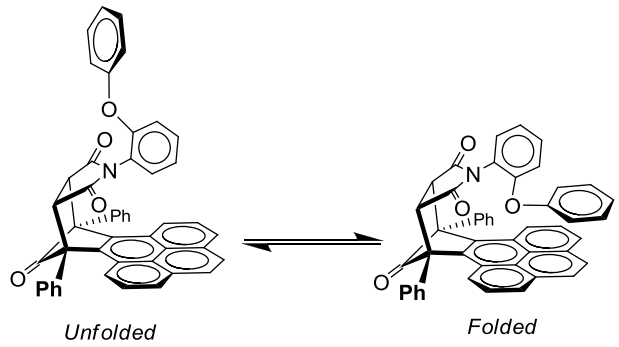

Figure 1.13: The equilibrium between *unfolded* and *folded* bicyclic molecular balances for measuring π–π stacking interactions.

1.4 CONCLUSION

In this chapter, the description and nature of non-covalent interactions with a specific focus on interactions of arenes were introduced. Several examples of recent molecular systems for the study of non-covalent interactions of arenes were presented. The purpose of this chapter was to show how important these weak interactions are, and what a challenge to understand and predict their nature. Thus, designing new molecular balances for the further study of the non-covalent interactions is of great significance and importance.

In the following chapters of this thesis, the study of non-covalent CH–π interactions using the molecular balances developed in our group will be presented. Different aspects of the CH–π interactions were studied, such as sterics, conformational entropy, cooperativity, deuterium isotope effect, substitution effects, and solvent effects.

CHAPTER 2

GENERAL EXPERIMENTAL DESIGN FOR THE MEASUREMENT OF CH–Π INTERACTIONS WITH MOLECULAR BALANCES

The new bicyclic *N*–arylimide molecular balances introduced at the end of Chapter 1 were shown to be effective on measuring face-to-face π–π stacking interactions (Figure 2.1).[74] Compared with the other systems described in Chapter 1, the new balance system possesses several advantages. First, the balances have suitably high rotational barriers, so that the two confirmations show distinct peaks in the ^{1}H NMR spectrum at room temperature, which simplified the measurement of the *folded*/*unfolded* rations in solution. Second, the balances were easier to synthesize, which made it more convenient to switch the interacting groups and study different non-covalent interactions. Finally, the balances showed good solubility in a wide range of solvents, which enabled the study of the solvent effects on the interactions.

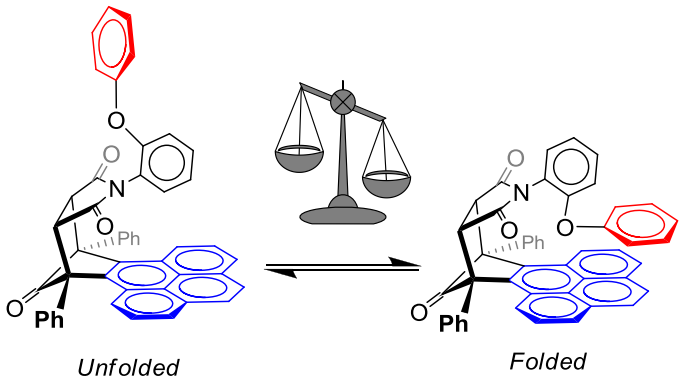

Figure 2.1: The equilibrium between folded and unfolded conformers of the bicyclic *N*-arylimide molecular balance for study the face-to-face π–π interaction.

The structures of the balances were modified to extend our study to other non-covalent interactions, but the experimental designs stayed similar regardless of the changes. In this chapter, general methods for the experimental measurement of CH–π interactions using molecular balances developed in our group will be introduced. Details of the introduction include the synthesis and characterization of balance molecules, the quantification of *folded* and *unfolded* conformations of the molecular balances, and the calculation of interacting energies, entropy values, and enthalpy values of each interaction.

2.1 STRUCTURES OF BALANCES

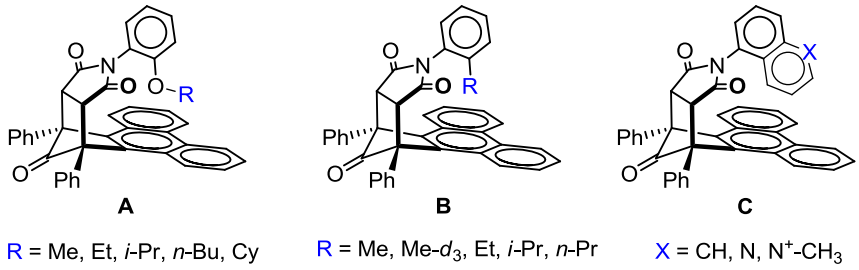

Figure 2.2: Molecular balances A and B designed to measure aliphatic CH–π interactions and balances C to measure aromatic CH–π interactions (or edge-to-face arene–arene interactions). All structures were shown in *folded* conformations.

The design of the balance system to measure CH–π interactions and edge-to-face arene–arene interactions (Figure 2.2) is based on an atropisomeric bicyclic *N*–arylimide framework that we have previously utilized to study face-to-face π–π interactions (Figure 2.1). Due to restricted rotation about the C_{aryl}–N_{imide} bond, the molecular balances adopt two distinct conformers. In the *folded* conformation, the *arm* group (phenyl ether) is positioned over the arene shelf forming an intramolecular interaction. In the *unfolded* conformation, the arm group points away from the arene shelf and cannot form an intramolecular interaction. The two conformations are in slow exchange in solution at

room temperature on the ^{1}H NMR timescale, which enables the easy characterization of *folded* and *unfolded* conformers by the distinct peaks on the ^{1}H NMR spectrums.

First, the phenyl ether on the arm position of the balance was replaced with alkyl ether groups to study aliphatic CH–π interactions (balances A, Figure 2.2).[75] The characterization in both solid-state and in solution proved the formation of desired interactions. However, due to the oxygen linker, the interacting surface area was limited, and only the interactions formed by methyl and ethyl groups could be effectively studied. The balances were then made with the alkyl groups directly linked to the phenyl rotor (balances B, Figure 2.2). Without the oxygen linker, we were able to study multiple CH–π interactions formed by various sized alkyl groups. The phenyl rotor was also replaced with 1-napthyl rings to form an edge-to-face arene–arene interaction with the arene shelves in the *folded* conformers (balances C, Figure 2.2). The formation of the intramolecular interactions was confirmed by modeling studies and the characterization data.

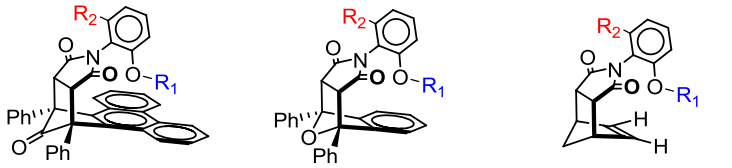

1a (R_1 = Me, R_2 = H)
1b (R_1 = Et, R_2 = H)
1c (R_1 = *i*-Pr, R_2 = H)
1d (R_1 = *n*-Bu, R_2 = H)
1e (R_1 = *c*-Hex, R_2 = H)
1f (R_1 = Me, R_2 = OMe)
1g (R_1 = Et, R_2 = OEt)

2a (R_1 = Me, R_2 = H)
2b (R_1 = Et, R_2 = H)
2c (R_1 = Me, R_2 = OMe)

3a (R_1 = Me, R_2 = H)

Figure 2.3: One-armed (**1a–e**), two-armed (**1f**, **1g**, and **2c**), and control (**2a–b**, **3a**) molecular balances designed to measure CH–π interaction.

For each new series of balances, control balances with smaller or no arene shelves (benzene, ethylene) were made (balances **2a**, **2b** and **3a**, Figure 2.3). They can help to measure the internal biases and secondary interactions that exist in each new balance

arisen from the framework and the central aromatic ring. "Two-armed" balances with two identical arms (**1f**, **1g**, and **2c**) were also made to force the balances to adopt the *folded* conformation. This allowed us to characterize the interactions in solid-state via X-ray crystallography when the *unfolded* conformation was more stable.

The balances with $–CH_3$ or $–OCH_3$ arm can also be applied to the study of deuterium isotope effect by comparisons of corresponding balances with $–CD_3$ or $–OCD_3$ arms.[76] These balances form CH–π interactions within relatively open and unconfined environments. Therefore, these model systems were less susceptible to steric effects arisen from the small difference in the size of $–CH_3$ and $–CD_3$ groups.

2.2 GENERAL SYNTHETIC ROUTE

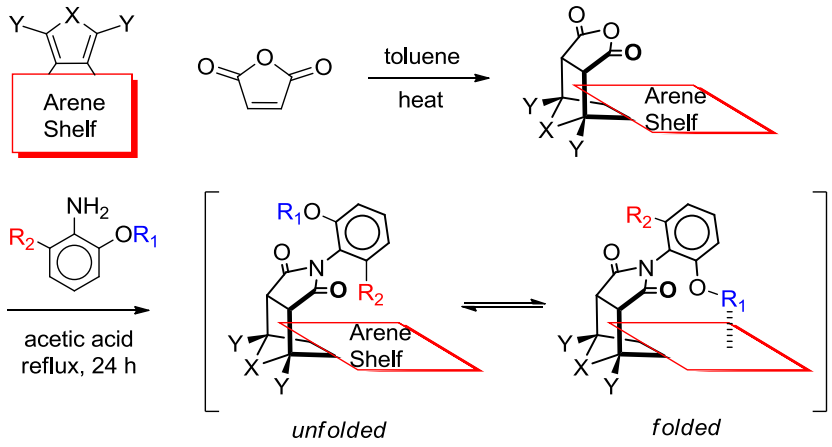

Figure 2.4: General route for the synthesis of balances **1–3** (X = CO, O, or CH_2; Y = H or Ph).

The balances were quickly assembled in modular fashion (Figure 2.4). First, the Diels-Alder reaction between a cyclic diene and maleic anhydride yielded the *endo*-bicyclic anhydride containing the arene-shelf. Then, the thermal condensation of the crude anhydride with an *ortho*-substituted aniline formed the *N*–arylimide linkage of the molecular balance. Both reactions proceeded in high yields of >80% in all cases. The efficiency of this synthesis is one of the most attractive features of the *N*–arylimide

framework, and facilitated the rapid variation of the size and structure of the arm group and the arene shelf.

2.3 QUANTIFICATION OF FOLDED AND UNFOLDED CONFORMERS

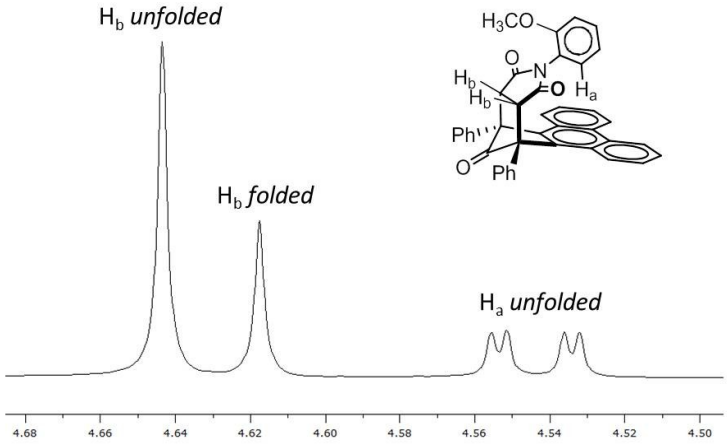

Figure 2.5: ^{1}H NMR spectra of balance **1a** in $CDCl_3$ allowed for quantification of *folded*/*unfolded* ratios.

Measurement of the concentrations of the two conformers in solution for most balances was based on the upfield shifted *ortho* proton on phenyl rotor (H_a, Figure 2.5) of the *unfolded* conformer in the ^{1}H NMR spectra. Due to its proximity to the arene shelf, the doublet-doublets of H_a is shift dramatically upfield from its normal position (~7 ppm) to a clear region of the ^{1}H NMR spectra. For balances with aromatic shelf (phenanthrene, pyrene, or benzene), the H_a peak will be shifted to the region between 4.0 and 5.0 ppm. The two conformers also showed separate signals for the two succinimide protons, usually between 4.5 and 5.0 ppm (H_b, Figure 2.5). One of the two H_b singlets, which had an area consistent with two times the area of *unfolded* H_a, was assigned as H_b *unfolded*. The other singlet was thus signed as H_b *folded*. Distinct peaks were also shown for the protons on the alkyl arm of the two conformers. The peaks for *folded* conformation were shifted upfield because of the shielding form the aromatic shelf.

For balances without an aromatic shelf, the signal for H_a in the *unfolded* conformation also showed an upfield shift form the *folded* H_a (Figure 2.6), but the difference was much smaller than the balances with aromatic shelves. Sometimes both H_a peaks overlapped with the other aromatic peaks and could not be clearly identified. In these cases, the conformers were assigned using NOEs between the alkyl peak and vinyl protons in the *folded* conformation.[75] The vinyl protons also showed split signals for the two conformers some times, but the relative position of for the two set of peaks was variable with the NMR solvents.

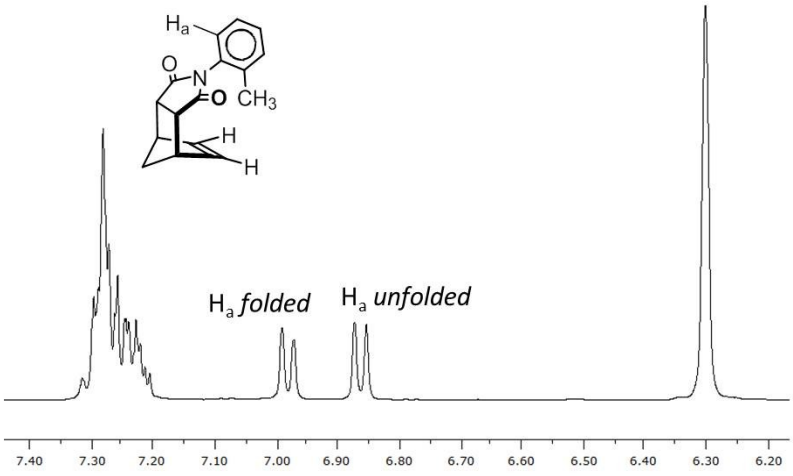

Figure 2.6: ^{1}H NMR spectra of a balance with ethylene shelf in $CDCl_3$ allowed for quantification of *folded*/*unfolded* conformations.

2.4 CALCULATION OF THE INTERACTING ENERGIES

The ratio of the *folded* and *unfolded* conformers provides a direct and accurate measure of the strength of the intramolecular interaction. The equation for the calculation of folding energy (ΔG_{fold}) of each balance is shown as Equation 2.1:

$$\Delta G_{fold} = -RT\ln(folded/unfolded) \qquad \text{(Equation 2.1)}$$

The *folded*/*unfolded* ratio for each balance was measured after the conformers were allowed to reach equilibrium. The equilibration time should be at least 10 half-lives,

and was calculated based on the rotational barrier of the C–N linkage. The barrier was primarily determined by the size of the *ortho* arm group on the phenyl rotor. For balances with oxygen atoms in the *ortho* position, the rotational barrier was 20–21 kcal/mol based on the kinetic studies,[74,75] which equates to a half-life of less than two minutes. Thus, the *folded*/*unfolded* ratios were usually measured after allowing the dissolved balances to stand at room temperature for two hours.

For most of the balances with aromatic shelves, the calculations of *folded*/*unfolded* ratios were based on the integrations of the H_a peaks on ^1H NMR spectra, because those peaks are usually in an unobscured region and were singlets, which allowed for easier integration and higher accuracy. The peaks for the protons on the alkyl arm groups can also be used for the calculation, and the ratios were almost identical with the results from the peaks of H_a. However, in order to be consistent, unless the two peaks were not well resolved, which was obscured in the spectrums of balances without aromatic shelves, the folding energies were still calculated based on the H_a peaks. The *folded*/*unfolded* ratios of the ethylene balances were based on the ratios of the two protons of the ethylene shelf. In cases of poor separation of these signals, the peaks for alkyl group were used to measure the *folded*/*unfolded* ratios.

The error of the analysis was calculated based on a conservative estimate of ±5% for the ^1H NMR integration error for each peak,[77-79] which means a ±0.03 kcal/mol error when transferred into folding energy. Spectral deconvolution method using VNMRJ software "fitspec" command at corresponding areas was applied when analyzing the spectrums to reduce the error.

2.5 THERMODYNAMIC STUDIES

Variable-temperature ^1H NMR (VT NMR) study of the balances enabled the

measurement of rotational barrier. For balances that showed distinct signals in the ^{1}H NMR spectrum for the two conformations at room temperature, the peaks corresponding to the same proton in the two conformers will shift closer and coalesce on heating. The coalescence temperature (T_c) can be used for the estimation of the rotational barrier ($\Delta G^{\ddagger}$) using Equation 2.2:[80,81]

$$\Delta G^{\ddagger} = aT\,[9.972+\log(T_c/\Delta v)] \qquad \text{(Equation 2.2)}$$

Where Δv stands for the maximum peak separation of the low-temperature limit (in Hz), and $a = 4.575 \times 10^{-3}$ kcal/mol.[80] For balance **1a**, the T_c was measured to be 135 °C in TCE–d_2. This equated to a rotational barrier of 20.5 kcal/mol.[75] For balances with an *ortho* methyl group, the barrier was measured to be 20.6 kcal/mol.[81]

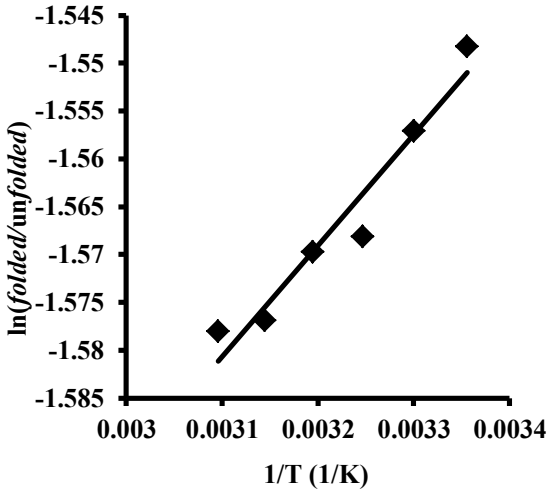

Figure 2.7: The van't Hoff plots of the molecular balance **1b** in $CDCl_3$ (25°C–55°C).

The VT NMR experiments were also used to measure the differences in enthalpy (ΔH) and entropy (ΔS) between the two conformers. The full ^{1}H NMR spectras were acquired at 10 °C intervals, and the van't Hoff plots were drawn with the ln(*folded*/*unfolded*) on the *y*-axis and the reciprocal of the temperatures on the *x*-axis. A typical van't Hoff plot is shown as Figure 2.7. Live fitting of the lines gave slopes

corresponding to $-\Delta H/R$ and y-intercepts to $\Delta S/R$. The ΔH and ΔS values were then calculated using Equations 2.3 and 2.4:

$$\Delta H = - slope \times R \qquad \text{(Equation 2.3)}$$

$$\Delta S = y_{int} \times R \qquad \text{(Equation 2.4)}$$

The errors for slopes and intercepts are measured by the regression add-in in excel.

The folding energies could also be calculated using the measured entropy and enthalpy values based on equation 2.5:

$$\Delta G_{fold} = \Delta H - T\Delta S \qquad \text{(Equation 2.5)}$$

The calculated ΔG values using the equation above were generally very close as the result calculated directly from the *folded*/*unfolded* ratios. These multiple point ΔG_{fold} values were used as reference measurements to verify the certainty of the data from single-point experiments.

2.6 CONCLUSION

A series of molecular balances were designed and prepared based on previous designed bicyclic phencyclone framework to measure non-covalent CH–π interactions. General procedures for the synthesis of the balances were described, and the methods for the characterization of the formed interactions in solution were illustrated. Also, by conducting VT NMR experiments, we were also able to estimate the rotational barriers and to measure the enthalpy and enthalpy changes between the two conformers of the balances. Studies using our molecular balances on measuring different non-covalent interactions will be presented with details in the following chapters.

CHAPTER 3

MOLECULAR BALANCES FOR MEASURING ALIPHATIC CH–π INTERACTIONS WITH THE EXISTENCE OF LONE PAIR–π INTERACTIONS

As introduced in Chapter 1, CH–π interactions are a series of important interactions with weak and non-directional nature. The direct and accurate measurement of CH–π interactions is thus difficult. The objective of this chapter is to introduce our first approach on measuring aliphatic CH–π interactions using molecular balances with O–Alkyl arms (Figure 3.1). As introduced in Chapter 1 and 2, all these balances were designed based on the same conformational dynamic framework previously developed in our group.

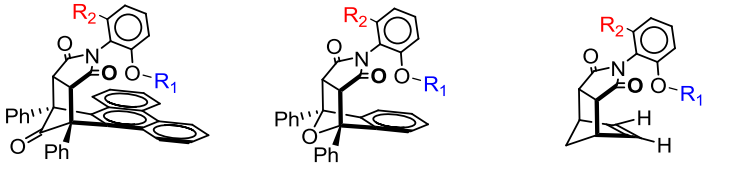

1a (R_1 = Me, R_2 = H)
1b (R_1 = Et, R_2 = H)
1c (R_1 = *i*-Pr, R_2 = H)
1d (R_1 = *n*-Bu, R_2 = H)
1e (R_1 = *c*-Hex, R_2 = H)
1f (R_1 = Me, R_2 = OMe)
1g (R_1 = Et, R_2 = OEt)

2a (R_1 = Me, R_2 = H)
2b (R_1 = Et, R_2 = H)
2c (R_1 = Me, R_2 = OMe)

3a (R_1 = Me, R_2 = H)

Figure 3.1: One-armed (**1a–e**), two-armed (**1f**, **1g**, and **2c**), and control (**2a–b**, **3a**) molecular balances designed with alkoxy arm groups to measure CH–π interaction.

This work benefited from the effort of a previously group member, William Carroll, who initiated this project, developed the synthesis route, and helped on synthesizing balances **1a**, **1b**, and **2a**. Major results presented in this chapter have been published in 2011[75] and were reprinted with permission (Copyright © 2011, American Chemical Society).

3.1 DESIGNS OF THE STRUCTURES OF MOLECULAR BALANCES

Three types of balances were studied for this study. Balances **1a–e** have alkoxy groups of varying sizes (R_1 = Me, Et, *i*-Pr, *n*-Bu, *c*-Hex) that can interact with a large phenanthrene surface. Control balances **2a–b** and **3a** have smaller benzene or ethylene surfaces. Finally, 'two-armed' balances **1f**, **1g**, and **2c** that have two identical *ortho*-alkoxy arms were made to force one of the alkoxy groups to position over the arene shelf (Figure 3.1). The purpose for have the oxygen linker in each of the balances is to 1) enable the systematic variation of the size of the alkyl group, and 2) compare with the balances with phenyl ether arm for studying face-to-face π–π interactions in previous study.[74]

3.2 CHARACTERIZATION OF CH–Π INTERACTIONS IN SOLID STATE

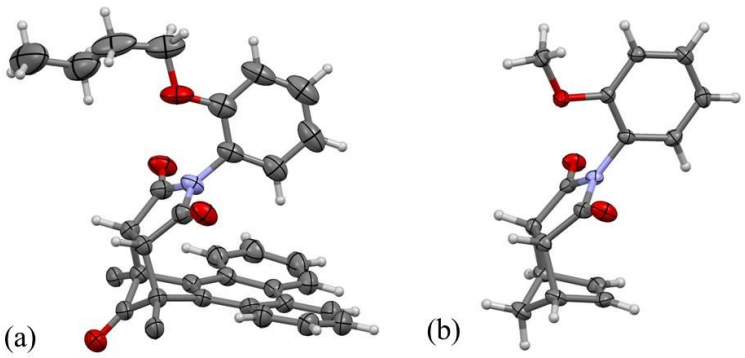

Figure 3.2: X-ray structures of (a) balance **1d**, and (b) balance **3a**, both shown in *unfolded* conformation. The bridge phenyl atoms of **1d** were hidden for better viewing clarity.

To verify the formation of an intramolecular CH–π interaction in the *folded* conformers, the solid-state structures of the balances were analyzed by X-ray crystallography. Unfortunately, the one-armed balances preferred to crystallize in the *unfolded* conformation (e.g. balance **1d** and balance **3**, Figure 3.2), due to the repulsive interaction between the ether oxygen linker and the arene shelf.

To force the molecule to crystallize in the *folded* conformation, two-armed balances **1f**, **1g**, and **2b** were synthesized that have identical alkyl-ether substituents at both *ortho*-aryl positions. Therefore, one of the two arms would always be in the *folded* configuration. The X-ray crystal structures of the two-arm balances **1f**, **1g**, and **2b** were then obtained (Figure 3.3).

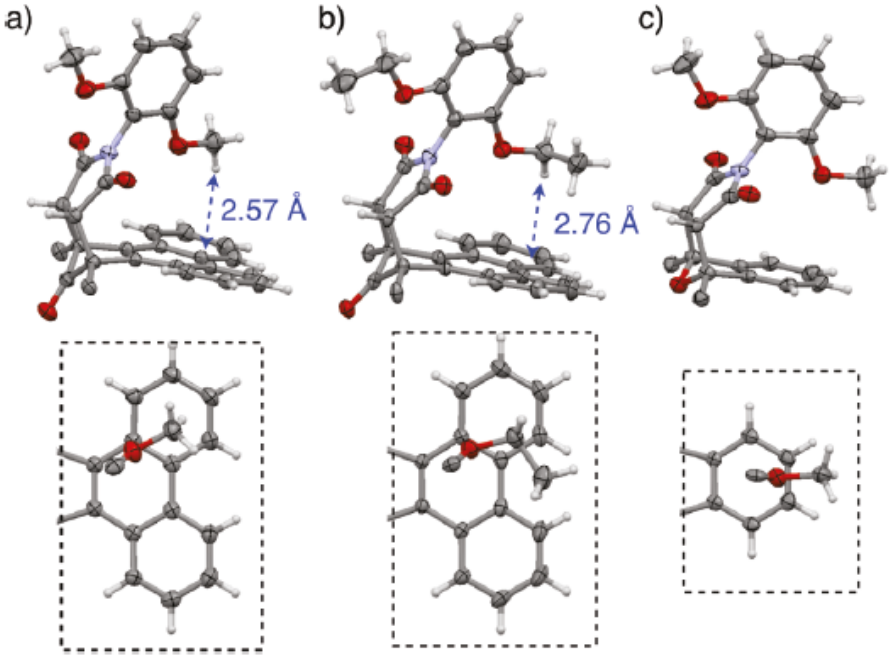

Figure 3.3: X-ray structures of the two-armed balances (a) **1f**, (b) **1g**, and (c) **2b**. The solvent molecules and the bridgehead phenyl groups are hidden for viewing clarity. The inset boxes show top-views of the interacting alkoxy and arene surfaces in each balance.

Geometries of the CH–π interactions obtained in the two-armed balances were analyzed. The OMe and OEt groups in **1f** and **1g** each form one well-defined CH–π interaction. A proton on the carbon bonded to the ether oxygen points down into the center of the outer ring of the phenanthrene shelf with atom to plane distances of 2.57 and 2.76 Å, respectively. These distances are less than the sum of the van der Waal's radii of the interacting H and C atoms (2.90 Å) and are also within the commonly used distance cut-off of 3.05 Å for the CH–π interaction.[32] In the solid-state, the terminal carbon of the

OEt group in **1g** does not form an additional CH–π interaction as it extends beyond the phenanthrene surface and is positioned over the central bay region (Figure 3.3, b). Similarly, control balance **2b** with the shorter benzene surface (Figure 3.3, c) does not form a CH–π interaction, as the methyl group extends beyond the benzene shelf. However, **2b** retains the repulsive lone pair–π interaction between the oxygen of the ether linker and the arene shelf that is also present in balance **1**. The oxygen-to-aromatic plane distance in **2b** is 3.37 Å, which is similar to distances for **1f** and **1g** (3.519 Å for OEt, 3.374 Å for OMe). Thus, comparison of the folding propensities of balances **1** and **2** provides a direct measure of strength of the intramolecular CH–π interaction.

3.3 QUANTIFICATION OF CH–Π INTERACTIONS IN SOLUTION

As introduced in Chapter 2, the strengths of the CH–π interactions were measured by monitoring the *folded*/*unfolded* conformational equilibrium by ^{1}H NMR. Due to restricted rotation around the C_{aryl}–N_{imide} single bonds, the *folded* and *unfolded* conformations were in slow exchange at room temperature. The rotational barrier about the C_{aryl}–N_{imide} bond in balance **1a** was measured to be 20.5 kcal/mol by VT NMR method (with a coalescence temperature of 135 °C in TCE-d_2), which equates to a half-life of 1.4 min at 23°C.

Separate peaks for the alkoxy-groups in different conformations were observed in the ^{1}H NMR spectra. For the phenanthrene balances **1a–g** that form intramolecular CH–π interactions, large upfield shifts of 1.4 to 1.6 ppm were observed for the alkoxy protons in the *folded* conformers due to the proximity of the arene shelf. In contrast, only small upfield shifts were observed for the *folded* conformers of control balances **2** (0.1 to 0.3 ppm) and **3** (0.01 ppm).

The folding propensities of the balances **1a–e** and control balances **2a–b** and **3a**

were measured. Integration of the peaks for the respective conformers yielded the *folded/unfolded* ratios (K_{eq}) and ΔG_{fold} values (Table 3.1). The singlets corresponding two *syn*-protons on the succinimide rings of the balances provided the most accurate *folded/unfolded* ratios as they fell in a clear region of the ^{1}H NMR spectra (4.2–4.8 ppm) and were well differentiated in most solvents. The conformers with aromatic shelves (**1a–e** and **2a–b)** were assigned by the upfield shifts of the alkoxy protons in the *folded* conformers. For balance **3a**, the conformers were assigned by NOEs between the methyl ether and vinyl protons in the *folded* conformer. Also, in order to verify that aggregation did not also attenuate the *folded*/*unfolded* ratio, the K_{eq} of balance **1a** was measured over a wide concentration range. The *folded/unfolded* ratio remained constant from 1.9 mM to 17 mM in $CDCl_3$, confirming that aggregation did not affect the *folded*/*unfolded* ratio.

Table 3.1: Comparison of *folded*/*unfolded* ratios and ΔG_{fold} values for one-armed balances as measured by ^{1}H NMR integrations, in $CDCl_3$ at 23 °C.

balances	alkoxy–arm	arene–shelf	K_{eq} [*folded*]/[*unfolded*]	ΔG_{fold} (kcal/mol)
1a	OMe	phenanthrene	0.46	0.45
1b	OEt	phenanthrene	0.20	0.94
1c	O*i*-Pr	phenanthrene	< 0.05	> 1.8
1d	O*n*-Bu	phenanthrene	0.13	1.2
1e	O*c*-Hex	phenanthrene	< 0.05	> 1.8
2a	OMe	benzene	0.09	1.40
2b	OEt	benzene	0.036	1.96
3a	OMe	Ethane	0.73	0.18

3.3.1 Comparison Between Methoxy and Ethoxy Balances

The differences in the folding energies ($\Delta\Delta G$) of balances **1** and **2**, that can and cannot form CH–π interactions respectively, provides a measure of the CH–π interactions. Therefore, the $\Delta\Delta G$ for the methoxy balances **1a** and **2a** yields an estimate of –0.95 kcal/mol for the CH–π interaction in $CDCl_3$ ($\Delta\Delta G$ = 0.45–1.40 kcal/mol). An analogous analysis with ethoxy balances **1b** and **2b** yielded a value of –1.04 kcal/mol. The similar

magnitudes of the CH–π interactions for the methoxy and ethoxy balances were in accord with the crystal structure analyses that found a single CH–π interaction in both balances. The magnitude of the CH–π interaction also compares favorably to previous measurements by Wilcox of –0.44 kcal/mol for an intramolecular alkyl CH–π interaction in $CDCl_3$.[62]

Although the CH–π interactions in **1a** and **1b** were attractive, the *folded* conformers were still not the major conformers. We hypothesized that this was due to an opposing repulsive interaction between the ether oxygen linkers and the arene surfaces. To measure the strength of the repulsive interaction, control balance **3a** was prepared, which lacked an aromatic surface. Therefore, the K_{eq} of **3a** provided a measure of the intrinsic conformational bias of the N–arylimide framework in the absence of the attractive CH–π and the repulsive oxygen–arene interaction. As expected, K_{eq} of **3a** was close to unity (0.73). The slight bias for the *unfolded* conformer was attributed to differences in dipole and solvation energy of the conformers. The $\Delta\Delta G_{\text{fold}}$ for **2a** and **3a** was +1.22 kcal/mol. This repulsive oxygen–π interaction was slightly larger than the attractive CH–π interactions in **1a** and **1b**, providing and explanation for the overall bias for the *unfolded* conformers in both balances.

3.3.2 Balances with Large Alkoxy Groups

Folding energies of balances **1a–e** with alkoxy arms of varying lengths and widths (OMe, OEt, O*i*-Pr, O*n*-Bu, and O*c*-Hex) were also compared (Table 3.1). In general, larger alkoxy arms appeared to weaken the intramolecular CH–π interactions. For balances **1c** and **1e**, only the *unfolded* conformer was observed, and thus a maximum *folded/unfolded* ratio of 0.05 in Table 3.1 was estimated based on a ^{1}H NMR integration accuracy of ±2%.

This trend could be explained for the branched O*i*-Pr and O*c*-Hex groups in **1c** and **1d**. Modeling showed that these secondary alkoxy groups create significant steric strain in the *folded* conformation. One of the two alkyl groups attached to the branch point was always pressed into the arene shelf. The destabilization of the balances with the longer linear alkoxy arms **1b** (OEt) and **1d** (O*n*-Bu) was more difficult to explain. X-ray and molecular modeling studies predicted that **1a**, **1b**, and **1d** should have similar folding energies because: 1) they all form only a single CH–π interaction between the protons on the carbon attached to the ether oxygen and the phenanthrene surface, and 2) the more flexible linear alkoxy groups can adopt conformations that minimize any destabilizing steric interactions. A possible explanation was that the observed differences in ΔG_{fold} were due to differences in conformational entropy (ΔS) of the alkoxy arms.

3.3.3 Comparison of Entropy and Enthalpy Values

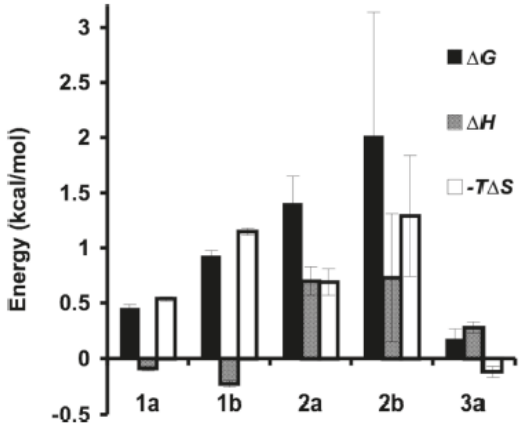

Figure 3.4: Folding energy (ΔG), enthalpy (ΔH) and entropy ($T\Delta S$) values with error bars in $CDCl_3$ for balance **1a**, **2a**, **1b**, **2b**, **3a** measured from van't Hoff plots (25–55 °C).

To test the theory above, the entropic and enthalpic terms of the folding equilibriums were measured for balances **1a**, **1b**, **2a**, **2b**, and **3a** (Table 3.6, Figure 3.4). The van't Hoff analysis for balances **1c, 1d,** and **1e** were not performed because of the large errors in the analysis for balances with *folded/unfolded* ratios < 0.1 or > 10.

The analysis confirmed that the apparent differences between the CH–π interactions formed in balances with OMe and OEt arms were due to differences in conformational entropy. For example, the $\Delta\Delta G$ of 0.47 kcal/mol for OEt and OMe balances, **1b** and **1a**, was due primarily to the differences in the entropic term, as $-T\Delta\Delta S > \Delta\Delta H$ **(**Table 3.2, entry 1). The additional methylene group of the OEt arm of **1b** forms only a slightly stronger CH–π interaction, as $\Delta\Delta H$ was small. The larger change was in the entropic term (0.61 kcal/mol), which can be attributed the loss of rotational freedom in the OEt arm when it is held against the phenanthrene shelf in the *folded* conformation. The same entropic penalty was observed for the smaller benzene-shelf balances **2b** and **2a** (Table 3.2, entry 2) that cannot form CH–π interactions, confirming that the entropic penalty in the OEt group was due to rotational isomerism around the O–CH_2 bond and not the CH_2–CH_3. The magnitude of the entropic penalty was also consistent with estimates of loss of rotational freedom around the O–C bond of an ethoxy group ($-T\Delta\Delta S$ = 0.43 kcal/mol).[82]

Table 3.2: Comparison of $\Delta\Delta G$, $\Delta\Delta H$ and $-T\Delta\Delta S$ values for balances for selected pairs of balances (in $CDCl_3$, 25°C).

entry	comparison	$\Delta\Delta G$ (kcal·mol^{-1})	$\Delta\Delta H$ (kcal·mol^{-1})	$-T\Delta\Delta S$ (kcal·mol^{-1})
1	**1b–1a**	0.47	–0.14	0.61
2	**2b–2a**	0.62	–0.03	0.60
3	**1a–2a**	–0.95	–0.79	–0.15
4	**1b–2b**	–1.10	–0.96	–0.14
5	**2a–3a**	1.23	0.42	0.81

The analyses in Table 3.2 also confirmed the validity of measuring the CH–π interaction via the difference in folding energies of the phenanthrene and benzene-shelved balances **1** and **2** (Table 3.2, entries 3 and 4). This comparison effectively removes the differences in conformational entropy in the *folded* and *unfolded* conformers,

isolating the enthalpic differences associated with the CH–π interaction. This can be seen by the dominant enthalpic terms ($|\Delta\Delta H| > |T\Delta\Delta S|$). Also, the $\Delta\Delta H$ terms for **1a**–**2a** and **1b**–**2b** were very similar (–0.79 and –0.96 kcal/mol), which is consistent with both OMe and OEt arms forming a single CH–π interaction.

3.3.4 Solvent Study

The excellent solubility of this balance system enables the study on solvent effect. In previous study on face-to-face arene–arene interactions, solvents were observed to have a great influence on the strength of the interactions due to solvophobic effect. In a solvent with higher polarity, the solvophobic effect would be stronger, and the non-covalent interaction would be stabilized.

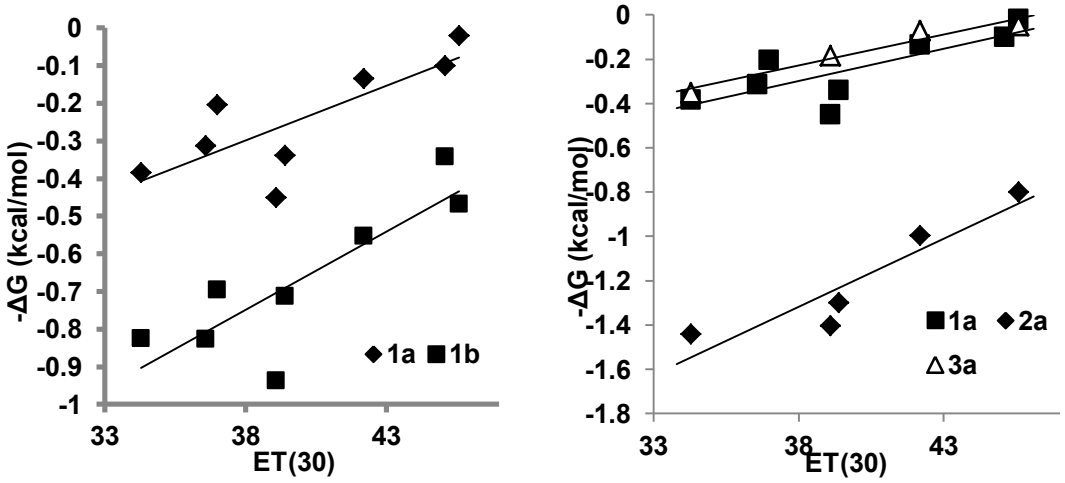

Figure 3.5: Measured –Δ*G* of (a) balance **1a** and **1b** and (b) balances **1a**, **2a** and **3a** in a series of solvents versus the $E_T(30)$ for each solvent. Solvent from left to right are deuterated benzene, THF, chloroform, TCE, acetone, DMSO, and acetonitrile at 23 °C.

In order to identify the magnitude of solvophobic effect on CH–π interactions, we attempt to study how polarity of solvent influent the strength of these interactions. Balances **1a** and **1b** was dissolved in a series of deuterated solvent (benzene, THF, chloroform, TCE, acetone, DMSO, acetonitrile), and the calculated –Δ*G* values were

plotted versus the $E_T(30)$ values of the solvents (Figure 3.5).

A linear correlation between the $-\Delta G$ and $E_T(30)$ values was observed. The polar solvents drive the balances into a higher folding degree, and trends of balances with different shelves or arms were close to parallel. The observation is consistent with Hunter's hypothesis that other than the attractive interaction formed in the *folded* conformers, the solvophobic effect is also important factor that determines the folding ratio. The molecules of solvent with high polarity are more intended to interact with each other rather than with the arm or shelf of the balance molecules, and thus stabilized the *folded* conformer by forcing the forcing the intramolecular interactions to happen. Thus, even though the balances form different interactions, the trends of the folding energies in different solvents were similar. The observation also matched up with the previous study on face-to-face arene–arene interactions.

3.4 CONCLUSION

In conclusion, a series of molecular balances based on the versatile bicyclic *N*–arylimide framework were designed, which can accurately measure intramolecular CH–π interactions. Due to the weak nature of the CH–π interaction (~1.0 kcal/mol) and the sensitivity of the balances, stability trends were easily masked by other weak forces such as rotational entropy and repulsive lone pair–π interactions. However, through comparison with carefully designed control balances, we can isolate the relative contribution of the CH–π interaction to the ΔG_{fold}. For example, the 0.45 kcal/mol ΔG_{fold} measured for balance **1a** is the sum of three terms: (1) the attractive CH–π interaction between the methyl and phenanthrene surfaces (–0.95 kcal/mol), (2) the repulsive oxygen–π interaction (1.23 kcal/mol), and (3) the slight conformational bias of the balances for the *unfolded* conformer (0.17 kcal/mol), which was estimated based on the

folded/*unfolded* ratio for control balance **3a** without form a CH–π interaction. The solvent effect on CH–π interactions was also studied, and the solvophobic effect was proved to be the main reason for changing folding energies in different solvents.

3.5 EXPERIMENTAL SECTION

NMR spectra were recorded on Varian 300 MHz and 400 MHz spectrometers. Chemical shifts are reported in ppm (δ) referenced to TMS. All chemicals were purchased from commercial suppliers and used as received unless otherwise specified. Flash chromatography was carried out using silica gel from Sorbent Technologies (60 Å, 200–400 mesh). Thin layer chromatography (TLC) was performed using pre-coated TLC plates (Merck pre-coated 0.25 mm silica gel 60 F254 plates).

3.5.1 Synthesis

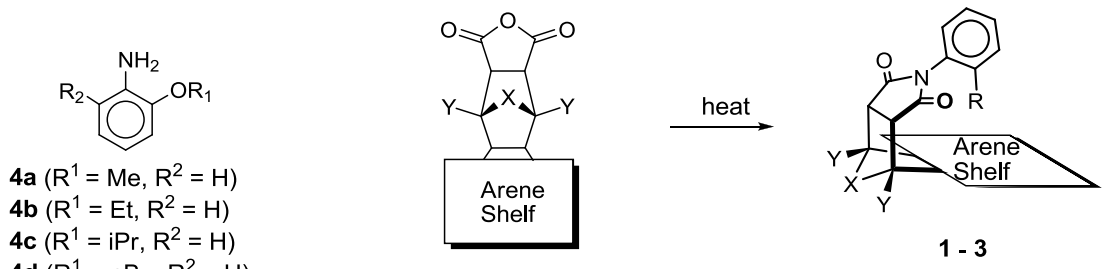

4a (R^1 = Me, R^2 = H)
4b (R^1 = Et, R^2 = H)
4c (R^1 = iPr, R^2 = H)
4d (R^1 = nBu, R^2 = H)
4e (R^1 = Cy, R^2 = H)
4f (R^1 = Me, R^2 = OMe)
4g (R^1 = Et, R^2 = OEt)

5a (X = C=O, Y = Ph, arene = phenanthrene)
5c (X = O, Y = Ph, arene = benzene)
5d (X = CH_2, Y = H, arene = ethene)

Figure 3.6: Overview of the synthesis of balances **1–3** via condensation between aniline **4** and anhydride **5**.

The general synthetic route for balances **1–3** (Figure 3.1) was as shown in Figure 3.6. All balances were synthesized via the condensation between anilines **4** with different arm groups and anhydrides **5** made via Diels-Alder reaction. The detailed synthesis of each of these compounds and the characterization data are shown as follows.

Procedures for Preparing Nitrophenylethers 6c–6e

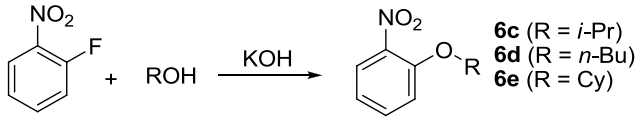

Compounds **6c–6e** are known molecules and were prepared via modified procedure from existing synthetic route.[83] To the mixture of potassium hydroxide or sodium hydride and alcohol, 1-fluoro-2-nitrobenzene was added drop-wise while stirring under nitrogen. After reacted for 24 h, the solvent was removed under vacuum. The residue was then diluted with 30 mL ethyl acetate and washed with 50 mL water for 3 times. The ethyl acetate was then removed under reduced pressure to afford accordingly substituted nitrobenzene.

Preparation of 1-*iso*-Propoxy-2-Nitrobenzene (**6c**)

Potassium hydroxide (0.27 g, 4.8 mmol), 1-fluoro-2-nitrobenzene (0.33 g, 2.4 mmol), and *iso*-propanol (5.0 mL) were used as reactants. 0.40 g product was obtained as yellow solid (94% yield). The spectra data were in agreement with reported.[84] ^{1}H NMR (400 MHz, $CDCl_3$) δ 7.77 (dd, J = 8.0 Hz, J = 1.4 Hz, 1 H), 7.47 (dt, J = 7.9 Hz, J = 1.4 Hz, 1 H), 7.07 (d, J = 8.4 Hz, 1 H), 6.97 (t, J = 7.8 Hz, 1 H), 4.65 (m, 1 H), 1.36 (d, J = 6.1 Hz, 6 H).

Preparation of 1-*n*-Butoxy-2-Nitrobenzene (**6d**)

Potassium hydroxide (0.23 g, 4.1 mmol), 1-fluoro-2-nitrobenzene (0.27 g, 1.9 mmol), and *n*-butanol (4.0 mL) were used as reactants. 0.33 g product was obtained as yellow oil, 90% yield. The spectra data were in agreement with reported.[85] ^{1}H NMR (300 MHz $CDCl_3$) δ 7.82 (dd, J = 8.0 Hz, J = 1.9 Hz, 1 H), 7.51 (dt, J = 8.0 Hz, J = 1.9 Hz, 1 H), 7.07 (d, J = 8.0 Hz, 1 H), 7.00 (t, J = 8.0 Hz, 1 H), 4.11 (t, J = 6.5 Hz, 2 H),

1.83 (m, 2 H), 1.46–1.59 (m, 2 H), 0.97 (t, J = 7.5 Hz, 3 H).

Preparation of 1-Cyclohexyloxy-2-Nitrobenzene (**6e**)

Sodium hydride (0.04 g, 1.0 mmol), 1-fluoro-2-nitrobenzene (0.13 g, 0.94 mmol) and cyclohexanol (3.0 mL) were used as reactants. 0.19 g product was obtained as yellow oil, 92% yield. The spectra data were in agreement with reported.[86] ^{1}H NMR (300 MHz $CDCl_3$) δ 7.75 (d, J = 7.5 Hz, 1 H), 7.47 (t, J = 7.5 Hz, 1 H), 7.08 (d, J = 7.5 Hz, 1 H), 6.96 (t, J =7.5 Hz, 1 H), 4.44 (m, 1 H), 1.25–1.95 (m, 10 H).

Procedures for Preparing Nitrophenylethers 6f, 6g

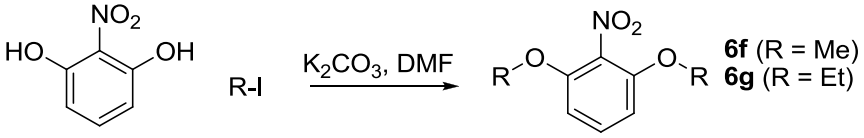

Compounds **6f** and **6g** are both known substances.[87,88] They were prepared via modified procedure from existing synthetic route of similar condensation reaction.[89] Iodoalkane was added drop wise to the mixture of potassium carbonate, 2-nitroresorcin and DMF while stirring under nitrogen. After stirred for 24 h, the reaction was poured into ice water mixture. The precipitate was then separated by filtration, washed with ice-cold water and dried under vacuum to give the product.

Preparation of 2, 6-Dimethoxynitrobenzene (**6f**)

Iodomethane (0.19 g, 1.35 mmol), 2-nitroresorcin (0.10 g, 0.65 mmol), potassium carbonate (0.18 g, 1.29 mmol) were used as reactants. Product was obtained as 0.085 g white powder, 71% yield. ^{1}H NMR (300 MHz, $CDCl_3$) δ 7.24 (t, J = 8.5 Hz, 1 H), 6.57 (d, J = 8.5 Hz, 2 H), 3.81 (s, 6 H).

Preparation of 2, 6-Diethoxynitrobenzene (**6g**)

Ethyl iodine (1.12 g, 7.15 mmol), 2-nitroresorcin (0.50 g, 3.25 mmol) and

potassium carbonate (0.89 g, 6.45 mmol) were used as reactant. Product was obtained as 0.57 g white powder, 83% yield. ^{1}H NMR (300 MHz, $CDCl_3$) δ 7.26 (dt, J = 7.8 Hz, J = 1.4 Hz, 1 H), 6.58 (d, J = 8.6 Hz, 2 H), 4.10 (q, J = 13.8 Hz, J = 7.0 Hz, 4 H), 1.38 (t, J = 6.8 Hz, 6 H).

Procedures for Preparing Anilines 4c–4f

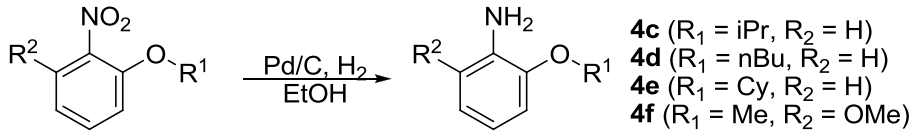

The synthetic routes of compounds **4c**–**4f** followed the general catalyzed hydrogenation method with Pd/C and H_2. The substituted nitrobenzene was dissolved in ethanol (40 mL) in a pressure vessel, and 20 mg of Pd/C (10% wt) was added. The vessel was pressurized at 40 psi with hydrogen gas and was stirred for 2 h. The resulting mixture was filtered through celite and the solvent was removed by rotary evaporation to afford the aniline product.

Preparation of 2-*iso*-Propoxyaniline (**4c**)

Compound **6c** (0.16 g, 0.89 mmol) was used as reactant. The product was obtained as brown liquid (0.13 g, 0.86 mmol, 97% yield). The spectra data were in agreement with reported.[84] ^{1}H NMR (300 MHz, $CDCl_3$) δ 6.90–6.70 (m, 4 H), 4.57 (hp, J = 6.1 Hz, 1 H), 3.80 (brs, 2 H), 1.38 (d, J = 6.1 Hz, 6 H).

Preparation of 2-*n*-Butoxyaniline (**4d**)

Compound **6d** (0.33 g, 1.7 mmol) was used as reactant. Product was obtained as brown oil (0.28 g, 1.7 mmol, 98% yield). The compound is known and has been reported.[90] ^{1}H NMR (300 MHz $CDCl_3$) δ 6.93–6.86 (m, 5 H), 4.07 (t, J = 6.4 Hz, 2 H), 1.91 (m, 2 H), 1.65 (m, 2 H), 1.12 (t, J = 7.4 Hz, 3 H).

Preparation of 2-Cyclohexyloxyaniline (**4e**)

Compound **6e** (0.27 g, 1.2 mmol) was used as reactant. Product was obtained as brown liquid (0.22 g, 1.1 mmol, 94% yield). The spectra data were in agreement with reported.[86] ^{1}H NMR (300 MHz $CDCl_3$) δ 6.94–6.60 (m, 4 H), 4.27 (m, 1 H), 3.83 (brs, 2 H), 1.30–2.10 (m, 10 H).

Preparation of 2, 6-Dimethoxyaniline (**4f**)

Compound **6f** (0.39 g, 2.1 mmol) was used as reactant and was reacted for two days. Product was obtained as yellow solid (0.31 g, 2.0 mmol, 95% yield). The spectra data were in agreement with reported.[91] ^{1}H NMR (300 MHz, $CDCl_3$) δ 6.69 (t, J = 8.1 Hz, 1 H), 6.53 (d, J = 8.1 Hz, 2 H), 3.85 (s, 6 H), 3.82 (s, 2 H).

Preparation of 2,6-Diethoxyaniline (4g)

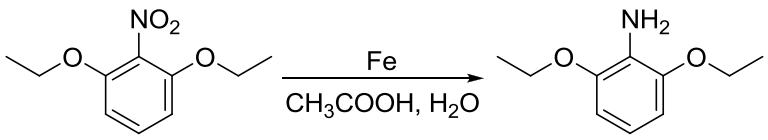

Compound **4g** is a known molecule.[92] The synthesis of **4g** follows the reduction of a similar nitrobenzene with different substituents.[93] To the mixture of compound **6g** (0.10 g, 0.55 mmol) and acetic acid (0.17 mL, 2.8 mmol) in water (5 mL), iron powder (0.31 g, 5.5 mmol) was added while stirring. The reaction was heated at reflux for 2 h and then neutralized by addition of saturated $NaHCO_3$ solution. The resulting suspension was extracted 3 times with 30 mL ethyl acetate. The organic layer was combined, and the solvent was removed by rotary evaporation to give compound **4g** (0.092 g, 0.51 mmol, 92% yield) as yellow oil. ^{1}H NMR (300 MHz, $CDCl_3$) δ 6.69 (m, 1 H), 6.54 (d, J = 6.5 Hz, 2 H), 4.06 (q, J = 13.9 Hz, J = 6.9 Hz, 4 H), 3.83 (brs, 2 H), 1.42 (t, J = 6.9 Hz, 6 H).

Preparation of anhydride 5a

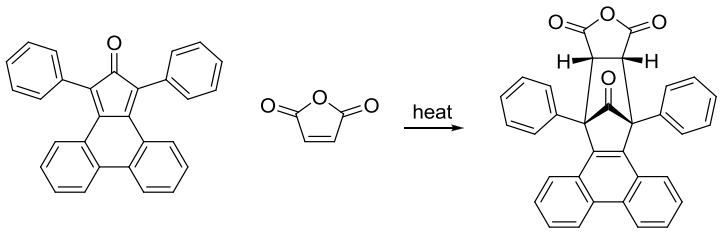

Anhydride **5a** was synthesized as described in reference.[94] Phencyclone (0.50 g, 1.3 mmol) and maleic anhydride (0.12 g, 1.3 mmol) were mixed in 5 mL of toluene and were heated with a heating gun until the dark green color faded. After cooling, the precipitated product was separated by filtration and washed with cold diethyl ether to give anhydride **5a** (0.49 g, 1.0 mmol, 77% yield) as white solid. The crude product was used for next step without further purification. The spectra data were in agreement with reported. ^{1}H NMR (300 MHz, $CDCl_3$) δ 8.69 (d, J = 8.0 Hz, 2 H), 7.12–7.76 (m, 16 H), 4.75 (s, 2 H).

Preparation of anhydride 5c

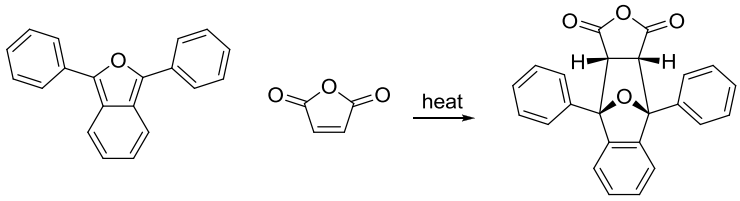

Anhydride **5c** is a known compound, and was synthesized via similar procedure as anhydride **5a**. For preparation, 1, 3-diphenylisobenzofuran (0.50 g, 1.9 mmol) and maleic anhydride (0.36 g, 3.7 mmol) were mixed in 5 mL of toluene, and the mixture was heated until the light yellow color faded. After cooling, the precipitated product was separated by filtration and washed with cold diethyl ether to obtain anhydride **5c** (0.57 g, 1.0 mmol, 84% yield) as white solid. ^{1}H NMR (300 MHz, $CDCl_3$) δ 7.94 (d, J = 6.8 Hz, 4 H), 6.94–7.70 (m, 10 H), 4.38 (s, 2 H).

Procedure for Preparing Molecular Balances 1a–1g, 2a–2c and 3

The anhydride and aniline were dissolved in 5 mL of acetic acid, and the reaction mixture was heated at reflux for 24 h. The solvent was then removed by rotary evaporation. The residue was dissolved in 25 mL EtOAc, washed once with 50 mL saturated sodium bicarbonate, and twice with 50 mL water. The solvent of organic layer was then removed under vacuum to give the crude product.

Preparation of Balance **1a**

Anhydride **5a** (0.50 g, 1.0 mmol) and anisidine **4a** (0.19 g, 1.5 mmol) were used as reactants, and 10 mL acetic acid was used as solvent. Purified by flash chromatography using silica gel ($MeOH/CH_2Cl_2$, v/v = 1/99). White solid, 0.54 g, 0.93 mmol, 93% yield. ^{1}H NMR (400 MHz, CDCl3) δ 8.64–8.76 (m, 2 H major, 2 H minor), 8.42 (d, *J* = 6.7 Hz, 2 H minor), 8.38 (d, *J* = 6.8 Hz, 2 H major), 7.09–7.80 (m, 13 H major, 13 H minor), 7.04 (td, *J* = 8.1 Hz, *J* = 2.5 Hz, 2 H major), 6.96 (dd, *J* = 7.8 Hz, *J* = 1.7 Hz, 2 H minor), 6.82 (td, *J* = 7.5 Hz, *J* = 0.9 Hz, 2 H minor), 6.74 (d, *J* = 8.6 Hz, 1 H major), 6.44 (dd, *J* = 8.5 Hz, *J* = 1.0 Hz, 1 H minor), 6.28 (td, *J* = 7.7 Hz, *J* = 1.4 Hz, 1 H major), 4.64 (s, 2 H major), 4.62 (s, 2 H minor), 4.54 (dd, *J* = 7.8 Hz, *J* = 1.7 Hz, 1 H major), 3.71 (s, 3 H major), 2.16 (s, 3 H minor). ^{13}C NMR (100 MHz, $CDCl_3$) δ 197.19, 173.15, 173.10, 154.22, 133.89, 133.80, 133.68, 133.57, 131.44, 131.11, 131.04, 130.89, 130.51, 130.44, 129.35, 129.28, 129.23, 128.61, 128.46, 128.41, 128.33, 128.30, 127.59, 127.18, 126.84, 126.59, 126.48, 126.32, 126.25, 125.90, 122.96, 122.76, 120.52, 120.07, 119.60, 111.73, 111.54, 63.58, 63.56, 55.72, 53.86, 45.33, 45.00, 29.72. HRMS (EI) calculated for $C_{40}H_{27}NO_4$: 585.1940; obs: 585.1939.

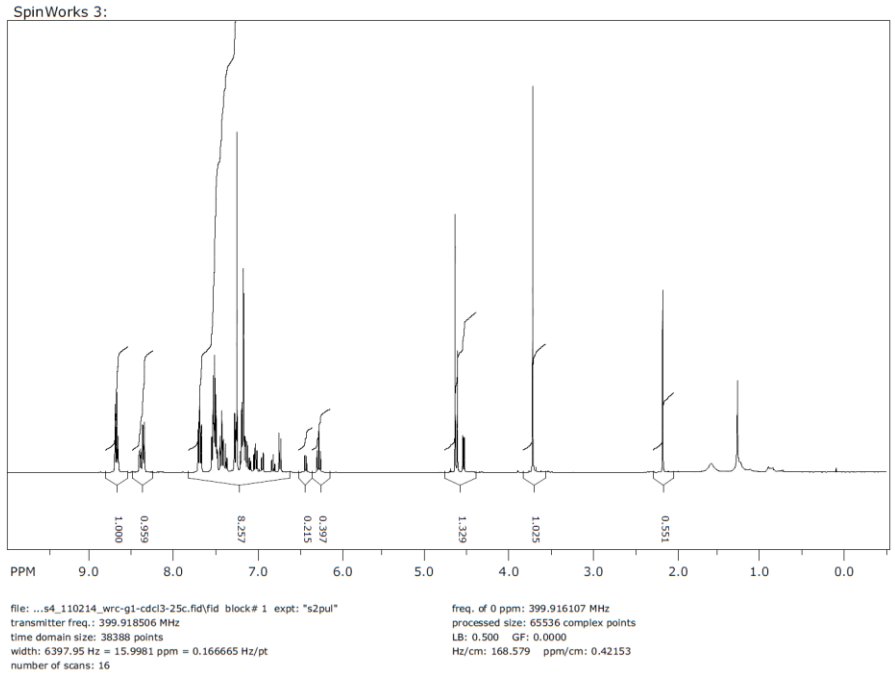

Figure 3.7: 400 MHz ^{1}H NMR spectrum of balance **1a** in $CDCl_3$.

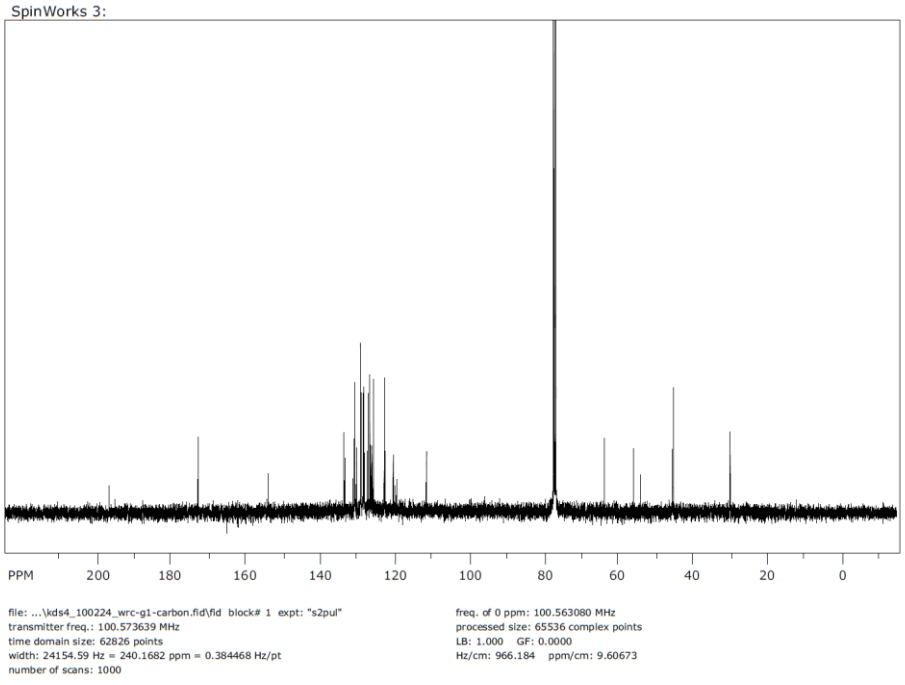

Figure 3.8: 100 MHz ^{13}C NMR spectrum of balance **1a** in $CDCl_3$.

Preparation of Balance **1b**

Anhydride **5a** (0.37 g, 0.77 mmol) and phenetidine **4b** (0.11 g, 0.77 mmol) were used as reactants. Purified by flash chromatography using silica gel ($MeOH/CH_2Cl_2$, v/v = 1/99). White solid, 0.36 g, 0.59 mmol, 73% yield. ^1H NMR (400 MHz, CDCl3) δ 8.3–8.4 (m, 2 H major, 2 H minor), 8.05 (dd, *J* = 7.9 Hz, *J* = 1.1 Hz, 2 H minor), 8.02 (dd, *J* = 6.6 Hz, *J* = 1.3 Hz, 2 H major), 6.4–7.4 (m, 15 H major, 16 H minor), 6.36 (dd, *J* = 8.4 Hz, *J* = 1.0 Hz, 1 H major), 6.06 (dd, *J* = 8.5 Hz, *J* = 1.0 Hz, 2 H minor), 5.90 (td, *J* = 7.7 Hz, *J* = 1.2 Hz, 1 H major), 4.26 (s, 2 H major), 4.22 (s, 2 H minor), 4.21 (dd, *J* = 7.8 Hz, *J* = 1.6 Hz, 1 H major), 3.58 (q, *J* = 7.0 Hz, 2 H major), 2.13 (q, *J* = 7.0 Hz, 2 H minor), 0.96 (t, *J* = 7.0 Hz, 3 H major), –0.21 (t, *J* = 7.0 Hz, 3 H minor). ^{13}C NMR (100 MHz, $CDCl_3$) δ 197.21, 173.04, 153.59, 133.84, 133.58, 131.13, 130.91, 130.33, 129.52, 129.41, 129.37, 129.33, 129.23, 128.67, 128.62, 128.41, 128.30, 127.58, 127.18, 126.83, 126.60, 126.44, 126.34, 125.91, 122.98, 122.74, 120.37, 119.90, 119.75, 112.58, 64.14, 63.56, 61.80, 45.38, 44.93, 29.73, 14.72, 12.76. HRMS (EI) calculated for $C_{41}H_{29}NO_4$: 599.2097; obs: 599.2116.

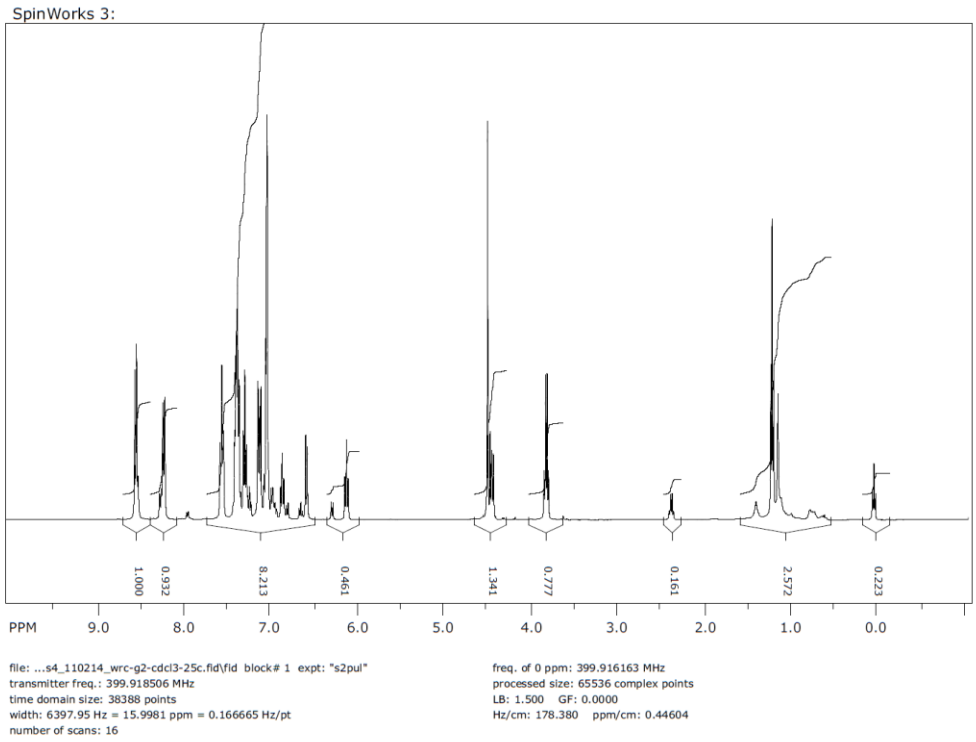

Figure 3.9: 400 MHz ^{1}H NMR spectrum of balance **1b** in $CDCl_3$.

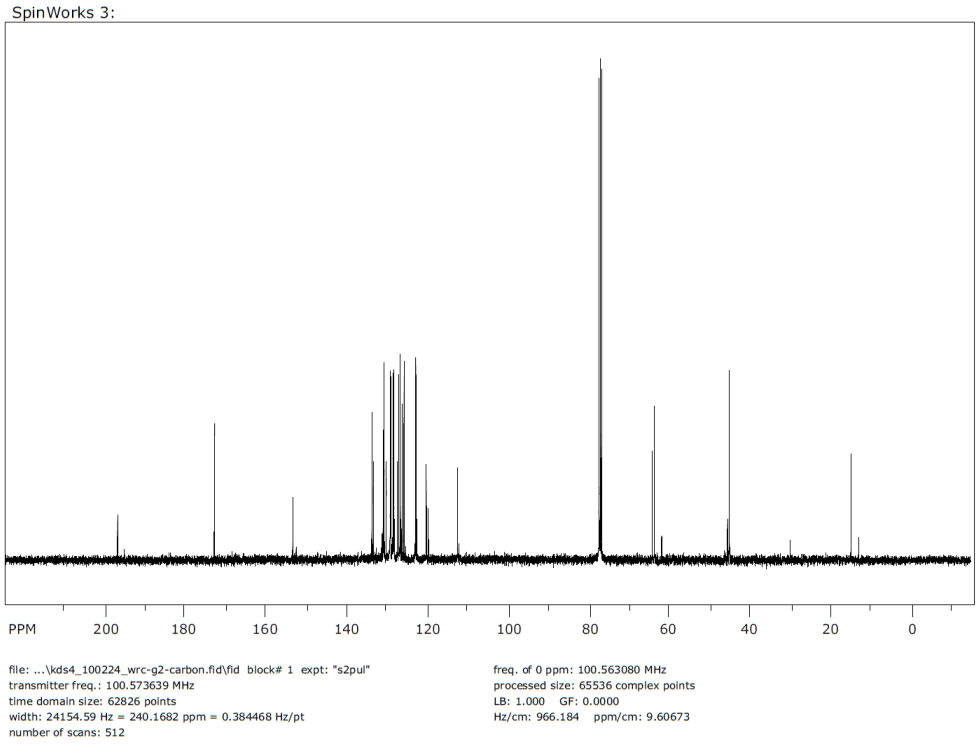

Figure 3.10: 100 MHz ^{13}C NMR spectrum of balance **1b** in $CDCl_3$.

Preparation of Balance **1c**

Anhydride **5a** (0.21 g, 0.43 mmol) and compound **4c** (0.13 g, 0.85 mmol) were used as reactants. Purified by flash chromatography using silica gel (EtOAc/Hexane, v/v = 1:5). Yellow crystal, 0.22 g, 0.36 mmol, 85% yield. ^{1}H NMR (400 MHz, $CDCl_3$) 8.71 (d, J = 8.3 Hz, 2 H), 8.37 (d, J = 7.8 Hz, 2 H), 6.81–7.91 (m, 15 H), 6.73 (d, J = 8.3 Hz, 1 H), 6.24 (t, J = 7.7 Hz, 1 H), 4.61 (s, 2 H), 4.55(dd, J = 7.7 Hz, J = 1.0 Hz, 1 H), 4.42 (m,1 H), 1.37 (d, J = 6.2 Hz, 6 H). ^{13}C NMR (100 MHz, $CDCl_3$) 197.43, 173.19, 153.95, 134.09, 133.81, 131.36, 131.14, 130.54, 129.57, 129.44, 128.84, 128.62, 127.81, 127.38, 127.04, 126.59, 126.05, 123.19, 120.56, 120.15, 112.76, 68.48, 63.78, 45.17, 31.27, 19.40, 14.13. HRMS (EI) calculated for $C_{42}H_{31}NO_4$: 613.2253; observed: 613.2256.

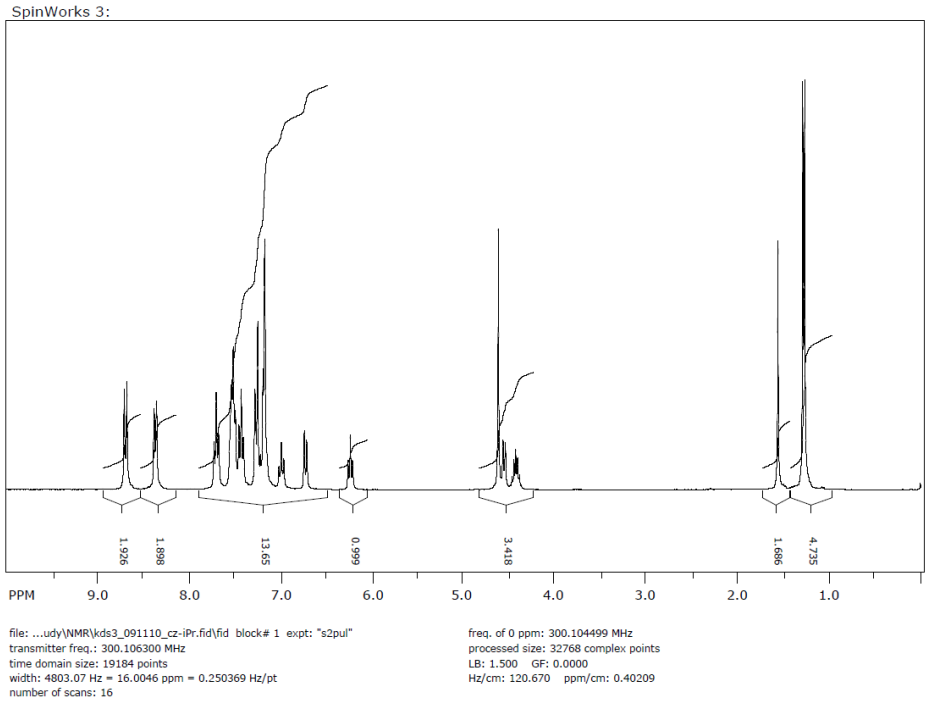

Figure 3.11: 300 MHz ^{1}H NMR spectrum of balance **1c** in $CDCl_3$.

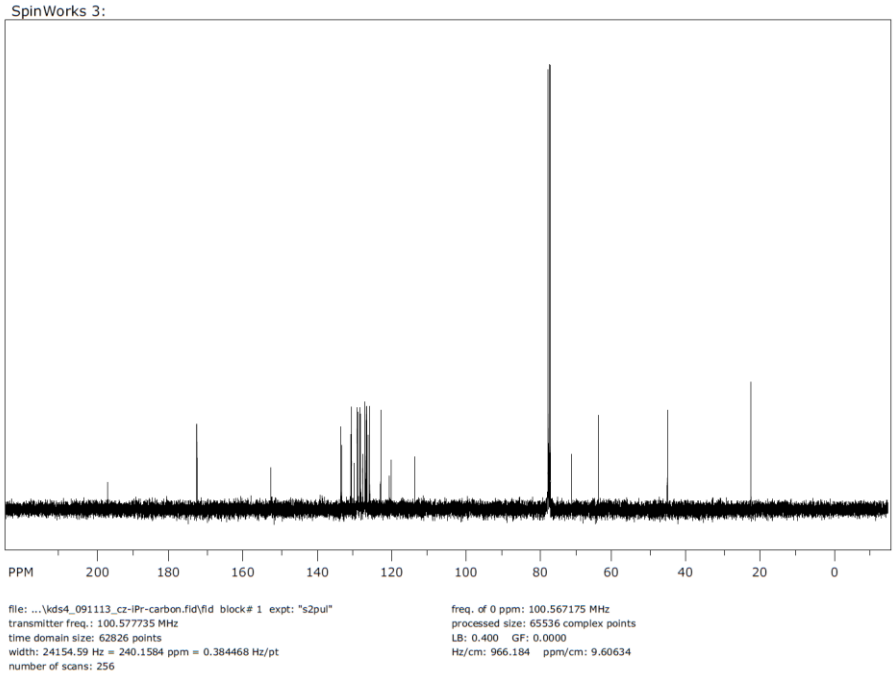

Figure 3.12: 100 MHz ^{13}C NMR spectrum of balance **1c** in $CDCl_3$.

Preparation of Balance **1d**

Anhydride **5a** (0.10 g, 0.21 mmol) and compound **4d** (0.068 g, 0.42 mmol) were used as reactants. Purified by flash chromatography using silica gel (MeOH/CH_2Cl_2, v/v = 1:99). Yellow crystal, 0.11 g, 0.17 mmol, 81% yield. ^{1}H NMR (300 MHz, $CDCl_3$) δ 8.70 (m, 2 H major, 2 H minor), 8.37 (m, 2 H major, 2 H minor), 7.71 (t, J = 7.6 Hz, 2 H major), 6.90–7.60 (m, 13 H major, 16 H minor), 6.79 (t, J = 8.0 Hz, 1 H minor), 6.73 (d, J = 8.6 Hz, 1 H major), 6.42 (d, J = 8.0 Hz, 1 H minor), 6.27 (t, J = 7.6 Hz, 1 H major), 4.62 (ds, 2 H major, 2 H minor), 4.60 (dd, J = 4.1 Hz, J = 1.3 Hz, 1 H major), 3.87 (t, J = 6.2 Hz, 2 H major, 2 H minor), 1.70 (m, 2 H major), 1.43 (m, 2 H major), 0.98 (t, J = 7.5 Hz, 3 H major), 0.34–0.80 (m, 7 H minor). ^{13}C NMR (100 MHz, $CDCl_3$) δ 197.21, 172.97, 153.71, 133.84, 133.57, 131.12, 130.90, 130.32, 129.35, 129.21, 128.61, 128.40, 127.57, 127.16, 126.81, 126.34, 125.91, 122.97, 122.86, 122.83, 120.13, 119.89, 112.51, 105.00, 68.23, 63.54, 44.93, 31.03, 19.18, 13.91. HRMS (EI) calculated for $C_{43}H_{33}NO_4$:

627.2410; observed: 627.2416.

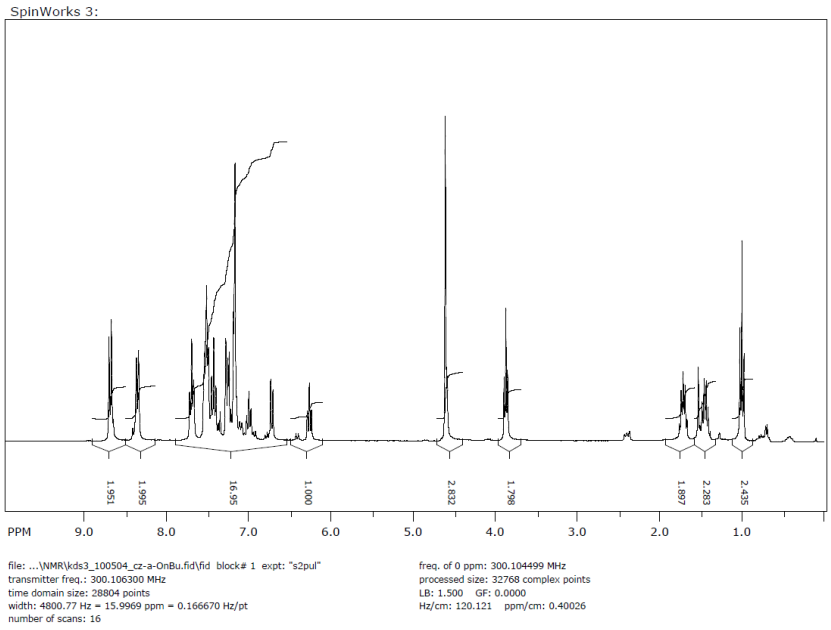

Figure 3.13: 300 MHz 1H NMR spectrum of balance **1d** in CDCl3.

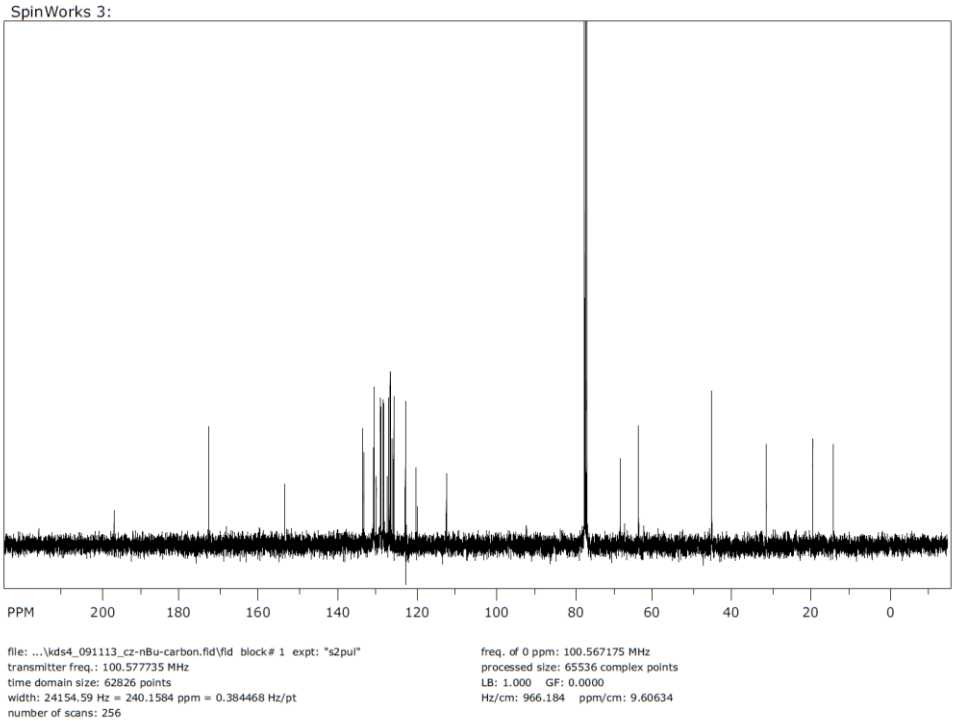

Figure 3.14: 100 MHz ^{13}C NMR spectrum of balance **1d** in $CDCl_3$.

Preparation of Balance **1e**

Anhydride **5a** (0.27 g, 0.57 mmol) and compound **4e** (0.22 g, 1.14 mmol) were used as reactants. Purified by flash chromatography using silica gel ($MeOH/CH_2Cl_2$, v/v = 1:99). Yellow solid, 0.29 g, 0.44 mmol, 78% yield. ^1H NMR (400 MHz, $CDCl_3$) δ 8.71 (d, J = 8.5 Hz, 2 H), 8.38 (d, J = 7.8 Hz, 2 H), 7.72 (t, J = 7.8 Hz, 2 H), 6.94–7.60 (m, 13 H), 6.73 (d, J = 8.5 Hz, 1 H), 6.24 (t, J = 7.8 Hz, 1 H), 4.61 (s, 2 H), 4.58 (dd, J = 7.8 Hz, J = 1.4 Hz, 1 H), 4.15 (m, 1 H), 1.20–1.92 (m, 10 H). ^{13}C NMR (100 MHz, $CDCl_3$) δ 197.25, 172.95, 152.64, 133.88, 133.58, 131.12, 130.91, 130.18, 129.36, 129.24, 128.60, 128.38, 127.81, 127.15, 126.81, 126.36, 125.94, 122.96, 120.58, 120.07, 133.62, 63.56, 44.88, 31.58, 25.49, 23.55. HRMS (EI) calculated for $C_{45}H_{35}NO_4$: 653.2566; observed: 653.2553.

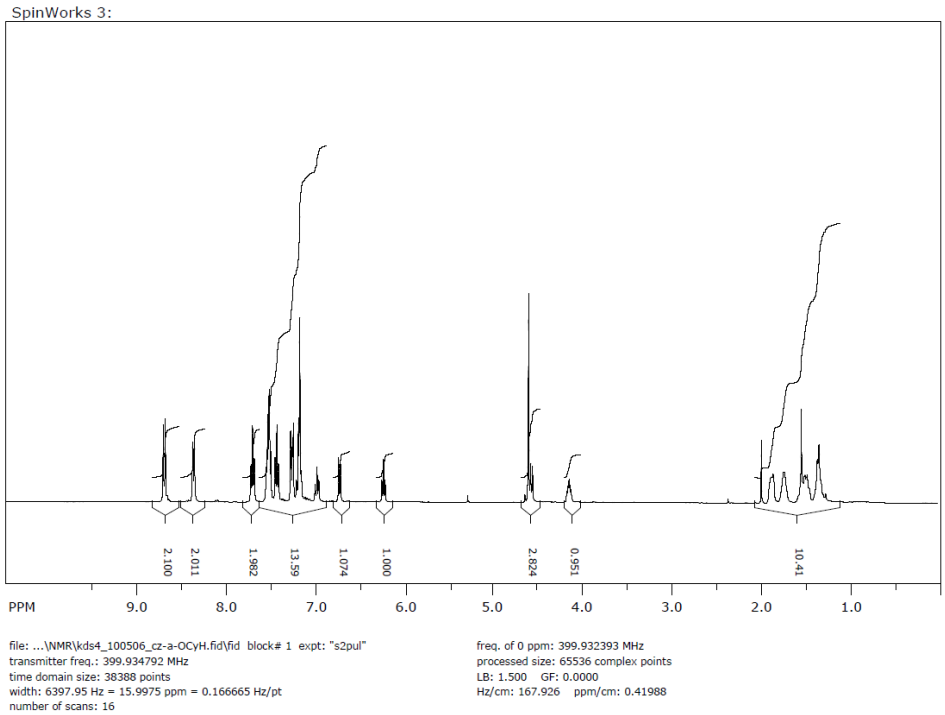

Figure 3.15: 400 MHz ^1H NMR spectrum of balance **1e** in $CDCl_3$.

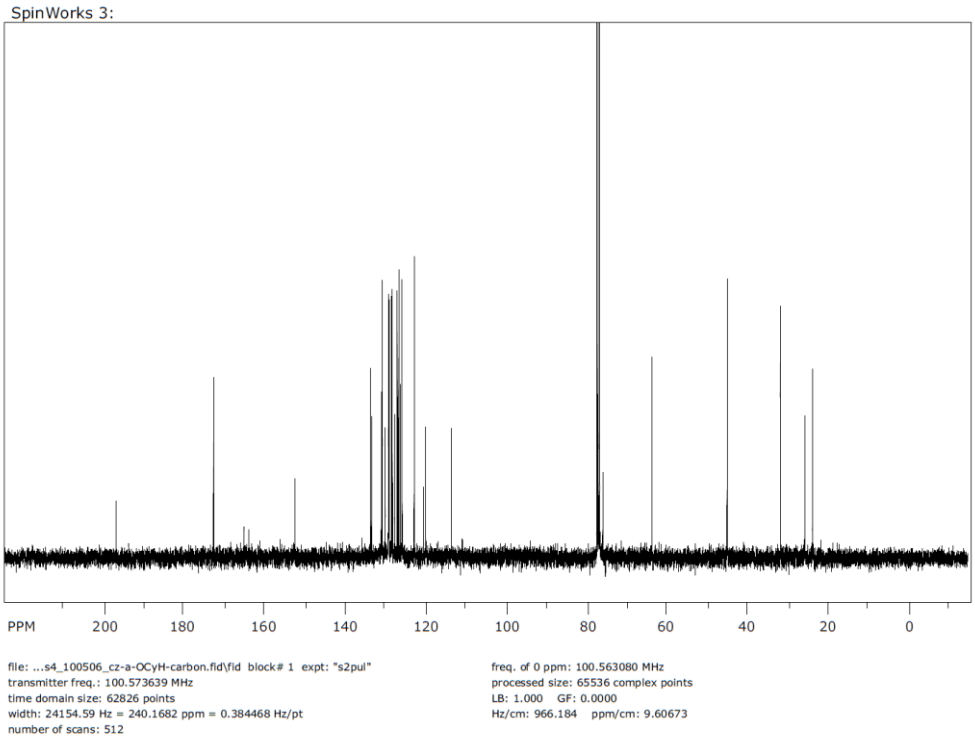

Figure 3.16: 100 MHz ^{13}C NMR spectrum of balance **1e** in $CDCl_3$.

Preparation of Balance **1f**

Anhydride **5a** (0.47 g, 0.99 mmol) and compound **4f** (0.30 g, 2.0 mmol) were used as reactants. The product was recrystallized from MeCN as white crystal, 0.35 g, 0.57 mmol, 58% yield. ^{1}H NMR (400 MHz, $CDCl_3$) δ 8.69 (d, J = 8.5 Hz, 2 H), 8.45 (d, J = 7.5 Hz, 2 H), 7.70 (t, J = 7.5 Hz, 2 H), 6.46–7.80 (m, 13 H), 6.42 (d, J = 8.5 Hz, 1 H), 6.05 (d, J = 8.5 Hz, 1 H), 4.66 (s, 2 H), 3.76 (s, 3 H), 2.17 (s, 3 H). ^{13}C NMR (100 MHz, $CDCl_3$) δ 195.96, 173.06, 155.75, 155.16, 134.03, 133.78, 131.43, 130.56, 129.46, 129.27, 128.40, 128.25, 126.75, 126.66, 126.44, 126.29, 122.67, 103.97, 103.38, 63.60, 56.10, 54.15, 45.29. HRMS (EI) calculated for $C_{41}H_{29}NO_5$: 615.2046; observed: 615.2043.

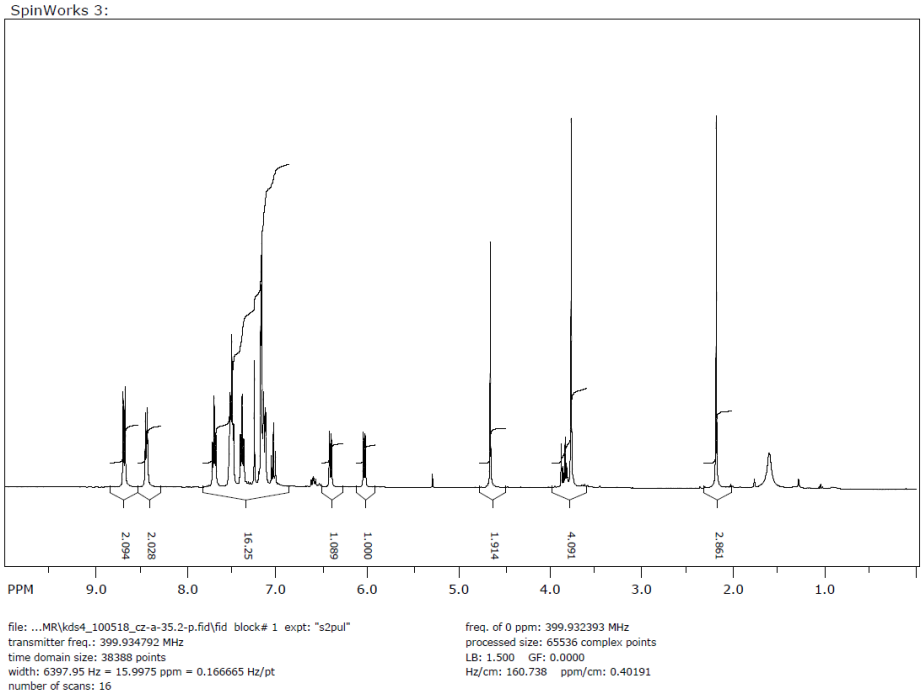

Figure 3.17: 400 MHz ^{1}H NMR spectrum of balance **1f** in $CDCl_3$.

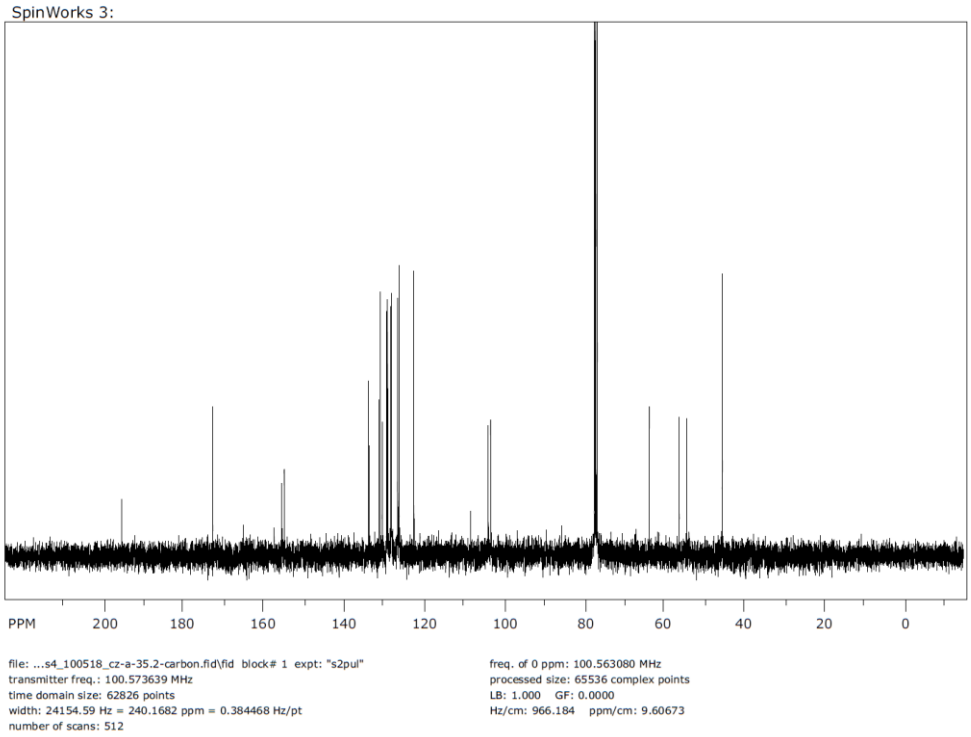

Figure 3.18: 100 MHz ^{13}C NMR spectrum of balance **1f** in $CDCl_3$.

Preparation of Balance **1g**

Anhydride **5a** (0.11 g, 0.22 mmol) and compound **4g** (0.08 g, 0.44 mmol) were used as reactants. Pale yellow solid, 0.12 g, 0.19 mmol, 88% yield. ^{1}H NMR (400 MHz, $CDCl_3$) δ 8.69 (d, J = 8.7 Hz, 2 H), 8.45 (d, J = 7.6 Hz, 2 H), 7.71 (t, J = 7.6 Hz, 2 H), 7.08–7.58 (m, 12 H), 7.01 (t, J = 8.5 Hz, 1 H), 6.37 (d, J = 8.3 Hz, 1 H), 6.04 (d, J = 8.3 Hz, 1 H), 4.63 (s, 2 H), 4.00 (q, J = 13.9 Hz, J = 6.95 Hz, 2 H), 2.56 (q, J = 13.9 Hz, J = 7.0 Hz, 2 H), 1.38 (t, J = 7.0 Hz, 3 H), 0.10 (t, J = 7.0 Hz, 3 H). ^{13}C NMR (100 MHz, $CDCl_3$) δ 195.91, 173.08, 154.66, 154.32, 134.06, 133.86, 131.38, 131.03, 130.26, 129.56, 129.41, 129.11, 128.51, 128.37, 128.07, 126.91, 126.66, 126.38, 122.68, 109.36, 104.54, 104.31, 104.08, 103.83, 64.33, 63.59, 62.16, 45.39, 45.11, 14.88, 14.79. HRMS (EI) calculated for $C_{43}H_{33}NO_5$: 643.2359; observed: 643.2372.

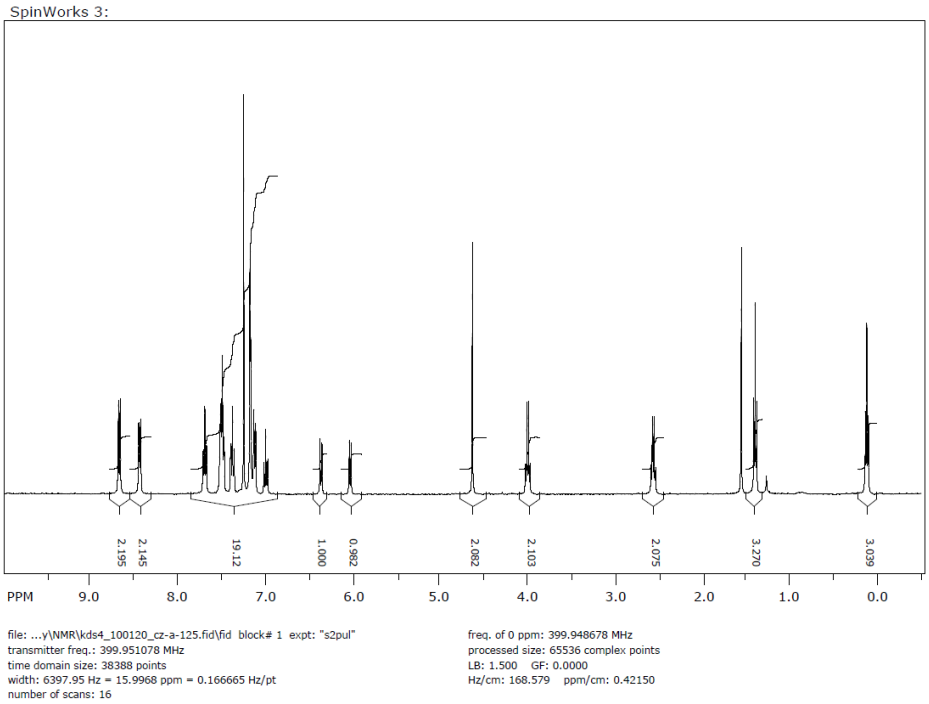

Figure 3.19: 400 MHz ^{1}H NMR spectrum of balance **1g** in $CDCl_3$.

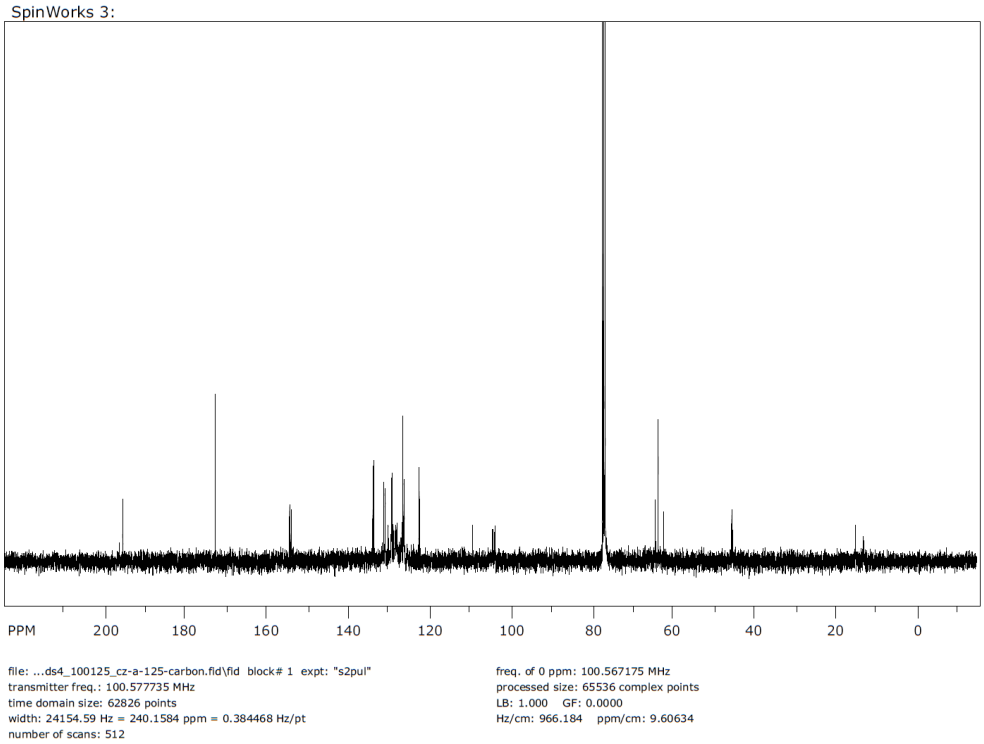

Figure 3.20: 100 MHz ^{13}C NMR spectrum of balance **1g** in $CDCl_3$.

Preparation of Balance **2a**

Anhydride **5c** (0.22 g, 0.59 mmol) and anisidine **4a** (0.11 g, 0.89 mmol) were used as reactants. Pale yellow solid, 0.23 g, 0.48 mmol, 82% yield. ^{1}H NMR (400 MHz, $CDCl_3$ δ 8.08 (m, 4 H major, 4 H minor), 6.78–7.60 (m, 13 H major, 14 H minor), 5.68 (dd, J = 7.7 Hz, J = 1.2 Hz, 1 H major), 4.31 (s, 2 H major), 4.28 (s, 2 H minor), 3.76 (s, 3 H major), 3.48 (s, 3 H minor). ^{13}C NMR (100 MHz, $CDCl_3$) δ 173.17, 154.77, 144.34, 136.46, 128.82, 128.58, 128.37, 128.00, 127.66, 127.39, 127.02, 120.96, 119.80, 90.53, 55.87, 55.65, 54.80, 54.72, 54.68. HRMS (EI) calculated for $C_{31}H_{23}NO_4$: 473.1627; observed: 473.1613.

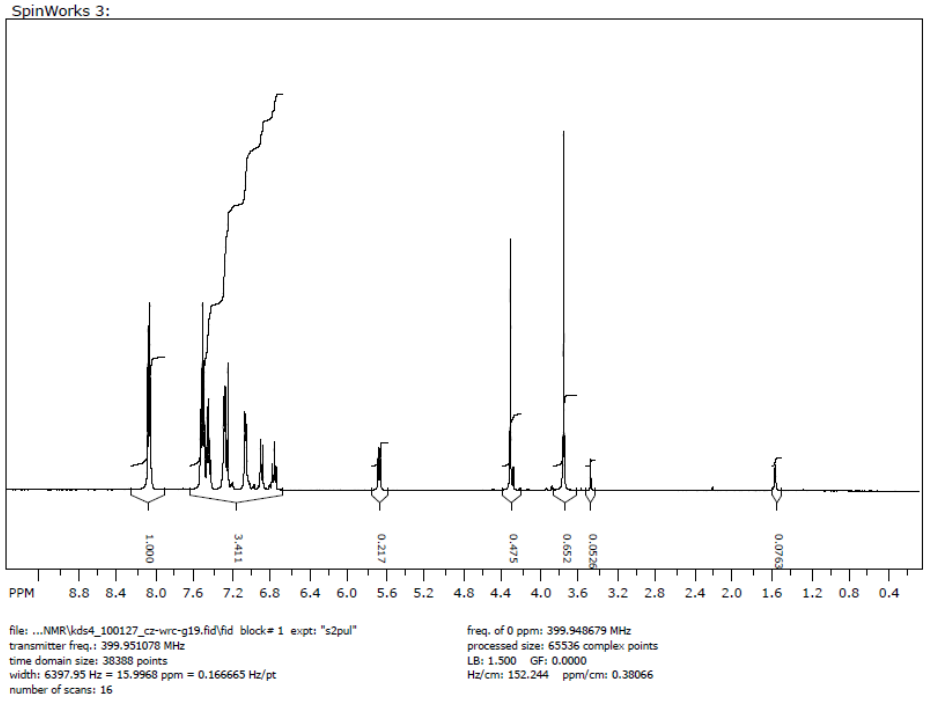

Figure 3.21: 400 MHz ^{1}H NMR spectrum of balance **2a** in $CDCl_3$.

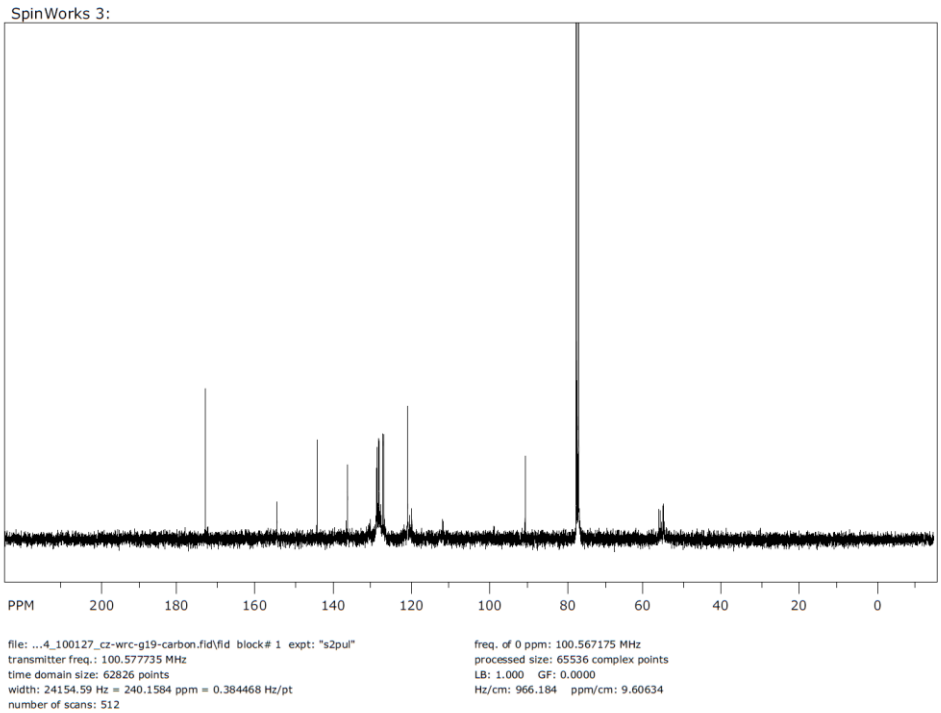

Figure 3.22: 100 MHz ^{13}C NMR spectrum of balance **2a** in $CDCl_3$.

Preparation of Balance **2b**

Anhydride **5c** (0.050 g, 0.13 mmol) and phenetidine **4b** (0.023 g, 0.16 mmol) were used as reactants. Pale yellow solid, 0.053 g, 0.11 mmol, 84% yield. ^{1}H NMR (300 MHz, $CDCl_3$) δ 8.08 (m, 4 H major, 4 H minor), 6.70–7.58 (m, 13 H major, 14 H minor), 5.69 (dd, J = 7.8 Hz, J = 1.7 Hz, 1 H major), 4.30 (s, 2 H major), 4.28 (s, 2 H minor), 4.00 (q, J = 14.0 Hz, J = 7.0 Hz, 2 H major), 3.91 (q, J = 14.0 Hz, J = 7.0 Hz, 2 H minor), 1.31 (t, J = 7.0 Hz, 3 H major), 1.12 (t, J = 7.0 Hz, 3 H minor). ^{13}C NMR (100 MHz, $CDCl_3$) δ 173.09, 154.12, 144.32, 136.50, 130.66, 128.62, 128.57, 128.46, 128.16, 128.12, 127.26, 127.18, 120.96, 120.44, 120.12, 112.83, 90.51, 64.16, 54.68, 14.65. HRMS (EI) calculated for $C_{32}H_{25}NO_4$: 487.1784; observed: 487.1778.

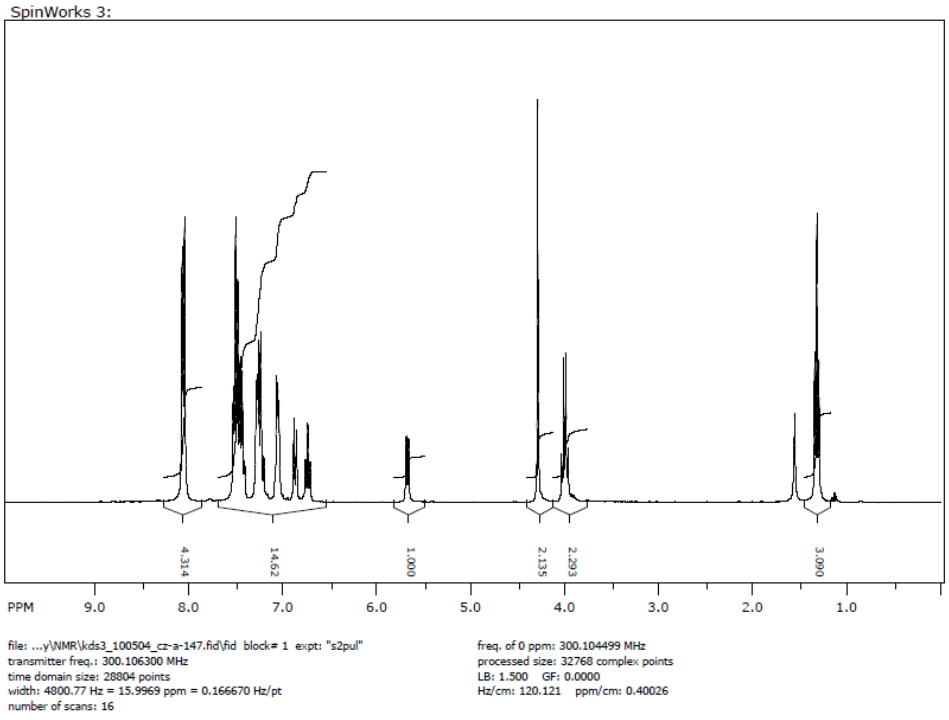

Figure 3.23: 400 MHz ^{1}H NMR spectrum of balance **2b** in $CDCl_3$.

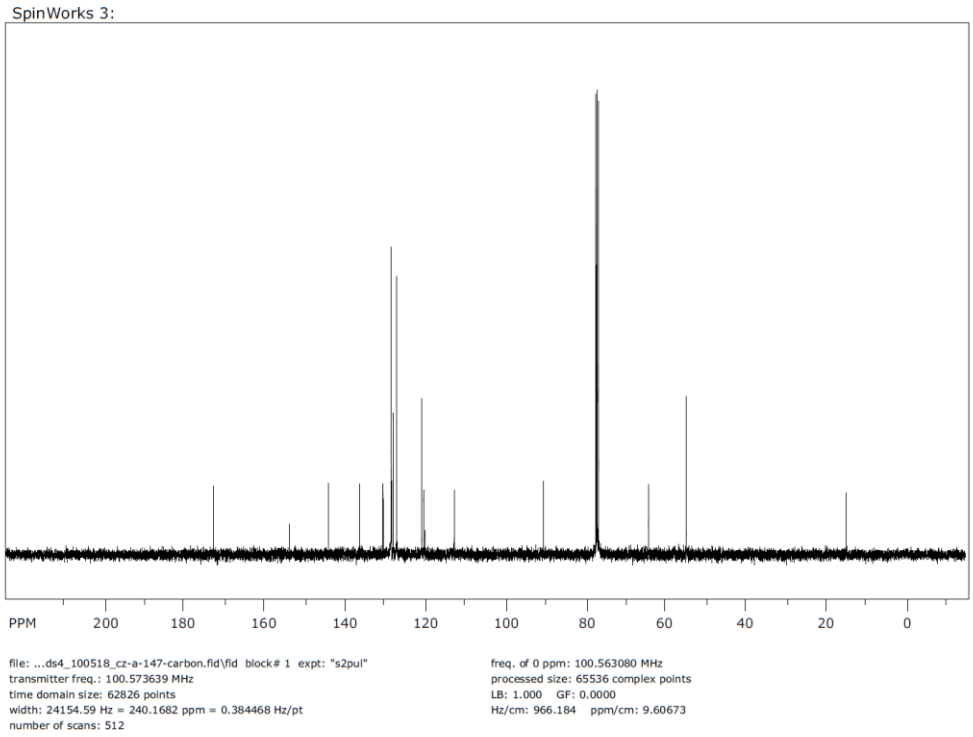

Figure 3.24: 100 MHz ^{13}C NMR spectrum of balance **2b** in $CDCl_3$.

Preparation of Balance **2c**

Anhydride **5c** (0.11 g, 0.30 mmol) and aniline **4f** (0.07 g, 0.45 mmol) were used as reactants. Yellow solid, 0.11 g, 0.23 mmol, 75% yield. ^{1}H NMR (400 MHz, $CDCl_3$) 8.07 (d, J = 7.5 Hz, 4 H), 6.96–7.59 (m, 11 H), 6.52 (d, J = 8.4 Hz, 1 H), 6.42 (d, J = 8.4 Hz, 1 H), 4.33 (s, 2 H), 3.74 (s, 3 H), 3.43 (s, 3 H). ^{13}C NMR (100 MHz, $CDCl_3$) δ 172.77, 156.18, 155.58, 144.60, 136.91, 128.77, 128.26, 127.78, 127.38, 127.00, 126.53, 124.64, 123.09, 120.88, 104.32, 104.06, 103.86, 103.58, 90.15, 56.20, 55.99, 55.74, 55.49, 54.76, 54.68. HRMS (EI) calculated for $C_{32}H_{25}NO_5$: 503.1733; observed: 503.1717.

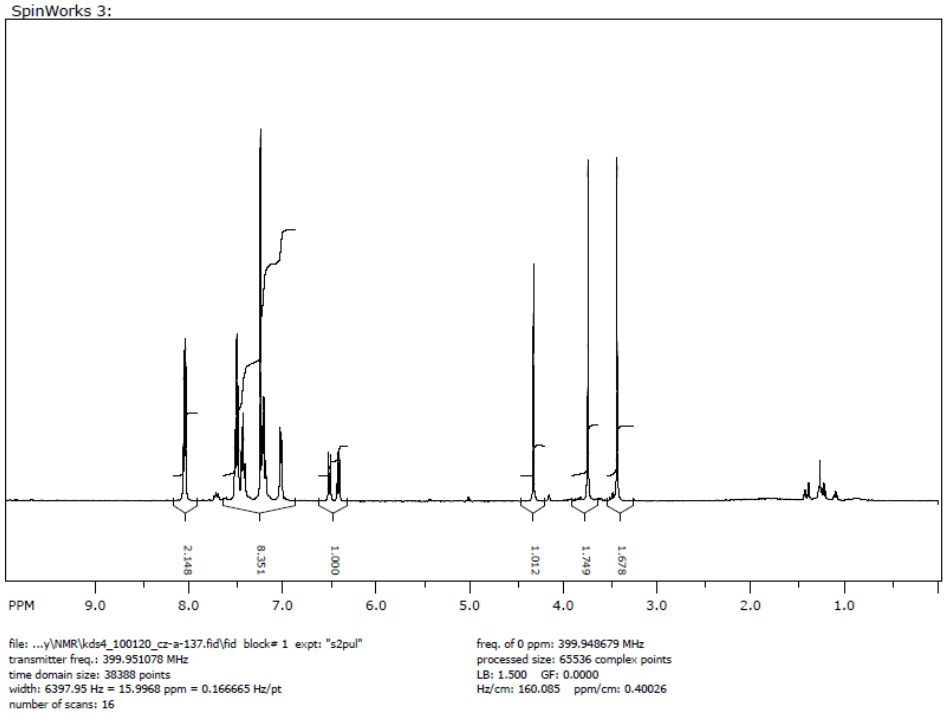

Figure 3.25: 400 MHz ^{1}H NMR spectrum of balance **2c** in $CDCl_3$.

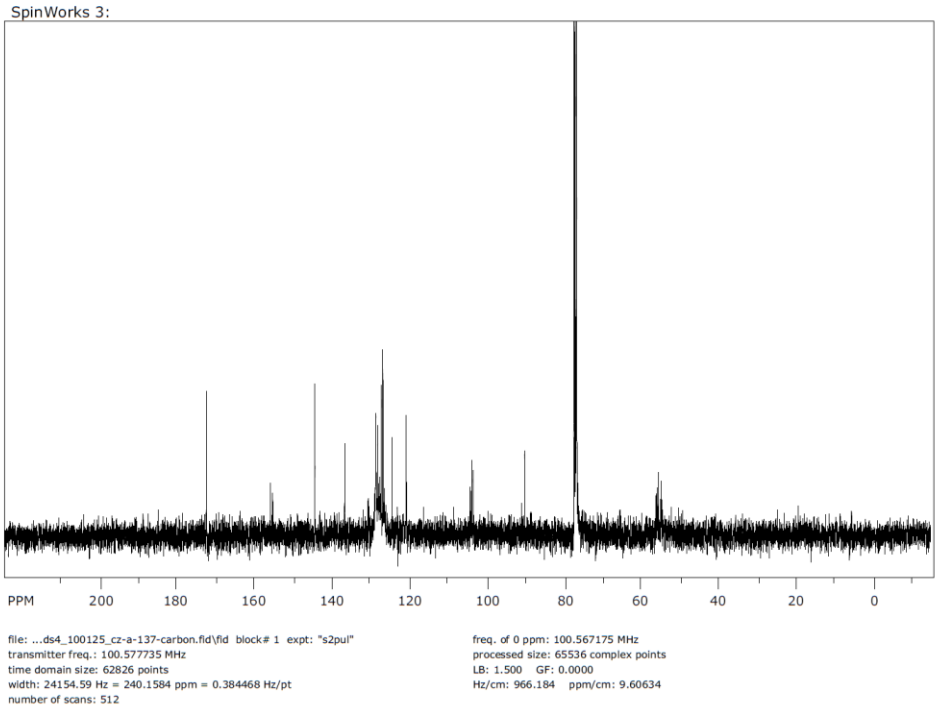

Figure 3.26: 100 MHz ^{13}C NMR spectrum of balance **2c** in $CDCl_3$.

Preparation of Balance **3a**

It is a known compound that has been reported.[95] Anhydride **5d** (0.11 g, 0.68 mmol) and *o*-anisidine (0.10 g, 0.81 mmol, 0.09 mL) were used as reactants. The crude product was heated in oven (130 °C) for 16 h to give the product as white crystal (0.12 g, 0.45 mmol, 66% yield). ^{1}H NMR (400 MHz, $CDCl_3$) δ 7.36 (dt, J = 7.8 Hz, J = 1.4 Hz, 1 H major, 1 H minor), 6.86–7.06 (m, 3 H major, 3 H minor), 6.28 (s, 2 H major), 6.21 (s, 2 H minor), 3.78 (s, 3 H major), 3.77(s, 3 H minor), 3.37–3.54 (m, 4 H major, 4 H minor), 1.54–1.82 (m, 2 H major, 2 H minor).

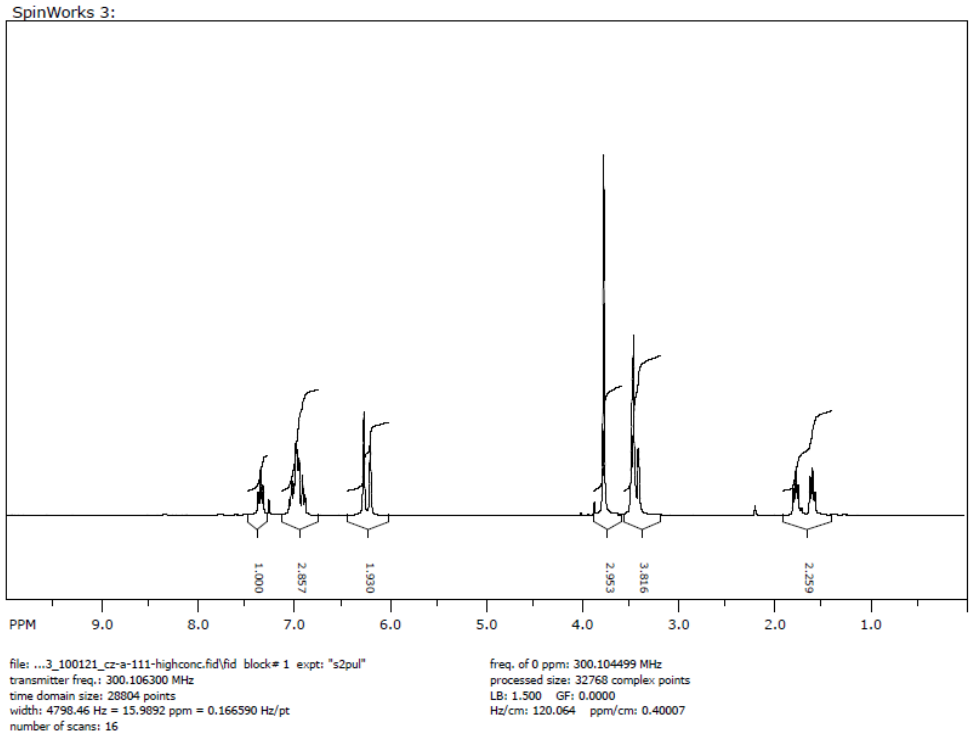

Figure 3.27: 300 MHz ^{1}H NMR spectrum of balance **3a** in $CDCl_3$.

3.5.2 Van't Hoff Plots

The van't Hoff plots of balances **1–3** were plotted based on the results from variable temperature ^{1}H NMR. The full spectra were acquired at 5°C intervals between 25°C–55°C, and the *folded*/*unfolded* ratios were obtained via spectral deconvolution of the succinimide alpha singlets (balance **1a**, **1b**, **2a**, **2b** in acetone-d_6), the methyl singlets or the CH2 quartet on the arm group (balance **1a**, **1b**, **2a**, **2b** in $CDCl_3$ because of the overlapped succinimide peaks), or the triplet for ethene protons (of balance **3a**). The *folded*/*unfolded* ratios were listed as Table 3.3–Table 3.5 and Table 3.7–Table 3.9, and the van't Hoff plots were as Figure 3.27 and 3.28.

Table 3.3: Spectral deconvolution integrations for variable temperature ^{1}H NMR of balance **1a** and **1b** in $CDCl_3$.

		balance **1a**			balance **1b**		
T (°C)	1/Temp (K^{-1})	Unfolded	Folded	ln(F/U)	Unfolded	Folded	ln(F/U)
25	0.003356	167.34	78.31	–0.75935	659.55	140.23	–1.54827
30	0.003300	310.15	144.32	–0.76502	637.06	134.26	–1.55709
35	0.003247	215.89	100.05	–0.76910	523.06	109.02	–1.56817
40	0.003195	216.3	100.75	–0.76402	565.21	117.62	–1.56974
45	0.003145	204.21	94.68	–0.76865	550.67	113.78	–1.57687
50	0.003096	236.82	109.41	–0.77220	540.52	111.55	–1.57806
55	0.003049	221.4	101.85	–0.77647	557.02	116.79	–1.56222

Table 3.4: Spectral deconvolution integrations for variable temperature ^{1}H NMR of balance **2a** and **2b** in $CDCl_3$.

		balance **2a**			balance **2b**		
T (°C)	1/Temp (K^{-1})	Unfolded	Folded	ln(F/U)	Unfolded	Folded	ln(F/U)
25	0.003356	0.915	0.085	–2.37627	0.954	0.034	–3.33430
30	0.003300	0.911	0.089	–2.32591	0.970	0.030	–3.47610
35	0.003247	0.910	0.090	–2.31363	0.965	0.031	–3.43814
40	0.003195	0.907	0.093	–2.27754	0.958	0.037	–3.25393
45	0.003145	0.906	0.094	–2.26574	0.956	0.035	–3.30741
50	0.003096	0.906	0.094	–2.26574	0.956	0.033	–3.36625
55	0.003049	0.906	0.094	–2.26574	0.952	0.036	–3.27505

Table 3.5: Spectral deconvolution integrations for variable temperature ^{1}H NMR of balance **3a** in $CDCl_3$.

		balance **3a**		
T (°C)	1/Temp (K^{-1})	Unfolded	Folded	ln(F/U)
25	0.003356	0.553	0.447	–0.212799
30	0.003300	0.559	0.441	–0.237105
35	0.003247	0.56	0.44	–0.241162
40	0.003195	0.561	0.439	–0.245221
45	0.003145	0.562	0.438	–0.249283
50	0.003096	0.565	0.435	–0.26148
55	0.003049	0.565	0.435	–0.26148

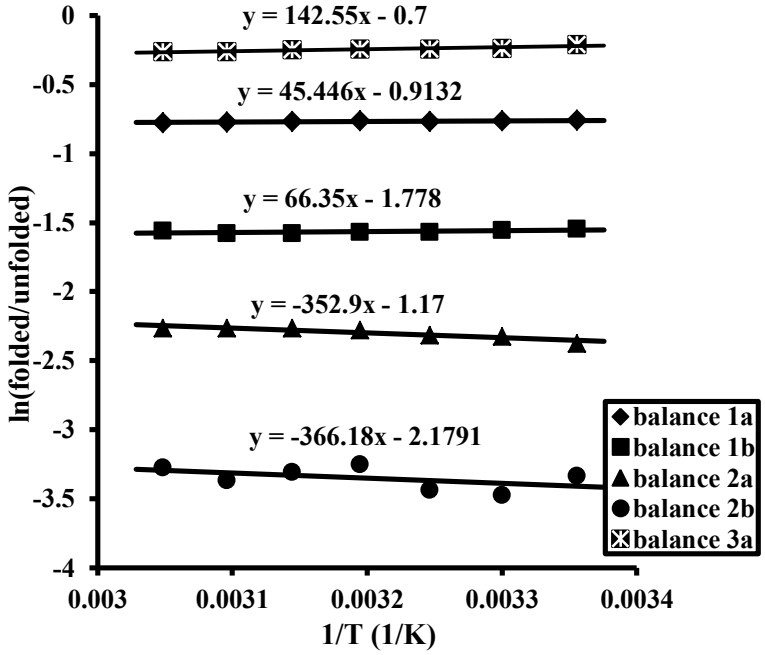

Figure 3.28: Van't Hoff plot of balances **1a**, **1b**, **2a**, **2b**, and **3a** in $CDCl_3$ based on the information in Table 3.3, Table 3.4, and Table 3.5.

Based on the equation in Chapter 2, the calculation of entropy/enthalpy values errors of balance **1a**, **1b**, **2a**, **2b**, and **3a** by VT NMR experiments in $CDCl_3$ are listed in Table 3.6. The errors for slopes and intercepts are measured by the regression add-in in excel.

Table 3.6: Calculation of ΔG, ΔH, ΔS, and $-T\Delta S$ and their errors of balance **1a**, **1b**, **2a**, **2b**, and **3a** by VT NMR experiments in $CDCl_3$.

balance	Slope	Intercept	ΔG (kcal/mol)	ΔH (kcal/mol)	ΔS (kcal/mol·K)	$-T\Delta S$@25°C (kcal/mol)
1a	45.5 ± 10.3	–0.913 ± 0.033	0.45 ± 0.04	–0.09 ± 0.02	–0.0018 ± 6.6×10^{-05}	0.54 ± 0.02
1b	116 ± 14	–1.94 ± 0.05	0.92 ± 0.06	–0.23 ± 0.03	–0.0039 ± 9.3×10^{-05}	1.20 ± 0.03
2a	–353 ± 65	–1.17 ± 0.21	1.4 ± 0.3	0.70 ± 0.13	–0.0023 ± 0.0004	0.69 ± 0.12
2b	–366 ± 291	–2.18 ± 0.93	2.0 ± 1.1	0.73 ± 0.58	–0.0043 ± 0.0019	1.30 ± 0.55
3a	–145 ± 26	0.200 ± 0.082	0.17 ± 0.10	0.29 ± 0.05	0.00040 ± 0.00016	–0.12 ± 0.05

Same analysis was done for the data measured in acetone-d_6. Although was not discussed in this chapter, the results lead to the same conclusion as date in $CDCl_3$

Table 3.7: Spectral deconvolution integrations for variable temperature ^{1}H NMR of balance **1a** and **1b** in acetone-d_6.

		balance **1a**			balance **1b**		
T (°C)	1/Temp (K^{-1})	Unfolded	Folded	ln(F/U)	Unfolded	Folded	ln(F/U)
25	0.003356	134.14	105.58	–0.23942	187.69	71.39	–0.9666
30	0.003300	152.4	116.98	–0.26451	225.04	75.56	–1.0913
35	0.003247	108.08	81.19	–0.28608	192.84	70.09	–1.0121
40	0.003195	161.14	120.54	–0.29029	242.65	83.63	–1.0652
45	0.003145	136.47	104.9	–0.26310	200.59	70.13	–1.0509
50	0.003096	155.97	112.2	–0.32938	221.21	74.83	–1.0839
55	0.003049	192.98	135.22	–0.35568	220.86	73.17	–1.1047

Table 3.8: Spectral deconvolution integrations for variable temperature ^{1}H NMR of balance **2a** and **2b** in acetone-d_6.

		balance **2a**			balance **2b**		
T (°C)	1/Temp (K^{-1})	Unfolded	Folded	ln(F/U)	Unfolded	Folded	ln(F/U)
25	0.003356	179.05	33.55	–1.6746	165.37	11.00	–2.710
30	0.003300	172.07	32.80	–1.6575	174.31	11.82	–2.691
35	0.003247	169.91	32.44	–1.6559	184.98	12.33	–2.708
40	0.003195	190.93	37.11	–1.6380	209.67	14.87	–2.646
45	0.003145	205.85	40.46	–1.6268	147.61	10.35	–2.658
50	0.003096	183.72	36.22	–1.6238	156.60	11.16	–2.641
55	0.003049	188.30	37.54	–1.6126	153.25	11.18	–2.618

Table 3.9: Spectral deconvolution integrations for variable temperature ^{1}H NMR of balance **3a** in acetone-d_6.

		balance **3a**		
T (°C)	1/Temp (K^{-1})	Unfolded	Folded	ln(F/U)
25	0.003356	0.54	0.46	–0.160343
30	0.003300	0.539	0.46	–0.158489
35	0.003247	0.545	0.456	–0.178293
40	0.003195	0.541	0.459	–0.164369
45	0.003145	0.543	0.456	–0.174617
50	0.003096	0.54	0.46	–0.160343
55	0.003049	0.54	0.46	–0.160343

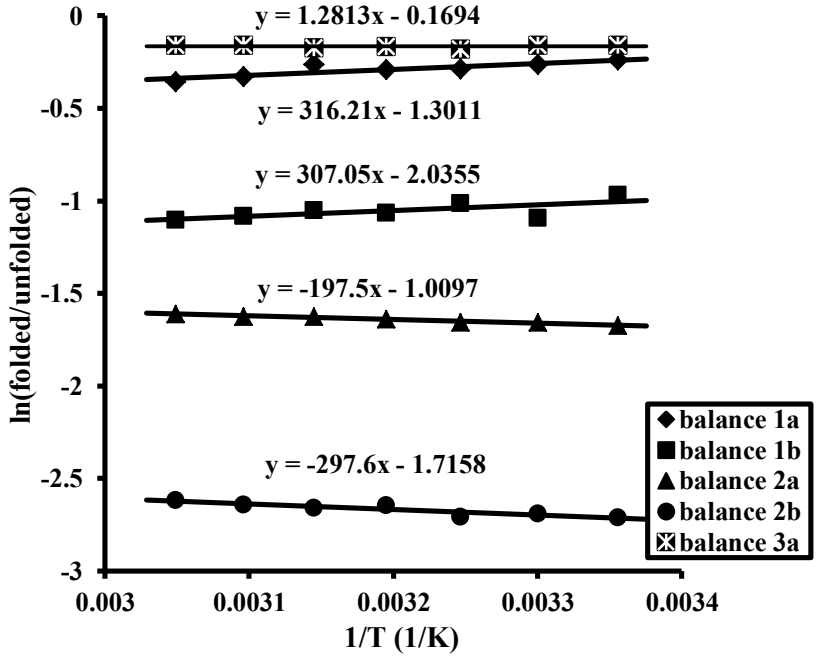

Figure 3.29: Van't Hoff plot of balances **1a**, **1b**, **2a**, **2b**, and **3a** in acetone-d_6 based on the information in Table 3.7, Table 3.8 and Table 3.9.

Table 3.10: Calculation of ΔG, ΔH, ΔS, and $-T\Delta S$ and their errors for balance **1a**, **1b**, **2a**, **2b**, and **3a** by VT NMR experiments in acetone-d_6.

balance	Slope	Intercept	ΔG (kcal/mol)	ΔH (kcal/mol)	ΔS (kcal/mol·K)	$-T\Delta S$@25°C (kcal/mol)
1a	316 ± 82	–1.30 ± 0.26	0.14 ± 0.32	–0.63 ± 0.16	–0.0026 ± 0.0005	0.77 ± 0.16
1b	307 ± 143	–2.04 ± 0.46	0.60 ± 0.56	–0.61 ± 0.28	–0.0040 ± 0.0009	1.20 ± 0.27
2a	–198 ± 14	–1.01 ± 0.05	0.99 ± 0.06	0.39 ± 0.03	–0.0020 ± 9.1×10^{-05}	0.60 ± 0.03
2b	–298 ± 58	–1.72 ± 0.19	1.6 ± 0.2	0.59 ± 0.12	–0.0034 ± 0.0004	1.02 ± 0.11
3a	1.28 ± 32	–0.169 ± 0.103	0.10 ± 0.12	–0.003 ± 0.064	–0.00034 ± 0.0002	0.10 ± 0.06

CHAPTER 4

MOLECULAR BALANCES FOR MEASURING MULTIPLE ALIPHATIC CH–π INTERACTIONS

In previous Chapter 3, our balances system was proved to be sufficiently pre-organized and sensitive to measure aliphatic CH–π interactions. However, because of the existence of lone pair–π interaction caused by the oxygen linker, those balances could only be used to look at single CH–π interaction, even for large alkyl groups with multiple CHs. In fact, in most CH–π interactions, the alkyl groups form multiple interactions with the aromatic surface.[96] The cooperativity of multiple CH–π interactions is commonly observed in solid-state structures,[97,98] and has been shown to enhance the stability of the polymers complexed inside of nano-channels[99,100] and stabilizing the interactions between sugars and aromatic side chains in enzyme active sites.[101,102] Thus, study about this property will be important in the design of supramolecular structures, polymer nano-composites and ligand targeted toward specific receptors. In this chapter, a new series of molecular balances that are able to form more than one intramolecular CH–π interactions were synthesized to study the coopertivity of multiple CH–π interactions.

4.1 DESIGNS OF THE STRUCTURES

The new series of balances (Figure 4.1) shared the same rigid bicyclic *N*–arylimide framework as our previous CH–π balances. To incorporate larger alkyl groups and form multiple CH–π interactions, the oxygen linkers in the former structures (balances **7e–10e**) was removed, allowing the alkyl groups connected directly to the phenyl rotor. Other than making shortened arms, a side benefit of the new design for

taking out the oxygen linker is that, it will eliminate the repulsive O–π interaction and can lead to higher *folded*/*unfolded* ratios. This result is supported by the conclusion of a recent computational study.[103]

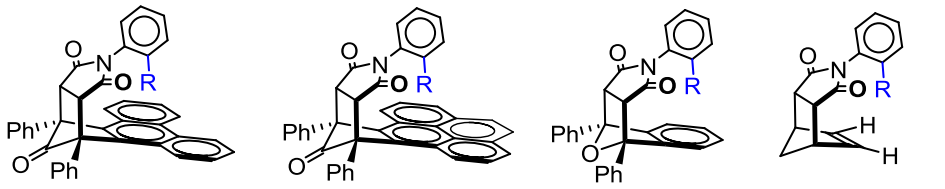

7a (R = Me)
7b (R = Et)
7c (R = *n*Pr)
7d (R = *i*Pr)
7e (R = OMe)

8a (R = Me)
8b (R = Et)
8c (R = *n*Pr)
8d (R = *i*Pr)
8e (R = OMe)

9a (R = Me)
9b (R = Et)
9c (R = *n*Pr)
9d (R = *i*Pr)
9e (R = OMe)

10a (R = Me)
10b (R = Et)
10c (R = *n*Pr)
10d (R = *i*Pr)
10e (R = OMe)

Figure 4.1: Structures of balances **7**–**10** designed for measuring multiple CH–π interactions.

Balances **7** and **8** have large phenanthrene or pyrene aromatic shelves were expected to form cooperative CH–π interaction as shown in Figure 4.2. Balance **9** are control balances with only one benzene ring on the shelf which can only form interaction with the first carbon on the alkyl group, and balances **10** are control balances without aromatic shelf. Balances **7e**–**10e** with methoxy arm were also used for comparison. Balance **7a** has been previously reported in literature for the study of CH–π interaction.[94,104] Balances **7e**, **9e**, and **10e** indicate the same structures as balances **1a**, **2a** and **3a** in Chapter 3.

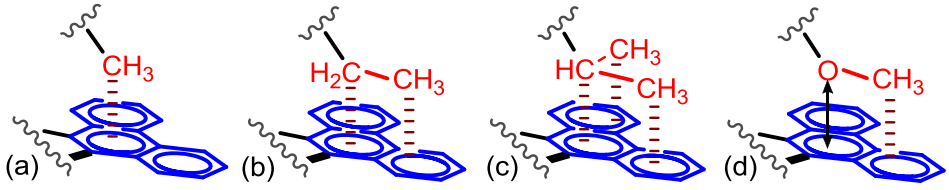

Figure 4.2: Illustration of (a) single CH–π interaction in balance **7a**, (b, c) multiple CH–π interactions in balance **7b** and **7d**, and (d) the long pair–π interaction in previous balance with oxygen linker.

4.2 SOLID-STATE STRUCTURES

The formation of multiple CH–π interactions in the *folded* conformers of the new balances were first verified and characterized in the solid-state (Figure 4.3). Crystals of the methyl balances **7a** and **8a**, ethyl balance **7b**, and *i*-Pr balance **7d** were obtained in their *folded* conformations. This was the first indication that the new balances could form more attractive CH–π interactions than previous series of CH–π balances which always crystalized as *unfolded* conformation. Control balance **9a** and **10a** crystalized in both *folded* and *unfolded* conformations.

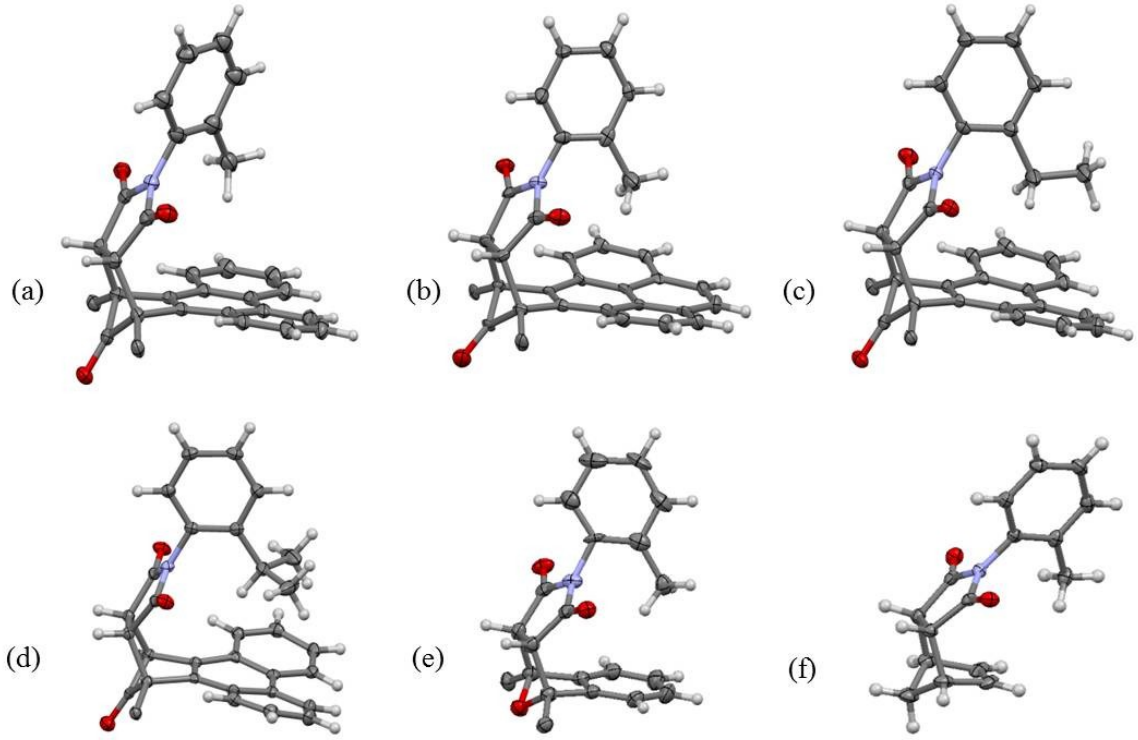

Figure 4.3: X-ray structures of balances (a) **7a**, (b) **8a**, (c) **7b**, (d) **7d**, (e) **9a** and (f) **10a** that obtain the *folded* conformation. The solvent molecules and the bridge-head phenyl groups for each balance (except **10a** with only proton on the bridge-head) are hidden for viewing clarity.

4.2.1 Geometries of CH_3–π Interactions

All of the solid-state structures obtained for methyl balances **7a**, **8a**, and **9a**

showed expected but slightly different intramolecular CH_3–π interactions. Their proton-to-aromatic plane distances (*d*) were all within the typical range of CH–π interactions (2.5–3.0 Å).[31] Balance **7a** forms one clear CH–π interaction with a proton-to-plane distance of 2.571 Å, and balance **8a** showed a similar interaction with slightly longer distance (d = 2.657 Å). The crystal structure of balance **9a** showed three set of *folded*/*unfolded* conformers. One of the three *folded* conformations showed one single CH–π interaction between methyl and the benzene ring (d = 2.571 Å), while the other two forms two CH–π interactions at the same time (d = 2.794 Å, 2.863 Å and d = 2.691 Å, 3.029 Å). The double-interaction geometry was only presented (and preferred) in balance **9a**, probably because the different back-side bridge atom (oxygen) on the framework of balance **9** leads to a more restricted environment compared with balances **7** and **8**, and the conformation with two protons pointing down to the arene shelf causes less sterics. The two types of CH_3–π interactions have similar stability because they showed up together in balance **9a**, but in a less restrict environment such as balance **7**, the single-interaction geometry is more stable because of a more proper proton-to-arene distance and a moderate sterics.

4.2.2 Geometries of Multiple CH–π Interactions

The solid-state structures of balances **7b** and **7d** showed expected multiple intramolecular CH–π interactions. In ethyl balance **7b**, the interaction between the first carbon and the central ring on arene shelf was shown as the double-interaction geometry (d = 2.717 Å, 2.864 Å), probably to adjust the extra steric caused by the additional CH_3 compared with **7a**. Because of the limitation of the shorter aromatic shelf, this is the only good CH–π interaction that can be formed in balance **7b**. The CH_3 of the ethyl group is centered over the bay region of the phenanthrene shelf (between the two outer rings),

forming an additional minor and weaker interaction. Although haven't obtained the crystal, it is possible that the *n*-Pr balance **7c** have similar situation with balance **7b** that with only one good interaction by the first carbon, and the second or third interaction are weak or non-exist. In *i*-Pr balance **7d**, all three carbons were found to form CH–π interactions in the *folded* structure, and the proton-to-plane distances were 2.785 Å, 2.594 Å (for two CH_3 groups) and 2.643 Å (for CH).

It is important to note that the solid-state structure only provides a snap-shot of one stable conformation of the alkyl arm. Modeling for the balances with longer alkyl groups predicts that the arm would sweep back and forth across the arene shelf in the *folded* conformer. Due to this uncertainty and the similar stability of the two types of interactions formed by the first carbon on alkyl group, the numbers of carbons that possibly form CH–π interaction were used for analysis and comparison, although some make different CH–π interaction than others.

4.2.3 Control Balances

No interaction was observed in control balance **10a** with no aromatic shelf, and both *folded* and *unfolded* conformers were found in its crystal structure. The distances between the methyl and double bond on the shelf is too long for any attractive or repulsive interaction. It also helps to make sure that the differences in dipole and solvation of the *folded* and *unfolded* conformers is not biasing the results.

4.3 MEASURING CH–Π INTERACTIONS IN SOLUTION

Next, the different intramolecular CH–π interactions were characterized and quantitatively measured in $CDCl_3$ solution. By analyzing the ^1H NMR spectrums, we were able to compare the strength of CH–π interactions formed in each of the balances (Table 4.1). As expected, due to the absence of the repulsive long pair–π interaction in

the new series, each of these balances was more *folded* than corresponding previous balance with oxygen linkers. This indicates that the replacement of the oxygen with CH_2 successfully replaced the repulsive lone pair–π interaction with an attractive interaction.

Table 4.1: The folding energies (ΔG) of molecular balances **7–10** in $CDCl_3$ at 25 °C.

Balance	**7**	**8**	**9**	**10**
shelf	phenanthrene	pyrene	benzene	ethylene
a (R = Me)	–0.13	–0.23	+0.84	+0.02
b (R = Et)	–0.27	–0.51	+0.84	+0.07
c (R = *n*-Pr)	+0.36	+0.07	+0.86	+0.02
d (R = *i*-Pr)	–0.91	–1.10	+0.89	–0.11
e (R = OMe)	+0.45	+0.25	+1.40	+0.18

4.3.1 Control Balances

The ΔG values are close to zero for control balances **10** without arene shelf, which proves that no interaction was formed and balances **10** are reasonable controls for the other balances. Balance **10d** showed a slightly lower folding energy because weak interaction might exist between the –*i*Pr group and the double bond, and balance **10e** showed a minor repulsion because of the lone pair on the oxygen linker, but in general, their folding energies were still close to each other.

Balances **9a–9d** with benzene shelf showed almost the same folding energy, which matched our expectation that all of these balances form only a single CH–π interaction. However, although being more *folded* than balance **9e** with oxygen linker, all these balances preferred the *unfolded* conformer. This suggests that sterics still exist between the first carbon on the alkyl group and the aromatic shelf in balances **9**. The sterics still possibly exist in balances **7** and **8** although they were more *folded* in its solution, but the repulsion should be weaker than that in **9** because with a different bridge group (C=O), their frameworks allow a wider space for the intramolecular interactions.

4.3.2 Strength of Multiple CH–π interactions

In the methyl, ethyl or *i*-propyl balances **7** and **8**, the ΔG values were all negative, demonstrating that the CH–π interactions were attractive. The interactions in balances **8** appeared to be stronger than that in balances **7**, because the extended arene shelf strength the dispersion effect. Generally, except for the *n*-propyl balances, the balances that can form more CH–π interactions showed lower folding energies, although the energies did not change linearly with the number of interactions. The folding energies for both balance series showed similar trends: **d** (–*i*Pr) < **b** (–Et) < **a** (–Me) < **c** (–*n*Pr).

Compared with balances **7a** and **8a** that formed single CH–π interaction, balances **7b** and **8b** showed the expected doubled ΔG values, while balances **7d** and **8d** showed a much lower folding energies that were more than three times of that of balances **7a** and **8a**. It is possible that due to the sterics exists between methyl group and arene shelf in balances **7a** and **7b**, the measured ΔG value turned out to be higher than the actually interaction. Also, in balances **7d** and **8d** where all three carbons on –*i*Pr group are able to form CH–π interactions with the aromatic surface, the cooperativity of the interactions may lead to a better geometric positioning, and thus strengthened the *folded* conformation more than three single interactions.

The balances **7c** and **8c** with linear –*n*Pr group were apparent exceptions among all balances as they favored the *unfolded* conformer and showed the highest folding energies. It is probably because while forming similar interactions as the ethyl balances due to the limited aromatic area, the alkyl group has less freedom to rotate and thus leads to a larger conformational entropy for the *n*-propyl group and thus increases the sterics and decreases the preference of their *folded* conformer.

4.4 ENTROPIC AND ENTHALPIC VALUES

To explain the discrepancies above in the folding trends, we hypothesized that they are due to the different entropic penalties imposed by pinning each alkyl group against the arene shelves. In this case, while a larger alkyl group forms more CH–π interactions, it also needs to pay a higher entropic penalty due to the loss of rotational freedom for each C–C single bond in the confined environment of the *folded* conformer.[105-108] To test this hypothesis, the enthalpy (ΔH) and entropy ($-T\Delta S$) values of CH–π interactions in balances **7–10** were measured using van't Hoff analysis (Table 4.2) of data from variable temperature ^{1}H NMR. The ΔG values from the analyses match up well with those from the single point r.t. measurement in Table 4.1.

Table 4.2: Comparison of ΔG, ΔH, and $-T\Delta S$ for balances **7–10** in $CDCl_3$ at 25 °C.

Balance	Arm	ΔG (kcal/mol)	ΔH (kcal/mol)	$-T\Delta S$ (kcal/mol)
7a	Me	–0.13 ± 0.06	–0.66 ± 0.03	0.53 ± 0.03
7b	Et	–0.27 ± 0.05	–0.96 ± 0.03	0.69 ± 0.02
7c	*n*Pr	0.36 ± 0.17	–0.34 ± 0.08	0.70 ± 0.09
7d	*i*Pr	–0.93 ± 0.59	–4.55 ± 0.30	3.62 ± 0.29
8a	Me	–0.16 ± 0.08	–0.71 ± 0.04	0.54 ± 0.04
8b	Et	–0.42 ± 0.19	–0.98 ± 0.10	0.56 ± 0.09
8c	*n*Pr	0.06 ± 0.30	–0.57 ± 0.15	0.63 ± 0.14
8d	*i*Pr	–1.09 ± 0.79	–2.74 ± 0.40	1.65 ± 0.38
9a	Me	0.84 ± 0.12	0.40 ± 0.06	0.44 ± 0.06
9b	Et	0.84 ± 0.06	0.46 ± 0.03	0.38 ± 0.03
9c	*n*Pr	0.86 ± 0.17	0.80 ± 0.09	0.06 ± 0.08
9d	*i*Pr	0.89 ± 0.08	0.67 ± 0.04	0.22 ± 0.04
10a	Me	0.02 ± 0.12	–0.62 ± 0.06	0.64 ± 0.06
10b	Et	0.08 ± 0.21	–0.47 ± 0.11	0.55 ± 0.10
10c	*n*-Pr	0.02 ± 0.07	–0.56 ± 0.04	0.59 ± 0.03
10d	*i*-Pr	–0.11 ± 0.45	–2.60 ± 0.23	2.49 ± 0.22

4.4.1 Comparison between Enthalpy Values

The observed enthalpy components ΔH for **7a–7d** followed the same trend as the folding energy: **7c** (–*n*Pr) > **7a** (–Me) > **7b** (–Et) > **7d** (–*i*Pr). Still, the enthalpy values did not show strict additivity: the ΔH of **7b** was less than two times of the ΔH of **7a**,

while balance **7d** showed an enthalpy that was more than three times of that of **7a**. It is possible that due to the sterics exists between methyl group and arene shelf in balance **7a**, the measured ΔH value turned out to be higher than that of the actual interaction. Without the repulsion, the ΔH value for a single CH–π interaction may be –1.5 kcal/mol or lower, based on the ΔH of balance **7d** which contains three CH–π interactions. The *n*-propyl balance **7c** still showed the lowest enthalpy. The balance **7d** with branched propyl group was much more stabilized than balance **7c** with linear propyl group, probably because the cooperativity of the interactions leads to a better geometric positioning.

4.4.2 Entropy-Enthalpy Compensation

The entropy term ($-T\Delta S$) of balances **7a–7d** showed generally similar but opposite sign as the ΔH values. One explanation is that larger alkyl group will lead to larger sterics in restricted environment. Similar trend of conformational entropy of Me, Et, *n*Pr and *i*Pr groups, from both calculation and experiments, have been observed in the conformational exchange between axial and equatorial conformers of alkyl-substituted cyclohexanes.[109-111]

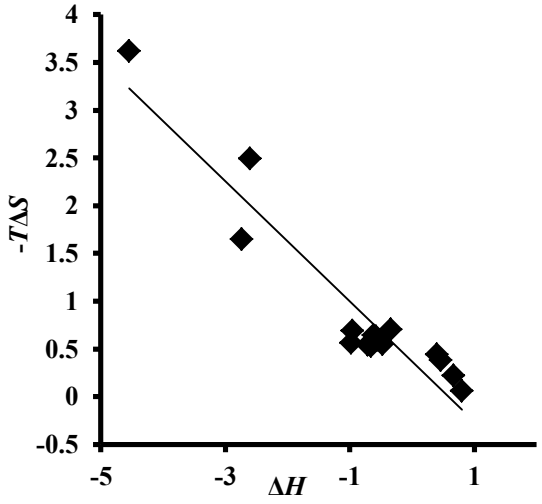

Figure 4.4: Polts showing the compensation between ΔH and $-T\Delta S$ values of balances **7–10**.

This can also be attributed to the increasing conformational restriction and entropic penalty of the balance system with higher enthalpic complexation energies, which is also known as the enthalpy/entropy compensation effect (Figure 4.4).[106,110] For example in balance **7d**, all three carbons on –*i*Pr group are able to form CH–π interactions with the phenanthrene surface, so only one rotamer for the –*i*Pr is able to be formed in the *folded* **7d** due to the highly restricted rotation of the C_{aryl}–C_{alkyl} bond. This leads to the highest conformational entropy while showing the lowest ΔH value among balance **7**.

4.5 SOLVENT EFFECTS

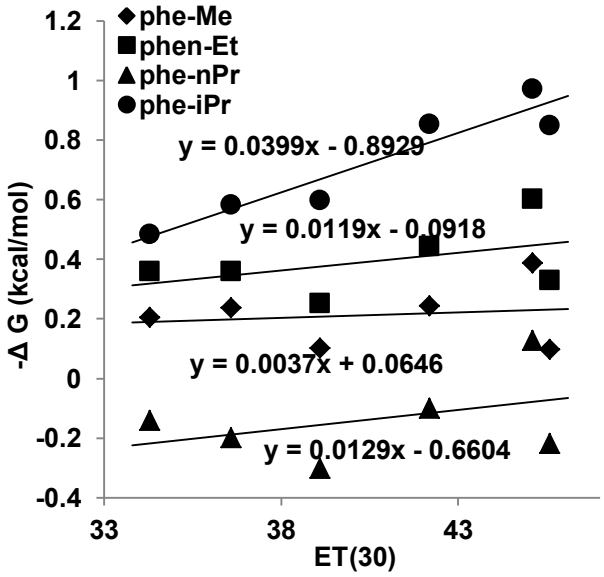

Figure 4.5: Solvent trends for balances **7a–7d** in a series of solvents with different $E_T(30)$ values. The solvents from left to right are: benzene-d_6, bromobenzene-d_5, $CDCl_3$, acetone-d_6, DMSO-d_6, and acetonitrile-d_3.

The solvent effect on multiple CH–π interaction was also studied. Same as previous balances, these compounds showed excellent solubility in a series of solvents with different polarity. Plots of folding energies vs. $E_T(30)$ of balances **7a–7d** in different solvents were shown in Figure 4.5. Different from result of previous balances

with oxygen linker, there was barely any trend for each of the balances. The strength of CH–π interaction did not change according to the solvent polarity (except for balance **7d** with *i*-Pr group). This suggests that maybe the solvent effect on CH–π interactions are too weak that it only shows up when multiple interactions were formed. It is also possible that the trend observed in previous studies were caused solely by the solvophobic effect of the lone pair–π interactions.

4.6 CONCLUSION

In conclusion, a series of molecular balances were synthesized to study the multiple CH–π interactions. By removing the oxygen linker and eliminate the repulsive O–π interaction, we successfully extended our study to the interactions formed by a larger range of alkyl groups. The geometries of several interactions were characterized in their solid-state, and their folding energies ($-\Delta G$) were compared. It turned out that the CH–π interactions can show certain additivity, but the total strength of the multiple interactions cannot be predicted by simply multiple the strength of one single interaction. The entropic penalty comes from the conformational restriction may be very important on determining the total strength of interactions, leading to the different behaviors of large alkyl groups such as –*n*Pr and –*i*Pr when forming interactions.

4.6 EXPERIMENTAL SECTION

NMR spectra were recorded on Varian 300 MHz and 400 MHz spectrometers. Chemical shifts are reported in ppm (δ) referenced to TMS. All chemicals were purchased from commercial suppliers and used as received unless otherwise specified. Flash chromatography was carried out using silica gel from Sorbent Technologies (60 Å, 200–400 mesh). Thin layer chromatography (TLC) was performed using pre-coated TLC plates (Merck pre-coated 0.25 mm silica gel 60 F254 plates).

4.6.1 Synthesis

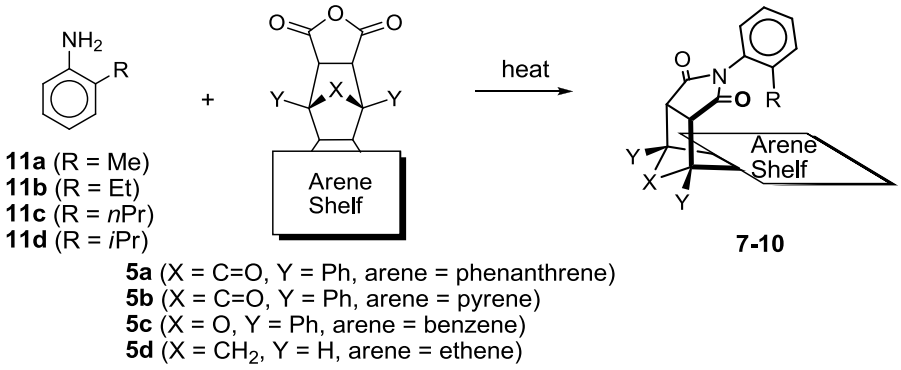

Figure 4.6: Overview of synthesis of balances **7–10** via condensation between aniline **11** and anhydride **5**.

The general synthetic route for balances **7–10** (Figure 4.1) was as shown in Figure 4.6. All balances were synthesized via the condensation between anilines **11** and anhydrides **5**. Anilines **11** are all commercially available, and the synthetic routes of anhydrides **5a**, **5c** and **5d** and balances **7e**, **9e** and **10e** (balances **1a**, **2a** and **3a** in Chapter 3)have been described in Chapter 3. The detailed synthesis for the rest of these compounds and the characterization data are shown as follows.

Preparation of pyrene-4, 5-dione

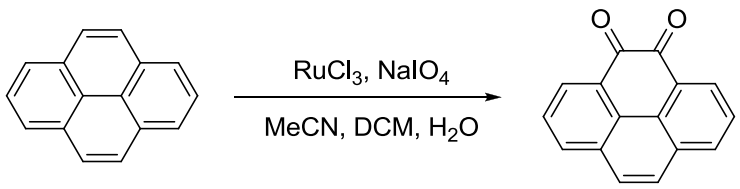

This precursor for making anhydride **5b** was prepared as described in reference.[74,112] To a solution of pyrene (2.0 g, 10 mmol) in 40 mL methylene chloride and 40 mL MeCN, $NaIO_4$ (10.0 g, 46.8 mmol), $RuCl_3$ (0.20 g, 0.96 mmol), and water (50 mL) were added. The dark brown suspension was stirred at rt. for 14 h. The reaction mixture was then poured into 500 mL water and the organic phase was separated. The

aqueous phase was extracted with methylene chloride (3×50 mL), and the extracts were combined and washed with water (3×200 mL) to give a dark orange solution. The solvent of combined organic phase was removed under pressure to give a dark orange solid (2.11 g) as crude product. Column chromatography was run with methylene chloride, and the pure product was given as an orange solid (1.13 g, 48.7% yield). 1H NMR (300 MHz, $CDCl_3$) δ 8.41 (dd, J = 0.9 Hz, J = 7.2 Hz, 2 H), 8.11 (dd, J = 1.2 Hz, J = 8.1 Hz, 2 H), 7.78 (s, 2 H), 7.70 (t, J = 7.5 Hz, 2 H).

Preparation of 9,11-diphenyl-10H-cyclopenta[e]pyren-10-one

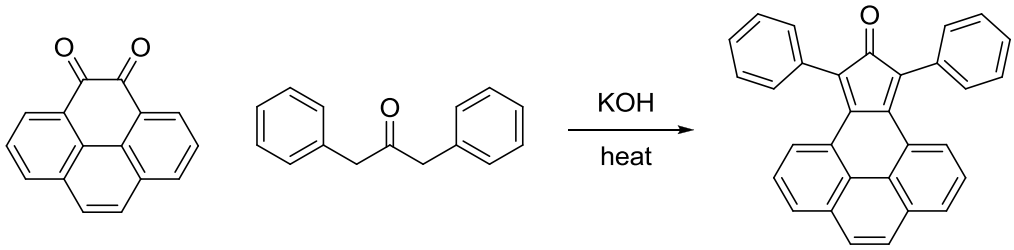

This is also a precursor for making anhydride **5b**, and was prepared as described in reference. Pyrene-4,5-dione (0.200 g, 0.86 mmol) and diphenyl acetone (0.199 g, 0.95 mmol) was dissolved in 100 mL methanol, and the mixture was heated to reflux. Potassium hydroxide (0.058 g, 1.03 mmol) in 50 mL of methanol was then added, and the reaction was heated at reflux for 2 h. The reaction mixture was then cooled down with ice water bath, and the precipitate was isolated via suction filtration and collected as the crude diene (dark green solid, 0.100g, 29% yield). The product was used for the next step directly without purification.

Preparation of anhydride 5b

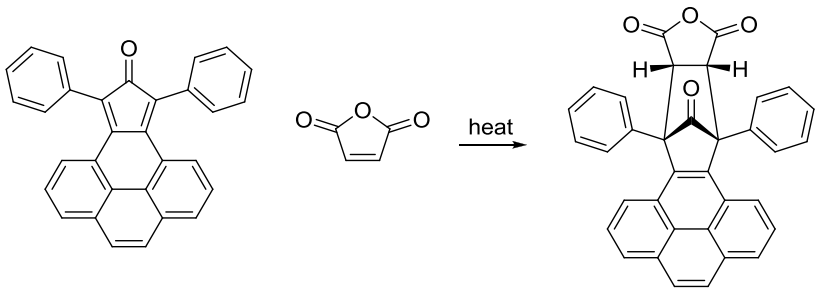

The crude diene (9,11-diphenyl-10H-cyclopenta[e]pyren-10-one) (0.099 g, 0.24 mmol) and maleic anhydride (0.060 g, 0.61 mmol) were mixed in 5 mL of toluene and were heated with a heating gun until the dark green color faded. After cooling with ice-water bath, the precipitated product was separated by suction filtration and washed with cold diethyl ether to give anhydride **5b** (0.080 g, 66% yield) as white solid. The crude product was used for next step without further purification. ^{1}H NMR (400 MHz, $CDCl_3$) δ 8.26 (d, J = 7.77 Hz, 2 H), 8.12 (d, J = 7.60 Hz, 2 H), 8.02 (s, 2 H), 7.78 (t, J = 7.60 Hz, 2 H), 7.65 (t, J = 7.98 Hz, 2 H), 7.60 (t, J = 7.41 Hz, 2 H), 7.47 (t, J = 7.60 Hz, 2 H), 7.37 (d, J = 7.98 Hz, 2 H), 7.27 (d, J = 7.60 Hz, 2 H), 4.81 (s, 2 H). ^{13}C NMR (100 MHz, $CDCl_3$) δ 168.46, 134.09, 132.69, 131.58, 130.97, 129.63, 128.91, 128.90, 128.58, 127.64, 126.56, 125.97, 125.48, 124.81, 123.13, 123.11, 63.34, 46.26. HRMS (EI) calculated for $C_{35}H_{20}O_4$: 504.1362; obs: 504.1363.

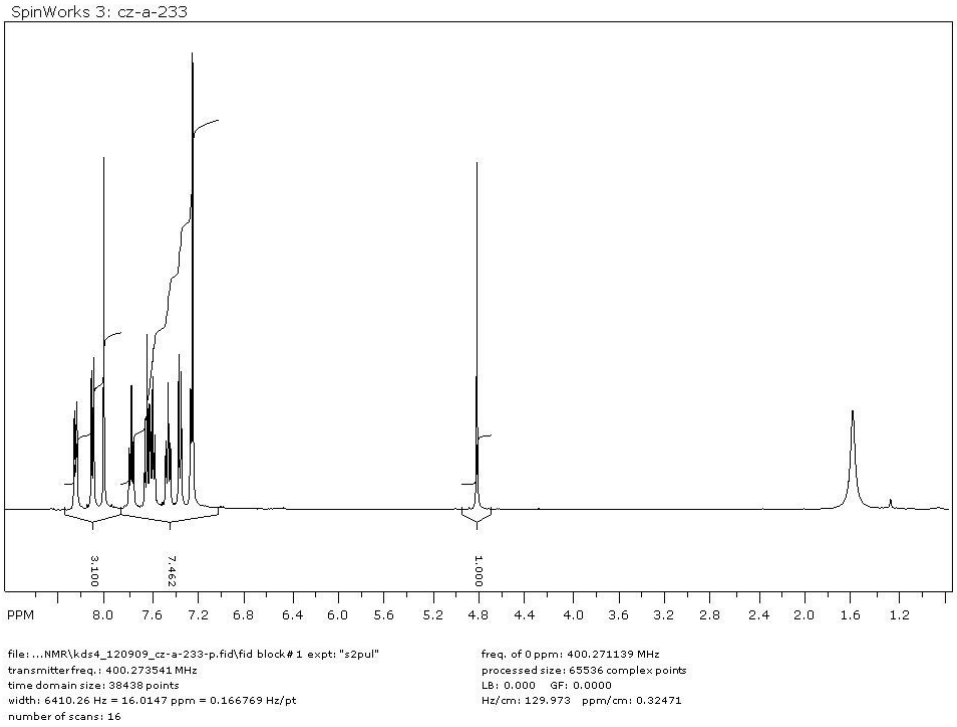

Figure 4.7: ^{1}H NMR spectrum of anhydride **5b** ($CDCl_3$, 400 MHz).

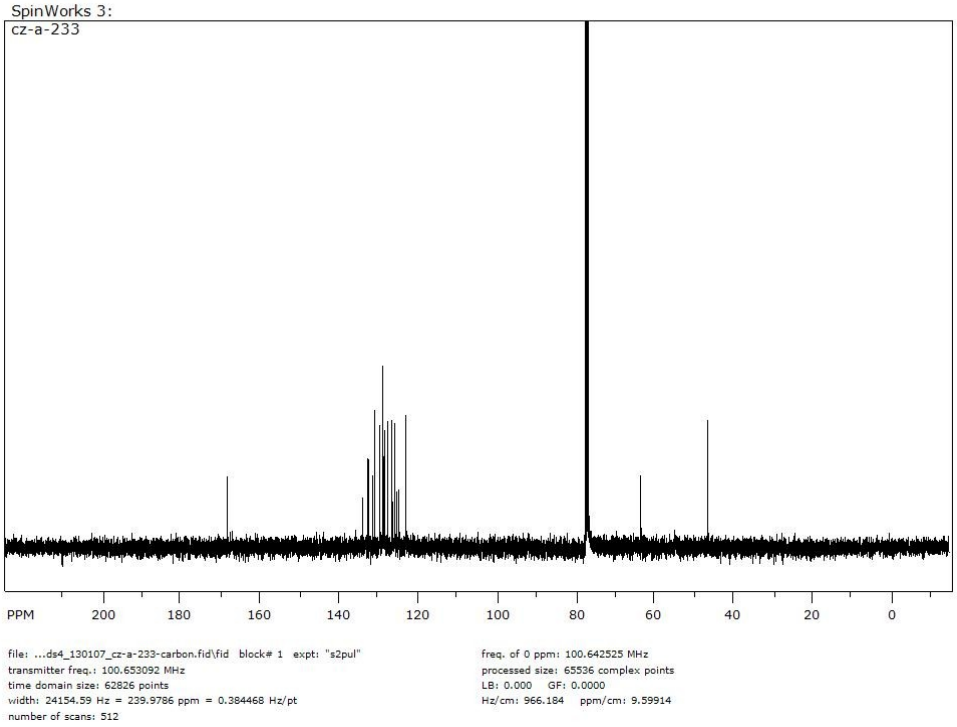

Figure 4.8: ^{13}C NMR spectrum of anhydride **6b** ($CDCl_3$, 100 MHz).

General procedure for preparing molecular balances 7–10

For the condensation reaction, the corresponding anhydride and aniline were dissolved in acetic acid, and the mixture was heated at reflux for 24 h. The solvent was then removed by rotary evaporation. The residue was dissolved in 25 mL EtOAc, washed once with 50 mL saturated sodium bicarbonate, and twice with 50 mL water. The solvent of organic layer was then removed under vacuum, and the crude product was purified via flash chromatography using silica gel ($MeOH/CH_2Cl_2$, v/v = 1/99). Among the balances that were synthesized, balances **7c**–**7d**, **8a**–**8e**, **9b**–**9d** and **10c** are new compounds. The other balances are known molecules, and their ^1H NMR spectra matched the previously reported spectra.

Preparation of balance **7a**

Without further purification, anhydride **5a** (0.100 g, 0.21 mmol) was reacted with *o*-toluidine (0.033 g, 0.31 mmol) in 5 mL acetic acid. After work-up and purification, balance **7a** was obtained as light yellow solid (0.081 g, 0.14 mmol, 67% yield). It is a known compound and its characterization data matched with the previous publication.[113] ^1H NMR (400 MHz, $CDCl_3$) δ 8.71 (d, J = 8.6 Hz, 2 H minor), 8.66 (d, J = 8.6 Hz, 2 H major), 8.37 (t, J = 8.6 Hz, 2 H), 7.80–6.86 (m, 17 H major, 16 H minor), 6.73 (d, J = 7.3 Hz, 1 H major), 6.46 (t, J = 7.3 Hz, 1 H minor), 4.64 (s, 2 H), 4.34 (d, J = 7.3 Hz, 1 H minor), 2.05 (s, 3 H minor), –0.03 (s, 3 H major).

Preparation of balance **7b**

Anhydride **5a** (0.100 g, 0.21 mmol) was reacted with 2-ethylaniline (0.037 g, 0.31 mmol) in 5 mL acetic acid. After work up and purification, balance **7b** was obtained as white solid (0.098 g, 0.17 mmol, 80% yield). It is a known compound, and the

characterization data was matched with the reference.[94] ^{1}H NMR (400 MHz, $CDCl_3$) δ 8.81–8.73 (m, 2 H minor, 2 H major), 8.47–8.39 (m, 2 H major, 2 H minor), 7.80–6.87 (m, 18 H major, 16 H minor), 6.50 (dt, *J* = 7.9 Hz, *J* = 1.1 Hz, 1 H minor), 4.81 (s, 2 H major, 2 H minor), 4.43 (dd, *J* = 7.9 Hz, *J* = 1.2 Hz, 1 H minor), 2.41 (q, *J* = 7.6 Hz, 2 H minor), 1.15 (t, *J* = 7.6 Hz, 3 H minor), 0.20 (q, *J* = 7.5 Hz, 2 H major), –0.08 (t, *J* = 7.4 Hz, 3 H major).

Preparation of balance **7c**

Anhydride **5a** (0.050 g, 0.10 mmol) was reacted with 2-propylaniline (0.028 g, 0.21 mmol) in 5 mL acetic acid. After work up and purification, balance **7c** was obtained as yellow solid (0.057 g, 0.095 mmol, 95% yield). ^{1}H NMR (400 MHz, $CDCl_3$) δ 8.80 (d, *J* = 8.5 Hz, 2 H major), 8.77 (d, *J* = 8.5 Hz, 2 H minor), 8.49–8.40 (m, 2 H major, 2 H minor), 7.85–6.88 (m, 16 H major, 18 H minor), 6.51 (t, *J* = 7.5 Hz, 1 H major), 4.72 (s, 2 H major), 4.70 (s, 2 H minor), 4.33 (d, *J* = 7.9 Hz, 1 H major), 2.38 (t, *J* = 7.5 Hz, 2 H major), 1.56 (m, 2 H major), 0.96 (t, *J* = 7.4 Hz, 3 H major), 0.52 (m, 2 H minor), 0.26 (t, *J* = 6.4 Hz, 2 H minor), –0.30 (t, *J* = 7.4 Hz, 3 H minor). ^{13}C NMR (100 MHz, $CDCl_3$) δ 196.93, 195.67, 173.81, 173.67, 139.40, 139.01, 133.84, 133.78, 133.72, 133.51, 131.54, 131.23, 131.18, 131.01, 130.92, 129.85, 129.46, 129.38, 129.34, 129.23, 129.18, 128.67, 128.54, 128.49, 128.42, 128.05, 127.83, 127.60, 127.31, 127.18, 126.93, 126.70, 126.61, 126.59, 126.39, 126.37, 126.32, 126.17, 125.96, 123.03, 122.99, 68.17, 63.62, 63.61, 45.51, 44.88, 38.74, 33.11, 30.38, 28.95, 28.44, 23.03, 19.42, 14.03, 11.45. HRMS (EI) calculated for $C_{42}H_{31}NO_3$: 597.2304; obs: 597.2303.

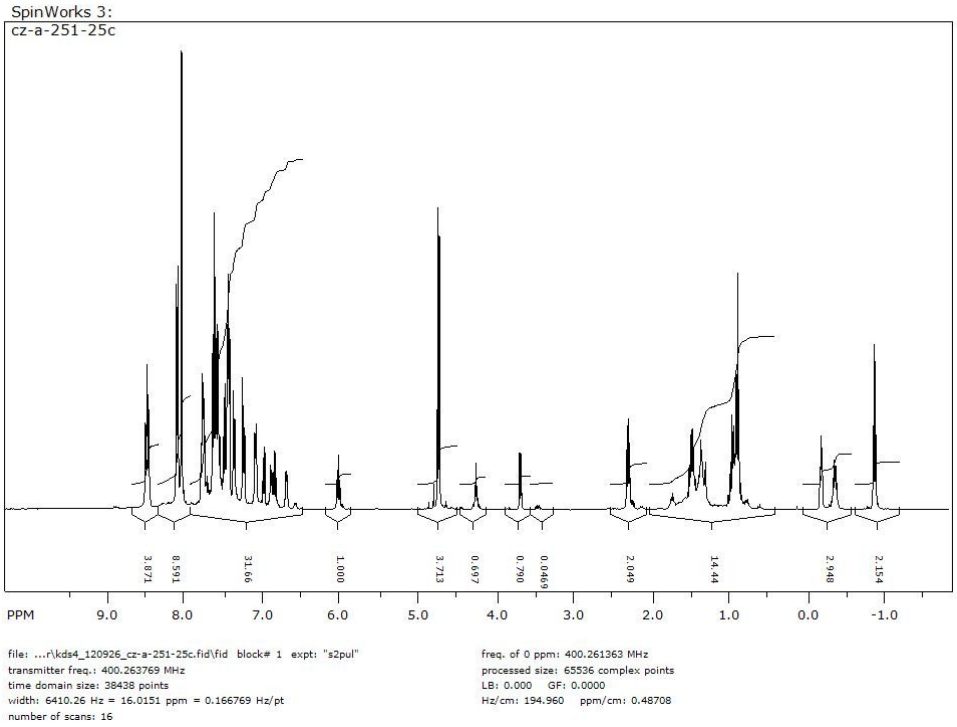

Figure 4.9: ^{1}H NMR spectrum of balance **7c** ($CDCl_3$, 400 MHz).

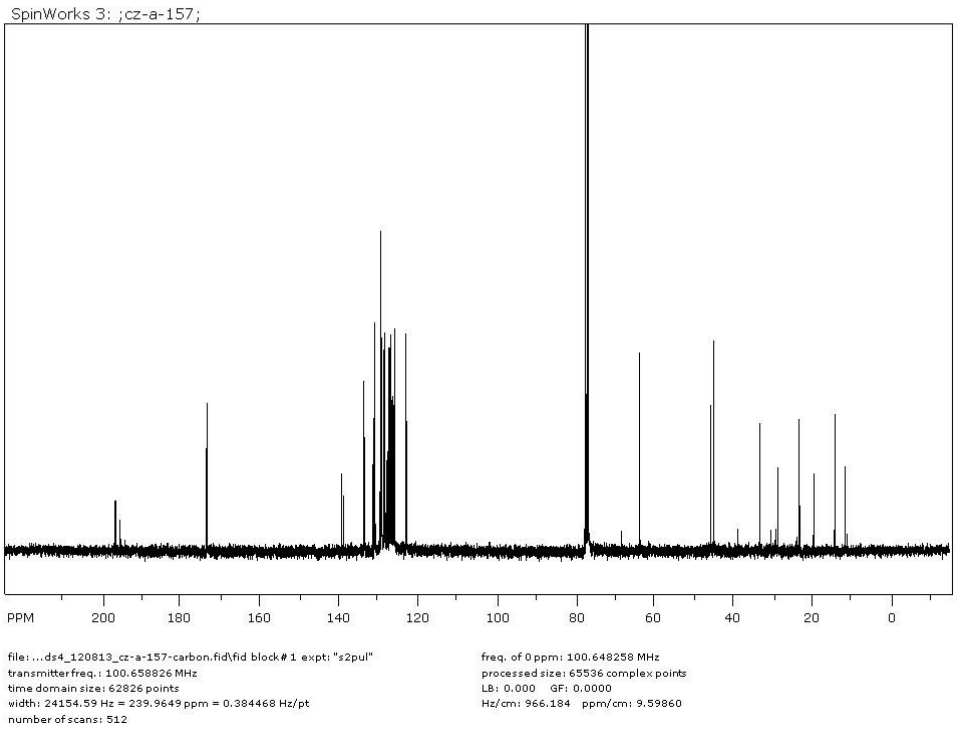

Figure 4.10: ^{13}C NMR spectrum of balance **7c** ($CDCl_3$, 100 MHz).

Preparation of balance **7d**:

Anhydride **5a** (0.050 g, 0.10 mmol) was reacted with 2-*iso*propylaniline (0.028 g, 0.21 mmol) in 5 mL acetic acid. After work up and purification, balance **7d** was obtained as white solid (0.055 g, 0.092 mmol, 92% yield). ^{1}H NMR (400 MHz, $CDCl_3$) δ 8.73 (d, J = 8.42 Hz, 2 H), 8.40 (d, , J = 7.74 Hz, 2 H major, 2 H minor), 7.76–6.82 (m, 18 H major, 17 H minor), 4.68 (s, 2 H major), 4.66 (s, 2 H minor), 4.17 (d, J = 8.04 Hz, 1 H minor), 2.62 (m, 1 H minor), 1.10 (d, J = 6.85 Hz, 6 H minor), –0.02 (m, 1 H major), –0.27 (d, J = 6.77 Hz, 6 H major). ^{13}C NMR (100 MHz, $CDCl_3$) δ 195.57, 173.98, 146.59, 133.82, 133.70, 131.54, 130.99, 129.78, 129.37, 129.27, 128.97, 128.51, 128.38, 127.42, 127.18, 126.60, 126.37, 126.18, 123.05, 63.63, 45.50, 27.62, 22.41. HRMS (EI) calculated for $C_{42}H_{31}NO_3$: 597.2304; obs: 597.2296.

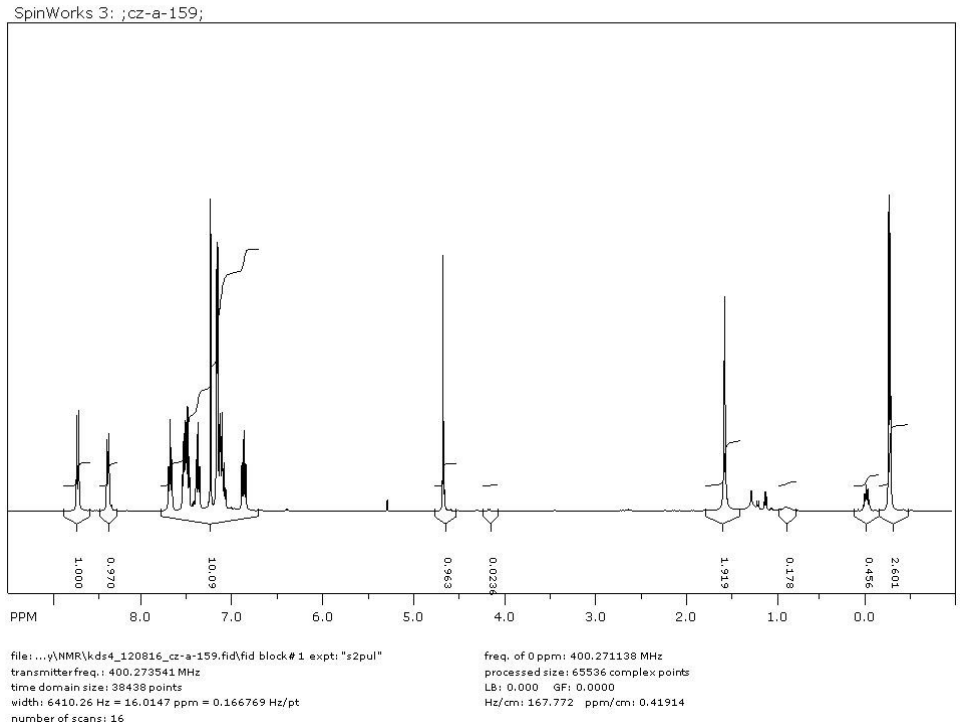

Figure 4.11: ^{1}H NMR spectrum of balance **7d** ($CDCl_3$, 400 MHz).

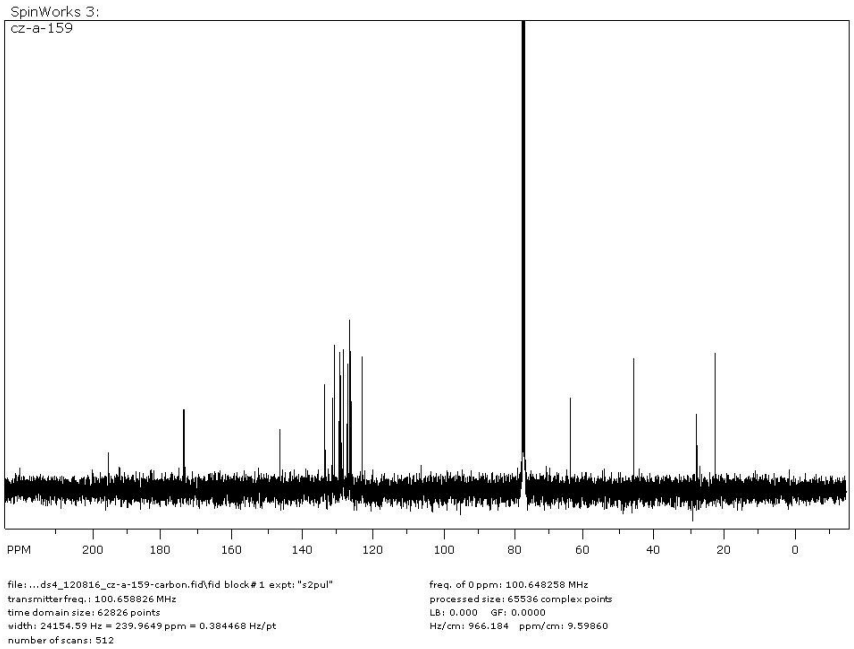

Figure 4.12: ^{13}C NMR spectrum of balance **7d** ($CDCl_3$, 100 MHz).

Preparation of balance **8a**:

Anhydride **5b** (0.050 g, 0.099 mmol) was reacted with *o*-toluidine (0.013 g, 0.12 mmol) in 5 mL acetic acid. After work up and purification, balance **8a** was obtained as a white solid (0.056 g, 0.094 mmol, 95% yield). ^{1}H NMR (400 MHz, $CDCl_3$) δ 8.52–8.40 (m, 2 H major, 2 H minor), 8.15–6.76 (m, 19 H major, 18 H minor), 6.55 (d, J = 7.8 Hz, 1 H major), 6.07 (t, J = 7.8 Hz, 1 H minor), 4.72 (s, 2 H minor), 4.70 (s, 2 H major), 3.78 (d, J = 7.9 Hz, 1 H minor), 2.02 (s, 3 H minor), –0.58 (s, 3 H major). ^{13}C NMR (100 MHz, $CDCl_3$) δ 197.34, 196.43, 173.56, 173.27, 135.61, 134.80, 134.53, 134.34, 133.73, 133.67, 131.40, 131.34, 131.15, 131.08, 130.59, 130.56, 130.44, 129.95, 129.46, 129.44, 129.33, 128.98, 128.70, 128.62, 128.58, 128.54, 127.59, 127.52, 127.33, 126.46, 126.21, 126.18, 126.12, 126.08, 125.98, 125.95, 125.57, 125.51, 125.34, 125.06, 123.53, 123.44, 63.86, 63.81, 45.46, 45.02, 17.58, 14.47. HRMS (EI) calculated for $C_{42}H_{27}NO_3$: 593.1991; obs: 593.1981.

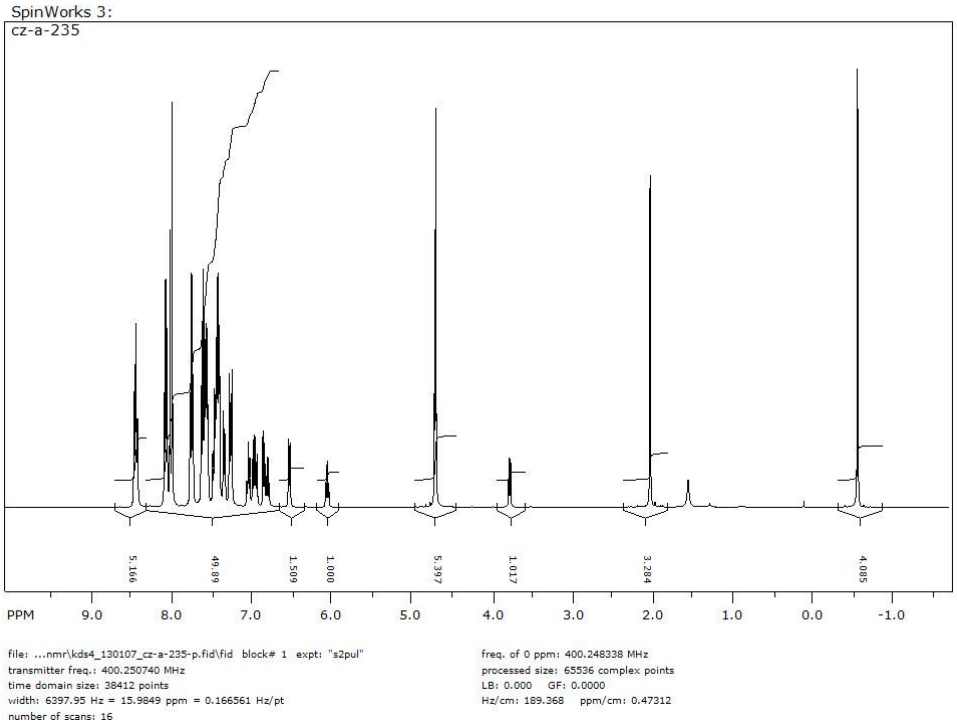

Figure 4.13: ^{1}H NMR spectrum of balance **8a** ($CDCl_3$, 400 MHz).

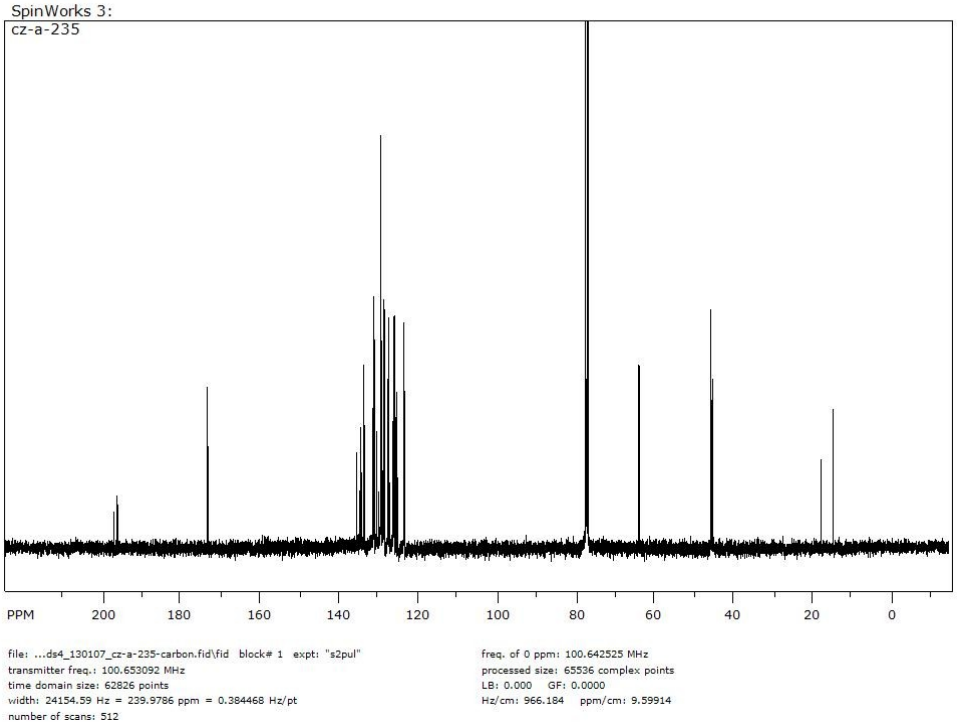

Figure 4.14: ^{13}C NMR spectrum of balance **8a** ($CDCl_3$, 100 MHz).

Preparation of balance **8b**:

Anhydride **5b** (0.050 g, 0.099 mmol) was reacted with 2-ethylaniline (0.018 g, 0.15 mmol) in 5 mL acetic acid. After work up and purification, balance **8b** was obtained as a white solid (0.050 g, 0.082 mmol, 83% yield). ^{1}H NMR (400 MHz, $CDCl_3$) δ 8.52–8.40 (m, 2 H major, 2 H minor), 8.14–6.52 (m, 20 H major, 18 H minor), 6.01 (t, J = 7.6 Hz, 1 H minor), 4.72 (s, 2 H minor), 4.70 (s, 2 H major), 3.66 (d, J = 7.9 Hz, 1 H minor), 2.31 (q, J = 15.2 Hz, J = 7.6 Hz, 2 H minor), 1.05 (t, J = 7.6 Hz, 3 H minor), –0.32 (q, J = 14.8 Hz, J = 7.6 Hz, 2 H major), –0.90 (t, J = 7.5 Hz, 3 H major). ^{13}C NMR (100 MHz, $CDCl_3$) δ 197.34, 196.21, 173.85, 173.63, 141.03, 140.65, 134.62, 134.36, 133.71, 133.68, 131.48, 131.40, 131.16, 131.07, 130.01, 129.51, 129.47, 129.42, 129.35, 129.23, 128.67, 128.55, 128.51, 127.95, 127.58, 127.56, 127.25, 126.31, 126.21, 126.19, 126.16, 126.11, 126.04, 125.98, 125.50, 125.38, 125.34, 125.06, 123.61, 123.48, 63.86, 63.84, 45.58, 45.05, 23.94, 20.88, 14.18, 10.08. HRMS (EI) calculated for $C_{43}H_{29}NO_3$: 607.2147; obs: 607.2149.

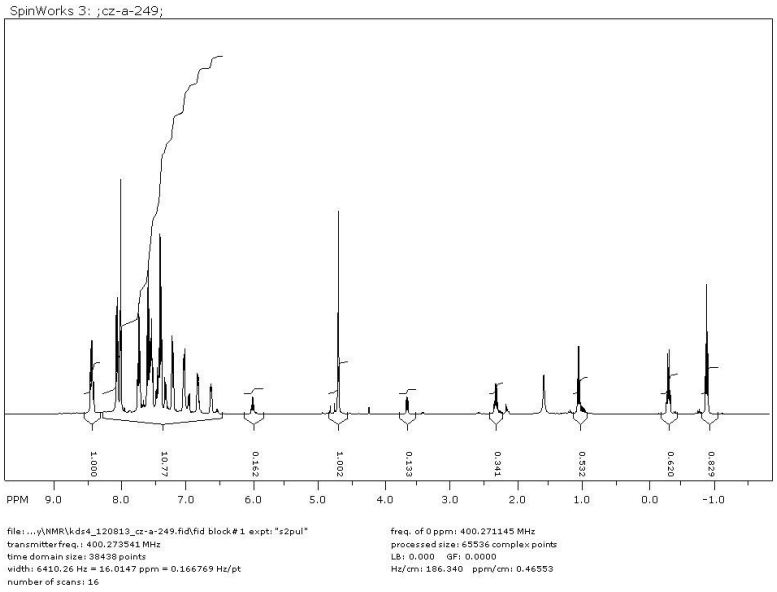

Figure 4.15: ^{1}H NMR spectrum of balance **8b** ($CDCl_3$, 400 MHz).

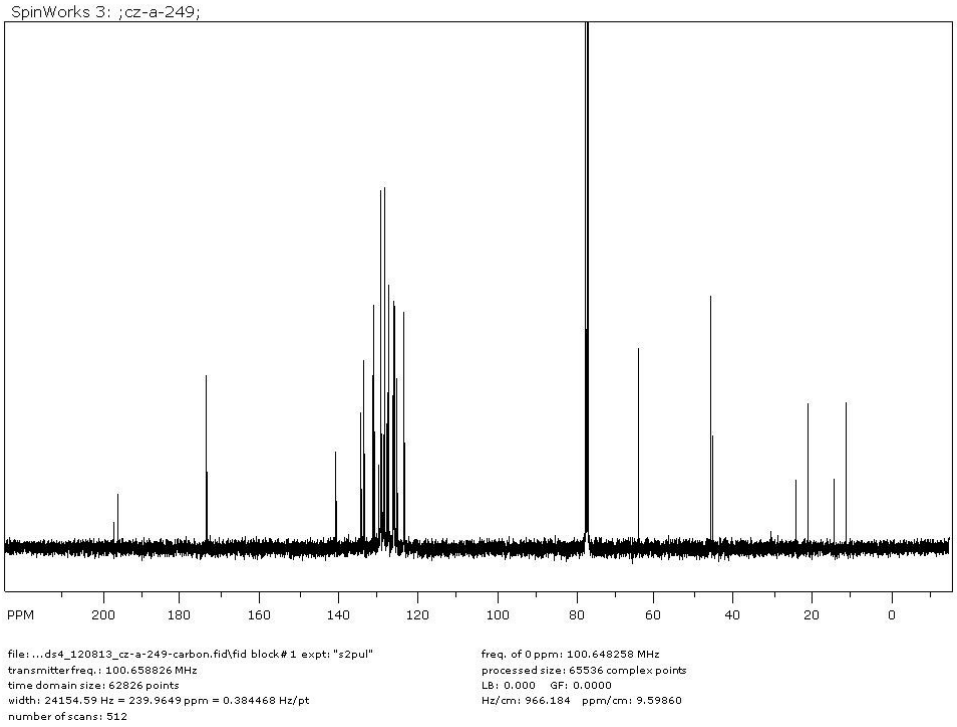

Figure 4.16: ^{13}C NMR spectrum of balance **8b** ($CDCl_3$, 100 MHz).

Preparation of balance **8c**:

Anhydride **5b** (0.050 g, 0.099 mmol) was reacted with 2-propylaniline (0.020 g, 0.15 mmol) in 5 mL acetic acid. After work up and purification, balance **8c** was obtained as a white solid (0.056 g, 0.094 mmol, 95% yield). ^1H NMR (400 MHz, $CDCl_3$) δ 8.56–8.43 (m, 2 H major, 2 H minor), 8.17–6.65 (m, 20 H major, 18 H minor), 6.03 (t, J = 7.8 Hz, 1 H major), 4.75 (s, 2 H major), 4.73 (s, 2 H minor), 3.68 (d, J = 7.8 Hz, 1 H major), 2.30 (t, J = 7.8 Hz, 2 H major), 1.55–1.40 (m, 2 H major), 0.88 (t, J = 7.8 Hz, 3 H major), –0.19 (t, J = 6.5 Hz, 2 H minor), –0.31- –0.43 (m, 2 H minor), –0.88 (t, J = 7.8 Hz, 3 H minor). HRMS (EI) calculated for $C_{44}H_{31}NO_3$: 621.2304; obs: 621.2294.

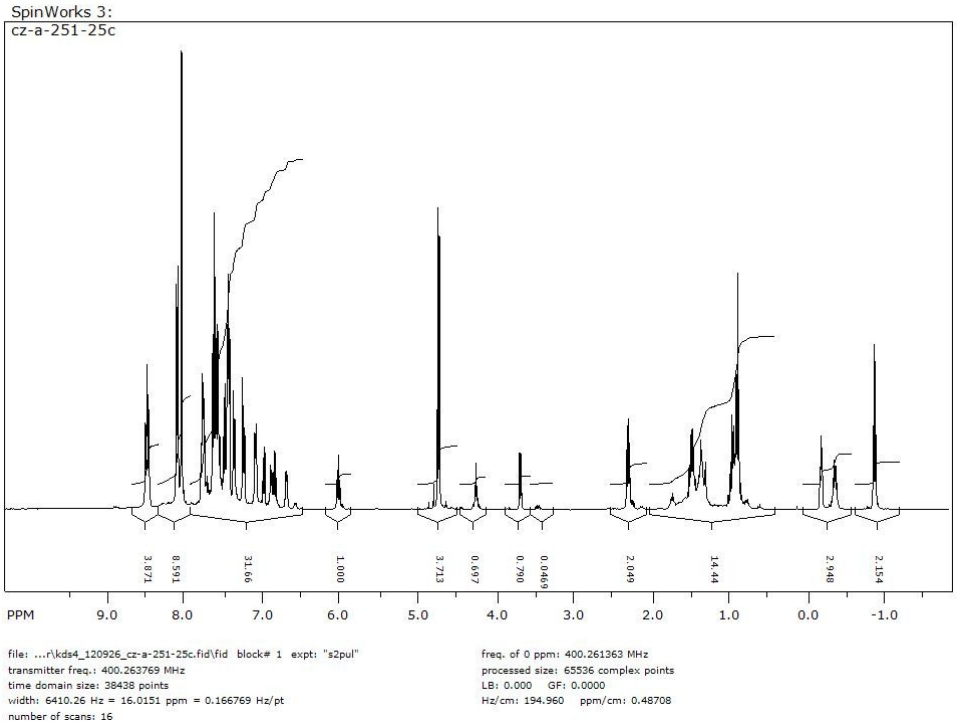

Figure 4.17: ^{1}H NMR spectrum of balance **8c** ($CDCl_3$, 400 MHz).

Preparation of balance **8d**:

Anhydride **5b** (0.050 g, 0.099 mmol) was reacted with 2-propylaniline (0.020 g, 0.15 mmol) in 5 mL acetic acid. After work up and purification, balance **8d** was obtained as a white solid (0.053 g, 0.085 mmol, 86% yield). ^{1}H NMR (400 MHz, $CDCl_3$) δ 8.55–8.43 (m, 2 H major, 2 H minor), 8.14–6.68 (m, 20 H major, 18 H minor), 5.97 (t, J = 7.6 Hz, 1 H minor), 4.76 (s, 2 H major), 4.74 (s, 2 H minor), 3.56 (d, J = 7.8 Hz, 1 H minor), 2.59 (m, 1 H minor), 1.07 (d, J = 6.8 Hz, 6 H minor), –0.38 (m, 1 H major), –0.95 (d, J = 6.7 Hz, 6 H major). ^{13}C NMR (100 MHz, $CDCl_3$) δ 196.10, 173.98, 146.46, 134.67, 133.67, 131.60, 131.17, 129.70, 129.46, 129.43, 128.52, 128.48, 127.57, 127.37, 126.48, 126.32, 126.04, 125.90, 125.49, 123.76, 63.84, 45.63, 27.25, 21.68. HRMS (EI) calculated for $C_{44}H_{31}NO_3$: 621.2304; obs: 621.2304.

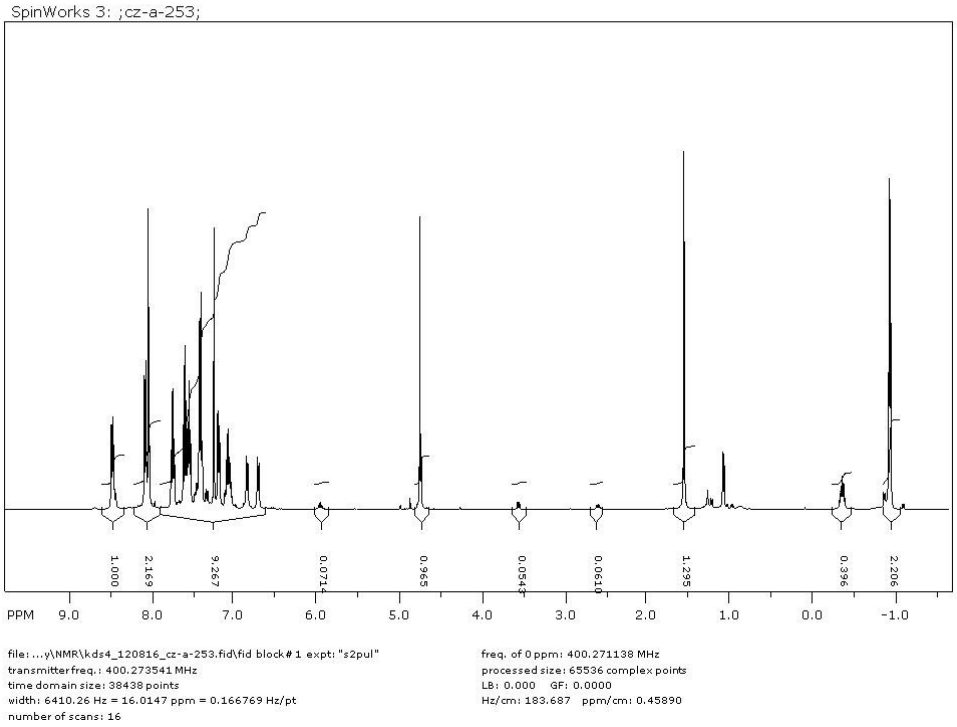

Figure 4.18: ^{1}H NMR spectrum of balance **8d** ($CDCl_3$, 400 MHz).

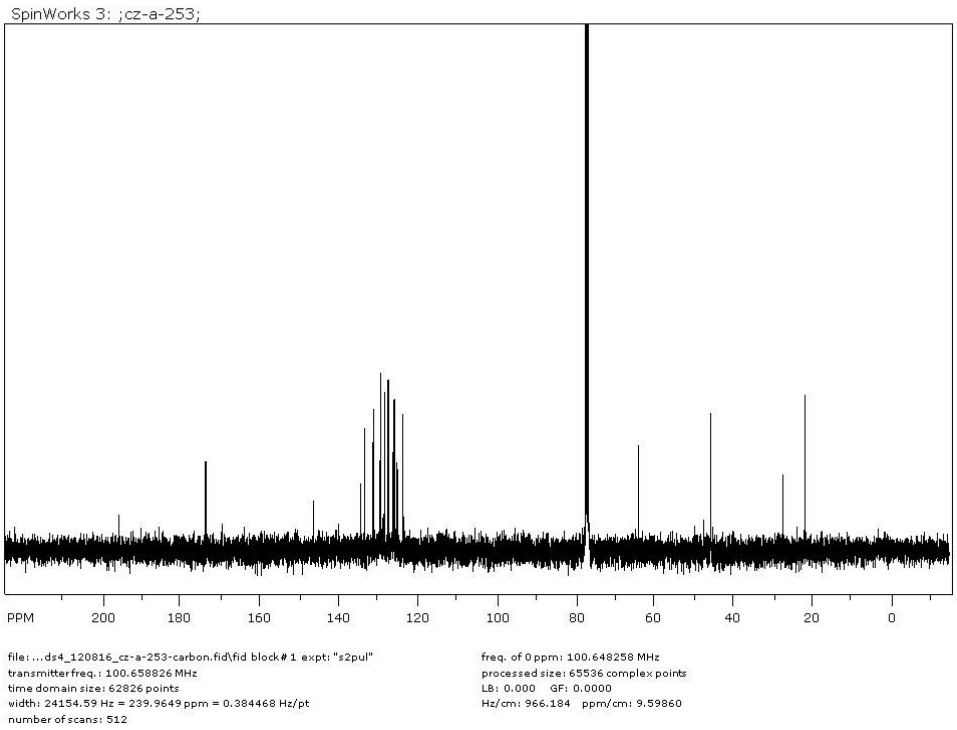

Figure 4.19: ^{13}C NMR spectrum of balance **8d** ($CDCl_3$, 100 MHz).

Preparation of balance **8e**:

Anhydride **5b** (0.050 g, 0.099 mmol) was reacted with *o*-anisidine (0.013 g, 0.11 mmol) in 5 mL acetic acid. After work up and purification, balance **8e** was obtained as a white solid (0.056 g, 0.091 mmol, 93% yield). ^{1}H NMR (400 MHz, $CDCl_3$) δ 8.57–8.40 (m, 2 H major, 2 H minor), 8.15–6.60 (m, 18 H major, 19 H minor), 6.23 (d, J = 8.2 Hz, 1 H minor), 5.93 (t, J = 7.5 Hz, 1 H major), 4.72 (s, 2 H major), 4.70 (s, 2 H minor), 3.98 (dd, J = 7.8 Hz, J = 1.1 Hz, 1 H major), 3.68 (s, 3 H major), 1.41 (s, 3 H minor).

Preparation of balance **9a**:

Anhydride **5c** (0.050 g, 0.14 mmol) was reacted with *o*-toluidine (0.022 g, 0.20 mmol) in 5 mL acetic acid to produce **9a** as light yellow solid (0.051 g, 0.11 mmol, 80% yield) after work-up and purification. ^{1}H NMR (400 MHz, $CDCl_3$) δ 8.00–8.12 (m, 2 H major, 2 H minor), 6.92–7.60 (m, 15 H major, 16 H minor), 5.51 (d, J = 7.8 Hz, 1 H major), 4.34 (s, 2 H minor), 4.30 (s, 2 H major), 2.09 (s, 3 H major), 1.08 (3 H minor). ^{13}C NMR (100 MHz, $CDCl_3$) δ 173.25, 144.29, 136.37, 135.55, 130.79, 130.35, 128.71, 128.67, 128.62, 128.34, 128.25, 121.03, 90.56, 54.63, 54.59, 17.68. HRMS (EI) calculated for $C_{31}H_{23}NO_3$: 457.1678; obs: 457.1680.

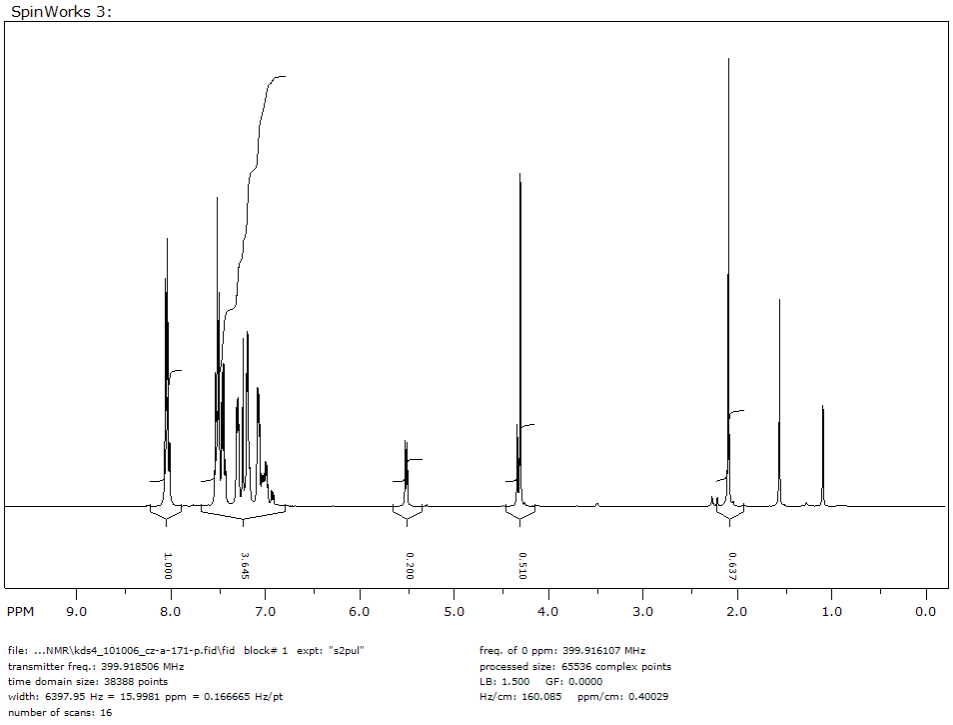

Figure 4.20: ^{1}H NMR spectrum of balance **14a** ($CDCl_3$, 400 MHz).

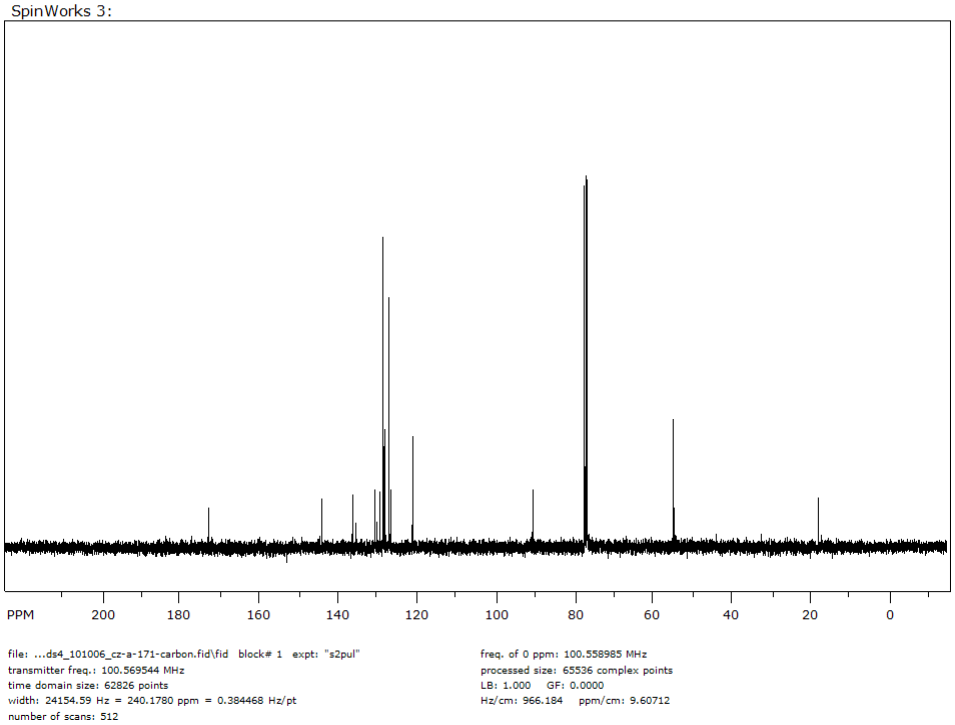

Figure 4.21: ^{13}C NMR spectrum of balance **14a** ($CDCl_3$, 100 MHz).

Preparation of balance **9b**:

Anhydride **5c** (0.100 g, 0.27 mmol) was reacted with 2-ethylaniline (0.039 g, 0.33 mmol) in 5 mL acetic acid to produce **9b** as light yellow solid (0.127 g, 0.27 mmol, 95% yield) after work-up and purification. ^{1}H NMR (400 MHz, $CDCl_3$) δ 8.11–8.01 (m, 2 H major, 2 H minor), 6.89–7.57 (m, 15 H major, 16 H minor), 5.43 (d, J = 7.9 Hz, 1 H major), 4.35 (s, 2 H minor), 4.31 (s, 2 H major), 2.38 (q, J = 7.5 Hz, J = 15.2 Hz, 2 H major), 1.13 (t, J = 7.6 Hz, 3 H major), 1.09 (q, J = 7.5 Hz, J = 15.2 Hz, 2 H minor), 0.85 (t, J = 7.5 Hz, 3 H minor). ^{13}C NMR (100 MHz, $CDCl_3$) δ 173.61, 144.34, 141.33, 136.38, 129.80, 129.72, 128.90, 128.69, 128.66, 128.61, 128.24, 128.17, 127.50, 127.13, 127.11, 126.65, 121.13, 121.05, 90.55, 54.74, 54.65, 24.06, 14.19. HRMS (EI) calculated for $C_{32}H_{35}NO_3$: 471.1834; obs: 471.1836.

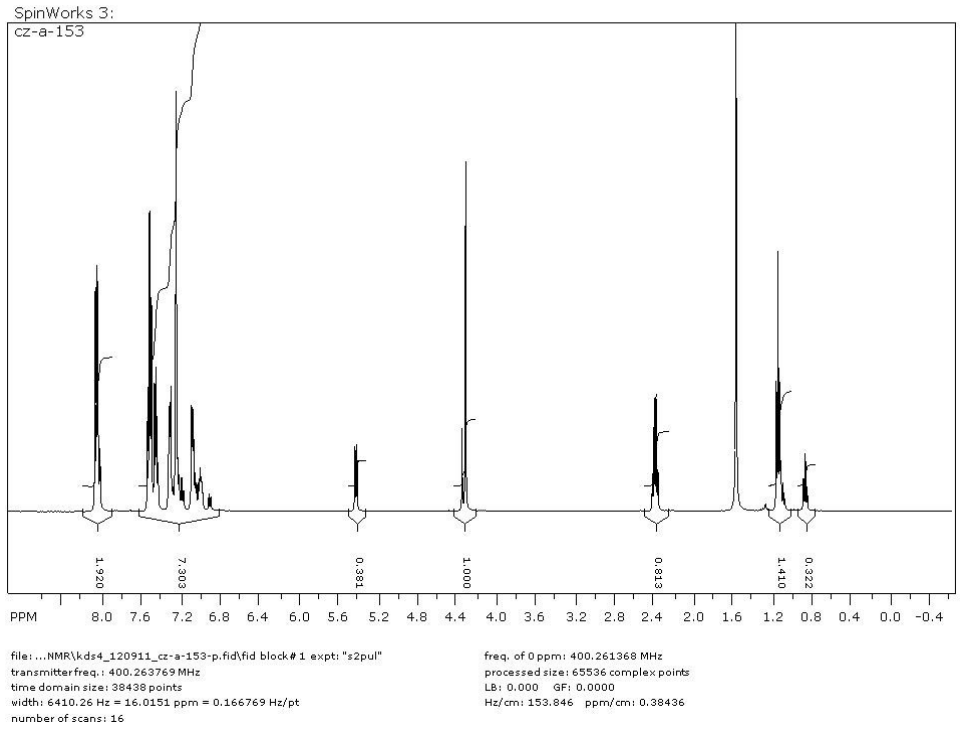

Figure 4.22: ^{1}H NMR spectrum of balance **9b** ($CDCl_3$, 400 MHz).

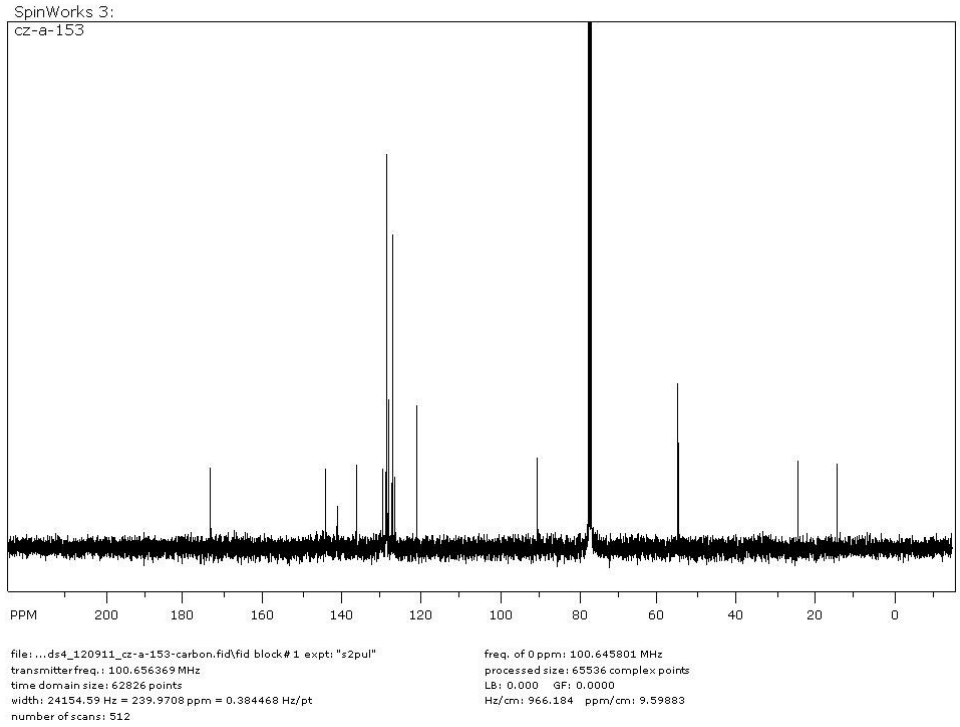

Figure 4.23: ^{13}C NMR spectrum of balance **9b** ($CDCl_3$, 100 MHz).

Preparation of balance **9c**:

Anhydride **5c** (0.100 g, 0.27 mmol) was reacted with 2-propylaniline (0.056 g, 0.41 mmol) in 5 mL acetic acid to produce **3c** as light yellow solid (0.134 g, 0.26 mmol, 95% yield) after work-up and purification. ^{1}H NMR (400 MHz, $CDCl_3$) δ 7.87–7.09 (m, 17 H major, 17 H minor), 6.90 (d, J = 7.7 Hz, 1 H major), 6.77 (d, J = 7.7 Hz, 1 H minor), 3.76 (s, 2 H minor), 3.72 (s, 2 H major), 2.28 (t, J = 7.8 Hz, 3 H minor), 1.13 (t, J = 7.8 Hz, 3 H major), 1.49–1.28 (m, 2 H minor, 2 H major), 0.91 (t, J = 7.3 Hz, 3 H major), 0.79 (t, J = 7.3 Hz, 3 H minor). ^{13}C NMR (100 MHz, $CDCl_3$) δ 196.61, 172.77, 172.68, 146.44, 146.42, 140.04, 140.02, 137.18, 134.00, 133.77, 133.01, 130.49, 130.38, 129.83, 129.78, 129.68, 129.44, 129.28, 128.34, 128.22, 127.87, 126.52, 126.52, 126.25, 126.04, 119.78, 91.24, 91.20, 53.99, 53.96, 33.28, 33.01, 23.30, 22.97, 14.20, 13.99. HRMS (EI) calculated for $C_{33}H_{27}NO_3$: 485.1991; obs: 485.1993.

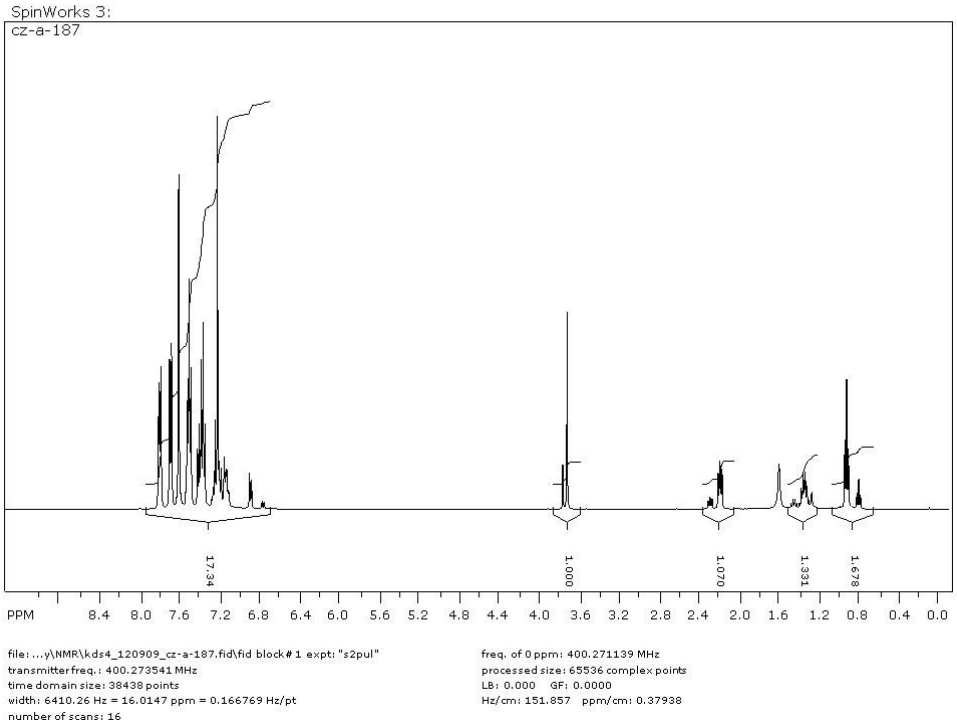

Figure 4.24: ^{1}H NMR spectrum of balance **9c** ($CDCl_3$, 400 MHz).

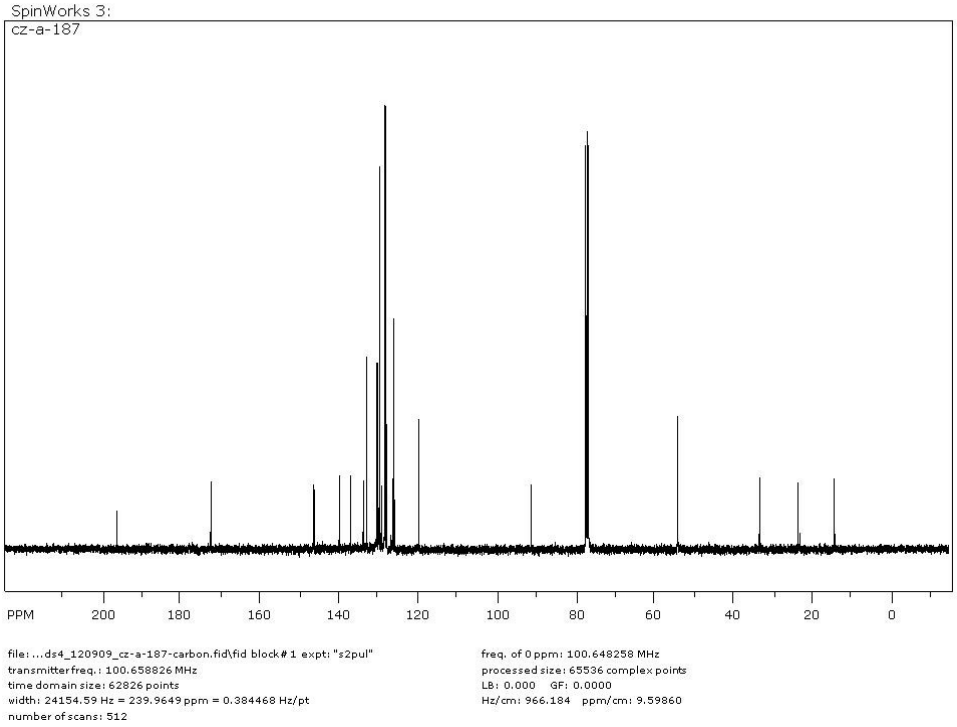

Figure 4.25: ^{13}C NMR spectrum of balance **9c** ($CDCl_3$, 100 MHz).

Preparation of balance **9d**:

Anhydride **5c** (0.100 g, 0.27 mmol) was reacted with 2-propylaniline (0.056 g, 0.41 mmol) in 5 mL acetic acid to produce **9d** as light yellow solid (0.114 g, 0.23 mmol, 85% yield) after work-up and purification. ^{1}H NMR (400 MHz, $CDCl_3$) δ 7.88–7.03 (m, 17 H major, 17 H minor), 6.90 (d, J = 7.6 Hz, 1 H major), 6.76 (d, J = 7.6 Hz, 1 H minor), 3.75 (s, 2 H minor), 3.70 (s, 2 H major), 2.71 (m, 1 H major), 2.58 (m, 1 H minor) 1.08 (d, J = 6.8 Hz, 6 H minor), 0.79 (t, J = 6.8 Hz, 6 H major). ^{13}C NMR (100 MHz, $CDCl_3$) δ 172.99, 172.72, 146.41, 146.32, 145.92, 140.02, 137.19, 134.01, 133.84, 133.01, 130.38, 129.90, 129.84, 129.68, 129.62, 129.45, 128.39, 128.34, 128.32, 128.24, 127.97, 127.87, 128.87, 126.51, 126.32, 126.25, 126.10, 126.01, 119.80, 104.48, 91.20, 91.15, 56.45, 54.18, 54.05, 28.62, 27.83, 23.59, 23.49. HRMS (EI) calculated for $C_{33}H_{27}NO_3$: 485.1991; obs: 485.1989.

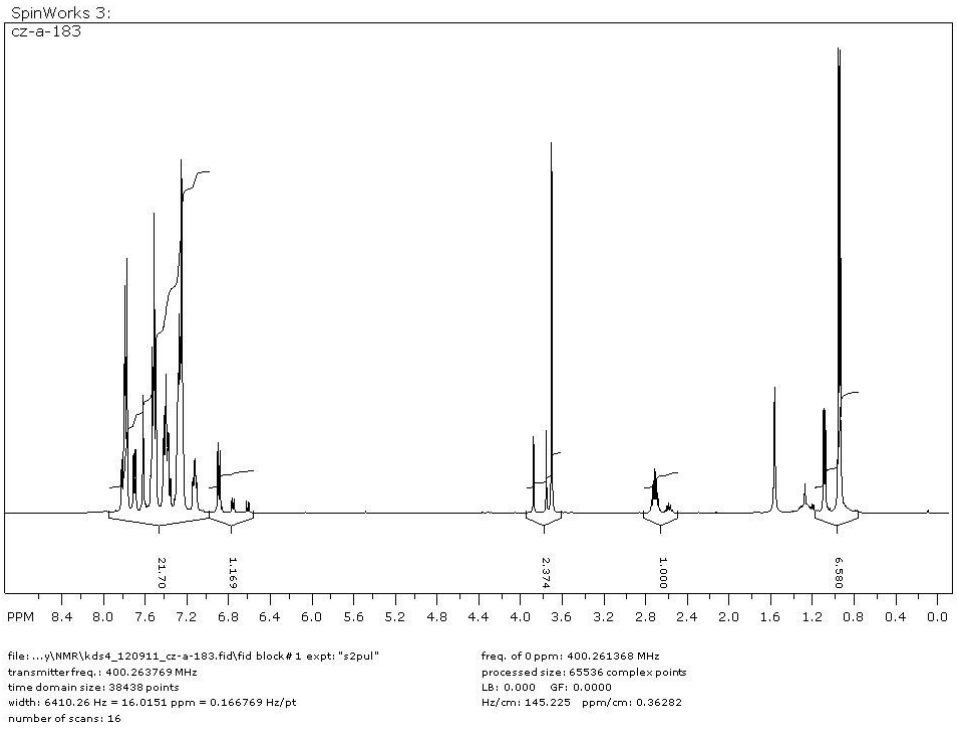

Figure 4.26: ^{1}H NMR spectrum of balance **9d** ($CDCl_3$, 400 MHz).

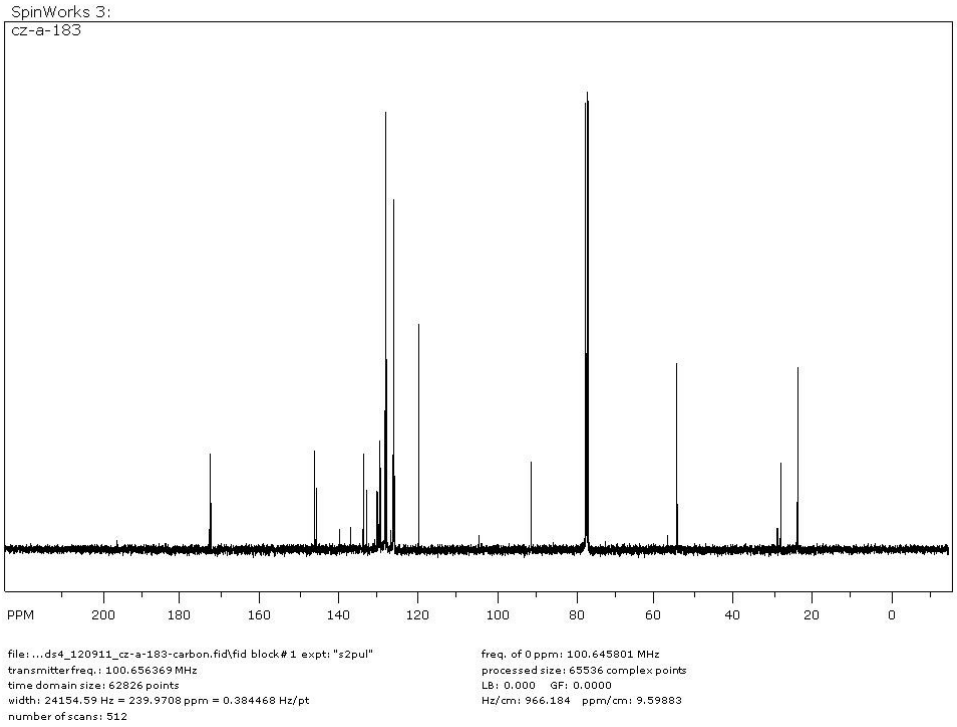

Figure 4.27: ^{13}C NMR spectrum of balance **9d** ($CDCl_3$, 100 MHz).

Preparation of balance **9e**:

Anhydride **5c** (0.22 g, 0.59 mmol) was reacted with anisidine (0.11 g, 0.89 mmol) in 5 mL acetic acid to produce balance **9e** as pale yellow solid (0.23 g, 0.48 mmol, 82% yield). ^1H NMR (400 MHz, $CDCl_3$) δ 8.08 (m, 4 H major, 4 H minor), 6.78–7.60 (m, 13 H major, 14 H minor), 5.68 (dd, J = 7.7 Hz, J = 1.2 Hz, 1 H major), 4.31 (s, 2 H major), 4.28 (s, 2 H minor), 3.76 (s, 3 H major), 3.48 (s, 3 H minor).

Preparation of balance **10a**:

Anhydride **5d** (*cis*-5-Norbornene-*endo*-2,3-dicarboxylic anhydride) (0.050 g, 0.30 mmol) and *o*-toluidine (0.039 g, 0.37 mmol) were heated to reflux in 5 mL acetic acid for 24 h. The solvent was removed under vacuum and the reaction mixture was heated in oven (120 °C) for another 12 h. Then balance **10a** was obtained as white solid (0.047 g, 0.19 mmol, 62% yield). Its characterization data matches up with the reference. ^1H

NMR (400 MHz, $CDCl_3$) δ 7.24–7.38 (m, 3 H), 7.03 (d, *J* = 7.5 Hz, 1 H minor), 6.91 (d, *J* = 7.5 Hz, 1 H major), 6.35 (t, *J* = 1.6 Hz, 2 H), 3.45–3.58 (m, 4 H), 2.18 (s, 3 H major), 2.15 (s, 3 H minor), 1.80–1.88 (m, 1 H), 1.60–1.69 (m, 1 H). HRMS (EI) calculated for $C_{16}H_{15}NO_2$: 253.1103; obs: 253.1099.

Preparation of balance **10b**:

Anhydride **5d** (0.100 g, 0.61 mmol) was reacted with 2-ethylaniline (0.089 g, 0.73 mmol) in 5 mL acetic acid. After work up and purification, balance **10b** was obtained as a white solid (0.142 g, 0.53 mmol, 87% yield). It is a known compound, and the characterization data was matched with the reference.[1] ^{1}H NMR (400 MHz, $CDCl_3$) δ 7.41–7.20 (m, 3 H), 6.97 (d, *J* = 7.8 Hz, 1 H minor), 6.86 (d, *J* = 7.8 Hz, 1 H major), 6.31 (s, 2 H), 3.54–3.39 (m, 4 H), 2.45 (q, *J* = 7.7 Hz, *J* = 15.2 Hz, 2 H major), 2.40 (q, *J* = 7.7 Hz, *J* = 15.2 Hz, 2 H minor), 1.79 (t, *J* = 9.0 Hz, 1 H), 1.60 (t, *J* = 7.9 Hz, 1 H), 1.22–1.08 (m, 3 H major, 3 H minor).

Preparation of balance **10c**:

Anhydride **5d** (0.050 g, 0.30 mmol) was reacted with 2-propylaniline (0.049 g, 0.37 mmol) in 5 mL acetic acid. After work up and purification, balance **10c** was obtained as a white solid (0.073 g, 0.26 mmol, 85% yield). ^{1}H NMR (400 MHz, $CDCl_3$) δ 7.34–7.10 (m, 3 H), 6.88 (d, *J* = 7.6 Hz, 1 H major), 6.78 (d, *J* = 7.6 Hz, 1 H minor), 6.31–6.18 (m, 2 H), 3.52–3.32 (m, 4 H), 2.40–2.19 (m, 2 H major, 2 H minor), 1.75 (t, *J* = 10.3 Hz, 1 H), 1.54 (t, *J* = 8.9 Hz, 1 H), 1.52–1.37 (m, 2 H major, 2 H minor), 0.89 (t, *J* = 7.3 Hz, 3 H minor). 0.84 (t, *J* = 7.3 Hz, 3 H major). ^{13}C NMR (100 MHz, $CDCl_3$) δ 177.23, 176.98, 140.45, 140.11, 135.18, 134.65, 130.86, 130.80, 130.04, 129.90, 129.47,

[1] Curran, D. P.; Geib, S.; DeMello, N. Tetrahedron **1999**, *55*, 5681.

129.44, 128.53, 128.15, 126.96, 126.84, 52.96, 52.32, 46.85, 45.77, 45.44, 45.16, 33.51, 33.24, 23.67, 23.06, 14.12, 14.10. HRMS (EI) calculated for $C_{18}H_{19}NO_2$: 281.1416; obs: 281.1418.

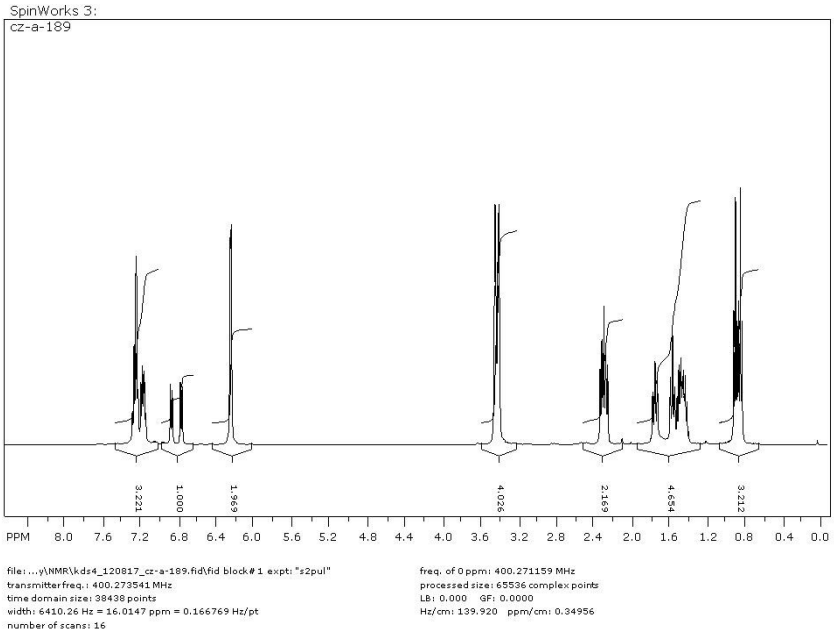

Figure 4.28: ^{1}H NMR spectrum of balance **10c** ($CDCl_3$, 400 MHz).

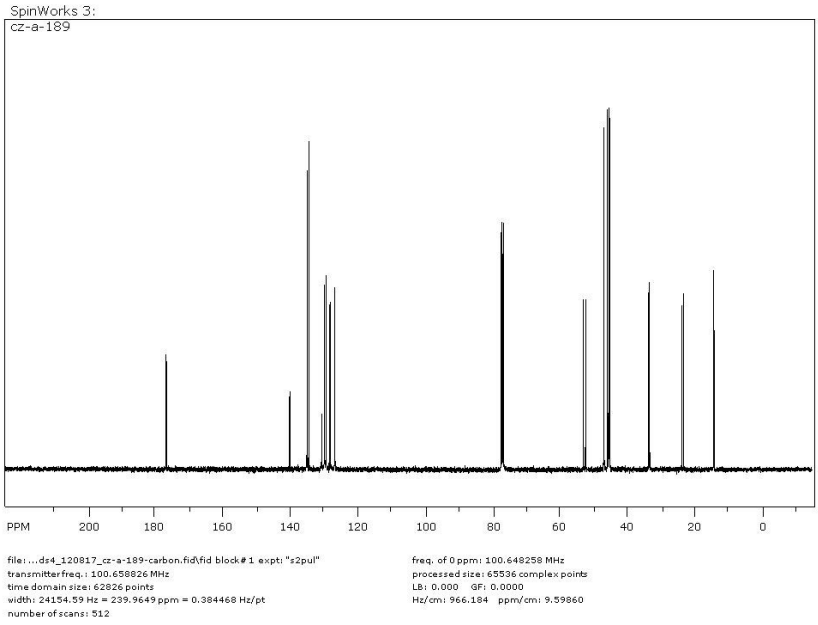

Figure 4.29: ^{13}C NMR spectrum of balance **10c** ($CDCl_3$, 100 MHz).

Preparation of balance **10d**:

Anhydride **5d** (0.100 g, 0.61 mmol) was reacted with 2-*iso*propylaniline (0.089 g, 0.73 mmol) in 5 mL acetic acid. After work up and purification with column, balance **10d** was obtained as a white solid (0.097 g, 0.34 mmol, 56% yield). It is a known compound, and the characterization data was matched with the reference.[1] ^{1}H NMR (400 MHz, $CDCl_3$) δ 7.43–7.31 (m, 2 H), 7.28–7.16 (m, 1 H), 6.92 (d, J = 7.7 Hz, 1 H major), 6.81 (d, J = 7.7 Hz, 1 H minor), 6.29 (m, 2 H minor, 2 H major), 3.53–3.39 (m, 4 H), 2.79–2.63 (m, 1 H major, 1 H minor), 1.79 (t, J = 9.5 Hz, 1 H), 1.60 (t, J = 8.3 Hz, 1 H), 1.17 (d, J = 6.9 Hz, 6 H minor), 1.14 (d, J = 6.9 Hz, 6 H major).

Preparation of balance **10e**:

Anhydride **5c** (0.11 g, 0.68 mmol) and *o*-anisidine (0.10 g, 0.81 mmol, 0.09 mL) were reacted in 10 mL acetic acid. The crude product was heated in oven (130 °C) for 16 h to give the product as white crystal (0.12 g, 0.45 mmol, 66% yield). ^{1}H NMR (400 MHz, $CDCl_3$) δ 7.36 (dt, J = 7.8 Hz, J = 1.4 Hz, 1 H major, 1 H minor), 6.86–7.06 (m, 3 H major, 3 H minor), 6.28 (s, 2 H major), 6.21 (s, 2 H minor), 3.78 (ds, 3 H major, 3 H minor), 3.37–3.54 (m, 4 H major, 4 H minor), 1.54–1.82 (m, 2 H major, 2 H minor).

4.6.2 Variable Temperature ^{1}H NMR Experiments:

The van't Hoff plots of balances **7–10** were plotted based on the results from variable temperature ^{1}H NMR. The full spectra were acquired at 5°C intervals between 25°C–55°C, and the *folded*/*unfolded* ratios were obtained via spectral deconvolution of the succinimide alpha singlets, the alkyl peaks (balances **7–9**), or the triplet for ethene protons (balances **10**). The *folded*/*unfolded* ratios (F/UF) were listed as Table 4.3–Table 4.10, and the van't Hoff plots were as Figure 4.30–4.33.

Table 4.3: Results from variable temperature ^{1}H NMR experiments of balance **7a** and **7b** in $CDCl_3$.

		balance **7a**		balance **7b**	
T (°C)	1/Temp (K^{-1})	F/UF	ln(F/UF)	F/UF	ln(F/UF)
25	0.003356	1.24834	0.22181	1.59186	0.4649
30	0.003300	1.2186	0.1977	1.54253	0.43343
35	0.003247	1.1973	0.18007	1.49766	0.4039
40	0.003195	1.18495	0.1697	1.46673	0.38303
45	0.003145	1.15324	0.14258	1.4332	0.35991
50	0.003096	1.14331	0.13393	1.39403	0.3322
55	0.003049	1.12463	0.11745	1.37348	0.31735

Table 4.4: Results from variable temperature ^{1}H NMR experiments of balance **7c** and **7d** in $CDCl_3$.

		balance **7c**		balance **7d**	
T (°C)	1/Temp (K^{-1})	F/UF	ln(F/UF)	F/UF	ln(F/UF)
25	0.003356	0.54037	–0.6155	4.64924	1.5367
30	0.003300	0.54806	–0.6014	4.56261	1.5179
35	0.003247	0.52531	–0.6438	3.70111	1.30863
40	0.003195	0.52575	–0.6429	3.42221	1.23029
45	0.003145	0.51902	–0.6558	2.88346	1.05899
50	0.003096	0.52648	–0.6415	2.65452	0.97626
55	0.003049	0.51393	–0.6657	2.43031	0.88802

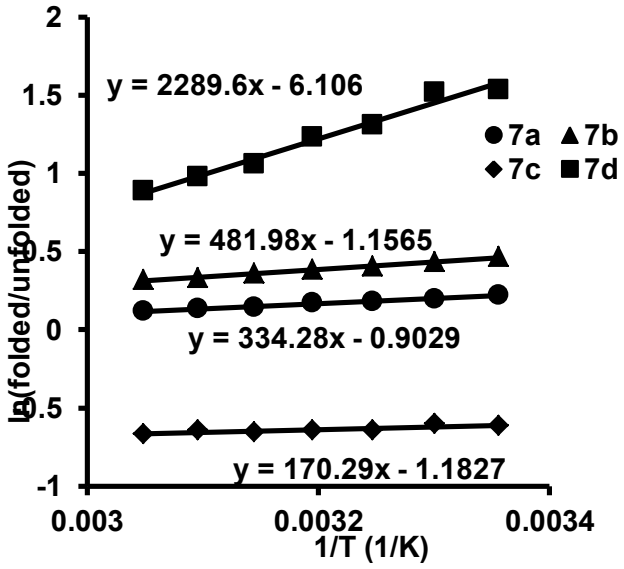

Figure 4.30: Van't Hoff plot of balances **7a–7d** in $CDCl_3$ based on the information in Table 4.3 and Table 4.4.

Table 4.5: Results from variable temperature ^{1}H NMR experiments of balance **8a** and **8b** in $CDCl_3$.

		balance **8a**		balance **8b**	
T (°C)	1/Temp (K^{-1})	F/UF	ln(F/UF)	F/UF	ln(F/UF)
25	0.003356	1.24834	0.22181	1.59186	0.4649
30	0.003300	1.2186	0.1977	1.54253	0.43343
35	0.003247	1.1973	0.18007	1.49766	0.4039
40	0.003195	1.18495	0.1697	1.46673	0.38303
45	0.003145	1.15324	0.14258	1.4332	0.35991
50	0.003096	1.14331	0.13393	1.39403	0.3322
55	0.003049	1.12463	0.11745	1.37348	0.31735

Table 4.6: Results from variable temperature ^{1}H NMR experiments of balance **8c** and **8d** in $CDCl_3$.

		balance **8c**		balance **8d**	
T (°C)	1/Temp (K^{-1})	F/UF	ln(F/UF)	F/UF	ln(F/UF)
25	0.003356	0.54037	–0.6155	4.64924	1.5367
30	0.003300	0.54806	–0.6014	4.56261	1.5179
35	0.003247	0.52531	–0.6438	3.70111	1.30863
40	0.003195	0.52575	–0.6429	3.42221	1.23029
45	0.003145	0.51902	–0.6558	2.88346	1.05899
50	0.003096	0.52648	–0.6415	2.65452	0.97626
55	0.003049	0.51393	–0.6657	2.43031	0.88802

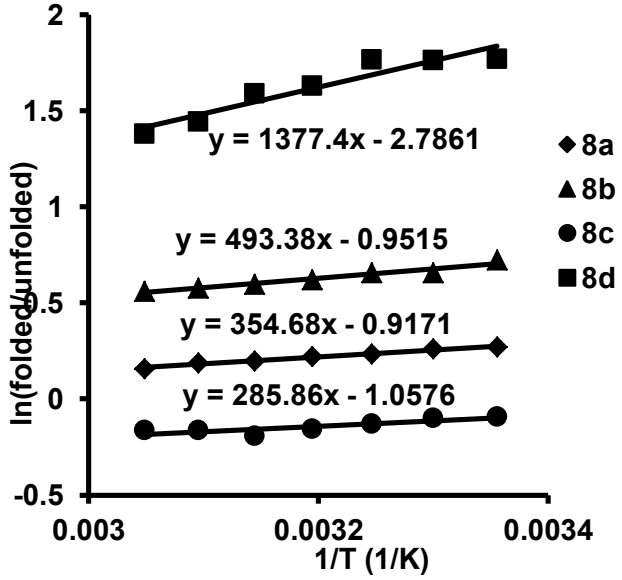

Figure 4.31: Van't Hoff plot of balances **8a–8d** in $CDCl_3$ based on the information in Table 4.5 and Table 4.6.

Table 4.7: Results from variable temperature ^{1}H NMR experiments of balance **9a** and **9b** in $CDCl_3$.

		balance **9a**		balance **9b**	
T (°C)	1/Temp (K^{-1})	F/UF	ln(F/UF)	F/UF	ln(F/UF)
25	0.003356	0.242322	–1.41749	0.242292	–1.41761
30	0.003300	0.257325		0.244667	–1.40786
35	0.003247	0.248561	–1.39207	0.247747	–1.39535
40	0.003195	0.247798	–1.39514	0.248764	–1.39125
45	0.003145	0.255321	–1.36523	0.253549	–1.3722
50	0.003096	0.255836	–1.36322	0.257114	–1.35824
55	0.003049	0.256991	–1.35871	0.259729	–1.34811

Table 4.8: Results from variable temperature ^{1}H NMR experiments of balance **9c** and **9d** in $CDCl_3$.

		balance **9c**		balance **9d**	
T (°C)	1/Temp (K^{-1})	F/UF	ln(F/UF)	F/UF	ln(F/UF)
25	0.003356	0.231847	–1.46168	0.221532	–1.50719
30	0.003300	0.238412	–1.43375	0.224027	–1.49599
35	0.003247	0.245156	–1.40586	0.229817	–1.47047
40	0.003195	0.248369	–1.39284	0.235478	–1.44614
45	0.003145	0.259957	–1.34724	0.239478	–1.4293
50	0.003096	0.25729	–1.35755	0.241582	–1.42055
55	0.003049	0.261652	–1.34074	0.244248	–1.40957

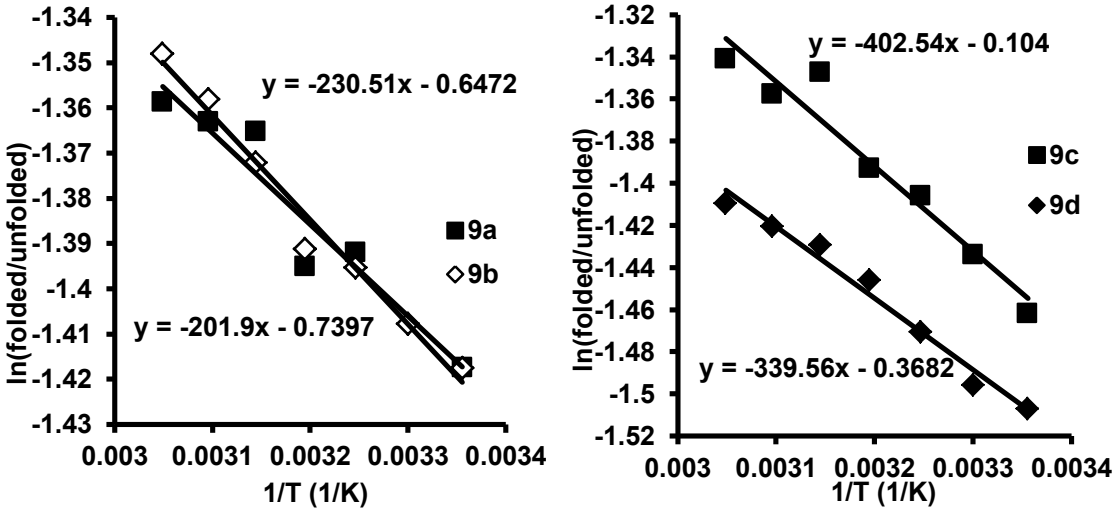

Figure 4.32: Van't Hoff plot of balances **9a–9d** in $CDCl_3$ based on the information in Table 4.7 and Table 4.8.

Table 4.9: Results from variable temperature ^{1}H NMR experiments of balance **10a** and **10b** in CDCl3.

		balance **10a**		balance **10b**	
T (°C)	1/Temp (K^{-1})	F/UF	ln(F/UF)	F/UF	ln(F/UF)
25	0.003356	0.967	–0.03356	0.886823	–0.12011
30	0.003300	0.950545	–0.05072	0.851496	–0.16076
35	0.003247	0.926327	–0.07653	0.855483	–0.15609
40	0.003195	0.930472	–0.07206	0.840507	–0.17375
45	0.003145	0.914783	–0.08907	0.85079	–0.16159
50	0.003096	0.885148	–0.122	0.832266	–0.1836
55	0.003049	0.87815	–0.12994	0.804918	–0.21702

Table 4.10: Results from variable temperature ^{1}H NMR experiments of balance **10c** and **10d** in $CDCl_3$.

		balance **10c**		balance **10d**	
T (°C)	1/Temp (K^{-1})	F/UF	ln(F/UF)	F/UF	ln(F/UF)
25	0.003356	0.964435	–0.03621	1.21065	0.191157
30	0.003300	0.945449	–0.05609	1.146235	0.136482
35	0.003247	0.937693	–0.06433	1.062383	0.060515
40	0.003195	0.926644	–0.07619	0.956232	–0.04476
45	0.003145	0.903053	–0.10197	0.878613	–0.12941
50	0.003096	0.892207	–0.11406	0.850126	–0.16237
55	0.003049	0.886356	–0.12064	0.844441	–0.16908

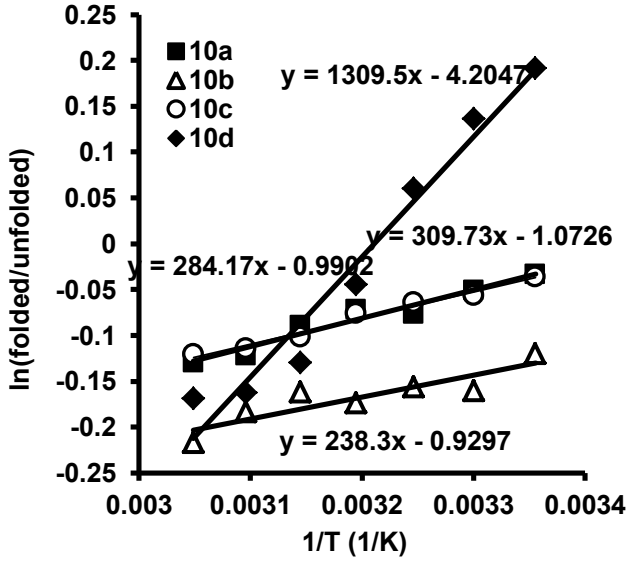

Figure 4.33: Van't Hoff plot of balances **10a–10d** in $CDCl_3$ based on the information in Table 4.9 and Table 4.10.

Based on the data above and the equation in Chapter 2, the calculation of entropy and enthalpy values of balance **7–10** with errors are listed in Table 4.11. The errors for slopes and intercepts are measured by the regression add-in in excel.

Table 4.11: Calculation of ΔG, ΔH, ΔS, and $-T\Delta S$ and their errors of balance **7–10** by VT NMR experiments in $CDCl_3$.

balance	Slope	Intercept	ΔG (kcal/mol)	ΔH (kcal/mol)	ΔS (kcal/mol·K)	$-T\Delta S$@25°C (kcal/mol)
7a	334.28 ± 14.81	–0.9029 ± 0.0474	–0.1296 ± 0.05749	–0.6642 ± 0.02943	–0.001794 ± 9.4×10^{-5}	0.5346 ±0.0281
7b	481.98 ±13.72	–1.1565 ±0.0439	–0.2729 ±0.05326	–0.9577 ±0.02726	–0.002298 ±0.000087	0.6848 ±0.0260
7c	170.29 ±40.94	–1.1827 ±0.1566	0.3619 ±0.1741	–0.3384 ±0.0814	–0.00235 ±0.00031	0.7003 ±0.1927
7d	2289 ±152	–6.106 ±0.486	–0.9339 ±0.5898	–4.549 ±0.302	–0.01213 ±0.00097	3.6155 ±0.2878
8a	354.88 ±19.78	–0.9171 ±0.0633	–0.1621 ±0.0768	–0.7051 ±0.0393	–0.001822 ±0.00013	0.5430 ±0.0375
8b	493.38 ±48.74	–0.9515 ±0.1560	–0.4169 ±0.1892	–0.9803 ±0.0969	–0.001891 ±0.00031	0.5634 ±0.0924
8c	285.86 ±76.13	–1.0576 ±0.2436	0.05823 ±0.2955	–0.5680 ±0.1513	–0.00210 ±0.00048	0.6262 ±0.1442
8d	1377.4 ±202.2	–2.7861 ±0.6472	–1.0872 ±0.7850	–2.7369 ±0.4018	–0.00554 ±0.00129	1.6497 ±0.3832
9a	–201.9 ±30.03	–0.7397 ±0.0956	0.8392 ±0.1163	0.4012 ±0.0597	–0.001470 ±0.00019	0.4380 ±0.0566
9b	–230.51 ±14.58	–0.6472 ±0.0466	0.8412 ±0.0565	0.4580 ±0.0290	–0.001286 ±0.000093	0.3832 ±0.0276
9c	–402.54 ±44.85	–0.1040 ±0.1435	0.8614 ±0.1741	0.7998 ±0.0891	–0.00021 ±0.00029	0.0616 ±0.0850
9d	–339.56 ±22.33	–0.3682 ±0.0714	0.8927 ±0.0867	0.6747 ±0.0444	–0.00073 ±0.00014	0.2180 ±0.0423
10a	309.73 ±31.99	–1.0726 ±0.1023	0.01968 ±0.12414	–0.6154 ±0.06356	–0.002131 ±0.0002	0.6351 ±0.0606
10b	238.3 ±53.5	–0.9297 ±0.1711	0.07700 ±0.20754	–0.4735 ±0.1062	–0.001847 ±0.00034	0.5505 ±0.1013
10c	284.17 ±17.69	–0.9902 ±0.0566	0.02168 ±0.06866	–0.5646 ±0.0351	–0.00197 ±0.00011	0.5863 ±0.0335
10d	1309.5 ±116.3	–0.2047 ±0.3722	–0.1123 ±0.4515	–2.6019 ±0.2311	–0.00835 ±0.00074	2.4897 ±0.2204

CHAPTER 5

INVESTIGATION OF DEUTERIUM ISOTOPE EFFECT ON ALIPHATIC CH–Π INTERACTIONS

Except for changing the environment and numbers of the interactions as we did in Chapter 3 and Chapter 4, another potentially powerful method for studying the interactions is to use the D/H isotope effects, which has been successfully applied to the study of other non-covalent interactions.[114] The presence of a pronounced D/H isotope effect for the CH–π interactions could be used to verify their formation and to probe their stability trends. The enhanced CH–π interactions of deuterated molecules could also be used to design better pharmaceuticals and asymmetric catalysts.

However, whether hydrogen and deuterium form different strength CH–π interactions remains unclear. Several studies have observed significant deuterium isotope effects: Rebek *et al.*[115,116] and Iwata *et al.*[117] found deuterated species forming stronger interaction within different molecular capsules, and differences on retention times between protic and deuterated species were observed in chromatographic studies.[118,119] Other studies have observed little or no D/H isotope effects for the CH–π interaction.[120,121] A possible reason for these discrepancies is that many of these studies were carried out within the confined environments of molecular capsules, which are very sensitive to small differences in molecular volume. Thus, the observed enhancements in the stability of deuterated guests could be due to their reduced steric interactions arising from their shorter C–D bonds, as opposed to stronger attractive CD–π interactions.

Therefore, the goal of this Chapter was to study the D/H isotope effect in CH–π interactions within less constrained environments in which steric interactions were minimized. An experimental approach was carried out using our molecular balance system (Figure 5.1), and only minor differences between CD–π and CH–π interactions was found. The computational approach was also carried out in collaboration with Dr. C. David Sherrill's group. They applied density functional theory (DFT) to a methane–benzene system, and the results also suggested the same conclusion.

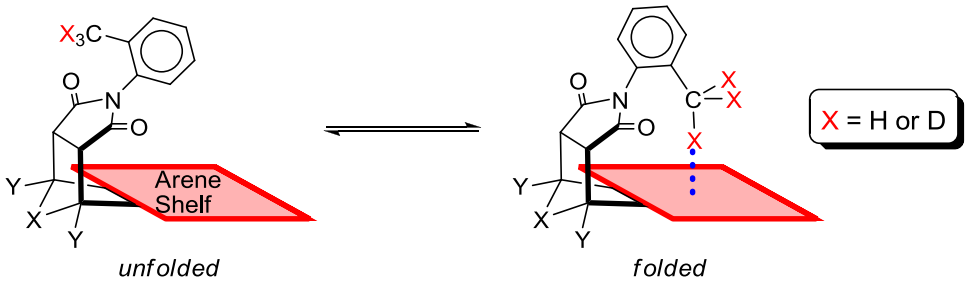

Figure 5.1: Schematic representation of the *folded*/*unfolded* conformational equilibrium of the molecular balances that can be used to measure changes in the strength of the intramolecular CH–π interactions in the folded conformer.

5.1 DESIGNS OF BALANCES

First, the differences in CH–π and CD–π interactions were experimentally studied using molecular balances **12–15** (Figure 5.2). These balances provide a range of different CH–π interaction geometries and environments, affording a comprehensive study of the interaction. For example, balances **12** and **13** have large phenanthrene aromatic shelves, whereas balances **14** and **15** have smaller benzene shelves. The geometry and steric interactions of the *ortho*-methyl group are attenuated by subtle differences in the bicyclic framework. Specifically, the different bridges (Z in Figure 5.1 = –CO–, –O–, –*m*-C_6H_4–) on the backside of the balances attenuate the distance and steric interactions between the methyl group and aromatic shelf.[122] Finally, balance **16** without aromatic shelf served as

controls which cannot form a CH–π interaction.

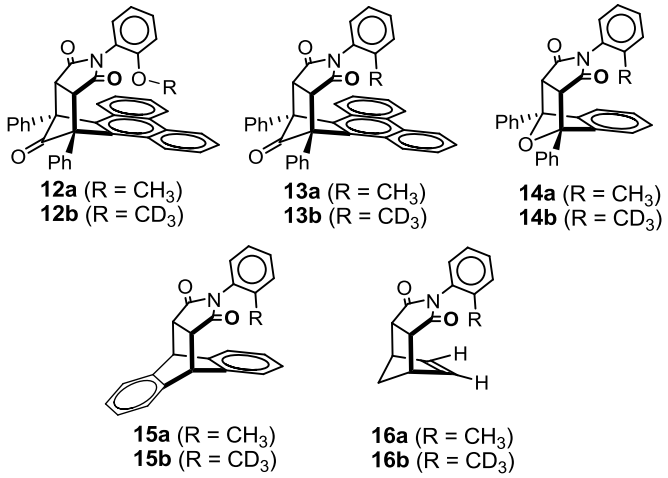

Figure 5.2: *Folded* conformers of protic and deuterated molecular balances **12**–**15** that were designed to form intramolecular CH–π interactions and control balance **16**.

Noticeable, the balances **12**–**15** form intramolecular CH–π interactions within relatively open environments with a minimum of steric interactions. Therefore, these model systems are less susceptible to repulsive interactions that could mask and attenuate the CH–π interactions of interest.

Balances **12**–**16** were all synthesized via similar modular routes, which allowed the preparation of protic (**12a**–**16a**) and deuterated (**12b**–**16b**) balances.[74,75] Protic balances **12a**, **13a**, **14a** and **16a** are same structures as balances **1a**, **7a**, **9a** and **10a** in Chapter 3 and 4. Balance **15a** had been previously described in the literature was used to study CH–π interactions.[81,113,123]

5.2 SOLID-STATE STRUCTURES

The solid-state structures of balances **13a**–**16a** by X–ray structure analyses was shown in Figure 5.3. The structures of balances **13a**, **14a** and **16a** have been discussed in Chapter 4 (as **7a**, **9a** and **10a**), and the crystal structure of balance **15a** was from the literature.[122] X-ray structure analysis confirms the existence of well-defined

intramolecular CH–π interactions in balances **13a**–**15a** (Figure 5.3, a–c). It also confirmed the absence of an intramolecular CH–π interaction in the *folded* conformation in the control balance **16a** (Figure 5.3, d).

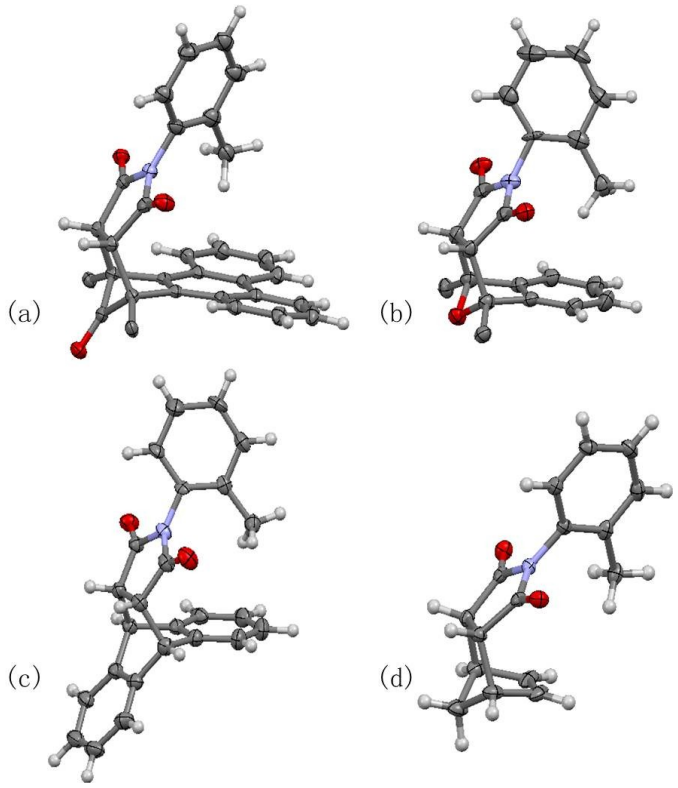

Figure 5.3: X–ray structures of the *folded* conformers of (a) **13a**, (b) **14a**, (c) **15a**, and (d) **16a**. The bridgehead phenyl groups in **13a** and **14a** were partially hidden for better viewing clarity. The *unfolded* conformers were also present in the crystal structures of **14a**, **15a**, and **16a** but are not shown.

Although balances **13a**–**15a** all formed intramolecular CH–π interactions, the number (one hydrogen versus two), geometry, and distances of these interactions varied considerably. The structural parameters (*d, θ,* and *α*) used to compare the balances are shown in Figure 5.4, and a comparison of the measurements from the crystal structures of the balances are shown in Table 5.2. The "hinge" angle (*θ*) defined by the succinimide and arene planes provides a measure of how closely the *ortho*-methyl group is held against the arene shelf. For example, balance **14a** has the smallest *θ*, fixing the *ortho*-

methyl tightly against the arene shelf. This strain is evident from the *N*–aryl group being pushed upward out of the succinimide plane (α = +21°). Balances **13a** and **15a**, in contrast, have larger θ values, positioning their *ortho*-methyl groups at more optimal distances with less strain (α = +5° and +4°).

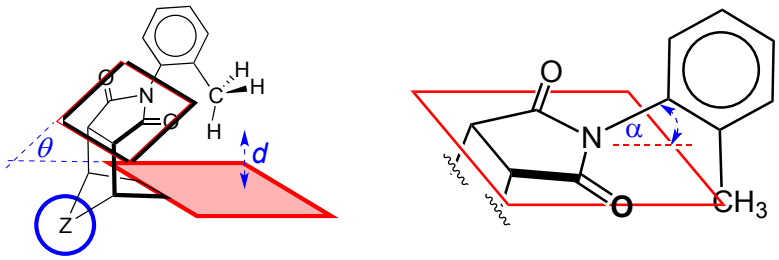

Figure 5.4: Definitions of the distance and angular measurements used to characterize balances **13a**–**16a**.

Table 5.1: The *d*, θ and α measured from the crystal structures of balances **13a**–**16a**.

balance	*d* (Å)	θ	α
13a	2.68	58°	5°
14a[a]	2.69	52°	21°
15a	2.61	58°	4°
16a	–	–	2°

[a] The d, θ, and α values were averages from the three unique folded conformers present in the unit cell of 14a.

The lager hinge angle θ of balances **14** with benzene shelf indicate that balances with the same benzene shelf and O bridge-atom may not be a good control for balances **13**. This also explains the observation that balances with the same framework as balances **14** always prefer the *unfolded* conformation. Thus, some comparisons made in Chapters **3** and **4** involving this series of balances may not be appropriate. In this chapter, they are only being considered as a different environment for the formation of CH–π interactions. The X–ray structure of deuterated balance **13b** was also examined and compared with its protic counterpart, **13a**. The structures were nearly identical.

5.3 COMPARISON OF FOLDING ENERGIES OF CH_3 AND CD_3 BALANCES

Next, the strengths of the CH–π interactions in balances **12–15** were measured in solution by ^{1}H NMR. In each case, separate peaks for the *folded* and *unfolded* conformers were observed at room temperatures, enabling facile measurement of the *folded*/*unfolded* ratios. In particular, large upfield shifts were observed for the *ortho*-methyl groups in the *folded* conformers, which are consistent with the formation of CH–π interactions. The *folded* methyl singlets of **12a**–**15a** were shifted upfield by –1.55 ppm, –2.08 ppm, –1.01 ppm and –1.04 ppm, respectively, compared with the peaks for the *unfolded* methyl groups. By comparison, control balance **16a**, which cannot form a CH–π interaction, had almost identical chemical shifts for the *folded* and *unfolded* methyl protons ($\Delta\delta$ = –0.03 ppm). The ^{1}H NMR spectra of the deuterated balances were identical to their protic counterparts except for the absence of the deuterated *ortho*–methyl peaks.

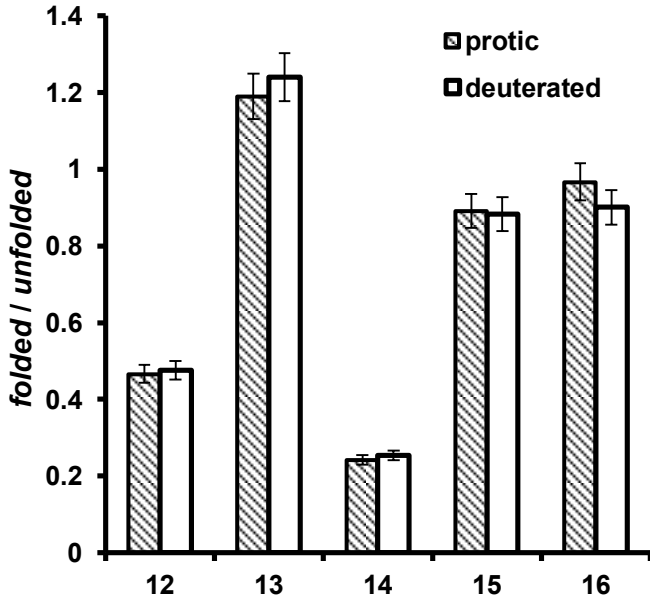

Figure 5.5: Comparison of the *folded*/*unfolded* ratios of balances **12**–**16** in $CDCl_3$ at 25°C measured by integration of the ^{1}H NMR spectra with a ±5% integration error.[77-79]

Comparison of the *folded*/*unfolded* ratios for the protic balances showed the differences in their CH–π interactions (Figure 5.5). These ratios were measured from the integration of the singlets for the succinimide protons in the ^{1}H NMR spectra. Integration of *ortho*–methyl groups also gave similar *folded*/*unfolded* ratios, but they were not used for comparisons because of the absence of this peak in the deuterated balances. As expected, control balances **16** had a nearly 1:1 *folded*/*unfolded* ratio, suggesting that differences in dipole and solvation of the conformers are not biasing the *folded*/*unfolded* ratios. Despite the presence of intramolecular CH–π interactions in balances **12–15**, only balance **13** displayed a preference for the *folded* conformer. We attribute this to the presence of repulsive interaction. The rigid bicyclic framework positions the methyl group slightly too close to the arene shelf, resulting in destabilizing steric interactions. As predicted from the crystal structures, the repulsive interaction is most evident in **14a**, which also has the lowest *folded*/*unfolded* ratio. The repulsive interactions complicate the measurement of the absolute strengths of the CH–π interactions. However, they do not diminish the utility of these balances in measuring the isotope effects of the CH–π interaction.

Differences in the strengths of intramolecular CH–π and CD–π interactions were assessed by comparison of the *folded*/*unfolded* ratios and the corresponding folding energies (Table 5.2). The folding energies for protic and deuterated balances **12–15** were almost identical. The differences ($\Delta\Delta G_{H-D}$) were very small and were within the error of the analysis (± 0.03 kcal/mol), which was calculated based on a conservative estimate of ± 5% for the ^{1}H NMR integration error.[18] The folding energies of the protic and deuterated balances were also compared in acetone–d_6 (see experimental section). Again,

nearly identical folding energies were observed with even smaller errors.

Table 5.2: The folding energies of protic (ΔG_H) and deuterated (ΔG_D) balances **12**–**16** in $CDCl_3$ at 25 °C.

balance	ΔG_H (kcal/mol)	ΔG_D (kcal/mol)	$\Delta\Delta G_{H-D}$ (kcal/mol)
12	0.45	0.44	+0.01
13	–0.10	–0.13	+0.03
14[a]	0.84	0.81	+0.03
15	0.07	0.07	0.00
16	0.02	0.06	–0.04

5.4 THERMODYNAMIC EXPERIMENT

To confirm the above single point measurements, more comprehensive multipoint van't Hoff analyses were carried out. The *folded*/*unfolded* ratios for balances **12–15** were measured over a range of temperatures (25°C to 55°C) in $CDCl_3$, and the ΔG_{fold} were calculated from the measured ΔH and ΔS values (Table 5.3). This study led to the same conclusion that the small differences in the ΔG_{fold} values of the protic and deuterated balances were well within the error of the analysis.

Table 5.3: Comparison of calculated ΔG_{fold} values between protic and deuterated balances **12**–**15** in $CDCl_3$ and acetone–d_6 at 25 °C with errors.

balance	ΔG_H in $CDCl_3$ (kcal/mol)	ΔG_D in $CDCl_3$ (kcal/mol)	ΔG_H in acetone–d_6 (kcal/mol)	ΔG_H in acetone–d_6 (kcal/mol)
12	0.44 ± 0.15	0.43 ± 0.12	0.14 ± 0.32	0.14 ± 0.09
13	–0.12 ± 0.05	–0.14 ± 0.11	–0.23 ± 0.16	–0.26 ± 0.37
14	0.83 ± 0.28	0.80 ± 0.19	0.66 ± 0.07	0.65 ± 0.07
15	0.07 ± 0.14	0.08 ± 0.38	–0.05 ± 0.26	–0.06 ± 0.10

5.5 CONCLUSION

The above experimental studies found only small differences in the strengths of the CH–π and CD–π interactions that were smaller than the experimental error of the analyses. These results were corroborated by theoretical calculations that compared the interaction energies of methane and benzene.[76] Therefore, we concluded that there was either no deuterium isotope effect for the CH–π interaction or that the effect was too

small to be accurately measured by our model system. Another explanation is that the isotope effects for the attractive CH–π and repulsive steric interactions perfectly cancel out in all three balances. However, this possibility was seems unlikely. First, the attractive and repulsive isotope effects would have to balance perfectly for all three models systems, despite their differences in geometries and conformational constraints. Second, the repulsive steric interactions in balances **12–15** are very small (<1.0 kcal/mol) and do not change significantly with small differences in the lengths of the C–D and C–H bonds. A third reason that this explanation is unlikely is because it requires the attractive CD-π interaction to be weaker than the CH-π interaction. However, all reports that observed deuterium isotope effects for the CH-π interaction found the opposite trend.

Thus, previous reports of isotope effects were probably due to other factors such as the size difference between CH_3 and CD_3 groups placed within more confined environments, rather than an attenuation of the CH–π interaction.[118,119] This steric hypothesis was supported by the theoretical calculations, which showed that differences in energy arose when the interacting groups were brought closer than the optimal CH–π interaction distance. While the lack of an isotope effect eliminates the possibility of using deuteration to enhance the CH–π interaction, it validates the use of deuteration for spectroscopic and labeling purposes, as this introduces a minimal perturbation of the system.[124] Results obtained in this Chapter have been published[76] and were reprinted with permission (Copyright © 2012, American Chemical Society).

5.6 EXPERIMENTAL SECTION

NMR spectra were recorded on Varian 300 MHz and 400 MHz spectrometers. Chemical shifts are reported in ppm (δ) referenced to TMS. All chemicals were

purchased from commercial suppliers and used as received unless otherwise specified. Flash chromatography was carried out using silica gel from Sorbent Technologies (60 Å, 200–400 mesh). Thin layer chromatography (TLC) was performed using pre-coated TLC plates (Merck pre-coated 0.25 mm silica gel 60 F254 plates).

5.6.1 Synthesis and Spectrums

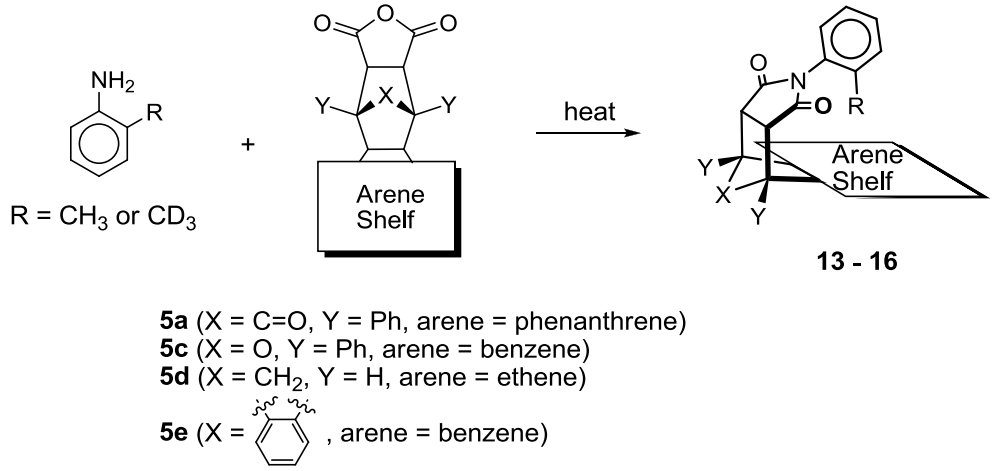

Figure 5.6: Overview of synthesis of balances **13–16** via condensation reactions between deuterated or protic *o*-toluidine and anhydride **5**.

General procedure for preparing molecular balances 12–16

For the condensation reaction, the corresponding anhydride and aniline were dissolved in acetic acid, and the mixture was heated at reflux for 24 h. The solvent was then removed by rotary evaporation. The residue was dissolved in 25 mL EtOAc, washed once with 50 mL saturated sodium bicarbonate, and twice with 50 mL water. The solvent of organic layer was then removed under vacuum, and the crude product was purified via flash chromatography using silica gel ($MeOH/CH_2Cl_2$, v/v = 1/99). The synthesis of balances **12a**, **13a**, **14a** and **16a** has been described in previous chapters as compound **1a** (Chapter 3), **7a**, **9a**, and **10a** (Chapter 4).

Preparation of *o*-Anisidine-d_3

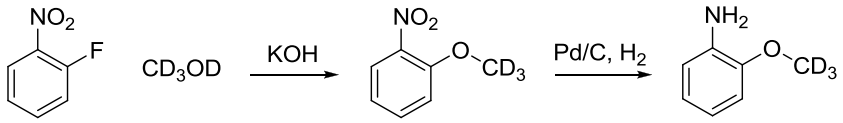

The corresponding deuterated nitrobenzene was synthesized first. To the stirring solution of potassium hydroxide (0.080 g, 1.42 mmol) in THF (3 mL), methanol-d_4 (0.100 mL, 2.49 mmol) and 1-fluro-2-nitrobenzene (0.100 g, 0.709 mmol) was added drop wise. The mixture was stirred for 24 h in room temperature. The solvent was then removed under vacuum, and the residue was dissolved with 30 mL ethyl acetate and washed with 50 mL water for 3 times. The solvent was dried to get deuterated 1-methoxy-2-nitrobenzene as yellow liquid (0.131 g, 0.84 mmol, > 95% yield). ^{1}H NMR (300 MHz, $CDCl_3$) δ 7.84 (dd, J = 7.84 Hz, J = 0.94 Hz, 1 H), 7.54 (dt, J = 7.52 Hz, 1.25 Hz, 1 H), 7.08 (d, J = 8.46 Hz, 1 H), 7.03 (t, J = 7.52 Hz, 1 H).

The nitrobenzene was then reduced via catalyzed hydrogenation with Pd/C and H_2. The deuterated 1-methoxy-2-nitrobenzene (0.131 g, 0.84 mmol) was dissolved in ethanol (20 mL) in a pressure vessel, and 20 mg of Pd/C (10% wt) was added. The vessel was pressurized at 40 psi with hydrogen gas and was stirred for 2 h. The resulting mixture was filtered through celite and the solvent was removed by rotary evaporation to afford the *o*-anisidine-d_3 as brown oil (0.130 g, > 95% yield). ^{1}H NMR (300 MHz, $CDCl_3$) δ 6.90–6.58 (m, 4 H), 3.72 (brs, 2 H).

Preparation of balance **12b**:

Anhydride **5a** (0.50 g, 1.0 mmol) and *o*-anisidine-d_3 (0.19 g, 1.5 mmol) were used as reactants, and 10 mL acetic acid was used as solvent. Purified by flash chromatography using silica gel (MeOH/CH_2Cl_2, v/v = 1/99). White solid, 0.49 g, 0.84

mmol, 84% yield. ^{1}H NMR (400 MHz, CDCl3) δ ^{1}H NMR (400 MHz, CDCl3) δ 8.64–8.76 (m, 2 H major, 2 H minor), 8.42 (d, *J* = 6.7 Hz, 2 H minor), 8.38 (d, *J* = 6.8 Hz, 2 H major), 7.09–7.80 (m, 13 H major, 13 H minor), 7.04 (td, *J* = 8.1 Hz, *J* = 2.5 Hz, 2 H major), 6.96 (dd, *J* = 7.8 Hz, *J* = 1.7 Hz, 2 H minor), 6.82 (td, *J* = 7.5 Hz, *J* = 0.9 Hz, 2 H minor), 6.74 (d, *J* = 8.6 Hz, 1 H major), 6.44 (dd, *J* = 8.5 Hz, *J* = 1.0 Hz, 1 H minor), 6.28 (td, *J* = 7.7 Hz, *J* = 1.4 Hz, 1 H major), 4.64 (s, 2 H major), 4.62 (s, 2 H minor), 4.54 (dd, *J* = 7.8 Hz, *J* = 1.7 Hz, 1 H major).

Preparation of balance **13b**:

Anhydride **5a** (0.10 g, 0.21 mmol) and *o*-toluidine-d_3 (0.034 g, 0.31 mmol) were reacted in 5 mL acetic acid. After work up steps and purification, balance **13b** was obtained as light yellow solid (0.098 g, 0.17 mmol, 81% yield). ^{1}H NMR (400 MHz, $CDCl_3$) δ 8.71 (d, *J* = 8.6 Hz, 2 H minor), 8.65 (d, *J* = 8.6 Hz, 2 H major), 8.37 (t, *J* = 8.5 Hz, 2 H), 7.80–6.86 (m, 17 H major, 16 H minor), 6.72 (d, *J* = 7.3 Hz, 1 H major), 6.46 (t, *J* = 7.3 Hz, 1 H minor), 4.64 (s, 2 H), 4.34 (d, *J* = 7.3 Hz, 1 H minor). ^{13}C NMR (100 MHz, $CDCl_3$) δ 196.94, 195.94, 173.56, 173.28, 135.79, 133.80, 133.75, 133.71, 133.50, 131.73, 131.24, 131.01, 130.95, 130.74, 130.56, 130.20, 129.41, 129.39, 129.27, 129.17, 129.14, 128.69, 128.60, 128.50, 128.46, 128.08, 127.84, 127.60, 127.41, 127.30, 127.19, 126.92, 126.76, 126.55, 126.51, 126.48, 126.33, 126.07, 125.95, 123.02, 122.99, 122.96, 63.62, 63.60, 45.35, 44.90. HRMS (EI) calculated for $C_{40}H_{24}D_3NO_3$: 572.2179; obs: 572.2181.

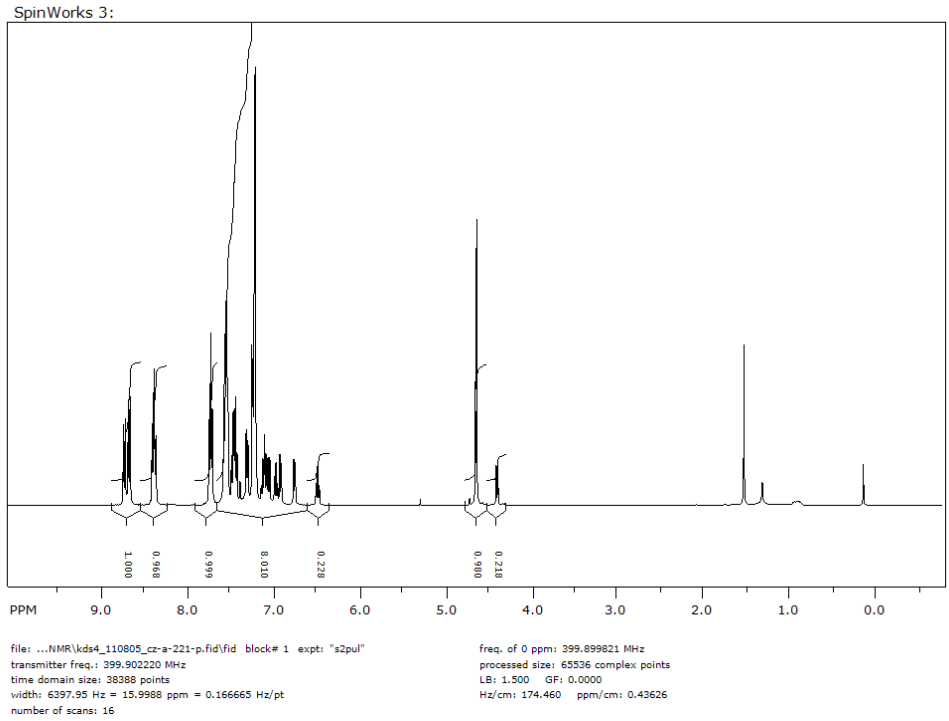

Figure 5.7: ^{1}H NMR spectrum of balance **13b** ($CDCl_3$, 400 MHz).

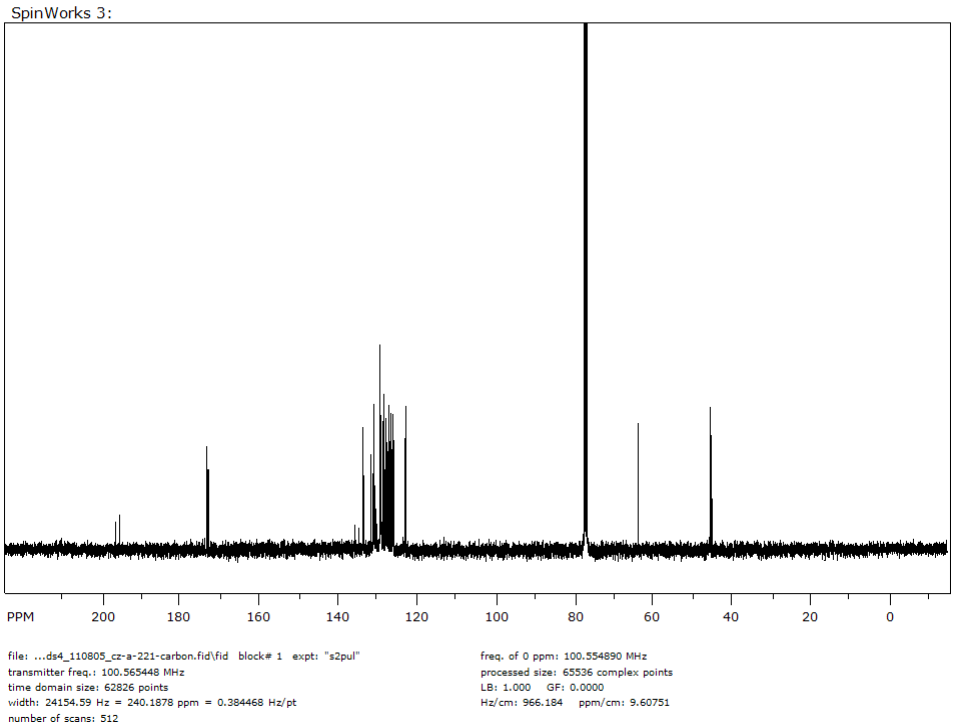

Figure 5.8: ^{13}C NMR spectrum of balance **13b** ($CDCl_3$, 100 MHz).

Preparation of balance **14b**:

Anhydride **5c** (0.050 g, 0.14 mmol) and *o*-toluidine-d_3 (0.022 g, 0.20 mmol) were reacted to give balance **14b** as light yellow solid (0.054 g, 0.12 mmol, 86% yield) after work up and purification. ^{1}H NMR (400 MHz, $CDCl_3$) δ 8.00–8.12 (m, 2 H major, 2 H minor), 6.92–7.60 (m, 15 H major, 16 H minor), 5.51 (d, J = 7.8 Hz, 1 H major), 4.33 (s, 2 H minor), 4.30 (s, 2 H major). ^{13}C NMR (400 MHz, $CDCl_3$) δ 173.26, 144.29, 136.37, 135.45, 130.78, 130.39, 128.71, 128.67, 128.62, 128.34, 128.25, 121.20, 121.03, 90.57, 54.63, 54.59. HRMS (EI) calculated for $C_{31}H_{20}D_3NO_3$: 460.1866; obs: 460.1871.

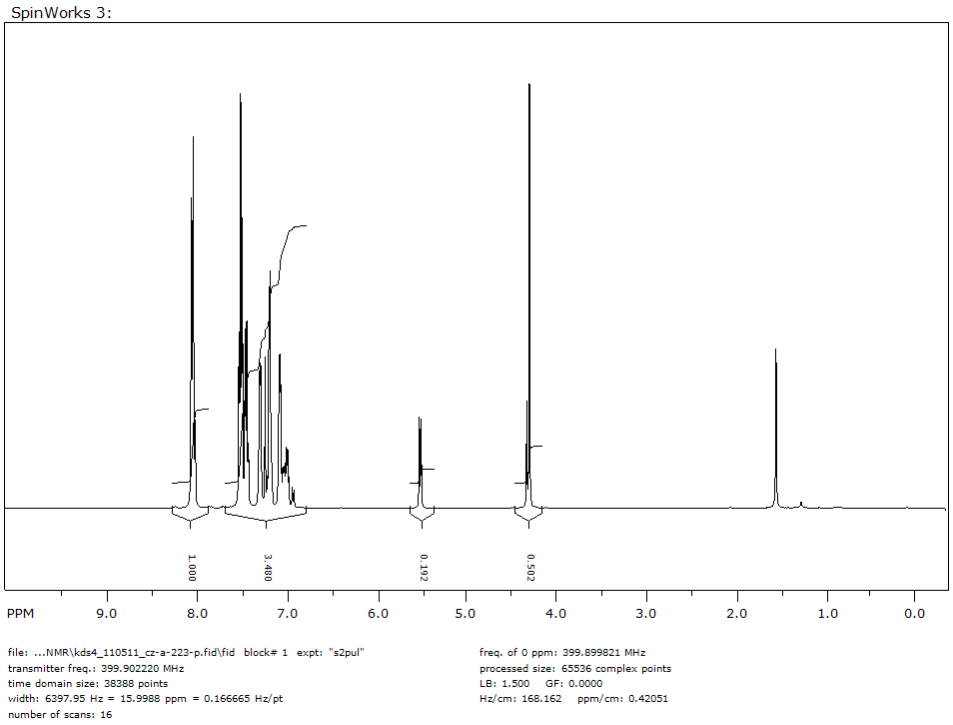

Figure 5.9: ^{1}H NMR spectrum of balance **14b** ($CDCl_3$, 400 MHz).

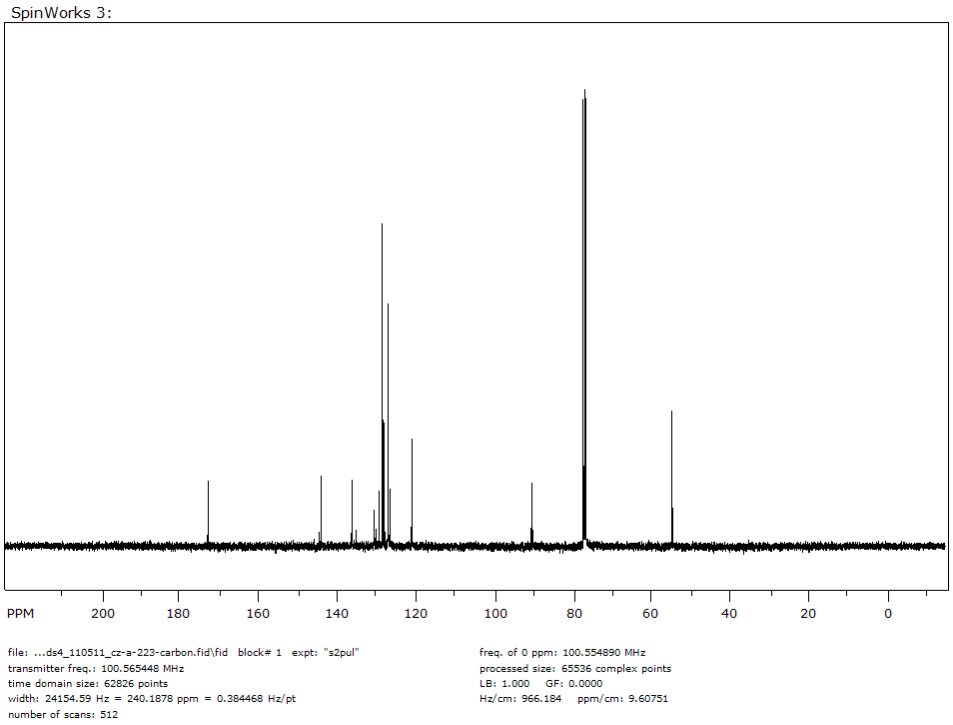

Figure 5.10: ^{13}C NMR spectrum of balance **14b** ($CDCl_3$, 100 MHz).

Preparation of anhydride **5e**:

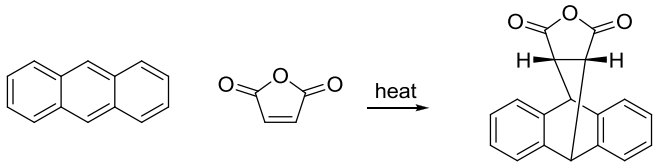

Anhydride **5e** was synthesized via the description in reference:[125] the mixture of anthracene (0.10 g, 0.56 mmol), maleic anhydride (0.06 g, 0.56 mmol) and 3 mL xylene were heated to reflux for 2 h under stirring. The reaction mixture was then cooled down to room temperature. After crystallized under ice-water bath for 30 min, the product was separated by filtration and washed with several drops of cold ethanol. The pure product was then obtained as white crystal (0.12 g, 0.43 mmol, 75% yield). ^1H NMR (400 MHz, $CDCl_3$) δ 7.52 (m, 2 H), 7.36 (m, 2 H), 7.17 (m, 4 H), 4.85 (s, 2 H), 3.55 (s, 2 H).

Preparation of balance **15a**:

Anhydride **5e** (0.050 g, 0.18 mmol) was reacted with *o*-toluidine (0.023 g, 0.22 mmol) to give balance **15a** as white solid (0.048 g, 0.13 mmol, 73% yield) after work up steps and purification. ^{1}H NMR (400 MHz, $CDCl_3$) δ 6.79–7.43 (m, 12 H major, 11 H minor), 5.43 (d, J = 7.6 Hz, 1 H minor), 4.76–4.88 (m, 2 H), 3.29–3.41 (m, 2 H), 1.98 (s, 3 H major), 0.97 (s, 3 H minor). HRMS (EI) calculated for $C_{25}H_{19}NO_2$: 365.1416; obs: 365.1411.

Preparation of balance **15b**:

Anhydride **5e** (0.033 g, 0.12 mmol) and *o*-toluidine-d_3 (0.020 g, 0.18 mmol) were heated to reflux in 3 mL acetic acid to produce balance 3b as white solid (0.037 g, 0.10 mmol, 83% yield) after purification. ^{1}H NMR (400 MHz, $CDCl_3$) δ 6.79–7.43 (m, 12 H major, 11 H minor), 5.43 (d, J = 7.6 Hz, 1 H minor), 4.77–4.88 (m, 2 H), 3.28–3.40 (m, 2 H). ^{13}C NMR (100 MHz, $CDCl_3$) δ 176.03, 175.92, 141.94, 141.30, 139.27, 138.85, 130.73, 129.44, 127.72, 127.37, 127.28, 127.18, 126.85, 126.75, 126.62, 125.48, 125.24, 124.34, 124.22, 47.18, 47.17, 45.85, 45.34. HRMS (EI) calculated for $C_{25}H_{16}D_3NO_2$: 368.1604; obs: 368.1604.

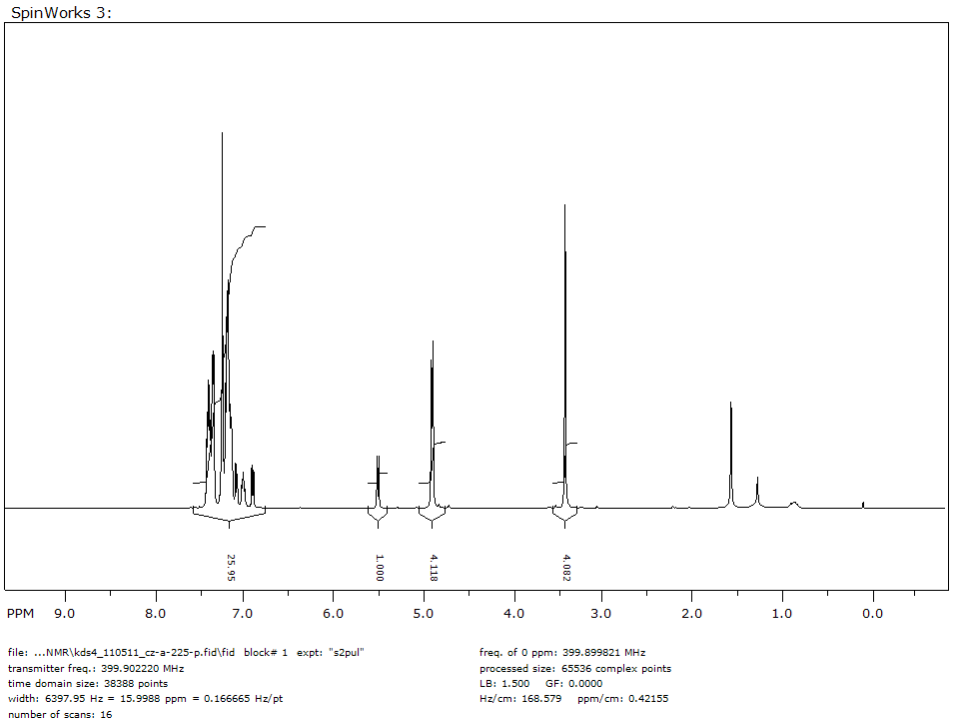

Figure 5.11: ^{1}H NMR spectrum of balance **15b** ($CDCl_3$, 400 MHz).

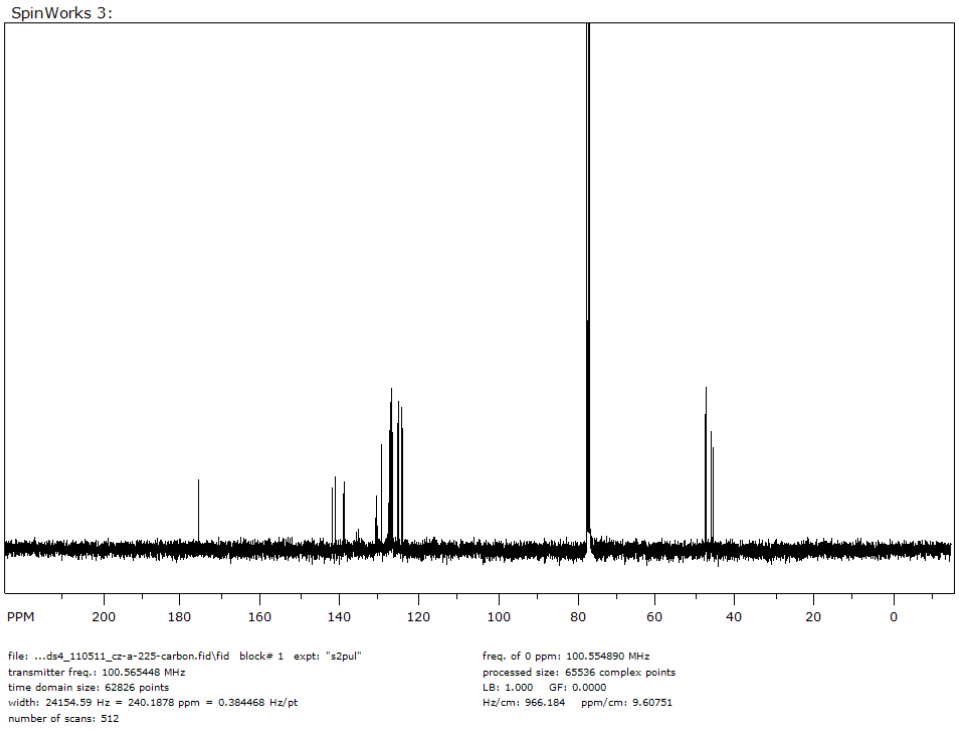

Figure 5.12: ^{13}C NMR spectrum of balance **15b** ($CDCl_3$, 100 MHz).

Preparation of balance **16b**:

cis-5-Norbornene-*endo*-2,3-dicarboxylic anhydride **5d** (0.031 g, 0.19 mmol) and *o*-toluidine-d_3 (0.025 g, 0.23 mmol) were heated to reflux in 3 mL acetic acid for 24 h. The solvent was removed under vacuum and the reaction mixture was heated in oven (120 °C) for another 12 h. Then balance 4b was obtained as white solid (0.038 g, 0.15 mmol, 78% yield). ^{1}H NMR (400 MHz, $CDCl_3$) δ 7.17–7.35 (m, 3 H), 6.82–7.02 (m, 1 H), 6.30 (t, J = 1.6 Hz, 2 H), 3.38–3.56 (m, 4 H), 1.75–1.85 (m, 1 H), 1.56–1.67 (m, 1 H). ^{13}C NMR (100 MHz, $CDCl_3$) δ 176.85, 176.56, 135.28, 134.62, 131.18, 131.03, 129.39, 129.33, 128.23, 127.82, 126.84, 126.78, 52.74, 52.33, 46.78, 45.81, 45.47, 45.17. HRMS (EI) calculated for $C_{16}H_{12}D_3NO_2$: 256.1290; obs: 256.1291.

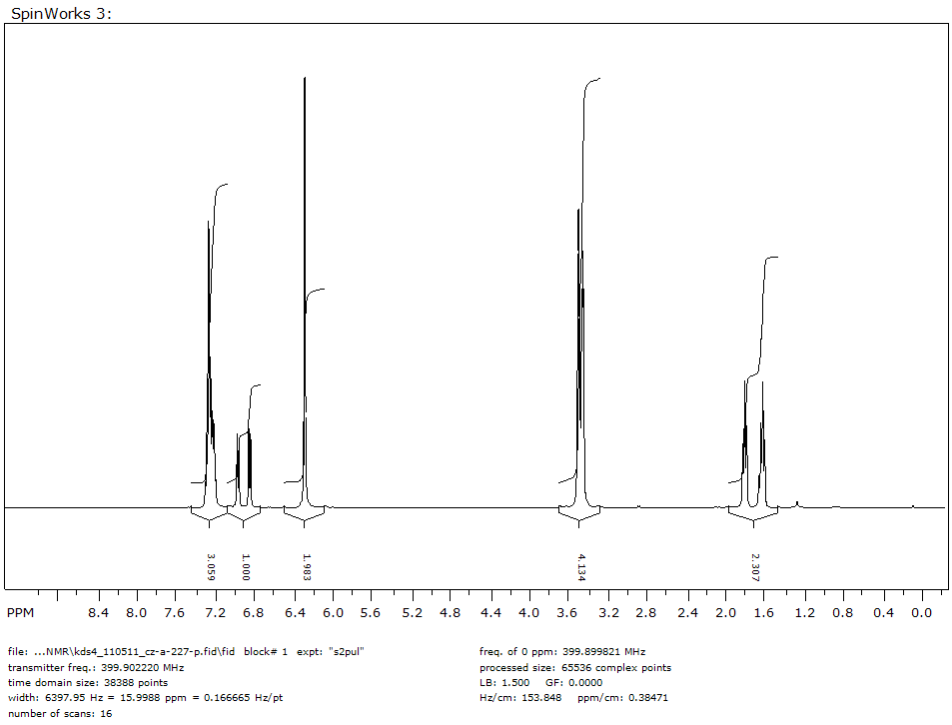

Figure 5.13: ^{1}H NMR spectrum of balance **16b** ($CDCl_3$, 400 MHz).

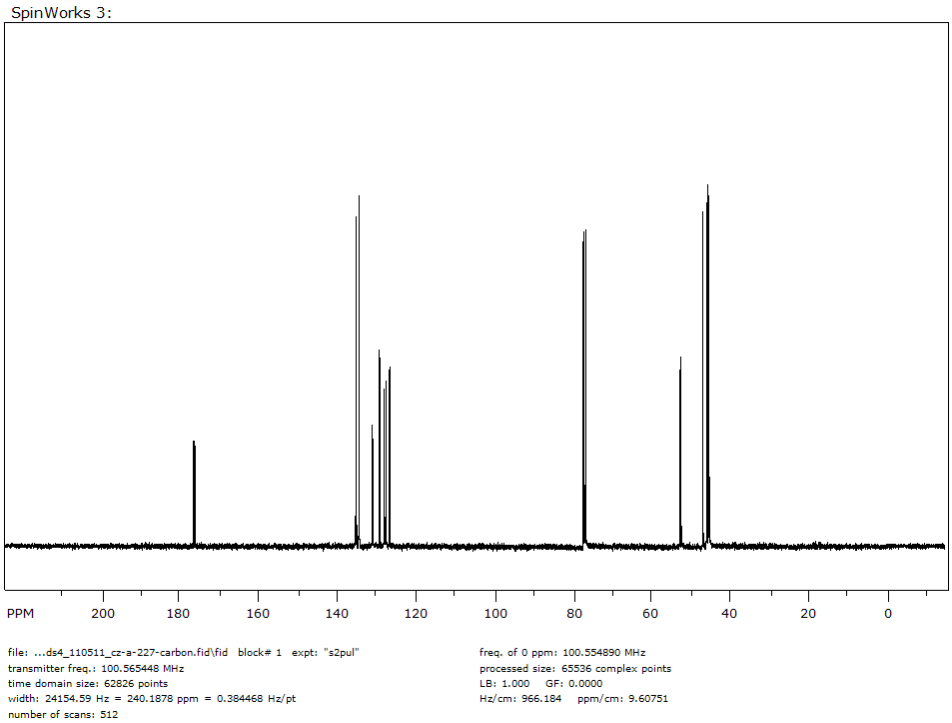

Figure 5.14: ^{13}C NMR spectrum of balance **16b** ($CDCl_3$, 100 MHz).

5.6.2 Folding Energies in Acetone-d_6

The folding energies of balances **12**–**16** in acetone-d_6 were also calculated based on the same qualification method, and the results are listed in Table S5.

Table 5.4: Comparison of folding energies of protic and deuterated balances 12–16 in acetone-d_6 at 25 °C.

balance	ΔG_H (kcal/mol)	ΔG_D (kcal/mol)	$\Delta\Delta G$ (kcal/mol)
12	0.13	0.14	–0.01
13	0.24	0.24	+0.00
14	–0.64	–0.64	+0.00
15	–0.05	–0.06	+0.01
16	0.01	–0.01	+0.02

5.6.3 Van't Hoff Plots

The van't Hoff plots of the ln(*folded*/*unfolded*) versus the reciprocal of temperature are linear. Curve-fits of these lines have slopes corresponding to $-\Delta H/R$ and y intercepts of $\Delta S/R$. The full spectra were acquired at 5°C intervals and the *folded* and *unfolded* ratio were obtained via spectral deconvolution using VNMRJ software "fitspec" command at corresponding areas on ^{1}H NMR spectra.

Table 5.5: *Folded*/*unfolded* ratios obtained from the integrations of corresponding peaks in variable temperature ^{1}H NMR spectrums of balances **13a** and **13b** in $CDCl_3$.

		balance **13a**		balance **13b**	
T (°C)	1/Temp (K^{-1})	F/UF	ln(F/UF)	F/UF	ln(F/UF)
25	0.003356	1.23	0.209	1.25	0.226
30	0.003300	1.20	0.186	1.23	0.207
35	0.003247	1.17	0.161	1.21	0.192
40	0.003195	1.15	0.140	1.20	0.183
45	0.003145	1.12	0.113	1.17	0.157
50	0.003096	1.11	0.104	1.13	0.125
55	0.003049	1.09	0.083	1.12	0.116

Table 5.6: *Folded*/*unfolded* ratios obtained from the integrations of corresponding peaks in variable temperature ^{1}H NMR spectrums of balances **13a** and **13b** in acetone-d_6.

		balance **13a**		balance **13b**	
T (°C)	1/Temp (K^{-1})	F/UF	ln(F/UF)	F/UF	ln(F/UF)
25	0.003356	1.49	0.401	1.49	0.399
30	0.003300	1.41	0.342	1.45	0.369
35	0.003247	1.41	0.345	1.40	0.335
40	0.003195	1.36	0.309	1.43	0.355
45	0.003145	1.33	0.286	1.33	0.286
50	0.003096	1.30	0.260	1.30	0.261
55	0.003049	1.27	0.236	1.24	0.211

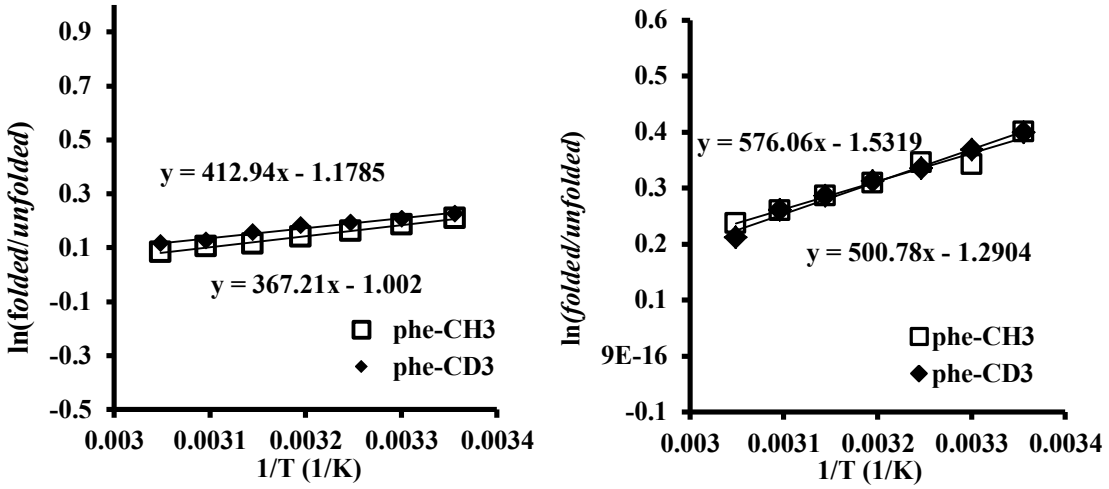

Figure 5.15: The van't Hoff plots of balances **13a** and **13b** in $CDCl_3$ and acetone-d_6.

Table 5.7: *Folded*/*unfolded* ratios obtained from the integrations of corresponding peaks in variable temperature ^{1}H NMR spectrums of balances **14a** and **14b** in $CDCl_3$.

		balance **14a**		balance **14b**	
T (°C)	1/Temp (K^{-1})	F/UF	ln(F/UF)	F/UF	ln(F/UF)
25	0.003356	0.242	–1.42	0.254	–1.37
30	0.003300	0.257	–1.36	0.261	–1.34
35	0.003247	0.249	–1.39		
40	0.003195	0.248	–1.40	0.269	–1.31
45	0.003145	0.255	–1.37	0.268	–1.32
50	0.003096	0.256	–1.36	0.264	–1.33
55	0.003049	0.257	–1.36	0.270	–1.31

Table 5.8: *Folded*/*unfolded* ratios obtained from the integrations of corresponding peaks in variable temperature ^{1}H NMR spectrums of balances **14a** and **14b** in acetone-d_6.

		balance **14a**		balance **14b**	
T (°C)	1/Temp (K^{-1})	F/UF	ln(F/UF)	F/UF	ln(F/UF)
25	0.003356	0.333	–1.10	0.335	–1.09
30	0.003300	0.328	–1.11	0.327	–1.12
35	0.003247	0.330	–1.11	0.336	–1.09
40	0.003195	0.333	–1.10	0.337	–1.09
45	0.003145	0.333	–1.10	0.337	–1.09
50	0.003096	0.335	–1.09	0.337	–1.09
55	0.003049	0.340	–1.08	0.341	–1.07

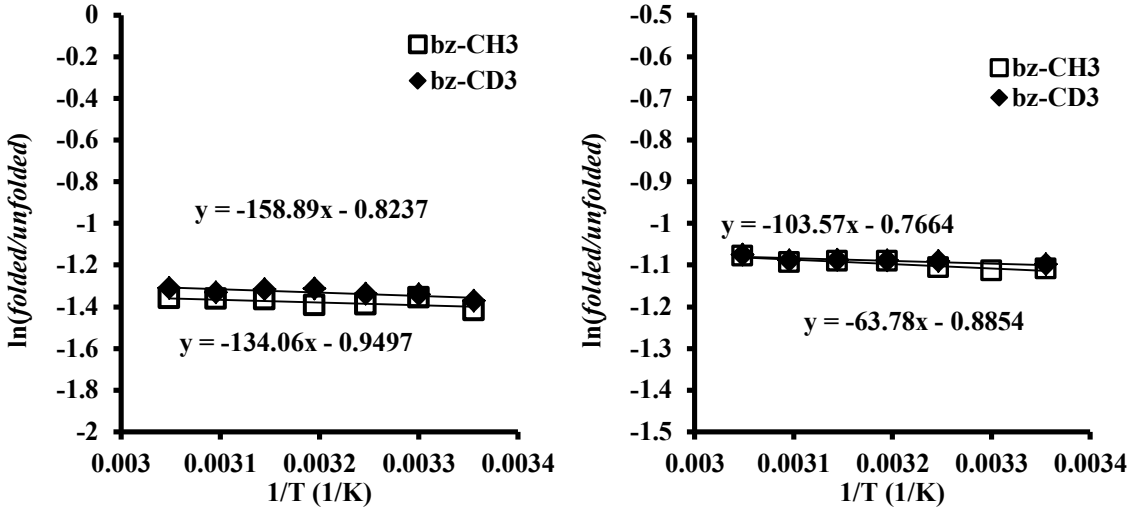

Figure 5.16: The van't Hoff plots of balances **14a** and **14b** in $CDCl_3$ and acetone-d_6.

Table 5.9: *Folded*/*unfolded* ratios obtained from the integrations of corresponding peaks in variable temperature ^{1}H NMR spectrums of balances **15a** and **15b** in $CDCl_3$.

		balance **15a**		balance **15b**	
T (°C)	1/Temp (K^{-1})	F/UF	ln(F/UF)	F/UF	ln(F/UF)
25	0.003356	0.891	–0.115	0.882	–0.125
30	0.003300	0.872	–0.137	0.857	–0.154
35	0.003247	0.868	–0.142	0.838	–0.177
40	0.003195	0.848	–0.165	0.848	–0.165
45	0.003145	0.840	–0.174	0.804	–0.218
50	0.003096	0.843	–0.171	0.837	–0.178

Table 5.10: *Folded*/*unfolded* ratios obtained from the integrations of corresponding peaks in variable temperature ^{1}H NMR spectrums of balances **15a** and **15b** in acetone-d_6.

		balance **15a**		balance **15b**	
T (°C)	1/Temp (K^{-1})	F/UF	ln(F/UF)	F/UF	ln(F/UF)
25	0.003356	0.915	–0.0884	0.903	–0.102
30	0.003300	0.938	–0.0640	0.932	–0.0704
35	0.003247	0.962	–0.0388	0.948	–0.0535
40	0.003195	0.951	–0.0501	0.950	–0.0513
45	0.003145	0.974	–0.0264	0.961	–0.0399
50	0.003096	0.984	–0.0160	0.977	–0.0231
55	0.003049	1.01	0.00599	0.993	–0.00732

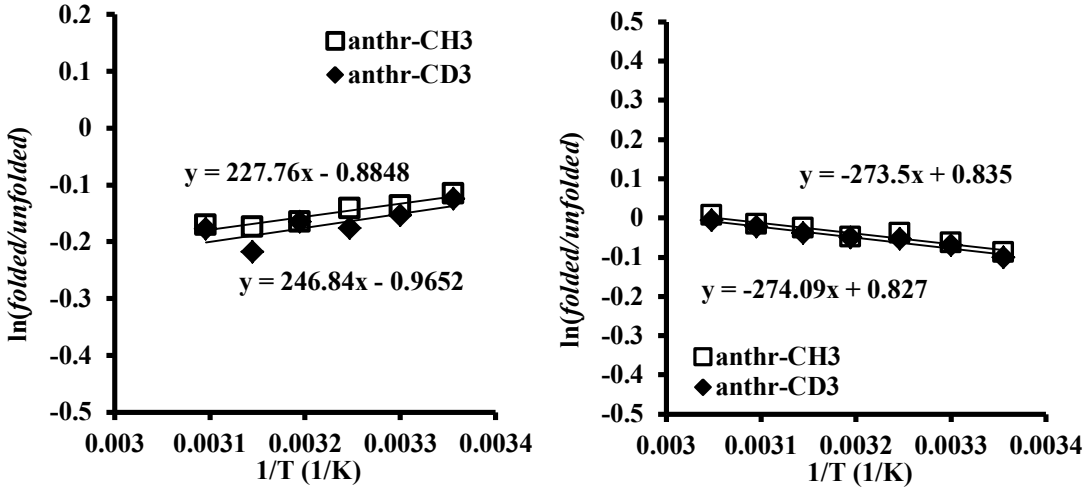

Figure 5.17: The van't Hoff plots of balances **15a** and **15b** in $CDCl_3$ and acetone-d_6.

Table 5.11: *Folded*/*unfolded* ratios obtained from the integrations of corresponding peaks in variable temperature ^{1}H NMR spectrums of balances **16a** and **16b** in $CDCl_3$.

		balance **16a**		balance **16b**	
T (°C)	1/Temp (K^{-1})	F/UF	ln(F/UF)	F/UF	ln(F/UF)
25	0.003356	0.967	–0.0336	0.901	–0.105
30	0.003300	0.951	–0.0507	0.895	–0.111
35	0.003247	0.926	–0.0765	0.890	–0.117
40	0.003195	0.930	–0.0721	0.884	–0.124
45	0.003145	0.915	–0.0891	0.874	–0.135
50	0.003096	0.885	–0.122	0.867	–0.143
55	0.003049	0.878	–0.130	0.863	–0.148

Table 5.12: *Folded*/*unfolded* ratios obtained from the integrations of corresponding peaks in variable temperature ^{1}H NMR spectrums of balances **16a** and **16b** in acetone-d_6.

		balance **16a**		balance **16b**	
T (°C)	1/Temp (K^{-1})	F/UF	ln(F/UF)	F/UF	ln(F/UF)
25	0.003356	1.07	0.0686	1.07	0.0714
30	0.003300	1.14	0.129	1.16	0.147
35	0.003247	1.05	0.0490	1.08	0.0742
40	0.003195	1.03	0.0255	1.08	0.0735
45	0.003145	1.04	0.0403	1.08	0.0793
50	0.003096	0.917	–0.0872	1.06	0.0580
55	0.003049	1.01	0.0110	1.17	0.157

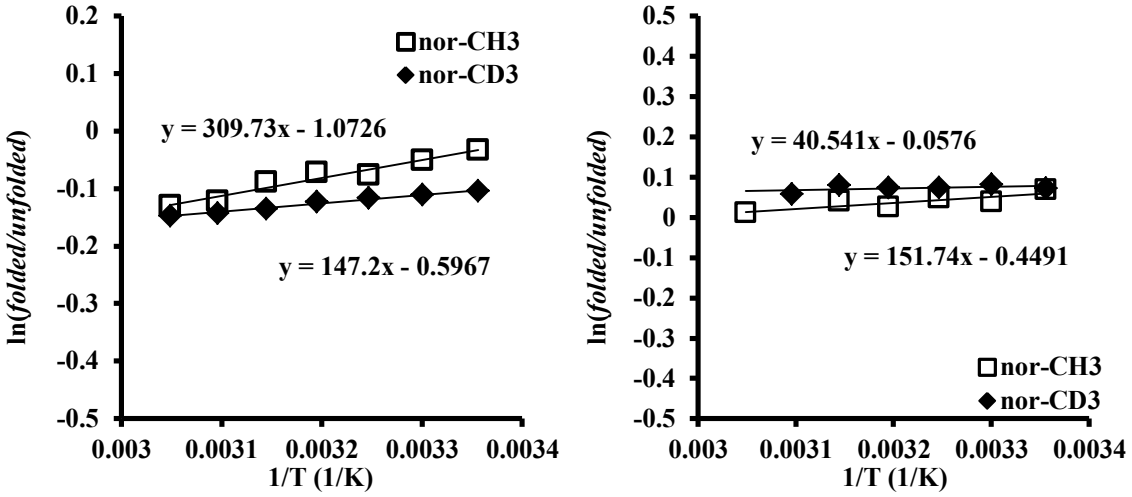

Figure 5.18: The van't Hoff plots of balances **16a** and **16b** in $CDCl_3$ and acetone-d_6.

The errors for slopes and intercepts are measured by the regression add-in in excel, and the calculated ΔH and $T\Delta$S values were summarized in Table 5.13 and Table 5.14:

Table 5.13: Calculated ΔG, ΔH, ΔS at 25°C and $T\Delta S$ for balance **13**–**16** in $CDCl_3$ with errors via VT ^{1}H NMR experiment.

balance	Slope	Intercept	ΔG (kcal/mol)	ΔH (kcal/mol)	ΔS (kcal/mol·K)	$-T\Delta S$@25°C (kcal/mol)
13a	413 ± 14	–1.18 ± 0.04	–0.123 ± 0.054	–0.821 ± 0.028	–0.00234 ± 0.00009	0.698 ± 0.026
13b	367 ± 28	–1.00 ± 0.09	–0.136 ± 0.108	–0.730 ± 0.056	–0.00199 ± 0.00018	0.593 ± 0.053
14a	–134 ± 72	–0.950 ± 0.231	0.829 ± 0.280	0.266 ± 0.144	–0.00189 ± 0.00046	0.562 ± 0.137
14b	–159 ± 48	–0.824 ± 0.154	0.803 ± 0.186	0.316 ± 0.095	–0.00164 ± 0.00031	0.488 ± 0.091
15a	228 ± 35	–0.885 ± 0.113	0.071 ± 0.137	–0.453 ± 0.070	–0.00176 ± 0.00022	0.524 ± 0.067
15b	247 ± 98	–0.965 ± 0.317	0.081 ± 0.383	–0.490 ± 0.195	–0.00192 ± 0.00063	0.572 ± 0.188
16a	310 ± 32	–1.07 ± 0.102	0.020 ± 0.124	–0.615 ± 0.064	–0.00213 ± 0.00020	0.635 ± 0.061
16b	147 ± 8	–0.597 ± 0.025	0.061 ± 0.030	–0.292 ± 0.016	–0.00119 ± 0.00005	0.353 ± 0.015

Table 5.14: Calculated ΔG, ΔH, ΔS (25°C) and $T\Delta S$ for balance **13–16** in acetone-d_6 with errors via VT ^{1}H NMR experiment.

balance	Slope	Intercept	ΔG (kcal/mol)	ΔH (kcal/mol)	ΔS (kcal/mol·K)	$-T\Delta S$@25°C (kcal/mol)
13a	501 ± 41	–1.29 ± 0.13	–0.231 ± 0.160	–0.995 ± 0.082	–2.56 ± 0.26	0.764 ± 0.078
13b	715 ± 95	–1.96 ± 0.31	–0.260 ± 0.370	–1.42 ± 0.19	–3.89 ± 0.61	1.16 ± 0.18
14a	–121 ± 18	–0.714 ± 0.057	0.664 ± 0.070	0.241 ± 0.036	–1.42 ± 0.11	0.423 ± 0.034
14b	–51.1 ± 17.4	–0.925 ± 0.055	0.649 ± 0.067	0.102 ± 0.034	–1.84 ± 0.11	0.548 ± 0.033
15a	292 ± 66	–0.897 ± 0.215	–0.049 ± 0.259	–0.580 ± 0.131	–1.78 ± 0.43	0.531 ± 0.128
15b	274 ± 26	–0.827 ± 0.085	–0.055 ± 0.103	–0.545 ± 0.053	–1.64 ± 0.17	0.490 ± 0.050
16a	178 ± 43	–0.529 ± 0.138	–0.040 ± 0.167	–0.353 ± 0.085	–1.05 ± 0.27	0.313 ± 0.081
16b	27.1 ± 43.3	–0.016 ± 0.139	–0.045 ± 0.168	–0.054 ± 0.086	–0.05 ± 0.28	0.0092 ± 0.0823

CHAPTER 6

MEASURING AROMATIC CH–Π INTERACTIONS USING MOLECULAR BALANCES

In addition to the previously described studies about face-to-face π–π stacking interactions and aliphatic CH–π interactions, the molecular balances can also be applied to the measurement of other non-covalent interactions via simple modification. In this chapter, the application of our phencyclone-based balance system on the study of aromatic CH–π interactions (edge-to-face arene–arene interactions) will be presented. Similar to aliphatic CH–π interactions, the edge-to-face arene–arene interactions are weakly directional and are results of several different forces of similar magnitudes. Therefore, the prediction of the strength, geometries and solvent dependence of edge-to-face arene–arene interactions is quite complex.

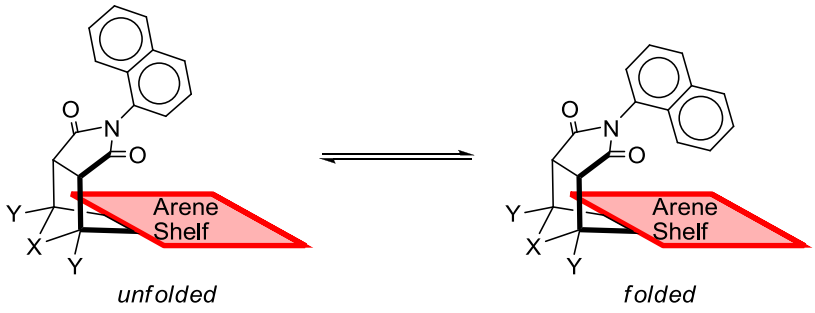

Figure 6.1: Equilibrium between the *unfolded* and *folded* conformers of molecular balances used for measuring edge-to-face arene–arene interaction between naphthalene and aromatic rings.

Several molecular models have been developed to study the edge-to-face arene–arene interactions.[62,126] By replacing the phenyl rotor with 1-naphthyl or 5-quinolyl rings, the balances can adopt intramolecular edge-to-face arene–arene interactions in their

folded conformation with well-defined geometry (Figure 6.1). Our balance system compares favorably with the other balance systems as it showed good solubility in a wider range of solvents and better control over the interacting geometry. It also enables the comparison between the stability of edge-to-face arene–arene interactions and the other non-covalent interactions that were studied using the same balance system.

6.1 BALANCE DESIGNS

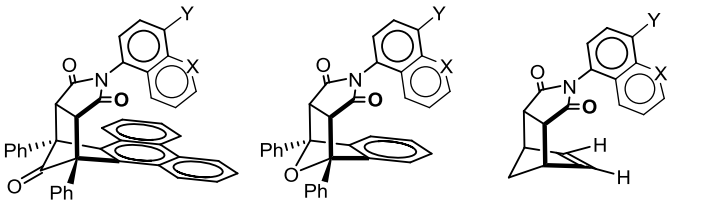

17a (X = C, Y = H)
17b (X = N, Y = H)
17c (X = N, Y = OH)
17d (X = N^+-CH_3, Y = H)

18a (X = C, Y = H)
18b (X = N, Y = H)

19a (X = C, Y = H)
19b (X = N, Y = H)
19c (X = N, Y = OH)

Figure 6.2: Structures of balances designed for measuring edge-to-face arene–arene interactions.

The structures of the edge-to-face balances **17**–**19** (Figure 6.2) were based on the same bicyclic *N*–arylimide framework used in previous chapters. The design of balance **17a** was previously shown to adopt the edge-to-face arene–arene geometry in its *folded* conformation, but this system was primarily used as a host molecule for small aromatic guests.[94] The new balance **17b** with a 5–quinolyl rotor was made for comparison containing a different electrostatic distribution and geometry of the edge ring. Substituted balance **17c** with –OH as Y group and balance **17d** with –CH3 at the *N*–position on the quinolyl ring were synthesized to study the substitution effect. Balances **18** and **19** with smaller shelves were made as control balances.

6.2 SOLID-STATE STRUCTURES

In order to confirm the presence and identify the exact geometries of the edge-to-

face arene–arene interactions in these molecular balances, the X-ray structures of balance **17a** and **17b** were analyzed. The crystal structure of balance **17a** was previously reported,[94] and the crystal structure of balance **17b** was obtained through single-crystal X-ray diffraction. Both structures crystallized as the *folded* conformation, which clearly displayed the edge-to-face interaction between the edge of the arene-rotor and the shelf (Figure 6.3).

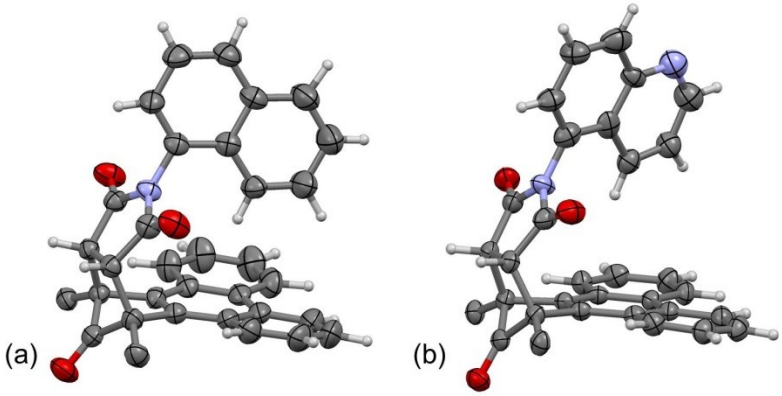

Figure 6.3: X-ray structures for *folded* conformers of balances **17a**[94] and **17b** suggesting edge-to-face interactions between the edge of rotor rings and phenanthrene-shelf. Parts of the phenyl rings at bridge position were hidden for better viewing clarity.

In the solid-state structure of balance **17a**, the 1–naphthyl group was fixed perpendicular to the phenanthrene-shelf with the C–8 proton pointing directly into the face of the center phenanthrene-ring. The hydrogen-to-plane distances for the two edge-protons (on C–8 and C–7) were 2.616 Å and 2.797 Å respectively. Both distances were within the sum of van der Waals' radii of H and C atoms (~ 2.9 Å), which suggested the formation of an attractive non-covalent interaction.

Similar edge-to-face geometry was observed in balance **17b** with the 5–quinolyl rotor, which showed the hydrogen-to-plain distances of 2.765 Å and 3.300 Å. The 8–proton of the quinoline ring was further away from the phenanthrene shelf than in **17a**. The bond-length of the C–N bond is shorter than the C–C bond, making the heterocyclic

quinoline ring slightly smaller than the naphthyl ring. The distance of 3.300 Å exceeded the typical range that can form a non-covalent bond, so it is possible that the second interaction in balance **17b** does not exist or only shows weak strength.

6.3 EDGE-TO-FACE ARENE–ARENE INTERACTIONS IN SOLUTION

The interactions were then quantified by the same methods described in Chapter 2 based on the integration of the succinimide peaks in ^{1}H NMR spectrum. Same as other molecular balances in our study, separate peaks for the *folded* and *unfolded* conformers were observed in the ^{1}H NMR spectrums. Assignment of the *folded* and *unfolded* peaks was based on the results from previous studies about balance **17a**.[94]

The larger aromatic rotors in these balances enhance the possibility of intermolecular aggregation. In order to rule out aggregation effects on this system, the concentration dependence of the *folded*/*unfolded* ratios was investigated. Over a concentration range of 1.6 to 15 mM, only a change of 0.02 kcal/mol in the folding energy was observed, which is within the error (0.03 kcal/mol) for this measurement. This indicates that the aggregation effects were either minor or no existent in the edge-to-face arene–arene balances.

6.3.1 Measurement of Rotational Barrier

The two conformers of these balances showed different R_f values on TLC plates, and exchanged overnight at room temperature or after a matter of minutes at elevated temperature. In one example, one of the conformers of **19a** was isolated via a quick column at room temperature. By tracking the change in the *folded/unfolded* ratio via ^{1}H NMR spectra over the course of one hour, the rotational barrier was calculated to be 22.8 kcal/mol (Figure 6.4). This equated to a half-life of 56 min at room temperature. This barrier is higher than that of previous balances such as balance **1a** with an OMe arm (20.5

kcal/mol), because the larger size and rigidity of the fused naphthalene ring compared with individual *ortho*-substituents on a phenyl ring. All the balances in this study were, therefore, allowed to equilibrate for at least 10 half-lives in solution before measurement of the *folded*/*unfolded* ratios.

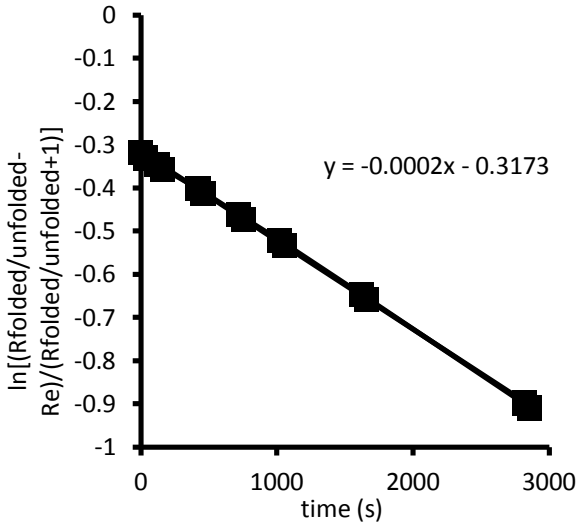

Figure 6.4: The value of $\ln[(R_{folded/unfolded}-R_{eq})/(R_{folded/unfolded}+1)]$ plotting versus time (at 21°C) indicating the rate for exchange between *folded* and *unfolded* conformers of balance **19a**.

6.3.2 Comparison of Balances with Naphthalene and Quinoline Rotors

The *folded*/*unfolded* ratios for balances **17–19** with naphthalene and quinoline rotors are listed in Table 6.1. With phenanthrene shelf, both rotors in balances **17a** and **17b** preferred the *folded* conformation in solution, which is consistent with an attractive intramolecular edge-to-face interaction between the rotor edge and the phenanthrene shelf. Balances **18a** and **18b** showed the lowest *folded*/*unfolded* ratios among balances, because only one edge proton–π was able to form an interaction. For control balances **19a** and 1**9b** without arene shelves, no interaction is possible, so the *folded*/*unfolded* ratios were close to 1.

Table 6.1: The *folded*/*unfolded* ratios of balance **17a–17b**, **18a–18b** and **19a–19b** in $CDCl_3$ at 25 °C.

rotor\shelf	**17** (shelf = phenanthrene)	**18** (shelf = benzene)	**19** (shelf = norborene)
a (rotor = naphthyl)	1.81	0.47	0.81
b (rotor = quinolyl)	2.98	0.61	0.93

Balance **17b** with quinolyl rotor showed a higher *folded*/*unfolded* ratio than balance **17a** with naphthyl rotor, which is in conflict with the observation that the quinolyl rotor forms fewer good interactions in crystal structures. One possible explanation is that the interaction is primarily driven by electrostatic force. The greater electronegativity of the nitrogen atom in the quinolyl ring of **17b** makes the edge of the rotor to have greater positive charge. Another possibility is that in balance **17a**, the proton at 8– position is too close to the arene shelf, so this interaction contains a greater repulsive component which destabilized its *folded* conformer. The lower *folded*/*unfolded* ratios of balances **18a** and **18b** with the benzene shelves agreed with the second hypothesis, because the *folded*/*unfolded* ratios of the two balances in solution were less than one. A third possibility is that the differences are due to a solvent effect. This possibility will be addressed in the following section 6.3.4.

6.3.3 Substituent Effect

To study the electrostatic contributions to the edge-to-face arene–arene interactions, we varied the electrostatic polarization of the aromatic rotors by introducing substituents on the quinolyl rotor of balances **17b**. Balance **17c** with an 8-hydroxyquinolyl rotor and balance **17d** with *N*–methylquinolyl rotor were prepared as balances with electron-rich and electron-poor substituents respectively.

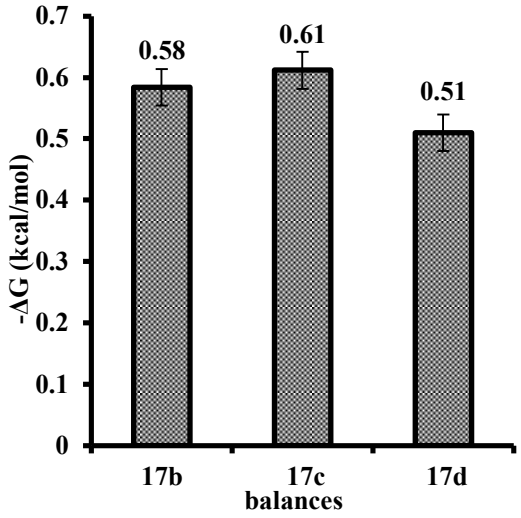

Figure 6.5: The folding energies (–Δ*G*, in kcal/mol) of balances **17b**–**17d** in acetonitrile–d_3 at 25 °C, shown with errors of 0.03 kcal/mol.

The folding energies (–Δ*G*) in acetonitrile–d_3 of balances **17b**–**17d** with different substituted quinolyl rotors were compared in Figure 6.5. Balance **17d** only showed good solubility in acetonitrile, so acetonitrile–d_3 was the only NMR solvent that dissolves all balances to allow this comparison. Balances **17b** with quinolyl rotor and **17c** with hydroxylquinolyl rotor showed almost identical folding energies, while balance **17d** with methylated quinolyl rotor showed slightly lower folding energy. The observation did not match with our expectation that the electron-rich hydroxyl-substituted balance **17c** should be less *folded* and the electron-poor *N*–methylquinoline balance **17d** should be more *folded* compared than balance **17b**. This discrepancy may be related to the solvent effect as discussed in the next section.

6.3.4 Solvent Effects

The solvophobic effect is one of the important factors that drive the folding of molecular balances, and may be able to explain the unexpected observations. To study the solvent dependent of the edge-to-face arene–arene interaction with balances **17a**–**17c**,

the folding energies ($-\Delta G$) of the two balances were calculated from the *folded/unfolded* ratios in various solvents and plotted versus the $E_T(30)$ values of the solvents (Figure 6.6). The folding trend of balance **17d** was not measured, because it only showed good solubility in acetonitrile.

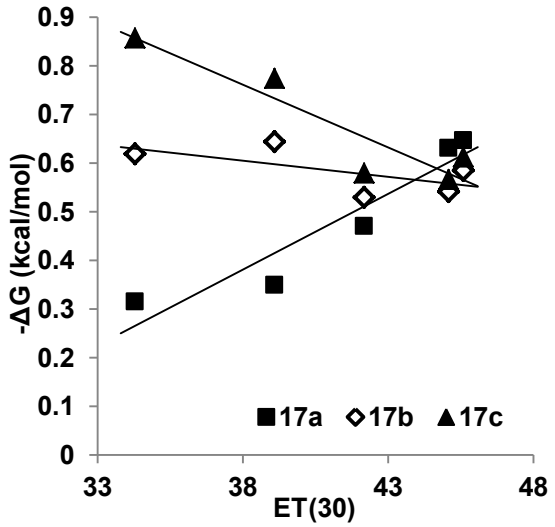

Figure 6.6: Measured $-\Delta G$ values for balances **17a–17c** in a variety of solvents at 25°C plotted versus $E_T(30)$ values of each solvent. Solvents from left to right are deuterated benzene, chloroform, acetone, DMSO, and acetonitrile.

The *folded* conformers were favored for **17a–17c** in all five solvents tested. For solvents with relatively lower polarity (benzene, $CDCl_3$, acetone), the folding energies of balance **17b** with quinolyl-rotor were stronger than that of balance **17a** with naphthyl-rotor. As the polarity of the solvent increased, balance **17a** became more *folded* while balance **17c** become less *folded*, and the *folded*/*unfolded* ratio of balance **17b** remained the same. Also, in solvents with relatively high polarity (DMSO and acetonitrile), the folding energies of balances **17a**–**17c** were almost identical.

One possibility for the different solvent trends of balances **17a**–**17c** is that the dipoles of *folded* and *unfolded* conformers of each balance are different. Based on the calculation, difference in dipole between *folded* in *unfolded* increases showed the

following order: hydroxyquinolyl > quinolyl > naphthyl. The theory was tested experimentally using control balances **19a–c** without aromatic shelves (Figure 6.7). However, the observation did not match with our expectation. The folding trends of balances **19a–c** in different solvents and did not show expected distinction as that of balances **17a–c**. Thus, the dipole difference was not the main reason to cause the folding trends. The other theories that can fully explain this observation are still under investigation.

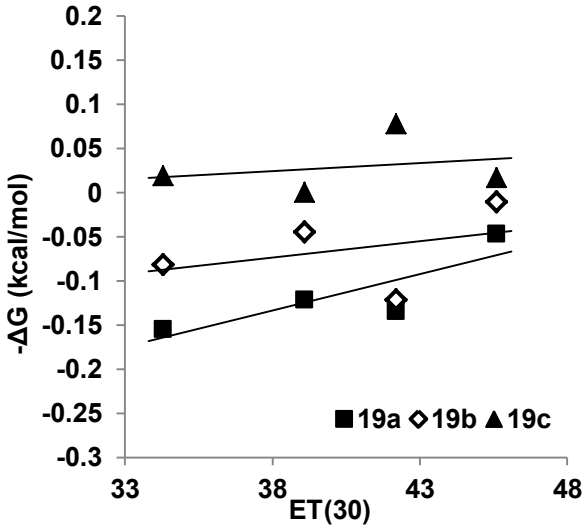

Figure 6.7: Measured $-\Delta G$ values for balances **19a–19c** in a variety of solvents at 25°C plotted versus $E_T(30)$ values of each solvent. Solvents from left to right are deuterated benzene, chloroform, acetone, and acetonitrile.

The solvent effects on the folding of the balances were also studied in mixed solvents. The folding energies of **17a–17c** were measured in the mixtures of methanol–d_4 and $CDCl_3$ with different ratios (Figure 6.8). Although the polarity of mixed solvents changed when the fraction of methanol increased, the folding energies for each balance stayed relatively consistent and were similar to those in pure $CDCl_3$. It is possible that because of the poor solubility of balances **17a–17c** in methanol, so changes on the concentration of methanol only have limited effect on the folding preference. Another

possibility is that methanol is an H-bond donor that could interact with the basic nitrogen on quinolyl rotor.

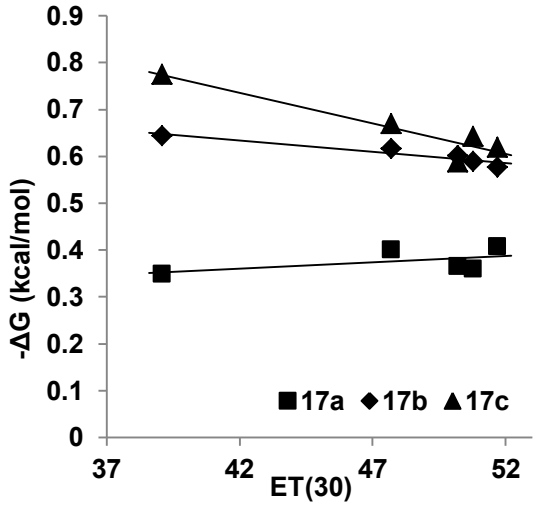

Figure 6.8: Measured –Δ*G* values for balances **17a–17c** in a series of mixtures of CDCl3 and methanol–d_4 at 25°C plotted versus $E_T(30)$ values. The fraction of methanol in each mixture was 0, 20%, 50%, 57% and 66% from left to right, and the $E_T(30)$ values were estimated based on literature.[127,128]

6.3.5 Balances with Quinoline and *iso*-Quinoline as Rotors

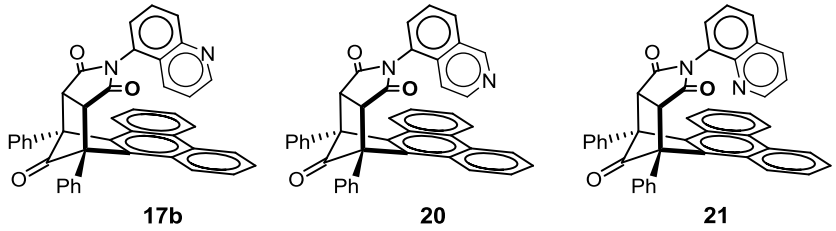

Figure 6.9: Structures of balances **17b**, **20** and **21** with quinoline and *iso*-quinoline arms.

Balances **20** and **21** with N atom at different position of the rotor ring were also made for comparison (Figure 6.9). The folding energies for balances **17b**, **20**, and **21** were compared in different solvents (Figure 6.10). Balance **17b** and **20** showed almost identical folding energies in each solvent being tested, and the energy values did not change according to the increaseing polarity. This indicates that the electrostatic property of the two protons interacting with the aromatic shelf was the same when the N atom on

the rotor ring is at 5– or 6– position. Their interactions with the solvent molecule did not change either. Balance **21** showed much lower folding ratios because of the existence of lone-pair π interaction in its *folded* conformer. It can also act as a good control because of its lack of edge-to-face interaction.

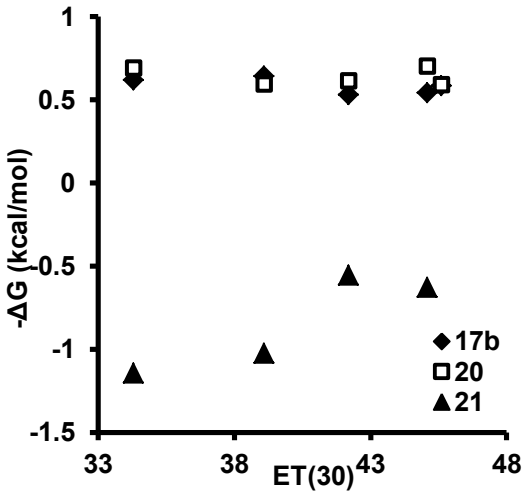

Figure 6.10: Folding energies of balances **17b**, **20** and **21** in different solvents at 25°C.

6.4 CONCLUSION

In summary, edge-to-face arene–arene interactions were verified by a series of control experiments. The geometries of edge-to-face interaction in the balances were characterized in the solid-state structure. Solvents and substitutions were found to affect the ratio of *folded* and *unfolded* conformers, but the relative magnitudes of forces that cause the observed trends are still unclear. Further studies will be conducted to give a better understanding on the questions remains unanswered.

6.5 SYNTHESIS

Edge-to-face balances **17a–b** and balances **18**–**21** were prepared from 1-naphthyl amine, 5-aminoquinoline, 5-aminoisoquinoline or 8-aminoquinoline in one step with corresponding anhydrides **5**. The reaction that made balances **17c** required the

participation of base. Balance **17d** was made from **17b** via methylation.

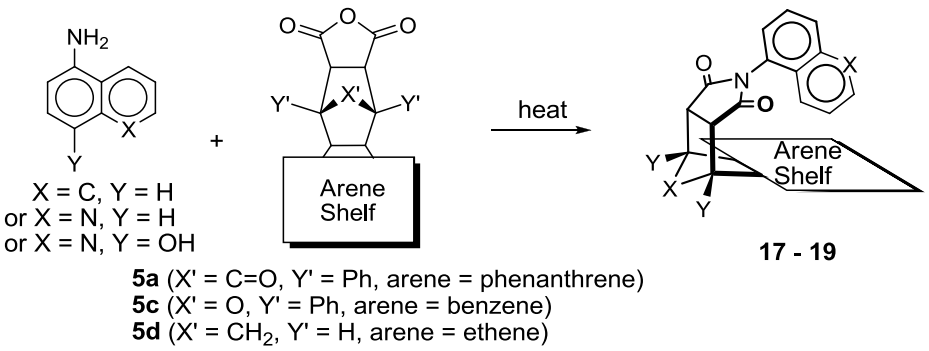

Figure 6.11: Overview of synthesis of balances **17a–b**, **18**, and **19** via condensation reactions.

Preparation of balance **17a**:

Anhydride **5a** (0.17 g, 0.35 mmol) and 1-naphthylamine (0.10 g, 0.70 mmol) were heated to reflux for 24 h in 5 mL acetic acid. After work up steps and purification, balance **17a** was obtained as white solid (0.19 g, 0.31 mmol, 90% yield). ^{1}H NMR (400 MHz, $CDCl_3$) δ 8.83 (d, J = 8.5 Hz, 2 H major), 8.76 (d, J = 8.5 Hz, 2 H minor), 8.41 (d, J = 7.8 Hz, 2 H major), 8.38 (d, J = 8.3 Hz, 2 H minor), 7.1–7.8 (m, 19 H major, 16 H minor), 7.02 (t, J = 7.6 Hz, 2 H minor), 6.74 (t, J = 7.9 Hz, 1 H major), 6.04 (t, J = 7.7 Hz, 2 H minor), 4.79 (s, 2 H minor), 4.75 (s, 2 H major), 4.65 (dd, J = 8.6 Hz, J = 0.8 Hz, 1 H major), 4.63 (dd, J = 7.4 Hz, J = 1.1 Hz, 1 H minor). Characterization data matched with the literature.[94]

Preparation of balance **17b**:

Anhydride **5a** (0.17 g, 0.35 mmol) and 5-aminoquinoline (97%, 0.10 g, 0.69 mmol) were heated to reflux for 24 h in 5 mL acetic acid. After work up steps and purification, balance **17b** was obtained as white solid (0.20 g, 0.33 mmol, 94% yield). ^{1}H NMR (300 MHz, $CDCl_3$) δ 8.82 (d, J = 8.44 Hz, 2 H major, 1 H minor), 8.76 (d, J = 8.44

Hz, 2 H minor), 8.47 (dd, J = 4.01 Hz, J = 1.19 Hz, 1 H major), 8.38 (d, J = 7.71 Hz, 2 H major), 8.35 (d, J = 7.71 Hz, 2 H minor), 7.96 (d, J = 8.62 Hz, 1 H major), 7.90–7.12 (m, 16 H major, 17 H minor), 6.98 (t, J = 8.19 Hz, 1 H minor), 6.05–5.98 (m , 1 H major), 4.94 (d, J = 8.29 Hz, 1 H major), 4.79 (s, 2 H minor), 4.78 (s, 2 H major), 4.68 (d, J = 7.46 Hz, 1 H minor).

Preparation of balance **17c**:

Anhydride **5a** (0.049 g, 0.102 mmol), potassium carbonate (0.028g, 0.204mmol) and 5-amino-8-hydroxyquinoline dihydrochloride (95%, 0.050 g, 0.204 mmol) were heated to reflux for 24 h in 5 mL acetic acid. After work up steps and purification, balance **17c** was obtained as purple solid (0.078 g, 0.129 mmol, > 90% yield). ^{1}H NMR (300 MHz, $CDCl_3$) δ 8.81 (d, J = 8.37 Hz, 2 H major), 8.75 (d, J = 8.75 Hz, 2 H minor), 8.69 (dd, J = 4.06 Hz, J = 1.16 Hz, 1 H minor), 8.46–8.27 (m, 3 H major, 2 H minor), 8.15 (brs, 1 H major), 7.91–6.96 (m, 16 H major, 17 H minor), 6.41 (d, J = 8.14 Hz, 1 H minor), 6.09 (dd, J = 8.39 Hz, J = 3.98 Hz, 1 H major), 4.88 (dd, J = 8.36 Hz, J = 1.02 Hz, 1 H major), 4.75 (s, 2 H minor), 4.74 (s, 2 H major), 4.58 (d, J = 8.19 Hz, 1 H minor).

Preparation of balance **17d**:

To a solution of balance **17b** (0.096 g, 0.158 mmol) in acetonitrile (10 mL), iodomethane (0.02 mL, 0.316 mmol) was added drop wise while stirring under nitrogen. After heated to reflux for 3 days, the solvent was removed *in* vacuum, and balance **17d** was obtained as yellow solid (0.089 g, 0.150 mmol, 95% yield). ^{1}H NMR (300 MHz, $CDCl_3$) δ 9.09 (d, J = 5.72 Hz, 1 H minor), 9.00 (d, J = 8.57 Hz, 2 H major), 8.90 (d, J = 8.57 Hz, 2 H minor), 8.70 (d, J = 5.72, 1 H major), 8.45–7.05 (m, 19 H major, 20 H minor), 6.57 (dd, J = 8.62 Hz, J = 5.80 Hz, 1 H major), 5.47 (d, J = 8.77 Hz, 1 H major),

5.12 (s, 2 H minor), 5.07 (s, 2 H major), 4.88 (d, J = 7.48 Hz, 1 H minor), 4.44 (s, 3 H minor), 4.35 (s, 3 H major).

Preparation of balance **18a**:

Anhydride **5c** (0.100 g, 0.26 mmol) and 1-naphthylamine (0.056 g, 0.40 mmol) were heated to reflux for 24 h in 5 mL acetic acid. After work up steps and purification, balance **18a** was obtained as white solid (0.113 g, 0.223 mmol, 85% yield). ^{1}H NMR (300 MHz, $CDCl_3$) δ 8.18–6.99 (m, 20 H major, 20 H minor), 5.79 (d, J = 7.14 Hz, 1 H major), 5.41 (d, J = 8.51 Hz, 1 H minor), 4.44 (s, 2 H major), 4.43 (s, 2 H minor).

Preparation of balance **18b**:

Anhydride **5c** (0.085 g, 0.23 mmol) and 5-aminoquinoline (0.050 g, 0.35 mmol) were heated to reflux for 24 h in 5 mL acetic acid. After work up steps and purification, balance **18b** was obtained as white solid (0.098 g, 0.20 mmol, 86% yield). ^{1}H NMR (300 MHz, $CDCl_3$) δ 8.96–8.78 (m, 1 H major, 1 H minor), 8.17–7.01 (m, 18 H major, 18 H minor), 5.88 (d, J = 7.36 Hz, 1 H major), 5.74 (d, J = 8.34 Hz, 1 H minor), 4.45 (s, 2 H major), 4.44 (s, 2 H minor).

Preparation of balance **19a**:

Anhydride **5d** (0.100 g, 0.61 mmol) and 1-naphthylamine (0.131 g, 0.91 mmol) were heated to reflux for 24 h in 5 mL acetic acid. After work up steps and purification, balance **19a** was obtained as white solid (0.158g, 0.546 mmol, 90% yield). ^{1}H NMR (300 MHz, $CDCl_3$) δ 7.96–7.17 (m, 6 H major, 7 H minor), 7.12 (d, J = 7.28 Hz, 1 H major), 6.55 (m, 2 H minor), 6.37 (m, 2 H major), 3.64–3.49 (m, 4 H major, 4 H minor), 1.97–1.60 (m, 2 H major, 2 H minor).

Preparation of balance **19b**:

Anhydride **5d** (0.095 g, 0.58 mmol) and 5-aminoquinoline (0.100 g, 0.69 mmol) were heated to reflux for 24 h in 5 mL acetic acid. After work up steps and purification, balance **19b** was obtained as white solid (0.145g, 0.50 mmol, 86% yield). ^{1}H NMR (300 MHz, $CDCl_3$) δ 8.97–8.88 (m, 1 H major, 1 H minor), 8.18 (d, J = 8.59 Hz, 1 H major, 1 H minor), 7.96–7.15 (m, 4 H major, 4 H minor), 6.51 (m, 2 H minor), 6.35 (m, 2 H major), 3.63–3.46 (m, 4 H major, 4 H minor), 1.93–1.59 (m, 2 H major, 2 H minor).

Preparation of balance **19c**:

Anhydride **5d** (0.033 g, 0.20 mmol), potassium carbonate (0.056g, 0.40mmol) and 5-amino-8-hydroxyquinoline dihydrochloride (95%, 0.050 g, 0.20 mmol) were heated to reflux for 24 h in 5 mL acetic acid. After work up steps and purification, balance **19c** was obtained as brown solid (0.066g, 0.20 mmol, >90% yield). ^{1}H NMR (300 MHz, $CDCl_3$) δ 8.85–8.74 (m, 1 H major, 1 H minor), 8.44 (brs, 1 H major), 7.85 (t, J = 10.05 Hz, 1 H major, 1 H minor), 7.50–7.40 (m, 1 H major, 2 H minor), 7.29–7.07 (m, 2 H major, 2 H minor), 6.50 (s, 2 H minor), 6.35 (s, 2 H major), 3.62–3.50 (m, 4 H major, 4 H minor), 1.93–1.60 (m, 2 H major, 2 H minor).

Preparation of balance **20**:

Anhydride **5a** (0.050 g, 0.104 mmol) and 5-aminoisoquinoline (0.018 g, 0.125 mmol) were heated to reflux for 24 h in 5 mL acetic acid. After work up steps and purification, balance **20** was obtained as white solid (0.059 g, 0.097 mmol, 93% yield). ^{1}H NMR (300 MHz, $CDCl_3$) δ 9.13 (s, 1 H minor), 8.95 (s, 1 H major), 8.83 (d, J = 8.59 Hz, 2 H major), 8.75 (d, J = 8.59 Hz, 2 H minor), 8.50 (d, J = 6.18 Hz, 1 H minor), 8.44–7.10 (m, 20 H major, 18 H minor), 6.89 (t, J = 7.83 Hz, 1 H minor), 4.84 (d, 1 H minor),

4.81 (s, 2 H minor), 4.78 (s, 2 H major), 4.42 (d, J = 5.98 Hz, 1 H major).

Preparation of balance **21**:

Anhydride **5a** (0.050 g, 0.104 mmol) and 8-aminoquinoline (0.018 g, 0.125 mmol) were heated to reflux for 24 h in 5 mL acetic acid. After work up steps and purification, balance **21** was obtained as white solid (0.058 g, 0.095 mmol, 91% yield). ^{1}H NMR (300 MHz, $CDCl_3$) δ 8.89–7.06 (m, 22 H major, 24 H minor), 6.89 (t, J = 7.77 Hz, 1 H major), 5.05 (dd, J = 7.12 Hz, J = 0.65 Hz, 1 H major), 4.84 (s, 2 H major), 4.75 (s, 2 H minor).

CHAPTER 7

OTHER NOTABLE WORKS

By varying the arm group on the structures of our molecular balances and comparing their folding energies, a number of studies about different types of non-covalent interactions were able to be conducted. In this chapter, some additional results that do not fit into any of the previous chapters will be presented.

7.1 DOUBLE-MUTANT CIRCLES FOR MEASURING NON-COVALENT INTERACTIONS

Molecular balances have been proved to be effective tools for measuring weak non-covalent interactions. However, because of the existence of weak secondary effects in the *folded* structures of balances, it is hard to isolate the actual strengths of each interaction from the total folding energies. In previous chapters, balances were compared with their control balances with smaller arene shelves to eliminate their secondary interactions. However, the single-mutation comparisons do not work perfectly, because some secondary effects still exist after the subtraction, especially when there is a linker between the arm and the phenyl rotor. In addition, the three frameworks used in this study (shelf = phenanthrene, benzene and norborene) have different bridge atom (C=O, O or CH_2) at the backside and may adopt slightly different angles between the rotor ring and the shelf planes.

Double-mutant cycles provide a way to isolate individual weak interactions from the multiple interactions (Figure 7.1). This method was originally proposed by Fersht et al in 1984,[129] and their application on quantification of non-covalent interactions has been

reviewed.[130] In this section, the double-mutant cycles designed with our balance system for a more precise measurement on the non-covalent interactions will be introduced.

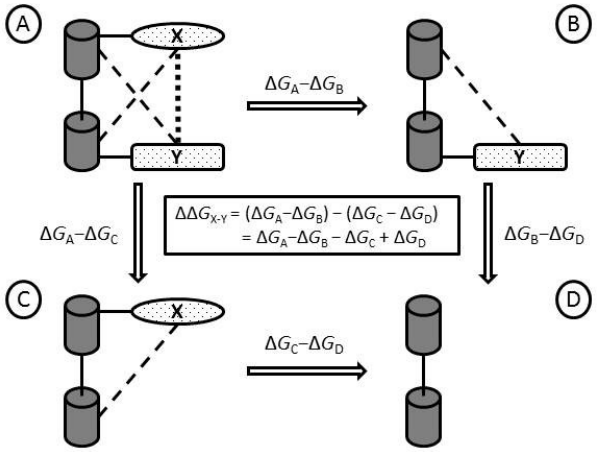

Figure 7.1: General schematic representing a supramolecular double-mutant cycle for measuring the intramolecular interaction between X and Y.

7.1.1 Structures of Molecular Balances

Balances **22** and **23** were synthesized to make double-mutant cycles that can isolate primary and secondary interaction of X and Y with the central and outer rings on the shelves (Figure 7.2). Balances **23b**, **23c** and **23e** have been previously studied as balances **9a**, **9b** in Chapter 4 and balance **2a** in Chapter 3. Balance **22** is similar to the previous balances with phenanthrene shelves, but their backside bridge was changed from a C=O into an O to match the *O*–bridge in balance **23**.

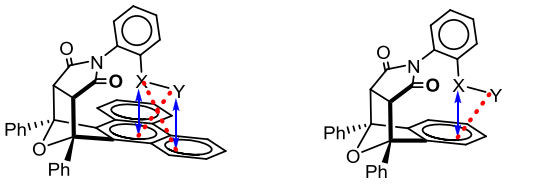

22a (X = CH_2, Y =Ph)
22b (X = CH_2, Y =CH_3)
22c (X = CH_2, Y = H)
22d (X = O, Y =Ph)
22e (X = O, Y =CH_3)

23a (X = CH_2, Y =Ph)
23b (X = CH_2, Y =CH_3)
23c (X = CH_2, Y = H)
23d (X = O, Y =Ph)
23e (X = O, Y =CH_3)

Figure 7.2: Molecular balances **22** and **23** designed for double-mutant cycles analyzing intramolecular primary interactions (blue arrows) and secondary interactions (red dash).

A range of different intramolecular interactions were formed by these molecular balances. In balances **22** with phenanthrene shelf (Y ≠ H), both the linker X and end group Y are able to form primary interactions with the aromatic surfaces below. In addition, the secondary interactions between Y and the central ring and X with the outer rings must be accounted for. In the corresponding balances **23** with the same X and Y combination, the interacting environment remains the same except for the absence of interaction between Y and the outer ring and the secondary interaction of X with the outer ring. This made balances **23** good reference balances in this mutation to isolate Y-to-outer ring interaction and X-to-central ring interaction. In cooperation with balances **22c** and **23c** that only forms interactions with X group, each of two primary and two secondary interactions were able to be isolated using the double mutant cycles.

7.1.2 Folding Energies of Balances **22** and **23**

Characterization of balances **22** and **23** in solution followed the same method as previous balances. The *folded*/*unfolded* ratios and folding energies of these balances were measured in CDCl3 at rt., and are listed in Table 7.1.

Table 7.1: *Folded*/*unfolded* ratios and folding energies of balances **22**–**23** measured in CDCl3 at 25 °C.

balances	shelf	X	Y	F/UF	ΔG (kcal/mol)
22a	phenanthrene	CH_2	Ph	0.41	0.53
22b	phenanthrene	CH_2	CH_3	0.58	0.32
22c	phenanthrene	CH_2	H	0.53	0.38
22d	phenanthrene	O	Ph	0.15	1.12
22e	phenanthrene	O	CH_3	0.18	1.01
23a	benzene	CH_2	Ph	0.16	1.10
23b	benzene	CH_2	CH_3	0.24	0.84
23c	benzene	CH_2	H	0.24	0.84
23d	benzene	O	Ph	0.10	1.39
23e	benzene	O	CH_3	0.09	1.40

7.1.3 General Design of Double-Mutant Cycles

The general double-mutant cycles designed for this study are shown in Figure 7.3. Balances A and B makes a single mutation. A parallel mutation between control balances C and D can cancel out the secondary effect between Y group and the central ring within the mutation between A and B. Similarly, the comparison between mutations from A to C and B to D cancels out the secondary interaction between X and the outer ring. The actual interacting energy between Y and the outer ring ($\Delta\Delta G$) can be calculated with equation:

$$\Delta\Delta G = (\Delta G_A - \Delta G_B) - (\Delta G_C - \Delta G_D) = \Delta G_A - \Delta G_B - \Delta G_C + \Delta G_D.$$

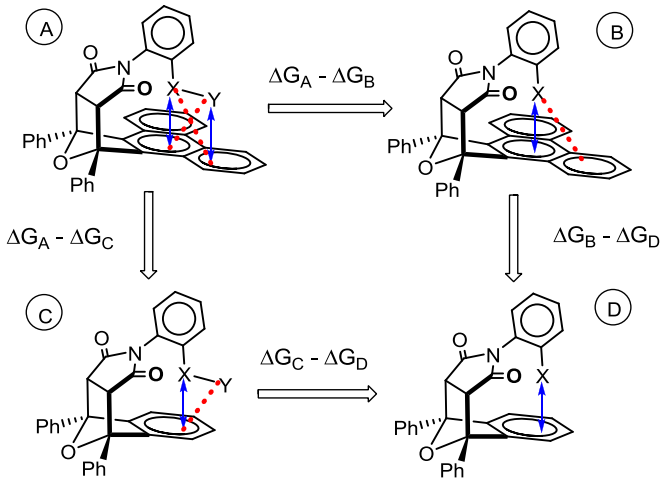

Figure 7.3: General design of the double-mutant cycle based on our molecular balances for measuring non-covalent interaction between Y and the outer ring on shelf.

Two double-mutant cycles were formed for the measurement of face-to-face π–π interaction (balances **22a**, **22c**, **23a**, **23c**) and CH–π interaction (balances **22b**, **22c**, **23b**, **23c**), respectively. Balances **22d**, **22e**, **23d**, **23e** were not able to form complete double-mutant cycles, because corresponding balances with X = O and Y = H showed very low rotational barriers and their *folded* and *unfolded* conformers did not show distinct set of peaks in the ^{1}H NMR spectra. However, balances **22d**, **22e**, **23d**, **23e** can still been used

for the comparison between π–π stacking and CH–π interactions, because they shared the same X (X = O) atom, and the difference on folding energies only comes from the difference between the two types of interactions.

7.1.4 Measuring π–π Stacking Interactions with Double-Mutant Cycle

The double-mutant cycle formed by balances **22a**, **22c**, **23a**, **23c** were used to calculate the face-to-face π–π interaction and the secondary effects within **22a** (Figure 7.4). Based on the equation ($\Delta G_{\mathbf{22a}} - \Delta G_{\mathbf{22c}} - \Delta G_{\mathbf{23a}} + \Delta G_{\mathbf{23c}}$), the π–π interaction between the phenyl arm and the outer ring was calculated to be –0.11 kcal/mol, which is attractive.

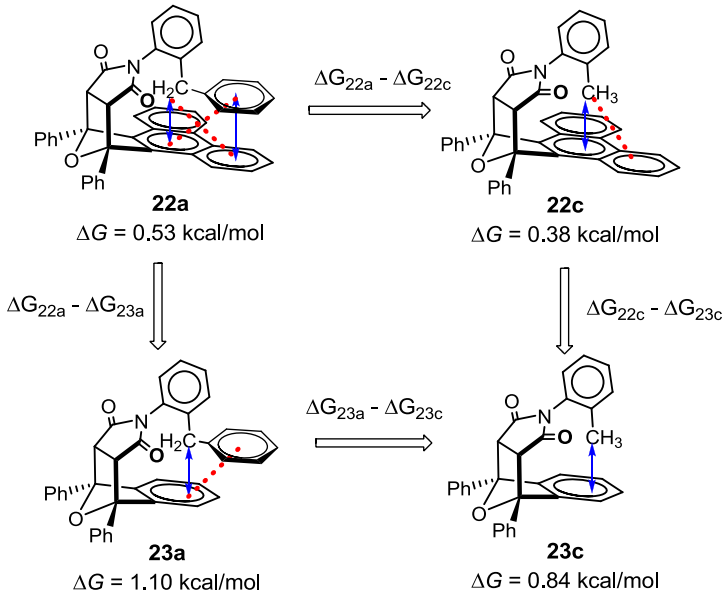

Figure 7.4: Double-mutant cycle formed by balances **22a**, **22c**, **23a**, **23c** for measuring π–π stacking interaction.

The secondary interaction between the phenyl arm and the central ring was calculated to be 0.26 kcal/mol ($\Delta G_{\mathbf{23a}} - \Delta G_{\mathbf{23c}}$). This repulsive effect may be caused by the increased sterics from the phenyl ring or the conformational entropy change of CH_2 linker because of the extra substitution. Another secondary interaction formed between

CH_2 and the outer ring was calculated to be –0.46 kcal/mol ($\Delta G_{\mathbf{23a}} - \Delta G_{\mathbf{23c}}$). This force is stabilizing, and it is possibly because larger arene shelf leads to stronger dispersion and more chance for the CH_3 form interaction.

7.1.5 Double-Mutant Cycle for Measuring CH–π Interactions

The double-mutant cycle formed by balances **22b**, **22c**, **23b**, **23c** were used to calculate the CH–π interactions and the secondary effects within **22b** (Figure 7.5). The interaction between CH_3 on ethyl and the side ring was calculated to be –0.06 kcal/mol ($\Delta G_{\mathbf{22b}} - \Delta G_{\mathbf{22c}} - \Delta G_{\mathbf{23b}} + \Delta G_{\mathbf{23c}}$). The interaction appeared to be very weak. The possibly reasons is that the CH_3 is located above the edge of arene surface, and may only form a minor interaction.

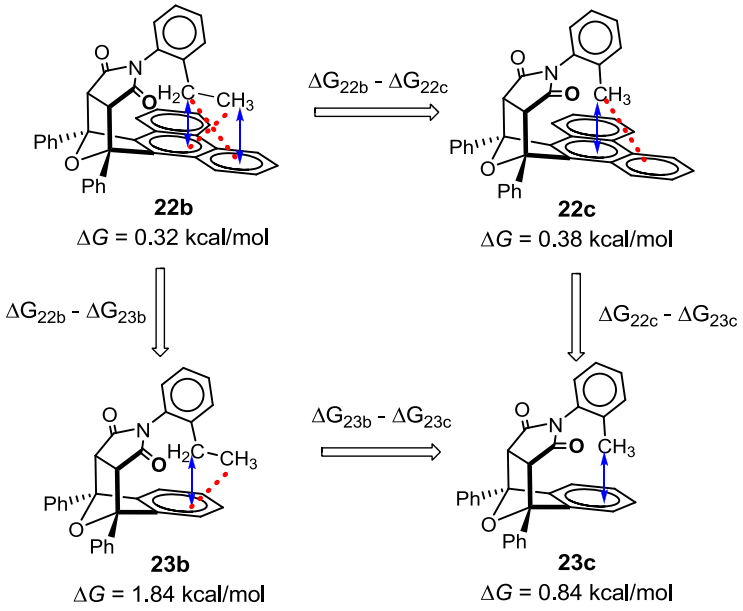

Figure 7.5: The double-mutant cycle formed by balances **22b**, **22c**, **23b**, **23c** for measuring π–π stacking interaction.

Balances **23b** and **23c** showed the same ΔG values, suggested that the second CH_3 on ethyl did not interact with the central ring. Compared with **23a** with phenyl arm, the CH_3 intend to cause smaller sterics and less rotational restriction for the CH_2 linker.

7.1.6 Double-Mutant Cycle for Comparing CH–π interactions to O–π and π–π Stacking Interactions

Other than isolating the primary non-covalent interaction from complicate environment, the double-mutant cycles can also be applied for the comparison between different interactions. This provides an indirect way to study some of the interactions that cannot be measured directly (e.g. O–π interaction). The difference between CH–π and O–π interactions at linker position was measured with two double-mutant cycles: (a) balances **22a**, **22d**, **23a** and **23d**, and (b) the balances **22b**, **22e**, **23b** and **23e**. The difference was calculated to be –0.30 kcal/mol and –0.13 kcal/mol, respectively. The two numbers are close enough considering the errors, and proved that CH–π interaction was more stabilizing than O–π interaction.

The difference between the π–π and CH–π interactions was also experimentally compared with two double-mutant cycles: (a) balances **22a**, **22b**, **23a** and **23b**, and (b) balances **22d**, **22e**, **23d** and **23e**. The difference was calculated to be –0.05 kcal/mol and 0.12 kcal/mol. This indicates that the two interactions showed very similar strength and the different folding energies of **22a** and **22b** primarily comes from the secondary interaction in balance, which was shown as the difference between balances **23a** and **23b** with benzene shelf.

7.1.7 Conclusion

In conclusion, a series of double-mutant cycles based on molecular balances were designed and were proved to be effective on isolating primary and secondary non-covalent interactions formed within the molecular balances. The strengths of weak non-covalent interactions, including face-to-face π–π interaction and CH–π interaction, were measured with high accuracy. This method also provides a more reliable way to measure

certain non-covalent interactions that could not be measured directly.

7.2 SOLVENT EFFECTS ON BALANCES WITH DIFFERENT LINKERS

In Chapter 3 and 4, the solvent dependent of balances **1** and **7** were discussed. Balance **1h** is from our previous study for measuring π–π stacking interactions. For each series of balances, the folding energies showed similar trends when measured in different solvents. It was true for balances with different interactions and even for control balances that could not form an interaction. However, the folding energies of the balances **1** and **7** showed different solvent trends. Thus, we hypothesized that the solvent trends might be primarily due to the linker atom between arm and the phenyl rotor.

The importance of linkers on determining the solvent effects was tested by comparing the solvent trends of balances with the same end group but different linkers on the arm. Several balances with same arm group (Me or Ph) and different linkers were then synthesized (Figure 7.6). In addition of balances **1** and **7** with oxygen and carbon linkers, balance **24** with N linker and **25** with S linker were also synthesized. The four linker groups have different abilities to associate with solvent molecules,[49] so we expected the balances to show different solvent trends.

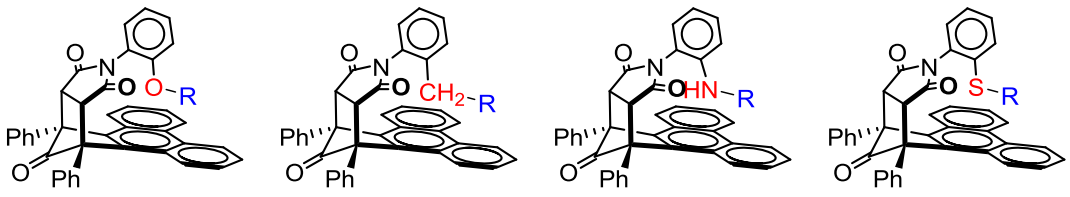

1a (R = Me)
1h (R = Ph)

7b (R = Me)
7e (R = Ph)

24 (R = Ph)

25 (R = Ph)

Figure 7.6: Structures of balances **1**, **7**, **24** and **25** with different linkers for the comparison of different solvent effect.

The folding energies ($-\Delta G$) of balances **1**, **7**, **24** and **25** were measured in different solvents, and the values were plotted according to the $E_T(30)$ values of each

solvent (Figure 7.7). The $E_T(30)$ values were used as the parameter indicating the polarities of solvents because it shows great correlation to the folding energies of balances in previous study.[74] The deuterated solvents used were (from left to right on the *x*-axis): benzene-d_6, bromobenzene-d_5, THF-d_4, $CDCl_3$, TCE-d_2, acetone-d_6, DMSO-d_6 and acetonitrile-d_3. Not all solvents were applied for study each of the balances because of the lack of data. The solvent trends of balances **1** and **7** should be consistent with less data because they are close to liner. The folding energies of balances **24** and **25** will be tested in more solvent in the future, but the difference on the solvent trends was obvious with the existing data.

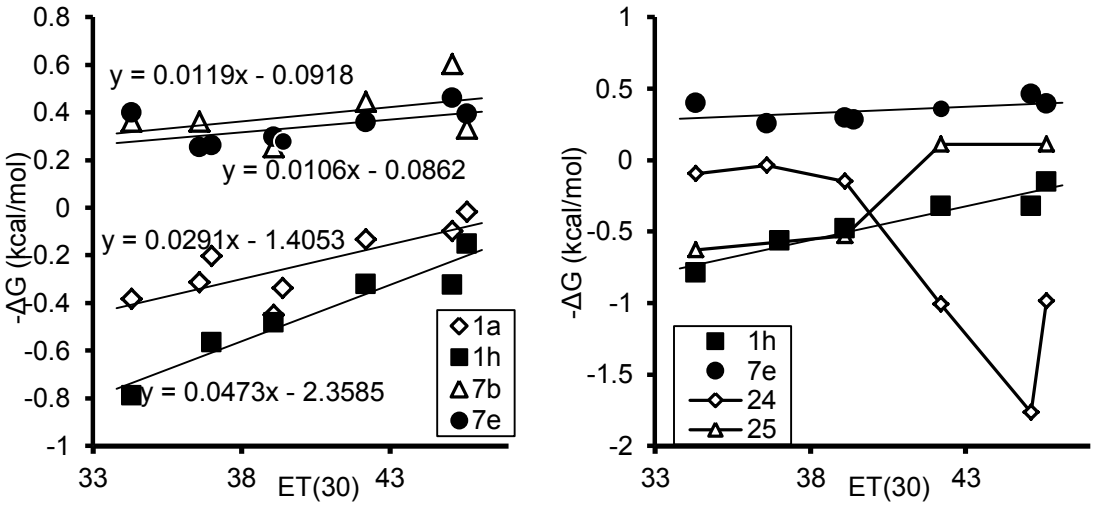

Figure 7.7: Comparison of the folding energies ($-\Delta G$) of balances **1a**, **1h**, **7b**, **7e** (left) and balances **1h**, **7e**, **24** and **25** (right) in different solvents.

Comparison among **1a**, **1h** with oxygen linkers and **7b**, **7e** with carbon linkers (Figure 7.7, left) showed that the trends were similar for balances with the same linker even when they formed different intramolecular interactions (CH–π or π–π stacking). Comparison of balances **1h**, **7e**, **24** and **25** (Figure 7.7, right) with the same π–π interaction but different linkers showed very different trends. It seems that for balance **24**

and **25**, the folding energies in acetone and acetonitrile were similar to each other, and were different from that in solvents with relatively low polarity. These observations were possibly caused by the different linker-solvent interactions or the solvophobic driving-force for the folding of balances. A complete set of solvent study and a deeper understanding of the polarity scales for both solvent and the linker groups are needed for a clear explanation.

7.3 MOLECULAR BALANCE FOR STUDY NH_2–Π INTERACTION

Molecular balance **26** with NH_2 as the arm group (Figure 7.8, left) was synthesized to measure the interaction between NH_2 group and the phenanthrene rings. Due to its restricted rotation of C_{aryl}–N_{imide} bond, the balance **26** was able to show separate peaks for the two conformations in ^{1}H NMR spectrum. This indicated a rotational barrier that was higher than that of the balance with OH arm (which are not able to show distinct signal on ^{1}H NMR spectrum). The reason for the enhanced barrier may be that the extra proton on the NH_2 group makes its conformation less flexible than OH group, and thus increases the energy for the transition-state during rotation.

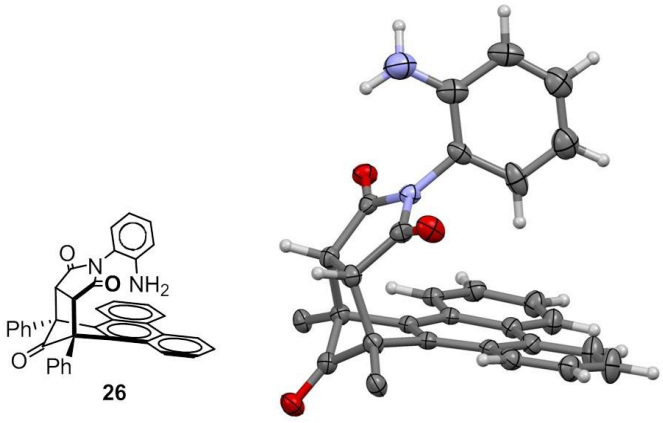

Figure 7.8: Structure of balance **26** that designed to form the NH–π interaction and its crystal structure obtained from X–ray analysis. The bridge phenyl groups in the crystal structure were hidden for better viewing clarity.

The balance **26** was able to be crystalized from its solution in acetonitrile. Only *unfolded* conformer was observed in the obtained solid-state structure (Figure 7.8, right). However, the *folded* conformation was favored in $CDCl_3$ in room temperature. The $-\Delta G$ value of balance **26** was measured to be 0.35 kcal/mol at 25°C in $CDCl_3$, which is stronger than CH_3–π interaction formed in **7a** under the same condition ($-\Delta G$ = 0.10 kcal/mol).

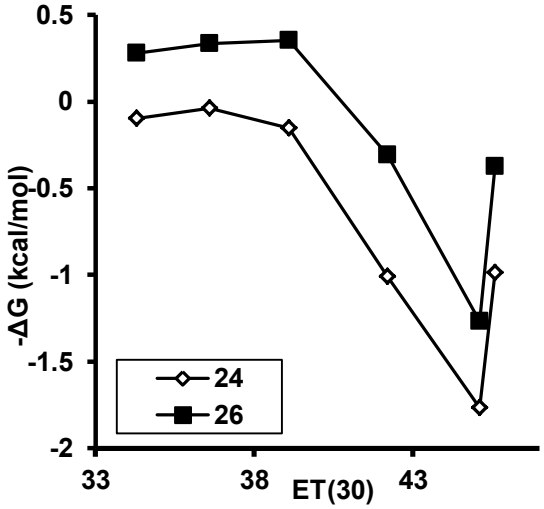

Figure 7.9: Comparison of the folding energies ($-\Delta G$) of balances **24** and **26** in different solvents.

Same as balance **24** mentioned on above section, the folding energy of balance **26** may show different values in solvents with different polarities (Figure 7.9). The trend is also very similar as balance **24**, which verified the importance of linker on determining the solvent effect. The factors that make up the solvent effect on the NH–π interaction are still under investigation.

7.4 MOLECULAR BALANCE FOR STUDY IMIDAZOLE–Π INTERACTION

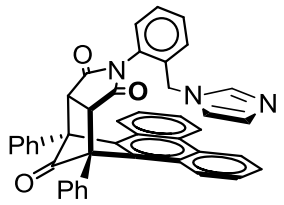

27

Figure 7.10: Structure of balance **27** that designed to form the imidazole–π interaction.

Balance **27** with imidazole arm (Figure 7.10) was synthesized to study the interaction between imidazole ring and the aromatic shelf. Its solid-state structure was characterization in crystal with X-ray analysis (Figure 7.11). A stacking interaction with was observed in the structure. Although the imidazole ring located above the central space between two side rings, the distance from the centroid of the five-member ring to the shelf plane (3.409 Å) was within a typical range of a non-covalent interaction, and one of the protons on the imidazole can still interact with the side ring. In addition, a clear CH–π interaction was also formed between the CH_2 linker and the shelf. It could be another stabilization force for the *folded* conformer of balance **27**.

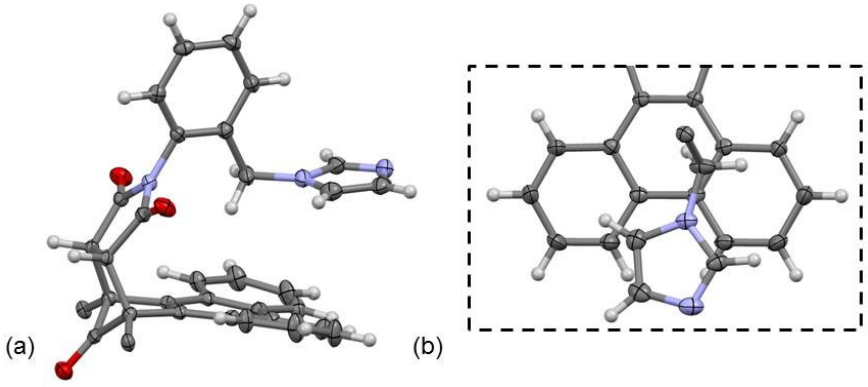

Figure 7.11: Crystal structure of balance **27** with (a) side view and (b) top view of the stacking interaction. Part of the structure was hidden for a better viewing clarity.

The *folded* conformer of balance **27** was favored in balance at room temperature in $CDCl_3$, and the accordingly $-\Delta G$ value was 0.19 kcal/mol. This interaction is slightly weaker compared with the phenyl–π interaction obtained in similar environment: the $-\Delta G$ value of balance **7e** with CH_2 linker and phenyl arm was measured to be 0.29 kcal/mol.

Containing imidazole structure, the balance **27** showed a potential ability to be soluble in solvents with high polarity. However, its solubility in water and methanol was poor based on the experiments. Further research about this balance could be the study on interactions formed by protonated or alkylated imidazole ring.

7.5 MOLECULAR BALANCE WITH SPLIT PHENYL RINGS ON SHELF

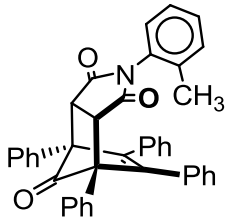

28

Figure 7.12: Structure of balance **28** with separate phenyl rings on the shelf.

The structure of balance **28** (Figure 7.12) contains two separate phenyl rings on the shelf (excluding the two bridge phenyl rings) were originally designed in hope of forming interactions between the two rings. However, the crystal structure obtained for this molecule (Figure 7.13) indicates that the space between the rings may not be enough for further interactions. Rather than twisting away and leave more space in between, the two rings intend to be parallel to each other. Still, one possible CH–π interaction was observed between the CH_3 and one of the side rings, but it was not within good geometry and cannot form strong interaction.

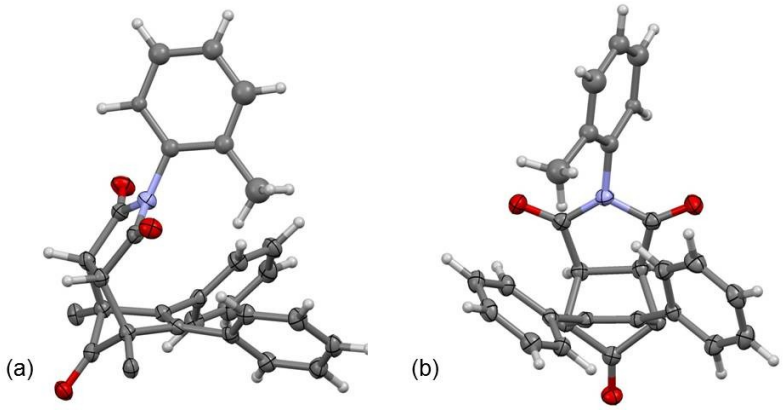

Figure 7.13: Crystal structure of balance **28** with (a) side view and (b) front view with both *unfolded* and *folded* conformers. Part of the structure was hidden for a better viewing clarity.

The assignment of folded and unfolded conformers was similar to that of previous balances. The interaction of this balance ($-\Delta G$ = –1.08 kcal/mol with *folded*/*unfolded* = 0.16) is much weaker than the balance **7a** ($-\Delta G$ = 0.13 kcal/mol with *folded*/*unfolded* = 1.25) with connected phenyl rings (phenanthrene shelf) and the methyl arm. Further investigation with similar structures containing larger alkyl arms is still undergoing by undergraduate student Darya Kaborda.

7.6 SYNTHESIS

7.6.1 Balances that forms Double-Mutant Cycles

The synthesis of balances **22** were via the Diels-Alder reaction between corresponding maleic imides **29** and diene **30** (Figure 7.14). The synthesis of balances **23** followed the same procedure as previous balances. Balances **22c**, **22d** and **22e** were synthesized by Ping li, and balances **23b**, **23c** and **23e** have been discussed in previous sections as balances **9b**, **9a** (or **14a**) and **2a**. Balances **23d** were synthesized for previous study.[74]

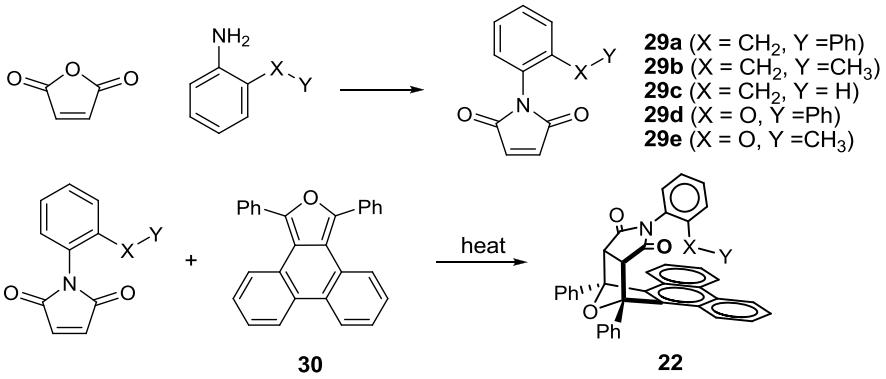

Figure 7.14: Overview of synthesis of balances **22** via Diels-Alder reaction between maleic imides **29** and the diene **30** with phenanthrene shelf.

To make imides **29**, maleic anhydride and corresponding aniline were heated to reflux in acetic acid for 2 d. The crude products were purified by running column with EtOAc/Hexane (v/v = 1/7).

Preparation of imides **29a**:

2-Benzylaniline (0.187 g, 1.02 mmol) was reacted with maleic anhydride (0.100 g, 1.02 mmol) in 10 mL acetic acid to produce imide **29a** as yellow oil (0.126 g, 0.48 mmol, 47% yield). ^{1}H NMR (300 MHz, $CDCl_3$) δ 7.51–6.90 (m, 9 H), 6.68 (s, 2 H), 3.89 (s, 2 H).

Preparation of imides **29b**:

2-Ethylaniline (0.494 g, 4.0 mmol) was reacted with maleic anhydride (0.400 g, 4.0 mmol) in 15 mL acetic acid to produce imide **29b** as yellow oil (0.477 g, 2.4 mmol, 59% yield). ^{1}H NMR (300 MHz, $CDCl_3$) δ 7.46–7.22 (m, 3 H), 7.08 (d, J = 7.83 Hz, 1 H), 6.87 (s, 2 H), 2.46 (q, J = 7.38 Hz, J = 14.75 Hz, 2 H), 1.15 (t, J = 7.38 Hz, 3 H).

Preparation of imides **29c**:

o-Toluidine (0.220 g, 2.0 mmol) was reacted with maleic anhydride (0.200 g, 2.0 mmol) in 10 mL acetic acid to produce imide **29c** as yellow oil (0.256 g, 1.37 mmol, 68%

yield). ^{1}H NMR (300 MHz, $CDCl_3$) δ 7.39–7.23 (m, 3 H), 7.11 (d, J = 7.14 Hz, 1 H), 6.85 (s, 2 H), 2.16 (s, 3 H).

Preparation of diene **30**:

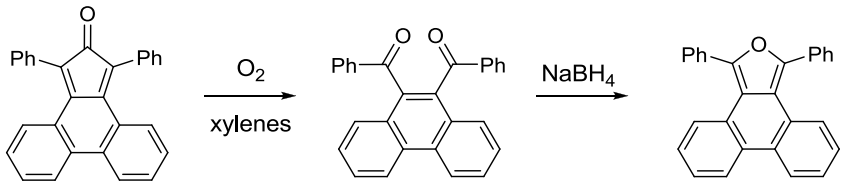

Phencyclone (2.0 g, 5.2 mmol) in xylenes (40 mL) was heated open to air to reflux for 24 h. The oxidation product was purified by running column with EtOAc and hexane (v/v = 1/10), and was obtained as colorless crystal (0.36 g, 0.93 mmol, 18% yield). ^{1}H NMR (300 MHz, $CDCl_3$) δ 8.81 (d, J = 8.7 Hz, 2 H). 7.66–7.90 (m, 8 H), 7.48–7.60 (m, 4 H), 7.30–7.42 (m, 4 H).

The acetone precursor (0.30 g, 0.78 mmol) was then dissolved in methanol (30 mL) and reacted with $NaBH_4$ (0.80 g, 21 mmol). After stirring for 3 h under nitrogen, HCl aqueous solution (3 N, 40 mL) was added to quench the reaction. The mixture was extracted with 30 mL CH_2Cl_2 for twice, and washed with 30 mL water and 30 mL brine. The organic layer was combined and dried under vacuum to get diene **30** as white solid (0.20 g, 0.54 mmol, 69% yield). ^{1}H NMR (300 MHz, $CDCl_3$) δ 8.37 (dd, J = 8.0 Hz, J =0.8 Hz, 2 H), 8.18 (dd, J = 8.0 Hz, J = 1.2 Hz, 2 H), 7.84 (dd, J = 7.7 Hz, J = 0.7 Hz, 4 H), 7.57–7.38 (m, 8H), 7.30–7.16 (m, 2H).

Preparation of balance **22a**:

Imide **29a** (0.034 g, 0.135 mmol) and diene **30** (0.050 g, 0.135 mmol) were dissolved in toluene (5 mL) and heated to reflux for 24 h. The crude product was purified by running column with EtOAc/Hex (v/v = 1/5), and balance 22a was obtained as white

solid (0.064 g, 0.128 mmol, 95% yield). ^{1}H NMR (300 MHz, $CDCl_3$) δ 8.74 (d, *J* = 8.27 Hz, 2 H minor), 8.61 (d, *J* = 8.44 Hz, 2 H major), 8.41–8.38 (m, 21 H major, 22 H minor), 6.22 (d, *J* = 7.36 Hz, 1 H minor), 5.98 (d, *J* = 7.36 Hz, 1 H major), 4.74 (2 H minor), 4.25–4.25 (m, 3 H major), 3.81 (2 H minor), 3.67 (s, 2 H major).

Preparation of balance **22b**:

Imide **29b** (0.029 g, 0.143 mmol) and diene **30** (0.053 g, 0.143 mmol) were dissolved in toluene (5 mL) and heated to reflux for 24 h. After work up steps and purification, balance **22b** was obtained as white solid (0.058 g, 0.105 mmol, 73% yield). ^{1}H NMR (300 MHz, $CDCl_3$) δ 8.81–8.67 (m, 2 H major, 2 H minor), 8.19 (brs, 2 H major, 2 H minor), 7.91–6.70 (m, 14 H major, 16 H minor), 6.49 (t, *J* = 7.62 Hz, 1 H major), 4.81 (s, 2 H minor), 4.75 (s, 2 H major), 4.25 (d, *J* = 7.62 Hz, 1 H major), 2.51 (q, *J* = 15.07 Hz, *J* = 7.67 Hz, 2 H major), 2.35 (q, *J* = 15.07 Hz, *J* = 7.67 Hz, 2 H minor), 1.20 (t, *J* = 7.39 Hz, 3 H major), 1.10 (t, *J* = 7.39 Hz, 3 H minor).

Preparation of balance **23a**:

The synthesis of **23a** was similar to previous balances with benzene shelves. Anhydride **5c** (0.100 g, 0.272 mmol) and 2-benzylaniline (0.054 g, 0.298 mmol) in acetic acid (5 mL) were heated to reflux for 24 h. After work up and purification steps, the balance **23a** was obtained as yellow oil (0.155 g, > 90% yield). ^{1}H NMR (300 MHz, $CDCl_3$ δ 8.10–7.90 (m, 4 H major, 4 H minor), 7.79–6.66 (m, 13 H major, 14 H minor), 5.56 (d, *J* = 7.72 Hz, 1 H major), 4.39 (s, 2 H major), 4.28 (s, 2 H minor), 3.76 (s, 3 H major), 3.48 (s, 3 H minor).

7.6.2 Balances used in Solvent Studies

The synthesis of balance **1a** and **7b** was discussed in Chapter 3 and Chapter 4, and balance **1h** have been synthesized for previous study.[74]

Preparation of balance **7e**:

The synthesis of **7e** was similar to balances in previous chapters with phenanthrene shelves. Anhydride **5a** (0.050 g, 0.104 mmol) and 2-benzylaniline (0.023 g, 0.125 mmol) in acetic acid (5 mL) were heated to reflux for 24 h. After work up and purification steps, the balance **7e** was obtained as white solid (0.063 g, 0.098 mmol, 94% yield). ^{1}H NMR (300 MHz, $CDCl_3$) δ 8.70 (d, J = 8.44 Hz, 2 H minor), 8.41 (d, J = 7.84 Hz, 2 H major), 8.21 (d, J = 7.84 Hz, 2 H minor), 8.06 (d, J = 8.44 Hz, 2 H major), 7.84–6.74 (m, 20 H major, 21 H minor), 6.56 (dt, J = 8.21 Hz, J =2.05 Hz, 1 H minor), 6.31 (d, J = 7.52 Hz, 1 H major), 5.94 (d, J = 7.21, 2 H major), 4.70 (s, 2 H minor), 4.42 (d, J = 7.65 Hz, 1 H minor), 4.14 (s, 2 H major), 3.99 (s, 2 H minor), 3.82 (s, 2 H major).

Preparation of balance **24**:

Anhydride **5a** (0.050 g, 0.104 mmol) and *N*-phenyl-*o*-phenylenediamine (0.023 g, 0.125 mmol) in acetic acid (5 mL) were heated to reflux for 24 h. After work up and purification steps, the balance **24** was obtained as yellow solid (0.056 g, 0.086 mmol, 83% yield). ^{1}H NMR (300 MHz, $CDCl_3$) δ 8.69 (d, J = 8.30 Hz, 2 H major), 8.40 (d, J = 7.47 Hz, 2 H minor), 8.29 (d, J = 7.47 Hz, 2 H major), 8.01 (d, J = 8.30 Hz, 2 H minor), 7.73 (t, J = 7.58 Hz, 4 H major), 7.64–6.64 (m, 16 H major, 21 H minor), 6.44–6.26 (m, 2 H major), 5.82–5.67 (m, 2 H minor), 5.41 (s, 1 H major), 4.70 (s, 2 H minor), 4.59 (dd, J = 7.94 Hz, J = 0.92 Hz, 1 H major), 4.38 (s, 2 H major), 3.23 (s, 1 H minor).

Preparation of balance **25**:

Anhydride **5a** (0.050 g, 0.104 mmol) and 2-aminophenyl-phenylsulfide (0.025 g, 0.125 mmol) in acetic acid (3 mL) were heated to reflux for 24 h. After work up and purification steps, the balance **25** was obtained as white solid (0.076 g, 0.114 mmol, >90% yield). ^{1}H NMR (300 MHz, $CDCl_3$) δ 8.79–8.62 (m, 2 H major, 2 H minor), 8.41 (d, *J* = 7.54 Hz, 2 H minor), 8.32 (d, *J* = 7.54 Hz, 2 H major), 8.15 (d, *J* = 7.54 Hz, 1 H minor), 8.08 (d, *J* = 8.55 Hz, 1 H major), 7.79–6.86 (m, 21 H major, 18 H minor), 6.69–6.54 (m, 2 H minor), 6.26 (d, *J* = 7.54 Hz, 2 H minor), 4.68 (s, 2 H minor), 4.58–4.48 (m, 3 H major).

7.6.3 Balance for Measuring NH–π Interaction

Anhydride **5a** (0.100 g, 0.208 mmol) and *o*-phenylenediamine (0.023 g, 0.208 mmol) in DMF (2 mL) were heated to reflux for 5 h. The mixture was quenched with 50 mL water and then extracted with 50 mL EtOAc for 3 times. The organic layer was combined and washed with 50 mL water for 3 times. The solvent was dried under vacuum, the balance **26** was obtained as white solid (0.130 g, 0.114 mmol, >90% yield). ^{1}H NMR (300 MHz, $CDCl_3$) δ 8.76–8.60 (m, 2 H major, 2 H minor), 8.47–8.27 (m, 2 H major, 2 H minor), 7.83–6.50 (m, 17 H major, 18 H minor), 6.19 (d, *J* = 8.44 Hz, 1 H major), 6.07 (t, *J* = 7.91 Hz, 1 H minor), 4.65 (s, 2 H major), 4.63 (s, 2 H minor), 4.36 (d, *J* = 7.91 Hz, 1 H minor).

7.6.4 Balance for Measuring Imidazole–π Interaction

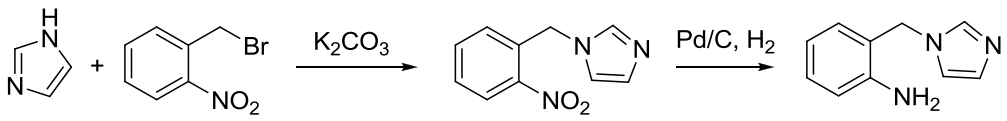

31 **32**

Balance **27** was obtained in three steps. First, nitrobenzene precursor **31** was made. To the stirring solution of imidazole (0.019g, 0.278 mmol) in DMF (5 mL), potassium carbonate (0.064 g, 462 mmol) and 2-nitrobenzyl bromide (0.050 g, 0.231 mmol) was added. The reaction was stirred under room temperature for 24 h, and was quenched with 30 mL water. The mixture was then extracted with 50 mL EtOAc for 3 times, and the combined organic layer was washed with saturate 50 mL $NaHCO_3$ (aq.) and dried with $MgSO_4$. After the removal of solvent under vacuum, compound **31** was then obtained as yellow liquid (0.048g, 0.24 mmol, 85% yield). ^{1}H NMR (300 MHz $CDCl_3$) δ 8.15 (d, J = 7.84 Hz, 1 H), 7.63–6.90 (m, 5 H), 6.80 (d, J = 7.61 Hz, 1 H), 5.57 (s, 2 H).

The nitrobenzene **31** was then reduced into aniline **32** via catalyzed hydrogenation. The substituted nitrobenzene **31** (0.048 g, 0.24 mmol) was dissolved with THF (5 mL) in a pressure vessel, then ethanol (20 mL) and of Pd/C (10% wt, 20 mg) was added. The vessel was pressurized at 40 psi with hydrogen gas and was stirred for 4 h. The resulting mixture was filtered through celite and the solvent was removed by rotary evaporation to afford the product **32** as yellow oil (0.044 g, 0.25 mmol, > 90% yield). ^{1}H NMR (300 MHz $CDCl_3$) δ 8.10 (s, 1 H), 7.19 (t, J = 7.58 Hz, 1 H), 7.13 (s, 1 H), 7.06 (d, J = 7.58 Hz, 1 H), 6.94 (s, 1 H), 6.79 (t, J = 7.58 Hz, 1 H), 6.71 (d, J = 8.08 Hz 1 H), 5.16 (s, 2 H), 5.04 (brs, 2 H).

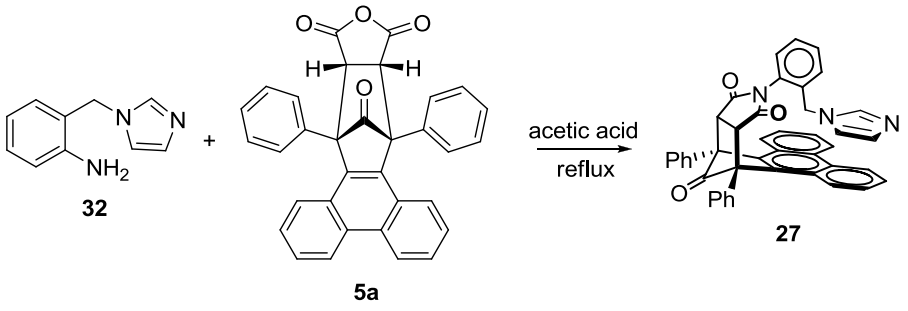

Aniline **32** was reacted with anhydride **5a** to produce balance **27**. Compounds **32** (0.043 g, 0.248 mmol) and **5a** (0.079 g, 0.166 mmol) were dissolved in 5 mL acetic acid and was heated to reflux for 24 h. After work up steps and purification, balance 27 was obtained as yellow solid (0.114 g, 0.179 mmol, > 90% yield). ^{1}H NMR (300 MHz $CDCl_3$) δ 8.62 (d, *J* = 8.40, 2 H major), 8.28 (d, *J* = 7.98 Hz, 2 H minor), 8.23 (d, *J* = 8.40 Hz, 2 H minor), 8.10 (d, *J* = 7.56 Hz, 2 H major), 7.73–6.86 (m, H major, H minor), 6.72 (s, 1 H minor), 6.33 (s, 1 H minor), 6.05 (d, *J* = 7.81 Hz, 1 H minor), 5.61 (s, 1 H minor), 4.66 (s, 2 H major), 4.65 (s, 2 H minor), 2.25 (s, 2 H minor), 1.97 (s, 2 H major).

7.6.5 Balance with Split Phenyl Shelf

Imide **29c** (0.045 g, 0.24 mmol) and tetraphenylcyclopentadienone (0.093 g, 0.24 mmol) were dissolved in benzene (5 mL) and heated to reflux for 24 h. After work up, the crude product was purified by running column with EtOAc/Hexane (v/v = 1/5). Balance **28** was then obtained as purple solid (0.121 g, 0.21 mmol, 88% yield). ^{1}H NMR (300 MHz $CDCl_3$) δ 7.91–6.63 (m, 22 H major, 22 H minor), 4.44 (s, 2 H minor), 4.41 (s, 2 H major), 2.25 (s, 3 H major), 2.05 (s, 3 H minor).

REFERENCES

(1) Deechongkit, S.; Nguyen, H.; Powers, E. T.; Dawson, P. E.; Gruebele, M.; Kelly, J. W. *Nature* **2004**, *430*, 101.

(2) Krueger, A. T.; Kool, E. T. *Curr. Opin. Chem. Biol.* **2007**, *11*, 588.

(3) Amabilino, D. B.; Stoddart, J. F. *Chem. Rev.* **1995**, *95*, 2725.

(4) Clayden, J. *Chem. Soc. Rev.* **2009**, *38*, 817.

(5) Lehn, J. M. *Science* **2002**, *295*, 2400.

(6) Anslyn, E. V.; Dougherty, D. A. *Modern physical organic chemistry*; University Science: Sausalito, Calif., 2006.

(7) Frieden, E. *J. Chem. Educ.* **1975**, *52*, 754.

(8) Hunter, C. A.; Anderson, H. L. *Angew. Chem. Int. Edit.* **2009**, *48*, 7488.

(9) Parthasarathi, R.; Subramanian, V.; Sathyamurthy, N. *J. Phys. Chem. A* **2006**, *110*, 3349.

(10) Grabowski, S. J.; Sokalski, W. A.; Dyguda, E.; Leszczynski, J. *J. Phys. Chem. B* **2006**, *110*, 6444.

(11) Grabowski, S. J. *J. Phys. Chem. A* **2007**, *111*, 3387.

(12) Pauling, L. *The nature of the chemical bond and the structure of molecules and crystals : an introduction to modern structural chemistry / by Linus Pauling*; 3rd ed.; Cornell University Press: Ithaca, N.Y., 1960.

(13) Takahashi, O.; Kohno, Y.; Nishio, M. *Chem. Rev.* **2010**, *110*, 6049.

(14) Grabowski, S. J.; Sokalski, W. A. *J. Phys. Org. Chem.* **2005**, *18*, 779.

(15) Hildebrand, J. H. *Proc. Natl. Acad. Sci. U. S. A.* **1979**, *76*, 194.

(16) Herzfeld, J. *Science* **1991**, *253*, 88.

(17) Dill, K. A. *Science* **1990**, *250*, 297.

(18) Dill, K. A. *Biochemistry* **1990**, *29*, 7133.

(19) Lins, L.; Brasseur, R. *Faseb J.* **1995**, *9*, 535.

(20) Hunter, C. A. *Chem. Soc. Rev.* **1994**, *23*, 101.

(21) Hunter, C. A.; Lawson, K. R.; Perkins, J.; Urch, C. J. *J. Chem. Soc., Perkin Trans. 2* **2001**, 651.

(22) Meyer, E. A.; Castellano, R. K.; Diederich, F. *Angew. Chem. Int. Edit.* **2003**, *42*, 1210.

(23) Brunsveld, L.; Folmer, B. J. B.; Meijer, E. W.; Sijbesma, R. P. *Chem. Rev.* **2001**, *101*, 4071.

(24) Beljonne, D.; Hennebicq, E.; Daniel, C.; Herz, L. M.; Silva, C.; Scholes, G. D.; Hoeben, F. J. M.; Jonkheijm, P.; Schenning, A.; Meskers, S. C. J.; Phillips, R. T.; Friend, R. H.; Meijer, E. W. *J. Phys. Chem. B* **2005**, *109*, 10594.

(25) Murai, T.; Aso, H.; Kato, S. *Org. Lett.* **2002**, *4*, 1407.

(26) Malkov, A. V.; Mariani, A.; MacDougall, K. N.; Kocovsky, P. *Org. Lett.* **2004**, *6*, 2253.

(27) Korenaga, T.; Kadowaki, K.; Sakai, T. *J. Fluor. Chem.* **2007**, *128*, 557.

(28) Hunter, C. A.; Sanders, J. K. M. *J. Am. Chem. Soc.* **1990**, *112*, 5525.

(29) Novoa, J. J.; Mota, F. *Chem. Phys. Lett.* **2000**, *318*, 345.

(30) Nishio, M.; Hirota, M. *Tetrahedron* **1989**, *45*, 7201.

(31) Nishio, M. *CrystEngComm* **2004**, *6*, 130.

(32) Nishio, M.; Umezawa, Y.; Honda, K.; Tsuboyama, S.; Suezawa, H. *CrystEngComm* **2009**, *11*, 1757.

(33) Takahashi, H.; Tsuboyama, S.; Umezawa, Y.; Honda, K.; Nishio, M. *Tetrahedron* **2000**, *56*, 6185.

(34) Nishio, M. *Tetrahedron* **2005**, *61*, 6923.

(35) Nishio, M.; Umezawa, Y.; Hirota, M.; Takeuchi, Y. *Tetrahedron* **1995**, *51*, 8665.

(36) Sakaki, S.; Kato, K.; Miyazaki, T.; Musashi, Y.; Ohkubo, K.; Ihara, H.; Hirayama, C. *J. Chem. Soc. Faraday T.* **1993**, *89*, 659.

(37) Ehama, R.; Tsushima, M.; Yuzuri, T.; Suezawa, H.; Sakakibara, K.; Hirota, M. *Bull. Chem. Soc. Jpn.* **1993**, *66*, 814.

(38) Arduini, A.; Giorgi, G.; Pochini, A.; Secchi, A.; Ugozzoli, F. *Tetrahedron* **2001**,

57, 2411.

(39) Arena, G.; Contino, A.; Longo, E.; Spoto, G.; Arduini, A.; Pochini, A.; Secchi, A.; Massera, C.; Ugozzoli, F. *New J. Chem.* **2004**, *28*, 56.

(40) Ma, J. C.; Dougherty, D. A. *Chem. Rev.* **1997**, *97*, 1303.

(41) Kearney, P. C.; Mizoue, L. S.; Kumpf, R. A.; Forman, J. E.; McCurdy, A.; Dougherty, D. A. *J. Am. Chem. Soc.* **1993**, *115*, 9907.

(42) Dougherty, D. A. *Science* **1996**, *271*, 163.

(43) Caldwell, J. W.; Kollman, P. A. *J. Am. Chem. Soc.* **1995**, *117*, 4177.

(44) Cockroft, S. L.; Hunter, C. A. *Chem. Comm.* **2006**, 3806.

(45) Mati, I. K.; Cockroft, S. L. *Chem. Soc. Rev.* **2010**, *39*, 4195.

(46) Schneider, H. J. *Angew. Chem. Int. Edit.* **2009**, *48*, 3924.

(47) Nakamura, M.; Oki, M.; Nakanish.H; Yamamoto, O. *Bull. Chem. Soc. Jpn.* **1974**, *47*, 2415.

(48) Oki, M. *Angew. Chem. Int. Edit.* **1976**, *15*, 87.

(49) Hunter, C. A. *Angew. Chem. Int. Edit.* **2004**, *43*, 5310.

(50) Oki, M.; Izumi, G.; Yamamoto, G.; Nakamura, N. *Chem. Lett.* **1980**, 213.

(51) Izumi, G.; Yamamoto, G.; Oki, M. *Chem. Lett.* **1980**, 969.

(52) Oki, M.; Izumi, G.; Yamamoto, G.; Nakamura, N. *Bull. Chem. Soc. Jpn.* **1982**, *55*, 159.

(53) Tamura, Y.; Yamamoto, G.; Oki, M. *Bull. Chem. Soc. Jpn.* **1987**, *60*, 1781.

(54) Tamura, Y.; Yamamoto, G.; Oki, M. *Chem. Lett.* **1986**, 1619.

(55) Oki, M. *Accounts Chem. Res.* **1990**, *23*, 351.

(56) Gung, B. W.; Xue, X. W.; Reich, H. J. *J. Org. Chem.* **2005**, *70*, 7232.

(57) Gung, B. W.; Zou, Y.; Xu, Z. G.; Amicangelo, J. C.; Irwin, D. G.; Ma, S. Q.; Zhou, H. C. *J. Org. Chem.* **2008**, *73*, 689.

(58) Gung, B. W.; Xue, X. W.; Reich, H. J. *J. Org. Chem.* **2005**, *70*, 3641.

(59) Gung, B. W.; Patel, M.; Xue, X. W. *J. Org. Chem.* **2005**, *70*, 10532.

(60) Gung, B. W.; Emenike, B. U.; Alverez, C. N.; Rakovan, J.; Kirschbaum, K.; Jain, N. *Tetrahedron Lett.* **2010**, *51*, 1648.

(61) Gung, B. W.; Wekesa, F.; Barnes, C. L. *J. Org. Chem.* **2008**, *73*, 1803.

(62) Paliwal, S.; Geib, S.; Wilcox, C. S. *J. Am. Chem. Soc.* **1994**, *116*, 4497.

(63) Kim, E.; Paliwal, S.; Wilcox, C. S. *J. Am. Chem. Soc.* **1998**, *120*, 11192.

(64) Ren, T.; Yin, Y. H.; Kim, K. S.; Kim, D. H. *J. Biomol. Struct. Dyn.* **1997**, *15*, 401.

(65) Hof, F.; Scofield, D. M.; Schweizer, W. B.; Diederich, F. *Angew. Chem. Int. Edit.* **2004**, *43*, 5056.

(66) Fischer, F. R.; Schweizer, W. B.; Diederich, F. *Chem. Comm.* **2008**, 4031.

(67) Bhayana, B.; Wilcox, C. S. *Angew. Chem.-Int. Edit.* **2007**, *46*, 6833.

(68) Fischer, F. R.; Schweizer, W. B.; Diederich, F. *Angew. Chem. Int. Edit.* **2007**, *46*, 8270.

(69) Cockroft, S. L.; Hunter, C. A. *Chem. Comm.* **2009**, 3961.

(70) Ribas, J.; Cubero, E.; Luque, F. J.; Orozco, M. *J. Org. Chem.* **2002**, *67*, 7057.

(71) Motherwell, W. B.; Moise, J.; Aliev, A. E.; Nic, M.; Coles, S. J.; Horton, P. N.; Hursthouse, M. B.; Chessari, G.; Hunter, C. A.; Vinter, J. G. *Angew. Chem. Int. Edit.* **2007**, *46*, 7823.

(72) Aliev, A. E.; Moise, J.; Motherwell, W. B.; Nic, M.; Courtier-Murias, D.; Tocher, D. A. *Phys. Chem. Chem. Phys.* **2009**, *11*, 97.

(73) Chong, Y. S.; Carroll, W. R.; Burns, W. G.; Smith, M. D.; Shimizu, K. D. *Chem.-Eur. J.* **2009**.

(74) Carroll, W. R.; Pellechia, P.; Shimizu, K. D. *Org. Lett.* **2008**, *10*, 3547.

(75) Carroll, W. R.; Zhao, C.; Smith, M. D.; Pellechia, P. J.; Shimizu, K. D. *Org. Lett.* **2011**, *13*, 4320.

(76) Zhao, C.; Parrish, R. M.; Smith, M. D.; Pellechia, P. J.; Sherrill, C. D.; Shimizu, K. D. *J. Am. Chem. Soc.* **2012**, *134*, 14306.

(77) Bauer, M.; Bertario, A.; Boccardi, G.; Fontaine, X.; Rao, R.; Verrier, D. *J. Pharm. Biomed. Anal.* **1998**, *17*, 419.

(78) Rizzo, V.; Pinciroli, V. *J. Pharm. Biomed. Anal.* **2005**, *38*, 851.

(79) Soininen, P.; Haarala, J.; Vepsalainen, J.; Niemitz, M.; Laatikainen, R. *Anal.*

Chim. Acta **2005**, *542*, 178.

(80) Zimmer, K. D.; Shoemaker, R.; Ruminski, R. R. *Inorg. Chim. Acta* **2006**, *359*, 1478.

(81) Srivastav, K. K.; Verma, A. K.; Verma, S. M. *Indian J. Chem. B* **1993**, *32*, 1143.

(82) Mammen, M; Shakhnovich, E. I.; Whitesides, G. M. *J. Org. Chem.* **1998**, *63*, 3168-3175.

(83) Arca, V.; Paradisi, C.; Scorrano, G. *J. Org. Chem.* **1990**, *55*, 3617-3621.

(84) Wolin, R. L.; Santillan, A.; Tang, L.; Huang, C.; Jiang, X. X.; Lovenberg, T. W. *Bioorgan.Med. Chem.* **2004**, *12*, 4511.

(85) Ueno, M.; Yonemoto, M.; Hashimoto, M.; Wheatley, A. E. H.; Naka, H.; Kondo, Y. *Chem. Comm.* **2007**, *22*, 2264-2266.

(86) Haquette, P.; Dagorne, S.; Welter, R.; Jaouen, G. *J. Organomet. Chem.* **2003**, *682*, 240.

(87) McNulty, J.; Nair, J. J.; Capretta, A. *Tetrahedron Lett.* **2009**, *50*, 4087-4091

(88) Turner, E. E. *J. Chem. Soc.Trans.* **1915**, *107*, 469-474.

(89) Xie, H.; Ng, D.; Savinov, S. N.; Dey, B.; Kwong, P. D.; Wyatt, R.; Smith, A. B.; Hendrickson, W. A. *J. Med. Chem.* **2007**, *50*, 4898–4908.

(90) Tong, Y. F.; Zhang, P.; Chen, F.; Hao, L. H.; Wu, S.; Ye, F.; Tian, J. Y. *Chinese Chem. Lett.* **2010**, *21*, 1415-1418.

(91) Hoshino, Y.; Okuno, M.; Kawamura, E.; Honda, K.; Inoue, S. *Chem. Comm.* **2009**, *45*, 2281-2283.

(92) Tortolani, D. R.; Poss, M. A. *Org. Lett.* **1999**, *1*, 1261–1262.

(93) Quideau, S.; Lyvinec, G.; Marguerit, M.; Bathany, K.; Ozanne-Beaudenon, A.; Buffeteau, T.; Cavagnat, D.; Chénedé, A. *Angew. Chem. Int. Ed.* **2009**, *48*, 4605-4609.

(94) Yoshitake, Y.; Misaka, J.; Setoguchi, K.; Abe, M.; Kawaji, T.; Eto, M.; Harano, K. *J. Chem. Soc., Perkin Trans. 2* **2002**, 1611.

(95) Bagmanov, B. T. *Russ. J. Org. Chem*. **2007**, *43*, 1635-1641.

(96) Ran, J.; Wong, M. W. *J. Phys. Chem. A* **2006**, *110*, 9702.

(97) Barnes, C. L.; Vanderhelm, D. *Acta Crystall. B -Stru.* **1982**, *38*, 2589.

(98) Chakrabarti, P.; Samanta, U. *J. Mol. Biol.* **1995**, *251*, 9.

(99) Sozzani, P.; Comotti, A.; Bracco, S.; Simonutti, R. *Chem. Comm.* **2004**, 768.

(100) Sozzani, P.; Comotti, A.; Bracco, S.; Simonutti, R. *Angew. Chem. Int. Edit.* **2004**, *43*, 2792.

(101) Umezawa, Y.; Nishio, M. *Biorg. Med. Chem.* **1998**, *6*, 2507.

(102) Muraki, M. *Protein Peptide Lett.* **2002**, *9*, 195.

(103) Nijamudheen, A.; Jose, D.; Shine, A.; Datta, A. *J. Phys. Chem. Lett.* **2012**, *3*, 1493.

(104) Eto, M.; Setoguchi, K.; Harada, A.; Sugiyama, E.; Harano, K. *Tetrahedron Lett.* **1998**, *39*, 9751.

(105) Page, M. I.; Jencks, W. P. *Proc. Natl. Acad. Sci. U. S. A.* **1971**, *68*, 1678.

(106) Jencks, W. P. *Proc. Natl. Acad. Sci. U. S. A.* **1981**, *78*, 4046.

(107) Franck, R. W. *Tetrahedron* **1983**, *39*, 3251.

(108) Searle, M. S.; Williams, D. H. *J. Am. Chem. Soc.* **1992**, *114*, 10690.

(109) Allinger, N. L.; Hirsch, J. A.; Miller, M. A.; Tyminski, I. J.; Vancatle.Fa *J. Am. Chem. Soc.* **1968**, *90*, 1199.

(110) Lumry, R.; Rajender, S. *Biopolymers* **1970**, *9*, 1125.

(111) Booth, H.; Everett, J. R. *J. Chem. Soc., Perk. T. 2* **1980**, 255.

(112) Hu, J.; Zhang, D.; Harris, F. W. *J. Org. Chem.* **2005**, *70*, 707-708

(113) Grossmann, G.; Potrzebowski, M. J.; Olejniczak, S.; Ziolkowska, N. E.; Bujacz, G. D.; Ciesielski, W.; Prezdo, W.; Nazarov, V.; Golovko, V. *New J. Chem.* **2003**, *27*, 1095.

(114) Wade, D. *Chem.-Biol. Interact.* **1999**, *117*, 191.

(115) Rechavi, D.; Scarso, A.; Rebek, J. *J. Am. Chem. Soc.* **2004**, *126*, 7738.

(116) Zhao, Y. L.; Houk, K. N.; Rechavi, D.; Scarso, A.; Rebek, J. *J. Am. Chem. Soc.* **2004**, *126*, 11428.

(117) Haino, T.; Fukuta, K.; Iwamoto, H.; Iwata, S. *Chem.-Eur. J.* **2009**, *15*, 13286.

(118) Turowski, M.; Yamakawa, N.; Meller, J.; Kimata, K.; Ikegami, T.; Hosoya, K.; Tanaka, N.; Thornton, E. R. *J. Am. Chem. Soc.* **2003**, *125*, 13836.

(119) Iyer, S. S.; Zhang, Z. P.; Kellogg, G. E.; Karnes, H. T. *J. Chromatogr. Sci.* **2004**,

42, 383.

(120) Liu, Y.; Warmuth, R. *Org. Lett.* **2007**, *9*, 2883.

(121) Mugridge, J. S.; Bergman, R. G.; Raymond, K. N. *J. Am. Chem. Soc.* **2010**, *132*, 1182.

(122) Bhayana, B.; Ams, M. R. *J. Org. Chem.* **2011**, *76*, 3594.

(123) Kishikawa, K.; Yoshizaki, K.; Kohmoto, S.; Yamamoto, M.; Yamaguchi, K.; Yamadab, K. *J. Chem. Soc., Perkin Trans. 1* **1997**, 1233.

(124) Ruschak, A. M.; Kay, L. E. *J. Biomol. NMR* **2010**, *46*, 75.

(125) Wu, X.; Kang, W.; Zhu, D.; Zhu, C.; Liu, S. *J. Organomet. Chem.* **2009**, *694*, 2981-2986.

(126) Jennings, W. B.; Farrell, B. M.; Malone, J. F. *Accounts Chem. Res.* **2001**, *34*, 885.

(127) Marcus, Y. *J. Chem. Soc. Perk. T. 2* **1994**, 1015.

(128) Mancini, P. M. E.; Terenzani, A.; Gasparri, M. G.; Vottero, L. R. *J. Phys. Org. Chem.* **1995**, *8*, 617.

(129) Carter, P. J.; Winter, G.; Wilkinson, A. J.; Fersht, A. R. *Cell* **1984**, *38*, 835.

(130) Cockroft, S. L.; Hunter, C. A. *Chem. Soc. Rev.* **2007**, *36*, 172.